

**Aus der Klinik mit Schwerpunkt
Rheumatologie und Klinische Immunologie
der Medizinischen Fakultät Charité - Universitätsmedizin Berlin**

**eingereicht über das
Institut für Tierpathologie
des Fachbereichs Veterinärmedizin
der Freien Universität Berlin**

HIF-stabilization to accelerate fracture healing – Evaluation of a new therapeutic strategy to treat delayed bone regeneration

**Inaugural-Dissertation
zur Erlangung des Grades eines
PhD of Biomedical Sciences
an der
Freien Universität Berlin**

**vorgelegt von
Dr. med. vet. Annemarie Lang
Tierärztin aus Halle/Saale**

**Berlin 2019
Journal-Nr.: 4163**

Aus der Klinik mit Schwerpunkt
Rheumatologie und Klinische Immunologie
der Medizinischen Fakultät Charité - Universitätsmedizin Berlin

eingereicht über das
Institut für Tierpathologie
des Fachbereichs Veterinärmedizin
der Freien Universität Berlin

**HIF-stabilization to accelerate fracture healing –
Evaluation of a new therapeutic strategy
to treat delayed bone regeneration**

Inaugural-Dissertation
zur Erlangung des Grades eines
PhD of Biomedical Sciences
an der
Freien Universität Berlin

vorgelegt von
Dr. med. vet. Annemarie Lang
Tierärztin aus Halle/Saale

Berlin 2019

Journal-Nr.: 4163

Gedruckt mit Genehmigung des Fachbereichs Veterinärmedizin
der Freien Universität Berlin

Dekan: Univ.-Prof. Dr. Jürgen Zentek
Erster Gutachter: Univ.-Prof. Dr. Robert Klopffleisch
Zweiter Gutachter: Prof. Dr. Frank Buttgereit
Dritter Gutachter: Univ.-Prof. Dr. Wolfgang Bäumer

Deskriptoren (nach CAB-Thesaurus):

bone fractures, regeneration, mineralization, tumor necrosis factor,
dexamethasone, osteotomy (MeSH), polymerase chain reaction

Tag der Promotion: 28.11.2019

Bibliografische Information der *Deutschen Nationalbibliothek*

Die Deutsche Nationalbibliothek verzeichnet diese Publikation in der Deutschen Nationalbibliografie; detaillierte bibliografische Daten sind im Internet über <<https://dnb.de>> abrufbar.

ISBN: 978-3-96729-026-4

Zugl.: Berlin, Freie Univ., Diss., 2019

Dissertation, Freie Universität Berlin

D188

Dieses Werk ist urheberrechtlich geschützt.

Alle Rechte, auch die der Übersetzung, des Nachdruckes und der Vervielfältigung des Buches, oder Teilen daraus, vorbehalten. Kein Teil des Werkes darf ohne schriftliche Genehmigung des Verlages in irgendeiner Form reproduziert oder unter Verwendung elektronischer Systeme verarbeitet, vervielfältigt oder verbreitet werden.

Die Wiedergabe von Gebrauchsnamen, Warenbezeichnungen, usw. in diesem Werk berechtigt auch ohne besondere Kennzeichnung nicht zu der Annahme, dass solche Namen im Sinne der Warenzeichen- und Markenschutz-Gesetzgebung als frei zu betrachten wären und daher von jedermann benutzt werden dürfen.

This document is protected by copyright law.

No part of this document may be reproduced in any form by any means without prior written authorization of the publisher.

alle Rechte vorbehalten | all rights reserved

© Mensch und Buch Verlag 2019

Choriner Str. 85 - 10119 Berlin

verlag@menschundbuch.de – www.menschundbuch.de

Meiner Familie & Mephisto

Table of Contents

LIST OF TABLES	IV
LIST OF FIGURES.....	V
ABBREVIATIONS.....	VIII
INTRODUCTION.....	1
CHAPTER 1: LITERATURE REVIEW.....	2
1.1 Fracture healing	2
1.1.1 <i>Consecutive phases during bone regeneration.....</i>	<i>2</i>
1.1.2 <i>The importance of the initial healing phase.....</i>	<i>3</i>
1.1.3 <i>The immunology of the initial healing phase</i>	<i>4</i>
1.1.4 <i>The microenvironment during the initial healing phase.....</i>	<i>8</i>
1.2 The pathophysiology of fracture healing.....	10
1.2.1 <i>Classification and risk factors of fracture healing disorders.....</i>	<i>10</i>
1.2.2 <i>Underlying mechanism – Immunological dysregulation and inhibited adaptation to hypoxia.....</i>	<i>11</i>
1.3 Current therapeutic interventions	12
1.3.1 <i>Conservative therapies, growth factors and biomaterials</i>	<i>12</i>
1.3.2 <i>Promising compounds – HIF-stabilizers.....</i>	<i>13</i>
1.4 Aims and Objectives of the Thesis.....	17
CHAPTER 2: MATERIALS AND METHODS.....	18
2.1 Materials	18
2.1.1 <i>Bone marrow donors – Cell source.....</i>	<i>18</i>
2.1.2 <i>Plastic-ware/Miscellaneous.....</i>	<i>19</i>
2.1.3 <i>Cell culture.....</i>	<i>19</i>
2.1.4 <i>FACS analysis.....</i>	<i>20</i>
2.1.5 <i>Cell staining</i>	<i>21</i>
2.1.6 <i>Protein isolation and mass spectrometry</i>	<i>21</i>
2.1.7 <i>Scanning electron microscopy</i>	<i>22</i>
2.1.8 <i>Animals and housing</i>	<i>22</i>
2.1.9 <i>Osteotomy – Medications and material for surgical procedure.....</i>	<i>23</i>
2.1.10 <i>Histology.....</i>	<i>24</i>
2.1.11 <i>Immunofluorescence.....</i>	<i>25</i>
2.1.12 <i>RNA-isolation, microarray and qRT-PCR.....</i>	<i>25</i>
2.1.13 <i>Instruments.....</i>	<i>26</i>
2.1.14 <i>Software and Online Services.....</i>	<i>27</i>
2.2 Methods.....	28
2.2.1 <i>hMSC isolation and expansion.....</i>	<i>28</i>

2.2.2 hMSC characterization	28
2.2.3 Osteogenic differentiation of hMSCs.....	29
2.2.4 Quantitative real time PCR (qRT-PCR).....	30
2.2.5 Cell vitality and cytotoxicity.....	31
2.2.6 Whole blood assay	32
2.2.7 Protein isolation and mass spectrometry (LC-MS/MS)	32
2.2.8 Scanning electron microscopy (SEM)	33
2.2.9 Animals, housing and osteotomy	33
2.2.10 Ex vivo micro computed tomography (μ CT).....	36
2.2.11 Histological staining.....	37
2.2.12 Histomorphometry	39
2.2.13 Microarray and qRT-PCR.....	40
2.2.14 Statistical analysis	42
CHAPTER 3: RESULTS	43
3.1 Characterization of bone marrow derived hMSCs	43
3.2 The effect of hypoxia or HIF-stabilizers on the inhibition of hMSC calcification by GCs in an <i>in vitro</i> setting	44
3.2.1 hMSC calcification was inhibited dose-dependent by GCs <i>in vitro</i>	44
3.1.2 HIF-stabilizers diminished the inhibiting effect of GCs on hMSC calcification.....	45
3.3 Identification of a suitable scaffold for local delivery of MIF and DFO into the fracture gap	48
3.3.1 ACS-L and ACS-H contained high contents of collagens and further potential bone regeneration-linked proteins	48
3.3.2 ACS-H and ACS-L showed structural differences	52
3.3.3 ACS-H inhibited <i>in vitro</i> calcification of hMSCs while osteogenic gene expression was not affected	53
3.3.4 ACS-H increased cell cytotoxicity and induced TNF α release from whole blood assay.	55
3.3.5 ACS-L delayed mineralized callus formation <i>in vivo</i>	57
3.3.6 ACS-L remained partially in the osteotomy gap during the observation period.....	58
3.3.7 Reduced cartilage formation and mineralization indicate inhibitory effect of ACS-L on transition from the soft to the hard callus phase.....	59
3.3.8 ACS-L diminished cell invasion and reduced CD31 ^{hi} Emcn ^{hi} vessel formation.....	60
3.3.9 ACS-L reduced TRAP ⁺ cells while the number of macrophages and osteoblasts were comparable between groups	64
3.4 Investigation on the influence of MIF and/or DFO on the regeneration process in a delayed healing model.....	66
3.4.1 Combined application of DFO and MIF and single application of DFO furthered the callus mineralization	66
3.4.2 MIF and/or DFO enhanced mineralized tissue formation and ACS degradation.....	67

3.4.3 Comparable amounts of macrophages and osteoblasts while TRAP ⁺ cells were more prominent in treatment groups.....	71
3.4.4 Amount of CD31 ^{hi} Emcn ^{hi} vessels obviously did not depend on treatment but on mineralization status.....	73
3.4.5 Vessel formation was guided by tissue formation.....	78
3.4.6 Upregulation of immune response-related genes and downregulation of matrix-associated genes characterized gene profile at day 3 and 7.....	81
CHAPTER 4: DISCUSSION	90
4.1 Characterization of bone marrow derived hMSCs.....	91
4.2 The effect of hypoxia or HIF-stabilizers on the inhibition of osteogenic hMSC differentiation by GCs in an <i>in vitro</i> setting.....	91
4.3 Identification of a suitable scaffold for local delivery of MIF and DFO into the fracture gap.....	95
4.4 Investigation on the influence of MIF and/or DFO on the regeneration process in a delayed healing model.....	102
4.5 Limitations.....	108
CHAPTER 5: CONCLUSION AND FUTURE PERSPECTIVES	111
SUMMARY.....	112
ZUSAMMENFASSUNG.....	114
REFERENCES.....	116
PUBLICATIONS.....	144
DANKSAGUNG.....	147
ANTEILSERKLÄRUNG VON DR. MED. VET. ANNEMARIE LANG.....	149
FINANZIERUNGSQUELLEN.....	150
INTERESSENSKONFLIKTE.....	150
SELBSTSTÄNDIGKEITSERKLÄRUNG.....	150

List of Tables

<i>Table 1: List of preclinical studies applying DFO in a fracture healing context.....</i>	<i>15</i>
<i>Table 2: List of preclinical studies applying DFO in a bone-related context</i>	<i>15</i>
<i>Table 3: Primer sequences</i>	<i>31</i>
<i>Table 4: Primer sequences</i>	<i>42</i>
<i>Table 5: List of identified proteins from mass spectrometric measurements – Part 1 [174].</i>	<i>49</i>
<i>Table 6: List of identified proteins from mass spectrometric measurements – Part 2 [174].</i>	<i>50</i>
<i>Table 7: List of query cover of potential bone regeneration-linked proteins [174].</i>	<i>51</i>
<i>Table 8: RNA concentration and RIN values of the samples used for microarray analyses.</i>	<i>82</i>
<i>Table 9: Gene expression profiles discriminating the different treatment groups normalized to the ACS group at day 3.</i>	<i>83</i>
<i>Table 10: Gene expression profiles discriminating the different treatment groups normalized to the ACS group at day 7.</i>	<i>84</i>
<i>Table 11: Gene expression profiles discriminating the different treatment groups normalized to the ACS group at day 7 continued from Table 10.</i>	<i>85</i>
<i>Table 12: qRT-PCR results of selected inflammation-related genes compared to the corresponding microarray results.</i>	<i>87</i>
<i>Table 13: qRT-PCR results of selected metabolism-related genes compared to the corresponding microarray results.</i>	<i>88</i>
<i>Table 14: qRT-PCR results of selected matrix-related genes compared to the corresponding microarray results.</i>	<i>88</i>
<i>Table 15: Results of the literature search on biological functions of selected proteins potentially being involved in bone-regeneration. Reproduced from [174].</i>	<i>97</i>

List of Figures

<i>Figure 1: Overview on the consecutive phases of fracture healing.</i>	<i>3</i>
<i>Figure 2: Involvement of immune cells in the initial phase of fracture healing.</i>	<i>5</i>
<i>Figure 3: Schematic representation of the cellular and cytokine/chemokine pattern described in the fracture hematoma when compared to the surrounding bone marrow as control.</i>	<i>7</i>
<i>Figure 4: Detailed separation of the consecutive phases including the overlap of pro-inflammatory and anti-inflammatory signaling.</i>	<i>8</i>
<i>Figure 5: The HIF signaling pathway.</i>	<i>9</i>
<i>Figure 6: Overview on differences in the fracture hematoma of immunologically restricted patients when compared to control patients as described by Hoff et al.</i>	<i>12</i>
<i>Figure 7: Preparation area and surgical procedure.</i>	<i>35</i>
<i>Figure 8: Experimental timeline including the outcome measurements, experimental groups and animal numbers indicated within the symbols.</i>	<i>36</i>
<i>Figure 9: Overview on scanned and analyzed VOIs during ex vivo μCT measurements.</i>	<i>37</i>
<i>Figure 10: Staining controls without primary antibody.</i>	<i>39</i>
<i>Figure 11: Image analysis pipeline using an ImageJ macro.</i>	<i>40</i>
<i>Figure 12: Image analysis pipeline using ImageJ.</i>	<i>40</i>
<i>Figure 13: Characterization of hMSCs.</i>	<i>43</i>
<i>Figure 14: In vitro hMSC calcification - Titration of Dex concentrations revealed significant reduction for 10^{-3} M Dex which was further used for the titration studies with MIF and/or DFO.</i>	<i>44</i>
<i>Figure 15: In vitro model simulating the inhibition of hMSC calcification via high concentration GC treatment showing the potential of HIF-stabilizers to counteract.</i>	<i>46</i>
<i>Figure 16: Double normalization to display the changes as percentage towards the Dex 10^{-3} M and 10^{-8} M demonstrate the superiority to combine MIF and DFO.</i>	<i>46</i>
<i>Figure 17: LDH-release indicated impact of Dex 10^{-3} M on cell survival.</i>	<i>47</i>
<i>Figure 18: Macroscopic images of the ACS-H and ACS-L after applying medium revealing a form-instability of the ACS-L.</i>	<i>52</i>
<i>Figure 19: Structural evaluation of ACS-L using electron microscopy showing collagen fiber structures and cell matrix production.</i>	<i>52</i>

<i>Figure 20: Structural evaluation of ACS-H using electron microscopy revealing a layer-like structures and little differences by cell application.</i>	<i>53</i>
<i>Figure 21: In vitro studies on hMSC calcification indicating a strong inhibiting effect of ACS-H.</i>	<i>54</i>
<i>Figure 22: In vitro studies on hMSC osteogenesis revealed no effects of ACS-L or ACS-H.</i>	<i>54</i>
<i>Figure 23: Cell cytotoxicity and immunogenicity showed negative effects of ACS-H on cell survival and TNFα release – cell vitality was also affected.</i>	<i>56</i>
<i>Figure 24: Ex vivo μCT analysis 14 and 21 days after osteotomy revealed effect of ACS-L on callus mineralization.</i>	<i>57</i>
<i>Figure 25: ACS-L was partially degraded in the osteotomy gap within 21 days.</i>	<i>58</i>
<i>Figure 26: Inhibited transition from soft to hard callus phase by decreasing cartilage formation and mineralization.</i>	<i>60</i>
<i>Figure 27: Diminished cell invasion and mineralization in ACS-L groups.</i>	<i>62</i>
<i>Figure 28: Reduced amount and expression of CD31^{hi} and Emcn^{hi} cells indicating disturbed vessel formation in the ACS-L groups.</i>	<i>63</i>
<i>Figure 29: Comparable amount of F4/80⁺ and Osx⁺ cells between groups while TRAP⁺ cells were reduced.</i>	<i>64</i>
<i>Figure 30: Marginal presence of TRAP⁺ cells in the ACS-L group 21 days after osteotomy.</i>	<i>65</i>
<i>Figure 31: Increased bone volume fraction (BV/TV) after MIF/DFO or DFO treatment.</i>	<i>67</i>
<i>Figure 32: MIF/DFO and DFO further mineralized tissue formation and ACS degradation.</i>	<i>68</i>
<i>Figure 33: Treatment with MIF and/or DFO influenced mineralization.</i>	<i>69</i>
<i>Figure 34: Treatment with MIF and DFO or DFO alone furthered degradation of ACS.</i>	<i>70</i>
<i>Figure 35: Comparable amounts of macrophages (F4/80) and osteoblasts (Osx) between groups.</i>	<i>72</i>
<i>Figure 36: Higher amounts of TRAP⁺ cells were found in the treatment groups at 14 days.</i>	<i>72</i>
<i>Figure 37: Different appearance of vessel formation can be observed depending on mineralization status.</i>	<i>74</i>
<i>Figure 38: MIF and/or DFO treatment did not markedly influence cell invasion and amount of CD31^{hi} Emcn^{hi} cells, but high mineralized areas show lower amount of vessels.</i>	<i>75</i>
<i>Figure 39: The amount of CD31^{hi} Emcn^{hi} cells negatively correlates with relative endosteal scaffold area (day 21).</i>	<i>76</i>
<i>Figure 40: Mean intensity of Emcn and CD31 was enhanced by treatments.</i>	<i>77</i>

<i>Figure 41: Different states of regeneration were accompanied by tissue dependent vessel formation – Part I.</i>	79
<i>Figure 42: Different states of regeneration were accompanied by tissue dependent vessel formation – Part II.</i>	80
<i>Figure 43: Vessel formation in cartilaginous areas seemed to be driven by $Emcn^{hi}$ cells and arterioles could be found in the gap area.</i>	81
<i>Figure 44: Correlation of fold change data from microarray and qRT-PCR.</i>	87
<i>Figure 45: qRT-PCR results of further interesting genes.</i>	88

Abbreviations

ACS	Adsorbable collagen-I scaffold
ACTB	Actin beta
ALP	Alkaline phosphatase
ANOVA	Analysis of variance
BMP	Bone morphogenic protein
BSA	Bovine serum albumin
CD	Cluster of differentiation
cDNA	Complementary DNA
Col I/II	Collagen Type I/II
Ct	Cycle threshold
CT	Computed tomography
CXCL	Chemokine (C-X-C motif) ligand
CXCR	Chemokine (C-X-C motif) receptor
DAPI	4',6-diamidino-2-phenylindole
DFO	Deferoxamine
DM	Diabetes mellitus
DMEM	Dulbecco's modified Eagle medium
DMOG	Dimethyloxaloylglycine
DNA	Deoxyribonucleic acid
Dex	Dexamethasone
EC	Endothelial cell
ECM	Extracellular matrix
EDTA	Ethylenediaminetetraacetic acid
ELISA	Enzyme linked immunosorbent assay
EMA	European Medicines Agency
EthD1	Ethidium homodimer-1
FBGC	Foreign body giant cells
FCS	Fetal calf serum
FDA	Food and Drug Administration
Gc	Glucocorticoid
GCR	Glucocorticoid receptor
HA	Hydroxyapatite
HIF	Hypoxia-inducible factor
IBAQ	Intensity-based absolute quantification

IL	Interleukin
LDH	Lactate dehydrogenase
M-CSF	Macrophage colony-stimulating factor
MIF	Macrophage migration inhibitory factor
MMP	Matrix-metalloproteinase
mRNA	Messenger RNA
MSC	Mesenchymal stromal cell
NaCl	Sodium-chloride
NSAID	Non-steroidal antiinflammatory drugs
OC	Osteocalcin
OD	Optical density
OPN	Osteopontin
Osx	Osterix
PBS	Phosphate buffered saline
PFA	Paraformaldehyde
PGK-1	Phosphoglycerate kinase 1
PHD	Prolyl hydroxylase
PMN	Polymorphnuclear neutrophils
PTH	Parathyroid hormone
qRT-PCR	qualitative Real-Time PCR
RA	Rheumatoid arthritis
RNA	Ribonucleic acid
ROS	Reactive oxygen species
RT	Room temperature
RUNX2	Runt-related transcription factor 2
s.c.	subcutaneous
SLRP	Small leucine-rich proteoglycans
TGF	Tissue-growth factor
TIMP	Tissue inhibitor of metalloproteinase
TNF	Tumor necrosis factor
TRAP	TNF-related activation protein
VEGF	Vascular endothelial growth factor

Introduction

“The healing of the fracture is one of the most remarkable of all the repair processes in the body since it results, not in a scar, but in the actual reconstruction of the injured tissue in something very like its original form.” Reproduced from [1].

Fracture healing is a temporally and spatially tightly regulated regeneration process leading to a complete restoration of the broken bone without fibrous scar formation. Fracture healing disorders are an important clinical problem, since up to 10 % of patients with fractures require further revision surgery due to delayed healing or formation of non-unions [2, 3]. Besides the economic burden for the society due to increasing costs of the health care system and the absence from work, the patients experience immobility, pain and a loss in life quality [4]. Anti-inflammatory treatments with non-steroidal anti-inflammatory drugs (NSAIDs) or glucocorticoids (GCs) in patients suffering from chronic inflammatory or auto-immune diseases can enhance the risk of non-unions which is also described for comorbidities such as Rheumatoid Arthritis (RA) or Diabetes Mellitus (DM). Patients with fracture healing disorders normally undergo several further surgeries where the physicians try to rebuild the bony structure within and around the fracture gap. The fixation is normally done with sophisticated plate systems or external fixators. During recent years, modern treatment methods have achieved high technology standards - plates, implants and comparable fixation systems have been adapted to the patients' needs. The gold standard for treating non-unions is bone marrow grafting [5]. Bone marrow is collected from the iliac crest of the patient and transferred into the fracture gap. This method is especially suitable for young patients while the regenerative capacity of bone marrow-derived mesenchymal stromal cells (MSCs) is significantly reduced over age. In addition, for old patients the collection of bone marrow from the iliac crest could lead to additional fractures when bone mass is lost due to the high age. Hence, the clinical setting is still often challenging and new approaches are needed. Therefore, regenerative medicine is becoming more and more of interest – including the application of stem cells and/or growth factors [6].

The aim of this of thesis was to investigate and evaluate a new therapeutic and regenerative approach towards fracture healing disorders by supporting the cellular adaptation towards the hypoxic microenvironment during the initial phase of fracture healing. Thus, a combination of two promising chemical stabilizers of the Hypoxia-inducible factor (HIF) – Deferoxamine (DFO) and Macrophage migration inhibitory factor (MIF) were tested *in vitro* and *in vivo*.

CHAPTER 1: Literature Review

1.1 Fracture healing

1.1.1 Consecutive phases during bone regeneration

Known forms of fracture healing are the direct and indirect healing, also named primary and secondary bone healing [7]. The direct healing requires the correct anatomical reduction of the fracture end with no fracture gap and no possibility for motion between the bone ends [8]. This form of fracture healing is the common goal of surgical interventions and stable fixations allowing for a direct remodeling of lamellar bone. Nevertheless, direct healing is not naturally occurring [9]. The most common form is the indirect healing including the endochondral and/or intramembranous bone healing while the complete restoration until mineralization and mechanical strength is achieved within 6 weeks [10]. Typical for this form is the natural occurrence without surgical intervention and it is characterized by some motions at the fracture site which can be beneficial for the regeneration process while overloading facilitates the formation of non-unions. Under normal conditions, the fracture healing can be divided into four phases, namely i) initial inflammatory or fracture hematoma phase, ii) fibrocartilaginous or soft callus, iii) mineralized or hard callus and iv) the remodeling phase (Fig. 1).

A strong mechanical insult onto the bone result in fracture and trauma of the surrounding tissue. Vessels within the bone are ruptured, the bone marrow channel is opened, and a blood-bone marrow mix enters the fracture gap starting to coagulate and forming the initial fracture hematoma. Besides the provision of a loose fibrin scaffold and template for the subsequent callus formation, the fracture hematoma comprises an unique microenvironment and several complex immunological and inflammatory processes that are known to initiate the following healing cascade [10-13]. These processes are essential for i) the reconstruction by recruiting monocytes and macrophages as well as mesenchymal stromal cells (MSCs) and endothelial cells (ECs), ii) bone matrix formation and iii) neovascularization [9]. The consecutive process of endochondral ossification is characterized by proliferation and differentiation of MSCs towards the chondrogenic lineage producing collagen (Col) I and II. In a next step, the formed soft callus is resorbed and replaced by a mineralized hard callus. This step is also supposed to reflect key elements of the embryological bone development including cellular proliferation and increasing matrix production. At this time point extensive neovascularization occur while sprouting vessels invade and vascularize the callus. Chondrocyte start to hypertroph and get into apoptosis being replaced by bone forming cells. Cartilage mineralization normally starts in the peripheral vascularized callus towards the center to form a hard callus which consists of calcified structures. In parallel,

intramembranous ossification takes place subperiostally between the distal and proximal ends of the fracture, closing the hard callus and completely bridging the fracture gap providing a semi-rigid stability to the fracture and allowing for weight-bearing which is essential for the following remodeling phase. The remodeling phase comprises the resorption of the formed woven bone by osteoclasts and the formation of lamellar bone structures with a medullary cavity by osteoblasts leading to the complete restoration of the biomechanical properties of the bone. However, this last step can take up to months and years in order to restore the complete bone structure depending on e.g. the age [7].

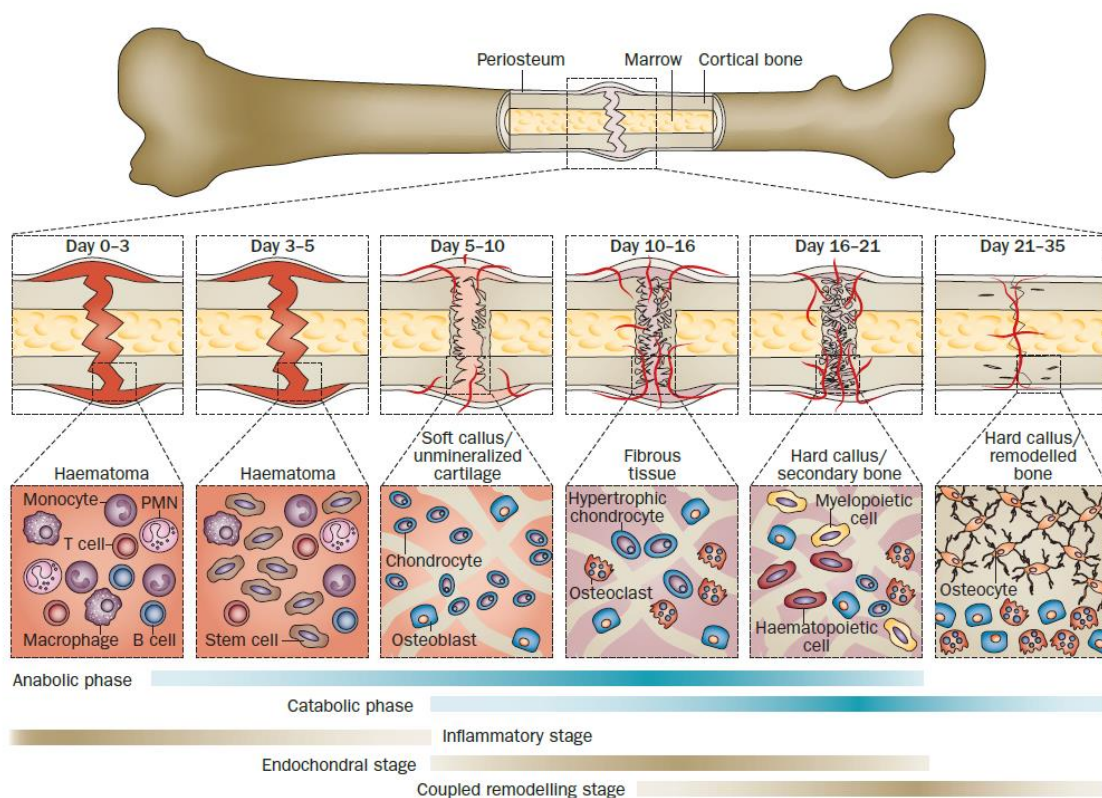


Figure 1: Overview on the consecutive phases of fracture healing.

The fracture hematoma phase, which is characterized by the complex interactions of immune cells and the recruitment of MSCs, is followed by the soft and hard callus phase where matrix formation, mineralization – in short, endochondral ossification is predominant. The remodeling phase finalizes the successful bone healing process without scar formation and with the re-establishment of the full function. Image reproduced and modified from [7].

1.1.2 The importance of the initial healing phase

Pro- and anti-inflammatory, pro-angiogenic and pro-osteogenic processes closely regulate the initial phase of fracture healing which is of great importance for the following regeneration cascade [10, 11]. The formation of the fracture hematoma is driven by the activation of the extrinsic coagulation pathway being initiated when tissue factors bind to plasma factor VII activating factor X and thrombin is provided [14]. Thrombin regulates the fibrin fiber formation by cleavage of fibrinogen. Additionally, leukocytes, fibroblasts and ECs can impact

the fibrin structure by secreting tissue factors that modulate thrombin production. The fibrin fiber organization determines the further function and progress since its structure supports cell infiltration, proliferation and differentiation and allows for binding of growth factors and the prevention of burst releases [13-15]. Moreover, thinner fibers can retain larger amounts of growth factors while thicker fibers allow for better fibrinolysis due to the higher porosity. Fibrinolysis is an important step in the initial healing phase facilitating the formation of granulation tissue [16, 17]. Plasminogen knockout mice exhibited disturbed bone formation which has been also shown in absence of fibrinolytic protease genes indicating the importance of degradation and resorption for the bone metabolism [18].

However, the surgical removal of a stable fracture hematoma within the first days after trauma have been proven to negatively affect the following healing outcome. Grundes and Reikeras showed in a rat femoral fracture model that the removal of the fracture hematoma two and 4 days after surgery leads to decreased mechanical properties after 4 weeks [19]. Similar observations were reported by Park *et al.* performing a repeated debridement and rinsing of the fracture gap in a middle tibia osteotomy in rabbits [20]. In a sheep tibial osteotomy model the removal of the fracture hematoma 4 and 7 days after surgery resulted in a delayed healing caused by an increased fraction of new hematoma tissue and a decreased woven bone formation [13]. Schell *et al.*, therefore, proposed that the secondary “naïve” hematoma, which was formed after the removal of the original one, is not able to provide the appropriate microenvironment resembling rather peripheral blood than a mature, fine adjusted and integrated hematoma [13]. The tight interplay and evolutionary balancing with the surrounding tissue is dramatically disturbed leading to delayed fracture healing. Transplanting the fracture hematoma in an ectopic location furthered bone formation which is also explained by the upregulation of osteogenic factors (runt-related transcription factor 2 - *RUNX2* and osteopontin - *SPP1*) within the first 72 h [12]. The fracture hematoma itself contains all important cells and factors to directly induce bone regeneration and is therefore of great importance for the physiology of fracture healing – like the engine of a car.

1.1.3 The immunology of the initial healing phase

During recent years, the importance of immune cells within the early phase of fracture healing has become clearer – although the precise underlying mechanism are still not fully characterized. The fracture hematoma contains e.g. several peripheral-blood-derived immune cells – as well as dead cells and debris attracting cells of the innate immune system such as neutrophils in the first hours after trauma [11, 21] (Fig. 2).

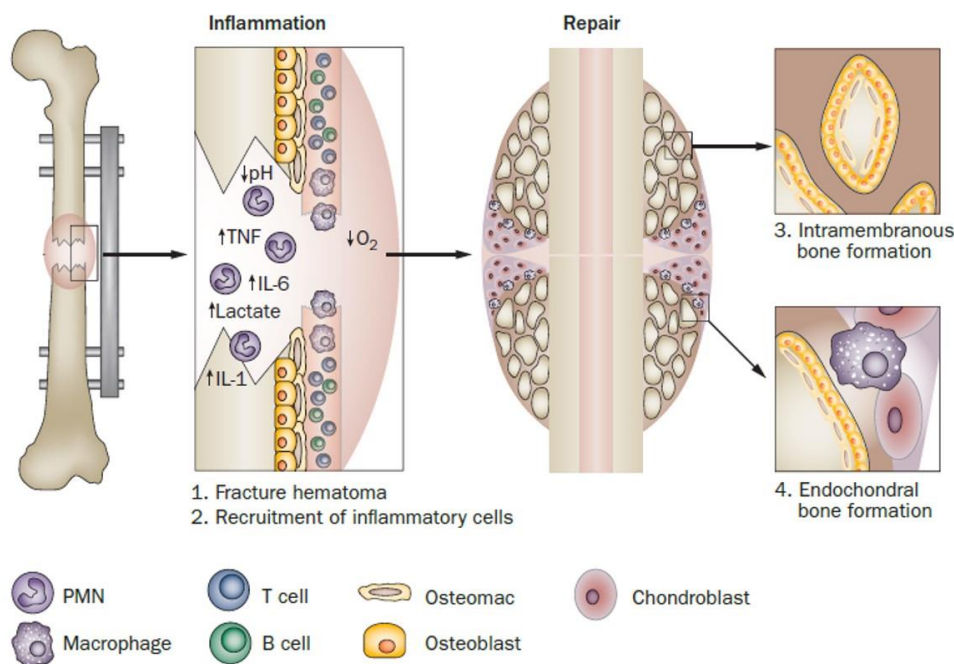


Figure 2: Involvement of immune cells in the initial phase of fracture healing.

Polymorphonuclear neutrophils (PMN) are the first cells invading the fracture site, followed by macrophages. The microenvironment is characterized by low pH and hypoxia. During intramembranous ossification only osteoblasts rebuild the tissue while endochondral ossification requires the complex interaction of different cell types such as osteoblast, macrophages and chondroblasts. Image reproduced and modified from [11].

Neutrophils phagocytize pathogens and cell debris and secrete reactive oxygen species (ROS), cytokines and chemokines such as interleukin (IL)-1 β , IL-6, IL-10, monocyte chemoattractant protein-1 (MCP-1), and chemokine (C-X-C motif) ligand (CXCL) 1 in order to recruit further immune cells especially monocytes and macrophages [12, 22-24]. While Chung *et al.* showed that the application of neutrophil-neutralising antiserum positively affect fracture healing, Bozlar *et al.* and Moukoko *et al.* demonstrated that the granulocyte-colony-stimulating (M-CSF) factor administered systemically, had a comparable effect [23, 25, 26]. A more precise method to study the importance of neutrophils was examined by Kovtun *et al.* applying an anti-Ly6G-antibody to reduce the number of neutrophils [24] (Ly6G - Lymphocyte antigen 6 complex locus G6D). Beside increased concentrations of cytokines and chemokines, higher numbers of monocytes and macrophages were found as well as an impaired bone healing after 21 days. This indicated the important role of the innate immune system within the regeneration process which is further supported when studying the relevance of macrophages – the key player to recover tissue integrity and function.

Therefore, two different types of macrophages can be distinguished. Tissue resident macrophages, which can be found closely to bone-lining cells, are named osteomacs and support intramembranous bone formation and endochondral ossification [27-29]. Recruited inflammatory macrophages are more pivotal in endochondral ossification which has been

shown by e.g. Schlundt *et al.* treating osteotomized mice with clodronate liposomes or Alexander *et al.* examining the macrophage subsets close to the periosteum during regeneration [28, 30]. Macrophages also modulate osteoblastic differentiation and therefore further mineralization of granulation tissue. Most recently, Vi *et al.* showed the ability of young macrophage cells to enhance osteogenesis of old precursor cells towards osteoblasts indicating that bone-marrow macrophages are affected by ageing leading to impaired bone regeneration [31].

In a next step, lymphocytes of the adaptive immune system are recruited to the fracture site consisting of T- and B-cells. Toben *et al.* reported that fracture healing was enhanced in RAG1(-/-) mice supposing a detrimental effect of adaptive immune cells [32]. Comparable inhibitory effects of γ/δ T-cells were described by Colburn *et al.* [33]. A negative impact was also demonstrated for CD8⁺ cytotoxic T-cells in human patients and a mouse-osteotomy-model [34]. In contrast, CD4⁺ cells have been shown to enhance osteogenic differentiation *in vitro* and upregulated osteogenic markers e.g. *RUNX2* or osteocalcin (*OC*) [35]. Nevertheless, the adaptive immune system was mainly assumed to have a regulatory function within the fracture healing process. Therefore, regulatory T cells (T_{Reg}), a subpopulation of CD4⁺ cells have been studied and described as positive modulating cell population – supported by several studies verifying the acceleration of bone formation by activating or additionally applying T_{Reg} [36-38]. Beside all the immune- and inflammation-related cells, several cytokines, chemokines, growth factors and enzymes characterize the microenvironment of the fracture hematoma as it has been shown in various studies using fracture patient's materials [12, 21, 39].

The pro-inflammatory phase is essential as it also initiates the attraction and promotion of MSCs – triggering a more anti-inflammatory phase during the subsequent regeneration process (Fig. 3). Different sources of those MSCs are discussed – surrounding soft tissue, bone marrow and systemic recruitment [7]. As attractants of MSCs, bone morphogenetic proteins (BMP), stromal cell-derived factor-1 (SDF-1) and the chemokine (C-X-C motif) ligand receptor (CXCR) 4 are described. The underlying mechanisms for the anti-inflammatory effect of MSCs has not been fully understood, but different factors such as transforming growth factor- β 1 (TGF- β 1), prostaglandin E2 (PGE2), hepatocyte growth factor (HGF), indoleamine-pyrrole 2,3-dioxygenase (IDO), nitric oxide (NO) and IL-10 [40] or soluble receptors such as soluble CTLA-4 have been described to be involved [41]. Besides controlling the inflammation, MSCs also differentiate into the osteoblastic lineage and therefore rebuild the bone matrix [42-44]. The differentiation is induced and influenced by several local conditions such as biomechanical properties of surrounding tissue, oxygen tension (stabilization of hypoxia-inducible factor 1 – HIF-1) and concentration of growth factors and cytokines

such as tumor necrosis factor α (TNF α) which has been shown to enhance osteogenesis *in vitro* [45-47]. Col I and II matrix production enables the soft callus formation which is additionally supported by migrating fibroblasts and regulated by members of the TGF- β family such as TGF- β 2, - β 2, GDF-5, BMP-5, and -6 [48].

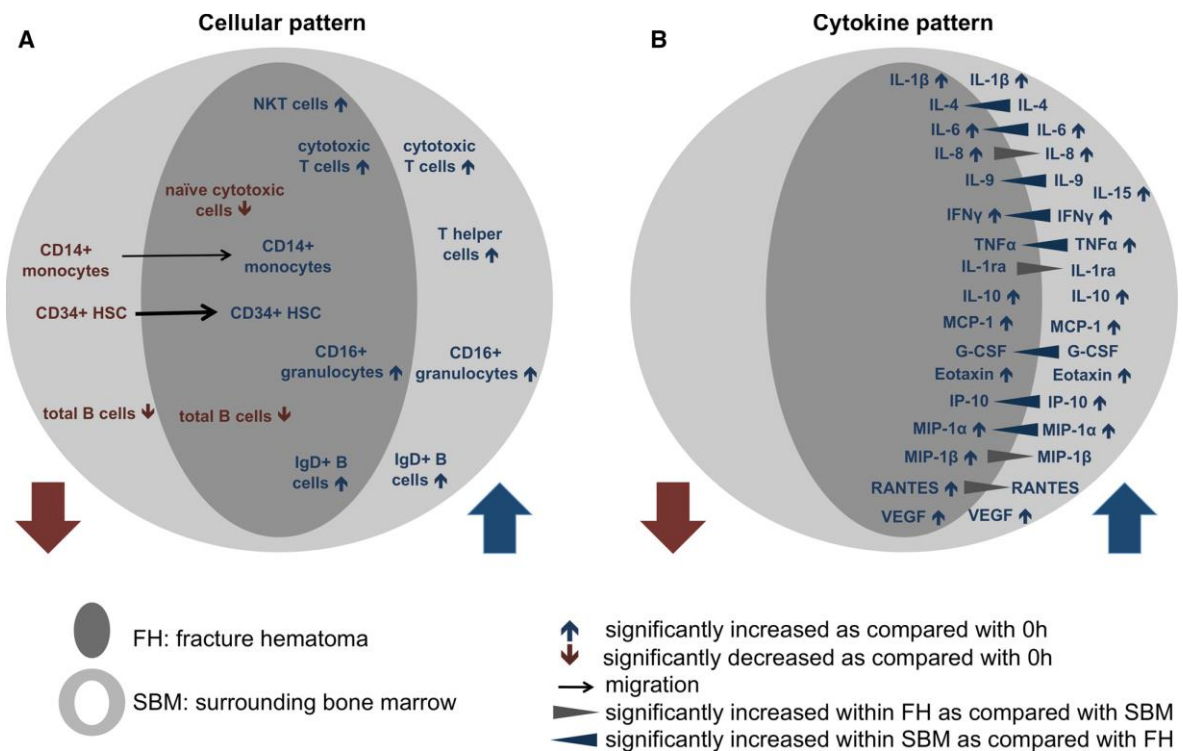


Figure 3: Schematic representation of the cellular and cytokine/chemokine pattern described in the fracture hematoma when compared to the surrounding bone marrow as control.

Migration of monocytes/macrophages and hematopoietic stem cells was enhanced as well as the proliferation of T helper and cytotoxic T cells. Additionally, high concentration pro-inflammatory, but also anti-inflammatory cytokines (IL-1Ra and IL-10) can be identified. Image reproduced and modified from [21]. Abbreviations: NKT – natural killer T cells; IFN γ – interferon γ ; IP-10 – interferon gamma-induced protein 10; MIP-1 – Macrophage inflammatory protein-1; RANTES – regulated on activation, normal T cell expressed and secreted; FH – fracture hematoma; SBM – surrounding bone marrow.

In addition, angiogenic factors e.g. vascular endothelial growth factor (VEGF) are produced as consequence of the hypoxic environment leading to the enhanced transcriptional activity of HIF-1 [49, 50] (Fig. 4). Vascularization is essential for fracture healing in order to supply cells with oxygen, remove debris and allow for recruitment circulating cells. Endothelial progenitors (CD31⁺ cells) migrate to the fracture site from the bone-marrow or pre-existing vessels of the periosteum [51, 52]. Interestingly, it has been proposed that the revascularization occurs at two time points during fracture healing: around day 7 (end of the inflammatory phase) and around day 21 (the woven bone formation) [53]. The drastic vascular plasticity between 7 and 21 days has been shown by Reisman *et al.* using a microendoscopic method

[54]. In addition, they described the same dynamic during steady-state which seems to be the result of a passive displacement caused by processes in the surrounding tissue [54].

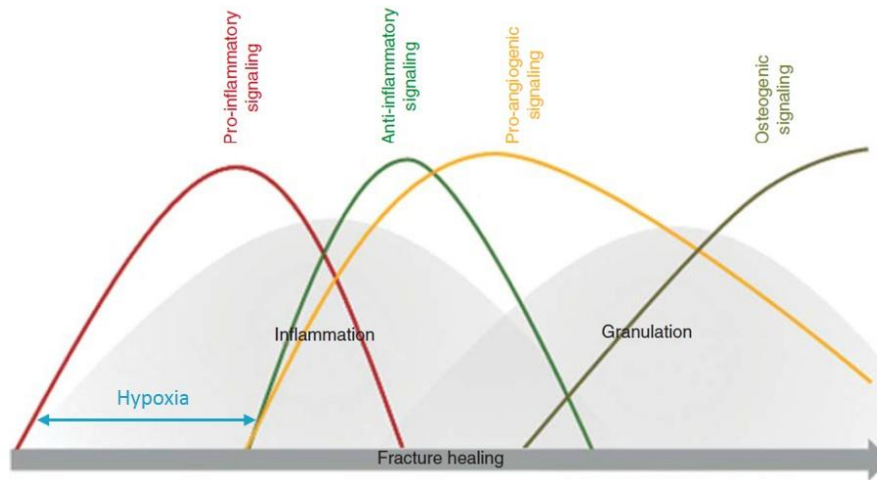


Figure 4: Detailed separation of the consecutive phases including the overlap of pro-inflammatory and anti-inflammatory signaling.

Hypoxic environment is prominent in the initial phase until new vessels have been formed. Anti-inflammatory signaling is redeemed by the osteogenic signaling driven by MSC. Image reproduced and modified from [9].

1.1.4 The microenvironment during the initial healing phase

Due to the disruption of vessels, cell death of e.g. erythrocytes and the lack of nutrients, the microenvironment of the fracture hematoma is described by hypoxia, high lactate and low pH – a cytotoxic environment whose downregulation is needed to attract regenerative cells. The oxygen tension within the fracture site is reduced over the first week after trauma being accompanied by the reduction (50 %) of blood flow [55-57]. Therefore, cellular adaptations mechanism are strongly activated – such as the HIF signaling pathway. HIF-1 and HIF-2 are essential for cells to survive hypoxic conditions and aim at increasing oxygen supply as well as reduction of oxygen consumption [58]. While HIF-1 β is constitutively expressed, HIF-1 α is oxygen-dependent activated and stabilized at < 5 % oxygen which is followed by the translocation to the nucleus, the dimerization with HIF-1 β and the activation of hypoxia-responsive genes [59] (Fig. 5). Under normoxic conditions, HIF-1 α is hydroxylated by the prolyl-hydroxylase domain enzyme/protein (PHD), ubiquitinated by phosphorylated von Hippel-Lindau tumor suppressor (pVHL) and degraded by cellular proteasomes. Under hypoxic conditions, the PHD, which is oxygen- and iron-dependent, is inhibited and HIF-1 α accumulates and is translocated to the nucleus leading to the upregulated expression of pro-angiogenic genes (*VEGF*, *IL-8*) or glycolytic enzymes (*LDHA* – *Lactate dehydrogenase A*, *PGK1* - *Phosphoglycerate Kinase 1*) [60].

The effect of HIF-1 α stabilization is different between cell types. It has been shown, that HIF-1 α in neutrophils and macrophages reduces cell aggregation, motility and invasiveness

while constitutive expression increases cell activation and function of stimulated immune cells [61]. In addition, immune cells are supposed to be highly dependent on glycolysis for mitochondrial adenosine triphosphate (ATP) synthesis [58]. In contrast, MSC differentiation is strongly influenced by oxygen tension, as the MSC niche normally has an oxygen tension of 2-8 % [47]. Hypoxia has been shown to enhance osteogenic and chondrogenic differentiation *in vitro* and *in vivo* - two key aspects of endochondral ossification [62-64]. However, hypoxia also affects osteoblasts e.g. inhibiting the matrix metalloproteinase (MMP)-13 and tissue inhibitor of metalloproteinase (TIMP)-1 expression or enhancing the expression of other matrix-related molecules (Col I and III) [65]. Moreover, beside regulation of VEGF, Wnt (wingless-related integration site) signaling, BMP-2 and insulin growth factor (IGF) expression in osteoblasts are additionally controlled by oxygen tension [66, 67].

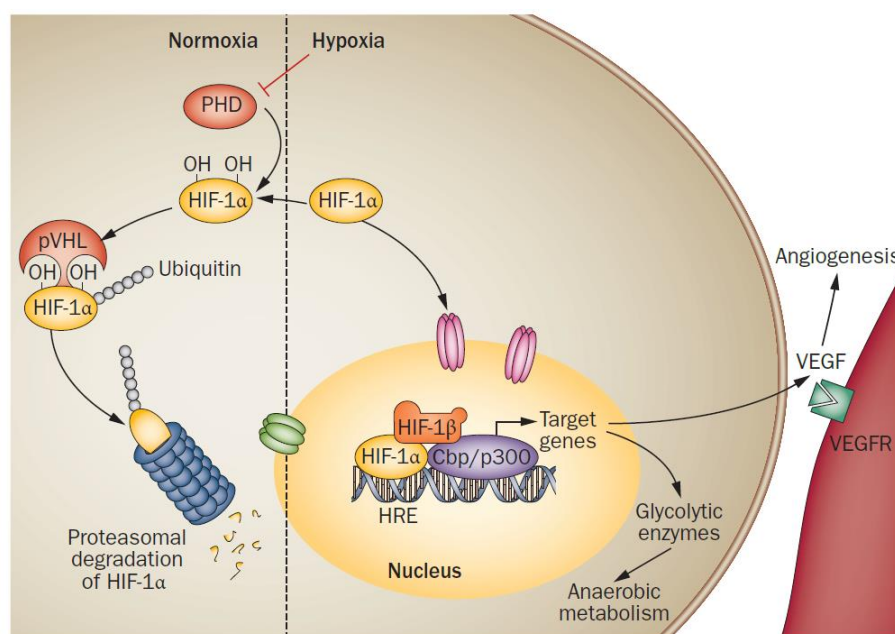


Figure 5: The HIF signaling pathway.

While HIF-1 α is degraded under normoxic conditions, it is translocated to the nucleus, dimerizes with HIF-1 β and activates target genes needed for cellular adaptation to hypoxia. Image reproduced and modified from [59]. Abbreviations: OH – hydroxy group; Cbp – CREB-binding protein; HRE – hypoxia-response element.

At the initial stage, the microenvironment in the fracture hematoma is acidotic and switched to neutral and slightly alkaline during the regeneration process [13]. The low pH at the beginning can be explained by accumulation of lactate as a result from the anaerobic energy supply [10, 56, 68]. Overall the effect of low pH on the cells has not yet been fully studied. Zhang *et al.* recently published a study providing evidence, that acidic pH induces autophagy in osteoblasts preventing cells from apoptosis [69]. The change towards a neutral and alkaline pH is explained by increasing concentrations of calcium resolved from the bone by the low pH and is also required during callus mineralization [70].

1.2 The pathophysiology of fracture healing

1.2.1 Classification and risk factors of fracture healing disorders

Although the healing time varies and depends on the fracture location – normal fracture healing processes are completed within the timeframe of 3 – 4 months. Healing processes that extend this timeframe are termed delayed union and when no bony regeneration has occurred after 6 - 9 months, it is termed non-union [71, 72]. There are several forms of non-unions. Hypertrophic non-unions are mainly caused by an inappropriate fixation or premature weight bearing that impedes an appropriate bridging of the fracture gap. A pseudarthrosis is characterized by a continuous soft callus formation building an artificial fibrous “joint-like” structure. Atrophic non-unions show reduced callus formation. While the therapeutic solution for hypertrophic non-unions is an improved fixation, atrophic non-unions and pseudarthrosis require a more advanced and individualized approaches using biomaterials and growth factors [6, 73].

Several risk factors have been described to potentially impair the fracture healing process [74]. At first, the trauma severity and location can determine the outcome [75]. Therefore, polytrauma – several fractures at different locations, segmental defects or tissue laceration can increase the risk for fracture healing disorders [2, 74, 76]. In contrast, Tsitsilonis *et al.* described the positive effect of traumatic brain injury on fracture healing [77]. However, it is known that the regeneration capacity of bone and other tissues is decreasing during aging, which is based on a general natural bone loss or pathological bone loss (post-menopausal osteoporosis) – osteoblast activity is decreased, osteoclast activity is enhanced and the multipotency of MSCs is diminished [78, 79]. Therefore, age can be a risk factor as well as lifestyle including obesity, smoking, alcohol abuse and physical inactivity. Smoking is supposed to reduce vessel formation and stimulate adverse reactions of the immune system [80-82]. Alcohol abuse and physical inactivity are related to a decreased bone formation rate and thus, an osteopenic effect on the skeleton [83].

However, comorbidities and medication use are mostly discussed as main risk factors. With regard to osteoporosis, studies during the last years mainly focused on the prevention of fractures in osteoporotic patients as it is still under debate whether osteoporosis really impairs fracture healing [84, 85]. Controversy results from animal models can be found in the literature and further studies are needed to show epidemiological correlations more clearly [86-88]. Moreover, osteoporotic fractures are a challenge to surgeons with regard to the appropriate fixation as the deterioration of the bone may lead to implant loosening and corresponding consequences [89]. Diabetes mellitus (DM) comprises several pathological alterations including a decline in bone biomechanical properties and an impaired fracture

healing. Beside the impaired vessel formation, which also strongly influences wound healing, osteopenia caused by reduced osteoblast activity can be observed especially in DM type I patients [90, 91]. Other chronic inflammatory diseases have been related to fracture healing disorders, such as Rheumatoid Arthritis (RA) or Systemic Lupus Erythematosus (SLE) [11, 92, 93]. Non-steroidal anti-inflammatory drugs (NSAIDs), commonly administered in orthopedic and post-traumatic settings for pain management, are controversially discussed to interfere with bone healing especially during the initial phase [94-96]. The same is described for long-term administration of glucocorticoids (GC) [97-99]. The overall hypothesis for both medication classes is the inhibition of the inflammation during the initial phase of the fracture healing which potentially may impair the whole process.

1.2.2 Underlying mechanism – Immunological dysregulation and inhibited adaptation to hypoxia

As explained above the fracture healing is a well-orchestrated process and inflammation is an important factor. The control of the pro-inflammatory cascade, the cartilage formation coupled with the invasion of vessels and cells and a sufficient mechanical stabilization are crucial elements for successful bone healing. Biomechanical conditions have shown to influence the inflammatory phase. Flexible fixation can lead to pronounced inflammation, based on high numbers of cytotoxic T-cells and other leukocytes [100]. Therefore, the pro-inflammatory M1 macrophage phenotype is predominantly activated and the anti-inflammatory M2 macrophage is inhibited explaining the prolongation of the inflammatory phase [30, 101]. In systemic chronic inflammatory processes such as DM, high concentrations of TNF α have been related to increased chondrocyte apoptosis, premature cartilage loss and increased osteoclast activity during diabetic fracture healing [90]. Hoff *et al.* examined fracture hematomas of immunologically restricted patients and described a reduced osteogenic differentiation due to reduced *RUNX2* expression, exaggerated immune reactions (*IL-8*, *CXCR4*) and high expression of *HIF1A* with inadequate expression of target genes while *VEGF* was normally expressed [102]. In another study, higher numbers of monocytes/macrophages, natural killer (NKT) cells and activated T cells were found in fracture hematomas of immunologically restricted patients accompanied by higher levels of IL-6, IL-8, TNF α , macrophage-migration inhibitory factor (MIF) and chemokines (e.g. Eotaxin) (Fig. 6) [39]. However, there is evidence that a local inflammatory milieu does not always impair fracture healing. Bogoch *et al.* examined the fracture healing in a lapin inflammatory arthritis model with the result that fracture healing was not impaired and bone loss was balanced in an intact bone [103]. Muinos-Lopez *et al.* supposed that a fracture non-union results from changes in the hematoma and the hypoxic microenvironment which therefore fail to activate BMP2 expression by MSCs [104].

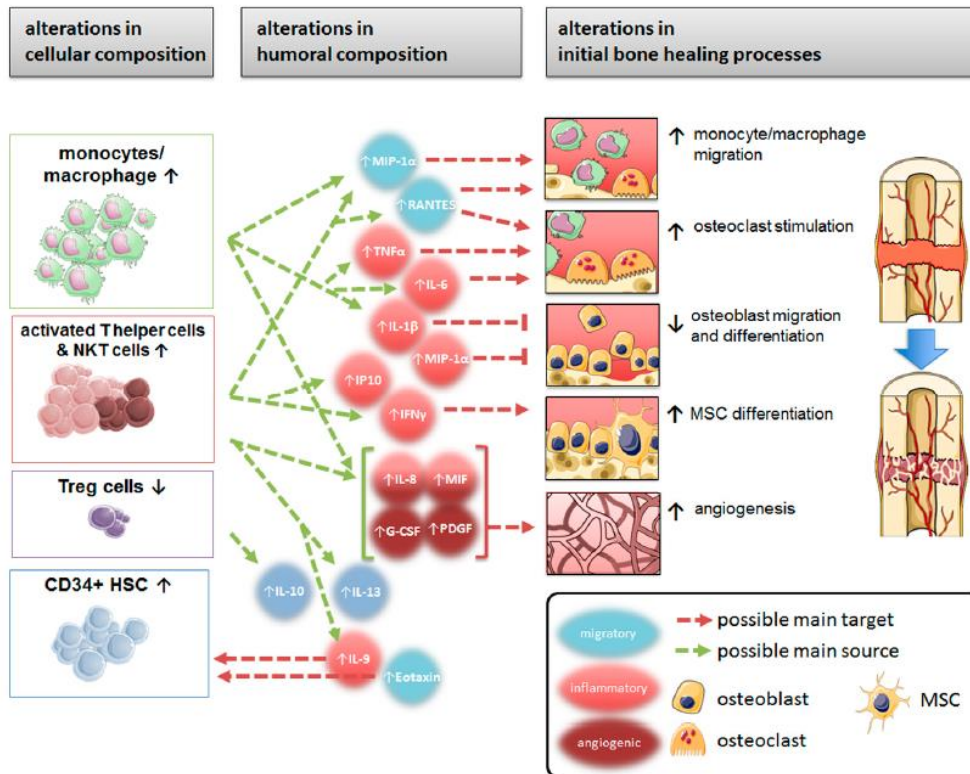


Figure 6: Overview on differences in the fracture hematoma of immunologically restricted patients when compared to control patients as described by Hoff *et al.*

Image reproduced and modified from [39]. Abbreviations: PDGF – platelet-derived growth factor

1.3 Current therapeutic interventions

1.3.1 Conservative therapies, growth factors and biomaterials

During recent years, modern treatment methods have achieved high technology standards – plates, implants and comparable fixation systems have been adapted to the patients' needs as well as the use of more sustainable materials and the combination with high-resolution imaging allowing for a detailed planning prior to surgery [6]. The gold standard for treating non-unions is bone marrow grafting [5]. Bone marrow is collected from the iliac crest of the patient and transferred into the fracture gap. This method is especially suitable for young patients while the regenerative capacity of MSCs is significantly reduced over age. In addition, for old patients the collection of bone marrow from the iliac crest could lead to additional fractures when bone mass is lost due to the high age. Hence, the clinical setting is still often challenging and new approaches are needed. Therefore, regenerative medicine is becoming more and more of interest – including the application of stem cells and/or growth factors [6]. Thus, new promising treatment strategies have been translated to the

clinic using potent growth factors such as recombinant human (rh) BMP-2 and rhBMP-7 for local delivery into the fracture gap [105, 106]. Controversially results on their effectiveness

and the observation of several adverse effects such as hematoma formation in the surrounding tissue, higher incidence of infection and heterotopic bone formation have been completely published. Thus, the use of rhBMP-2 is restricted and the FDA recommend no off-label use, while rhBMP-7 has been withdrawn from the market [107]. Nevertheless, it was shown that the use of rhBMP-2 treatment as prevention of non-unions after acute fracture could save costs about 9.000 € in Germany and France per affected patient [108]. The use of rhBMP-2 is solely permitted when applied on a bovine absorbable Col I scaffold (mainly used: ACS, Helistat; Integra LifeScience, Plainsboro, New Jersey) and marked under the commercial name INFUSE® (FDA approved), InductOs® (suspended by EMA) both from Medtronic and OP-1® (FDA approved) and Osigraft® (withdrawn from EMA) from Stryker Biotech. In addition, fibroblast growth factor 2 (FGF-2) and homodimeric platelet-derived growth factor subunit B (PDGF-BB) are promising candidates that have already been tested in clinical studies [109, 110].

Various biomaterials for bone regeneration are currently under investigation [6]. In general, those biomaterials can be divided into degradable materials such as collagen, chitosan, hydroxyapatite (HA), tricalcium phosphate (TCP) and non-degradable materials such as titanium alloy, bioglass [111]. Non-degradable materials are mainly used for implants. Degradable materials are commonly combined in order to bundle the advantageous properties. There are some scaffolds which have been approved by the FDA e.g. bovine Col I, Collagraft™ (HA + TCP + bovine collagen), OssiMend™ (porous bone mineral combined with collagen). In research bovine Col I scaffolds or sponges are most often used as delivery systems in explorative *in vivo* studies [30, 112-116]. However, the primary use of those sponges is to arrest bleeding by promoting platelet aggregation during invasive surgeries. Since Col I is the main extracellular component of bone, there are several *in vitro* and *in vivo* studies indicating its valuable contribution as provider of an infrastructure for the cell invasion and enhancer of chondrogenesis and osteogenesis [117-119].

1.3.2 Promising compounds – HIF-stabilizers

During the last decades many diseases have been identified in which pharmacological HIF stabilization can be seen as a promising therapeutic option for e.g. anemia associated with chronic kidney disease, limb ischemia, ischemic stroke, myocardial infarction or inflammatory bowel disease (IBD) [120, 121]. In general, these agents can be divided into those acting via PHD inhibition and those acting without PHD inhibition. PHD inhibitors can be classified into iron chelators, iron competitors, and 2-oxoglutarate (2OG) analogs, also called non-selective inhibitors while novel PHD inhibitors are more specific for e.g. either PHD2 or PHD3 [122]. Non-PHD inhibitors rely on other mechanism and include e.g. N-

acetylcysteine, miR-335, MG-132, a proteasome inhibitor or MIF. The iron chelator deferoxamine (DFO) and the iron competitor cobalt chloride (CoCl_2) are commonly used *in vitro* and *in vivo* inhibiting the PHD by binding or competing for endogenous iron (II).

➤ **Deferoxamine (DFO)**

Deferoxamine (DFO) is a siderophore, which binds Fe^{2+} , and is known as strong iron chelator produced by *Streptomyces pilosis* as growth factor. Since the late 1970s, DFO was used as infusion for treatment of iron poisoning (mesylate salt) and later on also for aluminum intoxication. In 2007, Wan *et al.* described the role of the HIF-1 α pathway during fracture healing in a genetic mouse model by knocking-out VHL and a pharmacological model by applying DFO [123]. They showed for the first time, the beneficial effect of DFO on fracture healing including enhanced vessel and bone formation within the fracture gap. Several studies followed over the last years indicating the broad range of applications. Therefore, DFO was applied in different calvarial defect or critical size defect models exhibiting a delayed healing or non-union [124-136]. An overview on the published studies can be found in Table 1. The application route was mainly done by local injection or loading onto a scaffold. The concentration was mainly 200 μM and the duration of local injection application lasted about several weeks. The general outcome was a strong enhancement of angiogenesis/vessel formation and bone regeneration independent of the species, model and evaluation methods. Several studies also tested the potential of DFO in other bone-related disorders such as postmenopausal osteoporosis, osteolysis or osteonecrosis with the same positive effect (Table 2) [137-141]. In contrast, Kuchler *et al.* combined a calvarial fracture model with a general induction of diabetes in rats comparing the effect of DFO and Dimethyloxalyglycine (DMOG) a 2OG analog. In this study, DFO treatment showed no significant enhancement of bone regeneration while DMOG induced vessel formation [142].

Table 1: List of preclinical studies applying DFO in a fracture healing context

Species	Bone	Model	Application Route & Concentration	Refs.		
Sprague-Dawley rats	<i>Ossa irregularia</i>	Mandibular distraction osteogenesis	Local injection every other day (5 doses); DFO = 200 µM	[127, 143, 144]		
		Mandibular osteotomy or distraction + Radiation	Local injection every other day (5 doses); DFO = 200 µM	[124-126, 130, 145-147]		
		Zygomatic arch critical-size bone defect	Local injection every other day (> 20 doses); DFO = 200 µM	[131]		
	Long bones		Stabilized midshaft femur defects	Application onto scaffold; DFO = 400 µM	[134]	
			Tibial non-union model	Application onto scaffold; DFO = 1 mg/kg	[148]	
			Femoral non-union model	Application onto scaffold; DFO = 1 mg/ml	[149]	
			Tibia cortical drilling + Hindlimb unloading	Local injection every other day (2-5 doses); DFO = 200 µmol/l	[132]	
Femoral drilling hole + Ovariectomy			Application onto scaffold; DFO = 2 µg	[150]		
C57BL/6 mice				Stabilized femur fracture model with intramedullary pin	Local injection every other day (6 doses); DFO = 200 µM	[123]
				Stabilized femur fracture model with intramedullary pin	Local injection every other day (5 doses); DFO = 200 mM	[135]
NZW rabbits		Segmental bone defects	Application onto scaffold DFO = 2 mM	[136]		
		Mid-shaft ulnar defect	Application onto scaffold DFO = 200 µM	[128]		

Table 2: List of preclinical studies applying DFO in a bone-related context

Model & Species	Application Route & Concentration	Ref.
Osteoporosis model induced by ovariectomy Rats	<i>i.p.</i> injection 5 days/weeks for 12 weeks DFO = 200 µM	[140]
Steroid-induced osteonecrosis femoral heads – core compression treatment New Zealand white rabbits	Application onto gelatin sponge DFO = 500 µM	[139]
Calvaria osteolysis model induced by ultra-high-molecular-weight polyethylene particles C57BL/6J mice	Application onto particles DFO = 10 mg/kg (low) and 30 mg/kg (high)	[137]
Bone loss during ageing 64 – 70 old C57BL/6J mice	Local injection on alternate days 4 – 5 weeks DFO = 15 mg/ml	[138]
Osteoporosis model induced by ovariectomy C57BL/6 mice	Local injection on alternate days 4 – 5 weeks DFO = 15 mg/ml	[141]
Osteoporosis model induced by ovariectomy C57BL/6 mice	Conjugated to a bone-seeking agent (SF) <i>i.p.</i> injection daily 4 weeks DFO = 40 mg/kg SF-DFO = 55.44 mg/kg	[151]

➤ **Macrophage Migration Inhibitory Factor (MIF)**

MIF was first recognized in 1932 by Rich and Lewis and described as a T-cell derived factor which inhibits the migration of macrophages in 1966 [152, 153]. MIF has multiple functions within and beyond the immune system playing a role in septic shock, chronic inflammation, tissue damage and autoimmune disease [154-156]. It is produced by a variety of cells: lymphocytes, monocytes, macrophages, ECs, fibroblasts or glia cells [157-160]. MIF mainly acts via binding to the CD74 receptor in the cell membrane which is expressed in several immune and cancer cells. The interaction with the receptor activates underlying signaling pathways such as the mTOR (mechanistic target of rapamycin) or MAPK (mitogen-activated protein kinase) pathway [12, 155]. CD44 activating non-receptor tyrosine kinases was identified as signaling component [161]. Nevertheless, Kleemann *et al.* described an intracellular activity in the cytoplasm after non-receptor mediated endocytosis which is accompanied by the binding and interaction with JAB-1 protein and inhibition of activator protein (AP)-1 activity and MAPK phosphorylation [162, 163]. From a functional point of view, MIF affects cell proliferation and differentiation of immune cells during inflammatory processes. In addition, MIF is described to balance GC effects on cells as an opponent. Therefore, two GC-dependent proteins are inhibited by MIF leading to the regulated activity of nuclear factor kappa B (NFκB) [164]. The investigation of all MIF-related pathways is quite complex as the effect seems to be mainly concentration- and environment- dependent regarding e.g. the oxygen availability [12]. Oda *et al.* described an increased HIF-expression via p53 after treating/overexpression with/of MIF in MCF-7 cells [165]. MIF is described a target gene of HIF-1α, but also regulates and enhances the HIF stabilization itself as it has been described in CD4⁺ T-cells [166]. With regard to bone metabolism and fracture healing, MIF has been identified in osteoblasts and is proposed to play an important role during fracture healing. Ondara *et al.* described higher mRNA expression levels of *MIF* during the fracture healing process which has been also described in other regenerative processes such as wound healing [167, 168]. MIF is able to increase MMP-9 and MMP-13 expression in osteoblasts also indirectly influencing the hypertrophic chondrocytes during endochondral ossification [169, 170]. MIF deficient mice showed impaired fracture healing caused by a reduced number of osteoclasts and increased osteoid production [171]. In accordance, Gu *et al.* showed the importance of MIF for the differentiation of osteoclasts via interacting with the receptor activator of nuclear factor kappa-B ligand (RANKL) pathway [172]. In contrast, Jaquin *et al.* reported an inhibitory effect of MIF on osteoclasts [173].

1.4 Aims and Objectives of the Thesis

Several factors and conditions are known to negatively influence the complex and fine orchestrated initial phase of fracture healing leading to an impaired regeneration process in the subsequent phases. There is definitively a clinical need to develop and test new therapeutic approaches, since sophisticated surgical techniques and prevention cannot treat or avoid all fracture healing disorders. As described in the literature e.g. anti-inflammatory treatments with NSAIDs or GCs in patients suffering from chronic inflammatory or autoimmune diseases can enhance the risk of non-unions which is also described for comorbidities such as RA or DM. It was previously confirmed that immunologically restricted patients lack an adequate adaptation to hypoxia which may result in impaired fracture healing [102]. However, during the initial fracture healing phase the hypoxic microenvironment is essential for activating the subsequent immune cell-driven healing cascade finally leading to regeneration. HIF-1 α is the key regulator of cellular adaptation under hypoxic conditions regulated by the activity of O₂ sensitive PHDs. Stabilization of HIF leads to activation of angiogenic, proliferative or osteogenic target genes which can be also achieved by factors such as DFO and/or MIF.

Given this background, the aim of this PhD thesis was to test a new approach to promote the cellular adaptation towards hypoxia to accelerate bone healing specifically under compromised conditions. Therefore, three main hypotheses were formulated:

Hypothesis I: Glucocorticoids (GC) inhibit the human MSC (hMSC) differentiation to the osteogenic lineage especially the calcification process which can be counteracted by targeting the HIF pathway.

Hypothesis II: Absorbable bovine Col I scaffolds (ACS) which are approved by the FDA and used routinely in research and clinic, are a suitable delivery system for new therapeutics to be tested in the fracture healing process.

Hypothesis III: The combination of two HIF-stabilizers especially DFO and MIF (synergy) addressing different mechanism is a promising approach to overcome compromised conditions leading to fracture healing disorders (delayed vs. non-union).

The first part of this work describes the *in vitro* testing of hypoxia and HIF-stabilizers (DFO + MIF) to counteract a delayed calcification approach induced by high concentrations of Dexamethasone (Dex) and to define an effective concentration for further *in vivo* testing. The second part focuses on the examination of two absorbable bovine Col I scaffolds (ACSs; Lyostypt[®], ACS-L; Helistat[®], ACS-H) that were tested for their suitability. In the last part, the combination of DFO and MIF was evaluated *in vivo* using a clinically relevant mouse-osteotomy-model.

CHAPTER 2: Materials and Methods

2.1 Materials

2.1.1 Bone marrow donors – Cell source

Bone marrow was provided by the Center for Musculoskeletal Surgery, Charité-Universitätsmedizin Berlin and distributed by the “Tissue Harvesting” Core Facility of the Berlin-Brandenburg Center for Regenerative Therapies (BCRT) from patients undergoing total hip replacement (ethical approval EA1/012/13).

Donor	Age	Gender	Cultivation condition	Charac-terization	Type of experiment
1	52	female	NM 1, OM 1	+	Dex Titration (2, 3, 4 weeks), MIF/DFO Titration (3, 4 weeks)
2	77	female	NM 1, OM 1	+	Dex Titration (2, 3, 4 weeks), MIF/DFO Titration (3, 4 weeks)
3	70	female	NM 1, OM 1	+	Dex Titration (2, 3, 4 weeks), MIF/DFO Titration (3, 4 weeks)
4	76	male	NM 1, OM 1	+	Dex Titration (2, 3, 4 weeks), MIF/DFO Titration (3, 4 weeks)
5	73	female	NM 1, OM 1	+	Dex Titration (2, 3, 4 weeks), MIF/DFO Titration (3, 4 weeks)
6	69	female	NM 1, OM 1	+	Dex Titration (3, 4 Weeks)
7	48	male	NM 1, OM 1	+	Dex Titration (3, 4 Weeks)
8	75	female	NM 1, OM 1	+	MIF/DFO Titration (3 weeks)
9	82	male	NM 1, OM 1	+	Dex, MIF/DFO LDH assay
10	56	female	NM 1, OM 1	+	Dex, MIF/DFO LDH assay
11	66	male	NM 1, OM 1	+	Dex, MIF/DFO LDH assay LDH
12	69	female	NM 2, OM 2	+	ACS-L osteogenic differentiation, LDH assay
13	57	male	NM 2, OM 2	+	ACS-L osteogenic differentiation, LDH assay
14	84	female	NM 2, OM 2	+	ACS-L osteogenic differentiation, LDH assay
15	65	male	NM 2, OM 2	+	ACS-H osteogenic differentiation, LDH assay
16	71	female	NM 2, OM 2	+	ACS-H osteogenic differentiation, LDH assay both ACS LIVE/DEAD staining, SEM
17	75	female	NM 2, OM 2	+	ACS-H osteogenic differentiation, LDH assay
18	82	male	NM 2, OM 2	+	ACS-H osteogenic differentiation
19	78	male	NM 2, OM 2	+	both ACS LIVE/DEAD staining, SEM
20	82	female	NM 2, OM 2	+	RNA expression, LIVE/DEAD staining
21	46	female	NM 2, OM 2	+	RNA expression, LIVE/DEAD staining
22	58	male	NM 2, OM 2	+	RNA expression, LIVE/DEAD staining
23	76	female	NM 2, OM 2	+	RNA expression, LIVE/DEAD staining
24	77	female	NM 2, OM 2	+	RNA expression, osteogenic differentiation, OPN and DAPI staining
25	53	male	NM 2, OM 2	+	RNA expression, osteogenic differentiation, OPN and DAPI staining
26	82	female	NM 2, OM 2	+	RNA expression, osteogenic differentiation, OPN and DAPI staining
27	86	female	NM 2, OM 2	+	RNA expression, osteogenic differentiation, OPN and DAPI staining

NM 1/2 = normal expansion medium 1/2; OM 1/2 = osteogenic medium 1/2; + = successful characterization

2.1.2 Plastic-ware/Miscellaneous

Plastic-ware was purchased from PEQLAB Biotechnologie (Erlangen), Greiner Bio One (Frickenhausen), Sarstedt (Nümbrecht) or Eppendorf (Hamburg) unless stated otherwise.

Description	Manufacturer	City, State
ELISA Plates 96-well flat bottom	NUNC	Wiesbaden, Germany
Millicell® Cell Culture Inserts, PET 8 µm, 24-Well	Merck Chemicals GmbH	Darmstadt, Germany
Sterile Filter (0.22 µm)		

2.1.3 Cell culture

Description	Manufacturer	City, State
Cytotoxicity Detection Kit (LDH)		
Deferoxamine mesylate salt	Sigma-Aldrich Biochemie GmbH	Hamburg, Germany
Dexamethasone water-soluble		
DMEM (1x) + GlutaMAX™	Thermo Fisher Scientific	Waltham, MA, US
Fetal calf serum (FCS)	PAA Laboratories GmbH	Cölbe, Germany
β-Glycerophosphate	Sigma-Aldrich Biochemie GmbH	Hamburg, Germany
Helistat® (InductOs®) kindly provided by Jochen Eichholtz	Medtronic, Inc.	Minneapolis, MN, US
Human TNFα DuoSet	R&D Systems	Minneapolis, MN, USA
L- L-ascorbic acid-2- phosphate	Sigma-Aldrich Biochemie GmbH	Hamburg, Germany
Lipopolysaccharides from <i>E. coli</i>		
Lyostypt®	B. Braun Melsungen AG	Melsungen, Germany
Macrophage migration inhibitory factor (MIF)	Lab own production	-
Phosphate-buffered saline (PBS)	German Rheumatism Research Center (DRFZ)	Berlin, Germany
Penicillin-Streptomycin (10,000 U/mL)	Thermo Fisher Scientific	Waltham, MA, US
RPMI medium		
StemMACS™ AdipoDiff Medium	Miltenyi Biotech	Bergisch Gladbach
StemMACS™ MSC Expansion Media Kit XF, human		
StemMACS™ OsteoDiff Medium		
TNF alpha Mouse ELISA Kit	Thermo Fisher Scientific	Waltham, MA, US
Trypsin/EDTA	PAA Laboratories GmbH	Cölbe, Germany

Description	Composition
Expansion Medium	NM 1 DMEM plus GlutaMAX™, 10% (v/v) FCS, 1% (v/v) Penicillin-Streptomycin
	NM 2 DMEM plus GlutaMAX™, 20% (v/v) StemMACS™, 10% (v/v) FCS, 1% (v/v) Penicillin-Streptomycin
Osteogenic Medium	OM 1 DMEM, 10% (v/v) FCS, 10 mM β-glycerophosphate, 10 ⁻⁸ M dexamethasone, 0.1 mM L-ascorbic acid-2- phosphate
	OM 2 StemMACS™ OsteoDiff Medium

2.1.4 FACS analysis

Description	Manufacturer	City, State
CD13 (clone WM15, Mouse IgG1, κ) APC	ImmunoTools GmbH	Friesoythe, Germany
CD14 (clone TM1, Mouse IgG1) Cy5	German Rheumatism Research Center (DRFZ)	Berlin, Germany
CD19 (clone BU12, Mouse IgG1) Cy5		
CD44 (clone MEM-263, Mouse IgG1) APC	eBioscience Thermo Fisher Scientific Inc.	Waltham, MA, US
CD45 (clone MEM-28, Mouse IgG1) APC	ImmunoTools GmbH	Friesoythe, Germany
CD90 (clone 5E10, Mouse IgG1) APC	eBioscience Thermo Fisher Scientific	Waltham, MA, US
CD105 (clone SN6, Mouse IgG1, κ) APC		
Bovine serum albumin (BSA)	Sigma-Aldrich Chemie GmbH	Steinheim, Germany
Flebogamma®	German Rheumatism Research Center (DRFZ)	Berlin, Germany
Sodium azide (NaN ₃)	Sigma-Aldrich Chemie GmbH	Steinheim, Germany

Description	Composition
PBS	137 mM NaCl; 2.7 mM KCl; 1.4 mM KH ₂ PO ₄ ; 4.3 mM Na ₂ HPO ₄ ; H ₂ O _{dest}
PBS/BSA	0,5 % (w/v) BSA in PBS
PBS/BSA/Azide	0,05 % (v/v) NaN ₃ in PBS/BSA

2.1.5 Cell staining

Description	Manufacturer	City, State
Alexa Fluor® 568 goat anti-rabbit IgG (H+L) antibody	Life Technologies Thermo Fisher Scientific	Waltham, MA, US
Alizarin Red	Sigma-Aldrich Chemie GmbH	Steinheim, Germany
BCIP/NBT Color Development Substrate	Promega Thermo Fisher Scientific	Waltham, MA, US
Cetylpyridinium chloride	AppliChem GmbH	Darmstadt, Germany
Isopropanol	Merck Chemicals GmbH	Darmstadt, Germany
LIVE/DEAD® Viability/Cytotoxicity Kit	Invitrogen Thermo Fisher Scientific	Waltham, MA, US
Oil Red O	Sigma-Aldrich Chemie GmbH	Steinheim, Germany
OPN antibody ab8448	Abcam	Cambridge, UK
Normal goat serum	Vector Laboratories	Burlingame, CA, US
Roti®-Histofix	Carl Roth GmbH + Co. KG	Karlsruhe, Germany
TritonX	Sigma-Aldrich Chemie GmbH	Steinheim, Germany
Tris Buffer, 1.0 M, pH 8.0	Merck Chemicals GmbH	Darmstadt, Germany

Description	Composition
Alizarin Red solution	0.5 % (w/v) Alizarin Red in H ₂ O _{dest} (pH 4)
Cetylpyridinium chloride solution	10 % (w/v) in H ₂ O _{dest}
Red Oil staining	<u>Stock solution:</u> 0.3 % (w/v) Oil Red in 100 % Isopropanol <u>Working solution:</u> 3 ml stock solution and 2 ml H ₂ O _{dest} 10 min incubation at RT, sterile filtration (0.45 µm)

2.1.6 Protein isolation and mass spectrometry

Description	Manufacturer	City, State
Guanidine hydrochloride	Sigma-Aldrich Chemie GmbH	Steinheim, Germany
DL-dithiothreitol		
Chloroacetamide	Merck Chemicals GmbH	Darmstadt, Germany
Endoproteinase LysC	Wako Chemicals GmbH	Neuss, Germany
Sequence grade modified trypsin	Promega	Madison, WI, US

2.1.7 Scanning electron microscopy

Description	Manufacturer	City, State
Conductive Carbon Adhesive Tabs	Electron Microscopy Sciences	Hatfield, PA, US
Ethanol, absolute	Carl Roth GmbH + Co. KG	Karlsruhe, Germany
Glutaraldehyde	Sigma-Aldrich Chemie GmbH	Steinheim, Germany
Hexamethyldisilazane		
Specimen Mounts for Scanning Electron Microscopes	Electron Microscopy Sciences	Hatfield, PA, US

2.1.8 Animals and housing

Number	Strain	Age	Sex	Body weight	Provider
107	C57BL/6N	12 weeks	female	20-25 g	Charles River Laboratories, Wilmington, MA, US

Description	Manufacturer	City, State
Eurostandard Type II	Tecniplast Deutschland GmbH	Hohenpeißenberg, Germany
Filter Top		
Lignocel FS 14	J. Rettenmaier & Söhne GmbH + Co. KG	Rosenberg, Germany
Standard mouse diet	ssniff-Spezialdiäten GmbH	Soest, Germany
Wire Lid	Tecniplast Deutschland GmbH	Hohenpeißenberg, Germany

2.1.9 Osteotomy – Medications and material for surgical procedure

	Description	Manufacturer	City, State
Medications	Clindamycin	Ratiopharm GmbH	Ulm, Germany
	NaCl 0.9%	B. Braun Melsungen AG	Melsungen, Germany
	Narketan®	Vetoquinol GmbH	Ismaning, Germany
	Temgesic®	RB Pharmaceuticals Limited	Heidelberg, Germany
	Tramal® Drops	Grünenthal GmbH	Stolberg, Germany
	Xylapan®	Vetoquinol GmbH	Ismaning, Germany
Surgical procedure	Isoflurane	CP-Pharma Handelsgesellschaft mbH	Burgdorf, Germany
	Bepanthen Eye Ointment	Bayer Pharma AG	Berlin, Germany
	Braunoderm B.	Braun Melsungen AG	Melsungen, Germany
	Drill bit 0.45 mm	RISystem	Davos, Switzerland
	Gigli wire saw		
	Lyostypt®	B. Braun Melsungen AG	Melsungen, Germany
	MouseExFix MountingPin 0.45mm	RISystem	Davos, Switzerland
	MouseExFix simple L		
	Opsite dressing spray	Smith & Nephew GmbH	Hamburg, Germany
	Prolene (4-0)	Johnson & Johnson Medical GmbH, Ethicon	Norderstedt, Germany
	Square box wrench 0.70 mm	RISystem	Davos, Switzerland

2.1.10 Histology

	Description	Manufacturer	City, State
Preparation: Emding & Cutting	Acetone	Sigma-Aldrich Chemie GmbH	Steinheim, Germany
	Cryofilm 2C (9)	Section-Lab Co. Ltd.	Hiroshima, Japan
	Embedding Medium SCEM		
	Microtome Blades SEC 35	Fisher Scientific	Schwerte, Germany
	n-Hexan	Carl Roth GmbH + Co. KG	Karlsruhe, Germany
	Paraformaldehyde Solution 20 % (v/v), EM grade	Electron Microscopy Sciences	Hatfield, PA, US
	Saccharose	Südzucker AG	Mannheim, Germany
	Superfrost™ Plus microscope slides	Thermo Fisher Scientific	Waltham, MA, US
	Tissue-Tek® O.C.T.™ compound	Sakura Finetek Germany GmbH	Staufen, Germany
Staining	Acetic acid	Carl Roth GmbH + Co. KG	Karlsruhe, Germany
	Acid alcohol	Merck Chemicals GmbH	Darmstadt, Germany
	Acid Phosphatase, Leukocyte (TRAP) Kit	Sigma-Aldrich Chemie GmbH	Steinheim, Germany
	Alcian blue	Carl Roth GmbH + Co. KG	Karlsruhe, Germany
	Alkaline ethanol		
	Brilliant crocein acid fuchsin	Chroma GmbH & Co. KG	Münster, Germany
	Fast Red Violet LB Salt	Sigma-Aldrich Chemie GmbH	Steinheim, Germany
	Iron hematoxylin (after Weigert)	Chroma GmbH & Co. KG	Münster, Germany
	L-(+)-Tartaric acid	Sigma-Aldrich Chemie GmbH	Steinheim, Germany
	Mayer's hemalum	Merck Chemicals GmbH	Darmstadt, Germany
	Naphthol AS-MX phosphate	Sigma-Aldrich Chemie GmbH	Steinheim, Germany
	N,N-dimethylformamide		
	Phosphotungstic acid	Chroma GmbH & Co. KG	Münster, Germany
	Saffron du Gâtinais		
	Silver nitrate (AgNO ₃)	Merck Chemicals GmbH	Darmstadt, Germany
	Sodium carbonate (Na ₂ CO ₃)	Merck Chemicals GmbH	Darmstadt, Germany
	Sodium thiosulfate	Merck Chemicals GmbH	Darmstadt, Germany
	Triton X-100	Sigma-Aldrich Chemie GmbH	Steinheim, Germany
	Xylene	Carl Roth GmbH + Co. KG	Karlsruhe, Germany
	Mounting	Cover slips 24 x 50 mm	Thermo Fisher Scientific
Vitro-Clud		R. Langenbrinck GmbH	Emmendingen, Germany
Aquatex® mounting medium		Merck Chemicals GmbH	Darmstadt, Germany

2.1.11 Immunofluorescence

Description	Manufacturer	City, State
Alexa Fluor® 568 donkey anti-goat IgG (H+L)	Life Technologies Thermo Fisher Scientific	Waltham, MA, US
Alexa Fluor® A647 goat anti-rat IgG (H+L)		
Alexa Fluor® 594 donkey anti-rat IgG (H+L)		
Alexa Fluor® 488 donkey anti-rabbit IgG (H+L)		
DAPI	German Rheumatism Research Center (DRFZ)	Berlin, Germany
goat anti-mouse CD31 (AF3628)	R&D Systems	Minneapolis, MN, US
rat anti-mouse Endomucin (V.7C7)	Santa Cruz Biotechnologies	Dallas, TX, US
rabbit anti-mouse OSX Santa Cruz (sc-22536-R)		
rat anti-mouse F4/80 (MCA497R)	Bio-rad	Hercules, CA, US
FluoroMount-G™		
Normal goat serum		
Normal donkey serum	Sigma-Aldrich Chemie GmbH	Steinheim, Germany
Normal rat serum		
Normal rabbit serum		
Tween® 20	Merck Chemicals GmbH	Darmstadt, Germany

2.1.12 RNA-isolation, microarray and qRT-PCR

Description	Manufacturer	City, State
Agilent RNA 6000 Nano	Agilent Technologies	Santa Clara, CA, US
β-Mercaptoethanol	Sigma-Aldrich Chemie GmbH	Steinheim, Germany
Chloroform	VWR International	Rednor, PA, US
DyNAmo ColorFlash SYBR Green qPCR Kit	Thermo Fisher Scientific	Waltham, MA, US
GeneChip™ Hybridization, Wash, and Stain Kit	Affymetrix Thermo Fisher Scientific	Waltham, MA, US
IVT-Express Kit		
Mouse Genome 430 2.0 Array		
RNeasy Mini Kit	Qiagen	Hilden, Germany
RNase Free DNase Set	Qiagen	Hilden, Germany
TaqMan Reverse Transcription Reagents Kit	Thermo Fisher Scientific	Waltham, MA, US
TRizol® Reagent	Invitrogen Thermo Fisher Scientific	Waltham, MA, US

2.1.13 Instruments

Description	Manufacturer	City, State
Affymetrix GeneChip™ Scanner 3000 7G	Affymetrix Thermo Fisher Scientific	Waltham, MA, US
Cell culture incubator	Binder GmbH	Tuttlingen, Germany
Computed tomography scanner μCT Viva 40	SCANCO Medical AG	Brüttisellen, Switzerland
Cryotome	Leica Mikrosysteme GmbH	Wetzlar, Germany
Electrospray ionization (ESI) source	Thermo Fisher Scientific	Waltham, MA, US
Electrophoresis Bioanalyzer In- strument 2100	Agilent Technologies	Santa Clara, CA, US
Fine Coater JFC-1200	Jeol GmbH	Tokio, Japan
Fluorescence microscop BZ-9000	Keyence GmbH,	Elmwood Park, IL, US
Fresco 17 Centrifuge	Thermo Scientific	Karlsruhe, Germany
GeneChip™ Fluidics Station 450 Hybridization Oven 640	Affymetrix Thermo Fisher Scientific	Waltham, MA, US
High-Performance Liquid Chroma- tography (HPLC) system	Thermo Fisher Scientific	Waltham, MA, US
JCM-6000 Plus Neo Scope™ SEM	Jeol GmbH	Freising, Germany
Labofuge 400R	Heraeus Instruments GmbH	Hanau, Germany
Light microscope	Leica GmbH	Wetzlar, Germany
Light microscope	Carl Zeiss Microscopy GmbH	Jena, Germany
MACSQuant® Analyzer	Miltenyi Biotech GmbH, Bergisch Gladbach	MACSQuant® Analyzer
Nano-Drop Spektrophotometer ND-1000	PeqLab Biotechnologie GmbH	Erlangen, Germany
Q-Exactive plus Orbitrap instru- ment	Thermo Fisher Scientific	Waltham, MA, US
Stratagene Mx3000P	Agilent Technologies	Santa Clara, CA, US
Synergy HT plate reader	BioTek Instruments	Winooski, VT, US

2.1.14 Software and Online Services

Description	Manufacturer	City, State
Affymetrix GCOS/MAS5 software	Affymetrix Thermo Fisher Scientific	Waltham, MA, US
AxioVision	Carl Zeiss Microscopy GmbH	Jena, Germany
FlowJo software	Tree Star	Ashland, OR, USA
GraphPad Prism V.5 software	GraphPad	San Diego, CA, USA
ImageJ	Open Source	-
MaxQuant software package V1.6.0.1	Computational Systems Biochemistry, Max Planck Institute of Biochemistry	Martinsried, Germany
MicroCT evaluation	SCANCO Medical AG	Brüttisellen, Switzerland
Stratagene Mx3000P Software	Agilent Technologies	Santa Clara, CA, US
Basic Local Alignment Search Tool (BLAST)	http://www.ncbi.nlm.nih.gov/tools/primer-blast/index.cgi?LINK_LOC=BlastHome	
BioRetis Database	www.bioretis-analysis.de	
Primer3 v. 0.4.0	http://bioinfo.ut.ee/primer3-0.4.0/	

2.2 Methods

2.2.1 hMSC isolation and expansion

Bone marrow was collected from patients undergoing total hip replacement at the Center for Musculoskeletal Surgery, Charité-Universitätsmedizin Berlin. Samples were registered and distributed by the “Tissue Harvesting” Core Facility of the BCRT. Written consents were gathered from all patients. All protocols were approved by the Charité-Universitätsmedizin Ethics Committee and performed according to the Helsinki Declaration. The bone marrow was transferred into a 175 ml cell culture flask, covered with 25 ml normal expansion medium (NM, see 2.1.3) and incubated at 37°C in 5% CO₂ atmosphere (app. 18% O₂). Medium was changed after 3-4 days when human MSCs (hMSCs) became adherent including a washing step with PBS to remove the remaining non-adherent cells and bone marrow material. Afterwards medium was changed weekly. Passaging was performed when a confluence of 80-90% was reached beginning with a PBS washing step followed by the application of Trypsin/EDTA and an incubation of 10-15 min at 37°C. Enzymatic reaction was stopped by supplementing DMEM with 10% (v/v) FCS and the cell suspension was transferred to a 50 ml tube and centrifuged (10 min, 300 x g). The cell pellet was washed with PBS, centrifuged, resolved in PBS and counted with a hemocytometer. 1x10⁶ cells were suspended in NM and placed in a new flask or used in other cell concentrations for subsequent experiments. Cells were used within passage 4-7.

2.2.2 hMSC characterization

After three passaging steps, hMSCs were characterized by flow cytometry (FACS) analysis and differentiation assays. Only those hMSCs which passed the characterization step were used in the experiments.

➤ FACS analysis

Cells (1x10⁶ cells) were fixed with ice-cold PBS and formaldehyde (4% v/v) and incubated for 20 min at room temperature (RT). After a washing step with PBS/BSA, cells were incubated for 10 min at 4°C with Flebogamma® (10 mg/mL) and subsequently stained individually for each antibody for 20 min at 4°C in the dark using the following dilutions: CD13-APC (1:100), CD14-Cy5 (1:250), CD19-Cy5 (1:500), CD44-APC (1:500), CD45-APC (1:100), CD90-APC (1:100), CD105-APC (1:100). Afterwards, the cells were washed twice with PBS/BSA and held in PBS/BSA/Azide protected from light until measurement at the MACSQuant® Analyzer. Data analysis was performed by FlowJo and a clear shift of cell population (>70%) was determined as positive.

➤ **Osteogenic differentiation**

For osteogenic differentiation, hMSCs were suspended in NM and transferred to a 96 well plate with a density of 1×10^4 cells/well and incubated at 37°C in 5% CO₂ atmosphere (app. 18% O₂). After 24 h medium was changed and osteogenic medium (OM; see 2.1.3) was applied. Medium was changed weekly, and Alizarin red staining was performed after 3 weeks. Therefore, adherent cells were fixed with 4% (v/v) formaldehyde (15 min RT), washed twice with PBS and stained with Alizarin red for 10 min at RT. ALP-staining was performed with the BCIP/NBT system from Promega/Thermo Fisher Scientific and performed according to the manufacturer's instructions. Finally, wells were washed once with PBS and four times with H₂O_{dest} and examined with a light microscope. Cellular calcifications were stained red and indicated positive osteogenic differentiation.

➤ **Adipogenic differentiation**

For adipogenic differentiation, hMSCs were suspended in NM and transferred to a 96 well plate with a density of 1×10^4 cells/well and incubated at 37°C in 5% CO₂ atmosphere (app. 18% O₂). After 24 h medium was changed and adipogenic medium (StemMACS™ Adipo-Diff Medium) was applied. Medium was changed weekly, and Red Oil staining was performed after 3 weeks. Adherent cells were fixed with 4% (v/v) formaldehyde (15 min RT), washed with H₂O_{dest} and 60% (v/v) isopropanol and stained with Red Oil working solution for 15 min at RT. Subsequently, wells were washed with 60% (v/v) isopropanol and H₂O_{dest} and examined with a light microscope. Lipid vacuoles were stained red and indicated positive adipogenic differentiation.

2.2.3 Osteogenic differentiation of hMSCs

➤ **Titration of Dexamethasone and MIF/DFO**

hMSCs were suspended in NM 1 and transferred to a 96 well plate with a density of 1×10^4 cells/well and incubated at 37°C in 5% CO₂ atmosphere. After 24 h or until cells reached a confluence of >90% OM 1 with Dexamethasone (Dex), MIF and/or DFO was applied. Therefore, Dex was solved in OM 1 in concentrations of 10^{-3} to 10^{-8} M. MIF and DFO were titrated in OM 1 with 10^{-3} Dex to reach the following final concentrations: 62.5, 125, 250, 500, 750, 1000 μM DFO; 50, 100, 125, 150, 250, 500 ng/ml MIF or in combinations of 125/50, 250/50, 62.5/50, 125/100, 250/100, 62.5/100, 125/150, 250/150, 62.5/150 μM DFO/ ng/ml MIF. Incubation was conducted at 37°C in 5% CO₂ atmosphere with app. 18% O₂ (normoxia) or 1% O₂ (hypoxia; incubator flushed by nitrogen) for two, three or four weeks. For each condition and donor at least 3 wells contained the same condition (> triplicates). Every experimental setup was accompanied by NM 1 and OM 1 controls. Afterwards quantitative Alizarin

red assay was performed as described below. Supernatants were collected for lactate dehydrogenase (LDH) assay. Double normalization was performed by first normalizing all data to OM 1 + Dex 10^{-3} M = 0% and afterwards to OM 1 + Dex 10^{-8} M = 100%).

➤ **Co-cultivation with ACS-L and ACS-H**

Uniformly, roundly punched out tape were placed into the middle of every well in a 24-well plate. hMSCs from different donors were seeded with 1×10^5 cells into the well and incubated for 24 h at 37°C in 5% CO₂ atmosphere (app. 18% O₂). The tape was removed and uniformly, round punched out ACS-L (Lyostypt®) or ACS-H (Helistat®) (6 mm) were applied to the middle of the well. OM 2 and NM 2 were applied accordingly. Medium was changed weekly for three weeks. Afterwards quantitative Alizarin red assay was performed as described below. Supernatants were used for LDH assay.

➤ **Quantitative Alizarin red assay**

Alizarin red staining was performed as described above (2.2.2). After the last washing step with H₂O_{dest} 10% (w/v) cetylpyridinium chloride solution was applied and incubated on a shaker for 30 min at RT. Supernatants were transferred to a new 96 well plate and measured with a Synergy HT plate reader at a wavelength of 562 nm (reference wavelength 630 nm) for quantification.

➤ **Osteopontin staining**

Osteopontin (OPN) staining was performed together with DAPI staining on fixed cells (4% (v/v) formaldehyde, 15 min RT) that have been blocked and permeabilized by 10% goat serum in 0.1% Triton X/PBS for 30 min at RT. For staining primary OPN antibody (1:250) was applied in PBS overnight at 4°C. The secondary Alexa Fluor® 568 goat anti-rabbit IgG antibody (1:500) together with DAPI (1:1000) was applied after washing for 1 h at RT. Pictures were taken with a fluorescence microscope Keyence BZ 9000. At least five pictures were quantitatively analyzed per sample. Quantification was performed with ImageJ. Therefore, positive stained areas were selected, and normalization was performed to the cell count (DAPI).

2.2.4 Quantitative real time PCR (qRT-PCR)

➤ **RNA isolation and cDNA synthesis**

Cells were removed with Trypsin/EDTA, washed with PBS and stored in RLT Buffer (+ 1% (v/v) β-Mercaptoethanol) at -20°C until further use. The following isolation steps were performed with RNeasy Mini Kit from Qiagen according to manufacturer's instructions including several buffer treatments, binding to special columns, washing and centrifugation steps. DNA contamination was removed by a one-step digestion step in between. After finishing the isolation, the RNA concentration was measured with a Nano-Drop Spektrophotometer

and stored at -80°C until further use. cDNA synthesis was performed with the TaqMan™ Reverse Transcription Reagents Kit following the manufacturer's instructions.

➤ qRT-PCR

RNA-expression was analyzed with the DyNAmo Flash SYBR Green qPCR Kit at a Stratagene Mx3000P using the standard protocol: 7 min at 95°C (initial denaturation); 45 cycles of 5 s at 95°C (denaturation), 7 s at 60°C (primer annealing), 9 s at 72°C (elongation); stepwise increase of the temperature from 50 to 98°C every 30 s (melting curve). Primers were purchased from TIB Molbiol (Table 3).

Table 3: Primer sequences

Gene	Forward	Reverse
<i>RUNX2</i>	TTACTTACACCCCGCCAGTC	TATGGAGTGCTGCTGGTCTG
<i>ALP</i>	GTACGAGCTGAACAGGAACAACG	CTTGGCTTTTCCTTCATGGTG
<i>EF1A</i>	GTTGATATGGTTCCTGGCAAGC	TTGCCAGCTCCAGCAGCCT

Data were normalized to the housekeeper gene expression *EF1A* and the NM 2 group using the $\Delta\Delta\text{Ct}$ -method.

2.2.5 Cell vitality and cytotoxicity

➤ LIVE/DEAD staining

For the LIVE/DEAD staining, 1×10^4 hMSCs in NM 2 were pipetted on uniformly, round punched out ACS-L or ACS-H (8 mm) which were placed in a cell culture insert. Cultivation was conducted for 1 week at 37°C in 5% CO_2 atmosphere (18% O_2). Staining was performed using the LIVE/DEAD® Viability/Cytotoxicity Kit. After washing the scaffolds twice with PBS the combined LIVE/DEAD® assay reagents were applied and incubated for 45 min at RT in the dark. As control, hMSCs were seeded in 24 well in NM 2 and were stained accordingly. Pictures were taken with a fluorescence microscope BZ 9000 at least two pictures were analyzed per sample using ImageJ (Color threshold). Quantification was performed marking positive stained areas and normalizing the results to the total area.

➤ LDH assay

The LDH assay was conducted using the Cytotoxicity Detection Kit with the collected supernatants according to the manufacturer's instructions. In order to avoid background measurements caused by phenol red (ingredient of DMEM), supernatants were diluted 1:20 in PBS, mixed with freshly prepared reaction mixture (1:1) and incubated for 30 min at RT protected from light. Absorbance was measured with a Synergy HT plate reader at a wavelength of 490 nm (reference wavelength 630 nm). Data were normalized to the NM OD values and the assay was performed in duplicates.

2.2.6 Whole blood assay

Human blood was sampled from 6 healthy voluntary donors (3 women and 3 men; aged 20-40). ACS-L and ACS-H were punched into round pieces (6 mm). The blood was mixed with RPMI medium (1:1) in round-bottom 96 well plates in duplicates per condition. The scaffolds were transferred to the wells and as a positive control, 100 ng LPS was supplemented in wells with blood but without scaffold. Co-cultivation was performed for 20 h at 37°C in 5% CO₂ atmosphere (app. 18% O₂). Plates were centrifuged (10 min, 300 x g, 4°C) and supernatants were collected and stored at -20°C until further use. TNF α DuoSet[®] ELISA was performed according to the manufacturer's instructions in duplicates. A seven-point standard dilution row with 2-fold serial dilutions were assayed in parallel. 96 well flat-bottomed plates were prepared with 100 μ l capture antibody diluted in PBS overnight at RT. After washing 3 times with washing buffer (0.05% (v/v) Tween[®] 20 in PBS), plates were blocked with 300 μ l reagent diluent (1% (w/v) BSA in PBS, pH 7.2-7.4) for 1 h at room temperature, followed by a washing step. Standards were dispensed that were incubated on the plate together with the samples for 2 h. After washing, 100 μ l of the detection antibody together with normal serum in PBS was applied for 1 h followed by a 20 min incubation with 100 μ l Streptavidin-HRP and a 20 min incubation with 100 μ l substrate solution addition. The reaction was stopped after 10 minutes with 50 μ l 2N H₂SO₄ and plates were read at 450 nm and 540 nm (wavelength correction). A standard curve was generated with a four-parametric logistic curve fit.

Whole mouse blood was collected from female C57BL/6N mice aged 12 weeks (n= 3). Assay was performed as the human whole blood assay. TNF α release in the supernatant was analyzed with the TNF alpha Mouse ELISA Kit.

2.2.7 Protein isolation and mass spectrometry (LC-MS/MS)

Protein isolation and mass spectrometry was performed by Dr. Marieluise Kirchner (BIH Proteomics Core Facility) and have been published previously [174]. Proteins were extracted from 1 mg ACS-L and ACS-H material comparing two different methods: *without* (Method 1) or *with* (Method 2) a cryo-pulverization of the sample before incubating the material in 6 M guanidine hydrochloride (100 mM HEPES; pH 8.0) for 15 min at 95°C. Afterwards, protein reduction was performed with 10 mM DL-dithiothreitol for 30 min at RT and alkylation with 55 mM chloroacetamide for 20 minutes in the dark at RT. 5 μ g of endoproteinase LysC was applied and incubated for 4 h at RT. Samples were diluted with 4x digestion buffer (50 mM ammonium bicarbonate in water (pH 8.0)) and 5 μ g sequence grade modified trypsin was added and incubated overnight at 37°C. Formic acid (2% (v/v) final concentration) was used to acidify samples and insoluble material was removed by centrifugation (15 min at 14,000 x g). The standard StageTip protocol [175] was used to extract

and desalt the peptides. For mass spectrometric measurements, peptides from 3 independent technical replicates were separated on a reversed-phase column over a 45 min and 85 min gradient with a 250 nl/min flow rate of increasing buffer B concentration (8-60%) on a High-Performance Liquid Chromatography (HPLC) system. Peptides were ionized using an electrospray ionization (ESI) source and analyzed on a Q-Exactive plus Orbitrap instrument. Mass spectrometry was performed in the data-dependent positive mode with one full scan (m/z range = 350-2,000; $R = 70,000$; target value: 3×10^6 ; maximum injection time = 5 ms). The ten most intense ions with a charge state greater than one were selected ($R = 35,000$, target value = 5×10^5 ; isolation window = 1.6 m/z ; maximum injection time = 120 ms). Dynamic exclusion for selected precursor ions was set to 30 s. For data analysis the MaxQuant software package was used (version 1.6.0.1). The internal Andromeda search engine was utilized to search MS^2 spectra against decoy *Bos Taurus* UniProt (BOVIN.2017-01) and contaminants database. Variable modifications of methionine oxidation, asparagine and glutamine deamination and N-terminal acetylation, and fixed modification of carbamidomethyl cysteine were included in the search. Minimal peptide length was restricted to seven amino acids and a maximum of 3 missed cleavages was allowed. The FDR (false discovery rate) was fixed to 0.01 for peptide and protein identifications. IBAQ intensity values were calculated. Only robust protein identifications (minimum of 3 peptides identified; detection in all 3 replicates) were used for further analyses.

2.2.8 Scanning electron microscopy (SEM)

For scanning electron microscopy, 1×10^4 hMSCs in NM 2 were applied on uniformly, round punched out ACS-L or ACS-H (8 mm) place in a cell culture insert and cultivated for 3 days at 37°C in 5% CO₂ atmosphere (18% O₂). As control, ACS-L and ACS-H were used dry and soaked with DMEM. Samples were dried in accordance with the following protocol: fixation with 2.5% (v/v) glutaraldehyde for 10 min, treatment with an immersion in ethanol series (10 min each step) 30%-100% (5 steps), incubation twice with hexamethyldisilazane for 10 min and subsequent air drying overnight. Dried samples were transferred to an adhesive tab placed on a specimen mount and gold coating was performed with a fine gold coater. A JCM-6000 Plus Neo Scope™ was used and for imaging with adjustment to the high vacuum and 5 - 15 V.

2.2.9 Animals, housing and osteotomy

➤ Animals and housing

Female C57BL/6N mice aged 10 weeks were purchased from Charles River Laboratories and used with an age of 12 weeks and a body weight between 20 and 25 g. They were housed in the Charité animal facility (FEM; Forschungseinrichtung für experimentelle Medizin). Mice were kept under obligatory hygiene standards monitored according to the

FELASA standards. Mice were randomly grouped into two and kept in groups two weeks prior to osteotomy provided with sufficient nesting material, but without pipes and houses after osteotomy to avoid possible entanglement with the used external fixator. Housing was semi-sterile in Eurostandard Typ II clear-transparent plastic cages covered with a wire lid with build-in u-shaped feed hopper closed with a filter top (outside the SPF barrier and without filtered air supply for the mice cages to support the development of a functional immune system). Food and water were available ad libitum and the temperature was (20 ± 2 °C) controlled with a 12 h light/dark period a humidity of 45-50%.

➤ **Osteotomy**

All experiments were carried out with ethical permission according to the policies and principles established by the Animal Welfare Act, the National Institutes of Health Guide for Care and Use of Laboratory Animals, and the National Animal Welfare Guidelines, the ARRIVE guidelines and were approved by the local legal representative animal rights protection authorities (Landesamt für Gesundheit und Soziales Berlin: G 0111/13, 0039/16). Pain management included a buprenorphine injection (0.1 mg/kg) s.c. as analgesic prior to the surgery and the application of tramadol (100 mg/l) via the drinking water for the first 3 post-operative days. Anesthesia was performed using isoflurane and O₂ supplementation applied in a Plexiglas box (Fig. 7A). After anesthetic induction, maintenance was achieved with a respiratory mask. Mice were prepared with eye ointment, clindamycin s.c. (0.02 ml) and the left femur area was shaved and disinfected. Osteotomy was performed as published previously [30] under aseptic conditions while mice were placed on a warm plate (Fig. 7B). In detail, a lateral longitudinal incision of the skin (2 mm) along an imaginary line from left knee to left hip was made. The femur was prepared bluntly between the *Musculus vastus lateralis* and *Musculus biceps femoris*, protecting the nerve. The pin placement (0.45 mm diameter) through the connector bar of the external fixator was performed by serial drilling to position the external fixator laterally parallel to the femur. A 0.70 mm osteotomy gap was created between the middle pins using a Gigli wire saw. The osteotomy gap was flushed with NaCl for all groups and left either empty (control), filled with PBS-soaked ACS-L (ACS-L group) or MIF and/or DFO solved in PBS applied on the ACS-L (treatment groups). ACS-L was trimmed in square shape with side lengths of 4-5 mm.

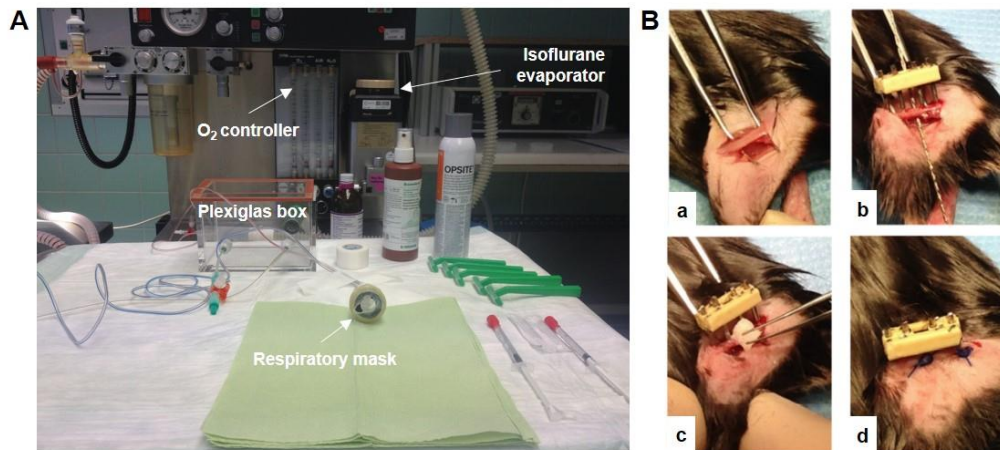


Figure 7: Preparation area and surgical procedure.

(A) Anesthesia was induced in a Plexiglas box. Mice were subsequently transferred to the preparation area and isoflurane and O₂ was provided via respiratory mask. Analgesic and antibiotic were injected, and operation area was shaved and disinfected. Afterwards, mice were transferred to the aseptic operative field together with the respiratory mask and placed on a warm plate. (B) The left femur was bluntly prepared (a) and connector bar of the external fixator was adjusted parallel to the femur by consecutive pin placement (b). The osteotomy gap was created with a Gigli wire saw (b) and filled with scaffold (-/+ treatment) or left empty (c) and the skin was closed (d).

After skin closure, mice received warmed NaCl (0.2 ml) s.c. and were returned to their cages with a prepared nest. For recovery from anesthesia an infrared radiator was provided under close observation. Blinding was not possible during surgery but was performed for further analysis. Mice were scored and weighted regularly during the following days in order to avoid suffering.

➤ Experimental groups and study design

Four time points were determined for endpoint measurements. In order to evaluate the effect of MIF/DFO on the initial fracture healing phase, early time points were chosen for RNA/microarray analysis (3 and 7 days). The healing outcome was investigated via *ex vivo* μ CT at day 7, 14 and 21 and histology at day 14 and 21 (Fig. 8). All analyses were performed blinded for the experimenter. Two operated animals were excluded due to infection in the osteotomy gap and one animal was partially excluded (only included for *ex vivo* μ CT) due to an oblique fixation.

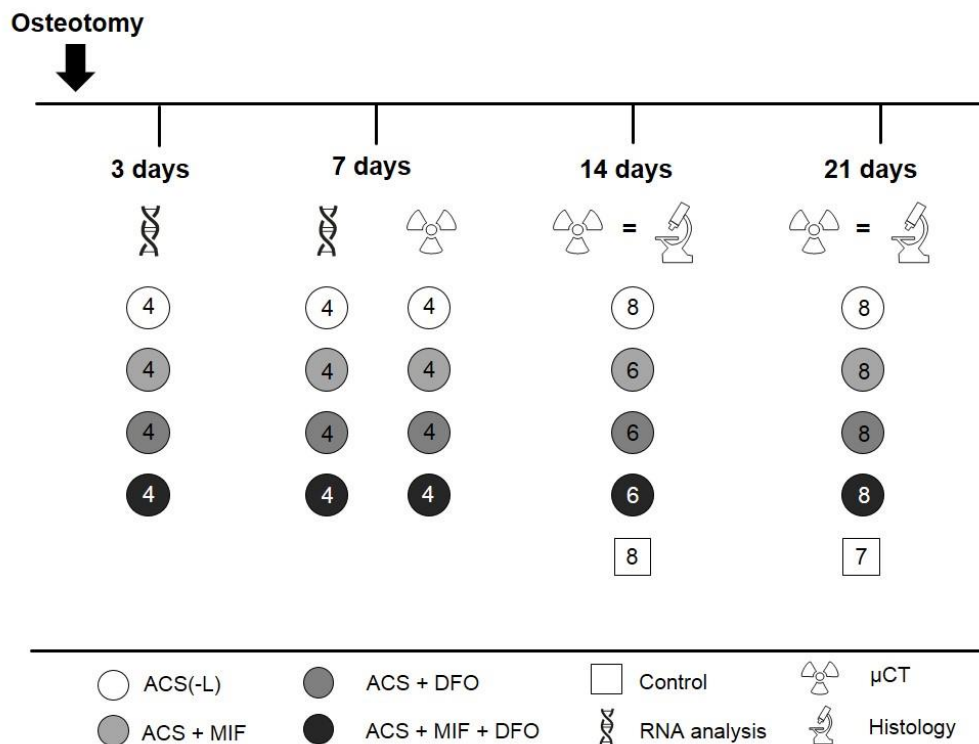


Figure 8: Experimental timeline including the outcome measurements, experimental groups and animal numbers indicated within the symbols.

➤ Euthanasia and sample collection

Animals were euthanized via cervical dislocation after 3, 7, 14 and 21 days in deep anesthesia (no deep pain perception) after intracardial blood collection. Left, osteotomized femora were collected and fixed with 4% (w/v) paraformaldehyde (PFA) for 6-8 h at 4°C (*ex vivo* µCT, histology). For RNA isolation, osteotomized femora were prepared, the fracture gap was cutted out, cryopreserved with liquid nitrogen and stored at -80°C until further use. The excised material contained the osteotomy gap as well as cortical bone from the adjacent bone. Additionally, liver, kidney and spleen were cryopreserved and stored at -80°C as retention sample in case of unexpected observations.

2.2.10 *Ex vivo* micro computed tomography (µCT)

PFA-fixed femora were treated with an ascending sugar solution (10%, 20%, 30%) for 24 h, respectively at 4°C and were scanned after removal of the pins and external fixator with an isotropic voxel size of 10.5 µm (70 KVp, 114 µA; SCANCO µCT Viva 40). The scan axis was aligned along the diaphyseal axis of the femora. The scanned volume of interest (VOI) comprised 191 slices between the middle pins to include the complete osteotomy gap. Further 3D reconstruction and analyses were performed using the provided software package. In detail, the osteotomy gap was defined for each sample from proximal half broken up cortical bone end to the distal one (analyzed VOI) (Fig. 9). During the post-processing, the VOI was manually determined and the cortical bone was manually excluded from the VOI.

A fixed global threshold of 240 mg HA/cm³ was applied for the automatic 3D callus tissue analysis. The total volume (TV; mm³), the bone volume (BV; mm³), the bone volume fraction and the bone mineral density (mg HA/cm³) were evaluated in the analysis. 3D images were exemplary created displaying the analyzed VOI. Nomenclature and analysis were conducted in accordance with published recommendations [176].

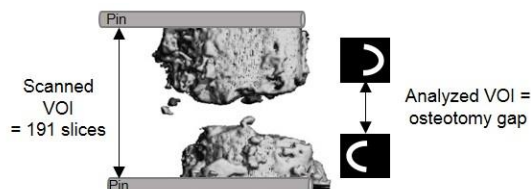


Figure 9: Overview on scanned and analyzed VOIs during *ex vivo* μ CT measurements.

Reproduced from [174].

2.2.11 Histological staining

➤ Embedding and cutting

After μ CT scanning, femora were cryo-embedded without decalcification in order to preserve the tissue's structures. The embedding and slice preparation was conducted according to the Kawamoto *et al.* method to prepare slices of undecalcified bones [177]. For cryo-embedding, a dewar vessel was one third filled with acetone and dry ice while a glass beaker filled with n-hexane was placed on top (cool down 10-15 min). Femora were placed in a metallic embedding form and filled with SCEM medium, the pins and external fixator were removed after a first short freeze on before samples were completely covered with the SCEM medium and frozen by pivoting in ice-cold n-hexane. Sample blocks were stored at -80°C until further use.

Slices were made with a cryotome allowing the frozen bone samples and the knife to acclimatize to the temperature of the cryotome (around -20°C) at the beginning. The sample blocks were fixed to the holder with Tissue-Tek[®] and trimming was performed until bone tissue became visible. As soon as the whole medullary canal was opened, consecutive sections of 7 μ m thickness were taken using cryofilms. The bone sections on the cryofilm were fixed with adhesive tape on an object slide, air dried and stored at -80°C until further use.

➤ Movat's pentachrome staining

Movat's pentachrome staining allows to distinguish between different tissues due to a combination of staining solutions as mineralized bone or mineralized cartilage appear yellow (Saffron du Gâtinais), hyaline cartilage green (alcian blue), cytoplasm reddish (brilliant crocein acid fuchsine), cell nuclei blue-black (iron hematoxylin) and the surrounding muscles are colored in reddish (brilliant crocein acid fuchsine). The staining procedure was conducted using a protocol already been published [30]. Briefly, bone sections were air dried

for 30 min, fixed with 4 % (v/v) PFA for 10 min and washed with H_2O_{dest} for 5 min. The next step included a pretreatment of 3 min in 3% (v/v) acetic acid, 30 min in alcian blue (1% (w/v) solution in 3% (v/v) acetic acid (pH 2.5)) and a short washing step in 3% (v/v) acetic acid. The sections were subsequently placed in H_2O_{dest} for 5 min and the staining was controlled with a light microscope. Afterwards, the sections were transferred to alkaline ethanol for 60 min and washed in tap water for 10 min, shortly rinsed with H_2O_{dest} and placed for 15 min in Weigert's hematoxylin. The following step comprised a washing in tap water for 15 min, followed by 15 min in crocein scarlet-acid fuchsin, 1 min in 0.5 % (v/v) acetic acid, 20 min phosphotungstic acid and again 1 min in 0.5 % (v/v) acetic acid. The staining process continued with a 100 % (v/v) ethanol series three times for 2 min, before transferring the sections to alcoholic Saffron du Gâtinais for 60 min. At the end, the sections were washed three times in 100 % (v/v) ethanol (2 min each) and put in xylene two times for 2 min. Mounting was performed with Vitro-Clud and sections were covered with a cover slip.

The combination of Von Kossa staining and Movat's pentachrome staining was conducted according the following protocol: air drying (30 min), fixation with 4% (w/v) PFA (10 min), washing step with H_2O_{dest} , 3% (w/v) silver nitrate solution (10 min), washing step with H_2O_{dest} , sodium carbonate formaldehyde solution (2 min), washing step with tap water, 5% (w/v) sodium thiosulphate solution (5 min), washing step with tap water and H_2O_{dest} . Afterwards Movat's pentachrome staining was performed as described above.

Images were taken with a light microscope in a 2.5x magnification and the program Axio-vision.

➤ **TRAP-staining**

For the TRAP-staining bone sections were air dried for 30 min, fixed with 4 % (v/v) PFA for 10 min and washed with H_2O_{dest} for 5 min. Buffer treatment was performed with L(+)-tartaric acid (pH 5) for 15 min followed by an incubation with the TRAP staining solution (L(+)-tartaric acid, naphthol AS-MX phosphate, N,N-dimethylformamide, Fast Red Violet LB Salt; dilution 1:15) for 15 min at 37°C. Sections were washed with H_2O_{dest} before getting counterstained with Mayer's hemalum and mounting with a cover slip. Pictures were taken with a light microscope. As a result, TRAP⁺ cells were stained violet. This method was used for representative images. For quantification and high throughput staining the Acid Phosphatase, Leukocyte (TRAP) Kit was used after immunofluorescence was imaged. Manufacturer's instructions were followed, and pictures were taken with a light microscope.

➤ **Immunofluorescence staining – CD31, Emcn, DAPI**

Immunofluorescence staining was performed as published earlier with minor adaptations [54]. Staining procedure was performed in a wet section staining chamber that allowed for

incubation in the dark after the blocking step. Briefly, bone sections were air dried for 20 min, rehydrated with PBS and blocked with PBS/ 5% (v/v) FCS for 30 min. Primary CD31 antibody (goat anti-mouse) was diluted 1:50 in PBS/ 5% (v/v) FCS/ 0.1% (v/v) Tween[®] 20, added to the sections and incubated for 2 h. After washing with 0.1% (v/v) Tween[®] 20, the secondary antibody (donkey anti-goat A568) was applied in a dilution of 1:500 in PBS/ 5% (v/v) FCS/ 0.1% (v/v) Tween[®] 20 for 1 h. A subsequent washing step was followed by a blocking step with PBS/ 10% (v/v) normal goat serum. Sections were subsequently incubated for 1 h with the primary endomucin (Emcn) antibody (rat anti-mouse endomucin; 1:500). After washing, the secondary antibody (goat anti-rat A647; 1:500) was added for 1 h. A washing step and DAPI (1:500; 1 mg/ml in PBS) finalized the staining. Pictures were taken with a fluorescence microscope BZ 9000 using the DAPI, TexasRed and Cy5 channels. To validate the staining controls with no primary antibodies were carried along the staining procedure (Fig. 10).



Figure 10: Staining controls without primary antibody.

No unspecific binding of the secondary antibodies was observed.

Reproduced from [174].

➤ Immunofluorescence staining – Osx, F4/80, DAPI

As described before bone sections were air dried for 20 min, rehydrated with PBS and blocked with PBS/ 10% (v/v) donkey serum for 30 min. Primary F4/89 (1:400; rat anti-mouse) and primary Osx (1:200; rabbit anti-mouse) were diluted PBS/ 5% (v/v) donkey serum/ 0.1% (v/v) Tween[®] 20, added to the sections and incubated for 1 h. After washing with 0.1% (v/v) Tween[®] 20, the secondary antibodies (donkey anti-rat A594; donkey anti-rabbit A488) were applied in a dilution of 1:500 in PBS/ 5% (v/v) donkey serum/ 0.1% (v/v) Tween[®] 20 for 1 h. A subsequent washing step was followed by a blocking step with PBS/ 10% (v/v) rat, rabbit and donkey serum for 30 min. A washing step and DAPI (1:500; 1 mg/ml in PBS) finalized the staining. Pictures were taken with a fluorescence microscope BZ 9000 using the DAPI, TRITC and GFP channels.

2.2.12 Histomorphometry

➤ Tissue composition

In order to provide quantitative data on tissue appearance, images were analyzed with a self-programmed ImageJ macro (by Mario Thiele, JWI, Berlin). The single analysis steps are depicted in Figure 11. Gained results were normalized to the corresponding area (Tt.Ar, Ec.Ar, Ic.Ar, Pc.Ar). Additionally, the relevant Void area (Vd.Ar) was subtracted before. As

the ACS-L showed a slight yellow color in the Movat's pentachrome staining, the differentiation between mineralized bone and scaffold was possible during image analysis. The nomenclature of the histomorphometry was conducted in accordance with published guidelines [178].

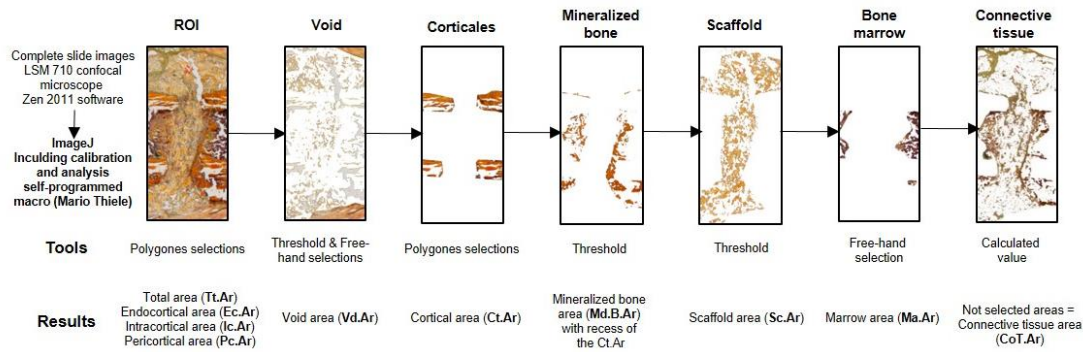


Figure 11: Image analysis pipeline using an ImageJ macro.
Reproduced from [174].

➤ Cell count, vessel formation, macrophages, osteoclasts and TRAP

Images were analyzed with ImageJ as depicted in Figure 12. Measurements were normalized to the Tt.Ar. Mean intensities were also determined with ImageJ with the provided tools. Analysis pipeline was adapted to every staining.

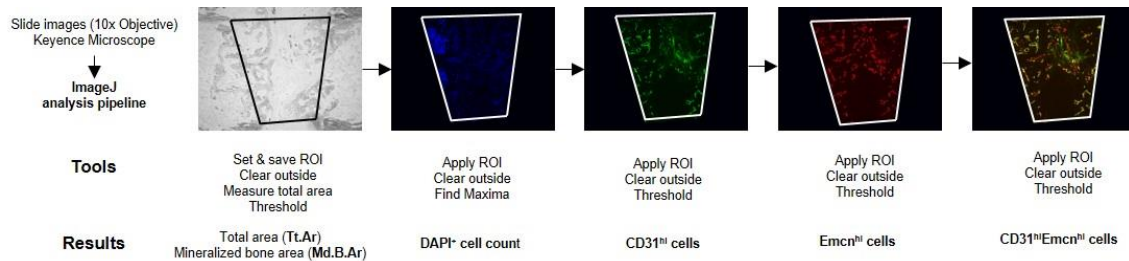


Figure 12: Image analysis pipeline using ImageJ.
Reproduced from [174].

2.2.13 Microarray and qRT-PCR

➤ RNA isolation

The tissue samples from the osteotomy gaps were cryo-pulverized in a grinding bowl under supplementation of liquid nitrogen to avoid thawing of the samples. The cryo-pulverized samples were transferred to a tube and solved in ice-cold TRIzol® (1 ml). In a next step, chloroform (200 µl) was added and the mixture was properly mixed and incubated for 10 min at RT, before centrifugation (10 min, 10,000 x g). The top aqueous phase was collected and mixed with 75% (v/v) ethanol (500 µl). The following isolation steps were performed with RNeasy Mini Kit from Qiagen according to manufacturer's instructions including several

buffer treatment, binding to special columns, washing and centrifugation steps. DNA contamination was removed by a one-step digestion step in between. After finishing the isolation, the RNA concentration was measured with a Nano-Drop Spektrophotometer and stored at -80°C until further use. A small aliquot of each sample was analyzed for the RNA integrity and quality via Agilent 2100 Bioanalyzer (service at Core facility, DRFZ, Berlin).

➤ **Affymetrix GeneChip hybridization and analysis of microarray data**

Affymetrix GeneChip (Mouse Genome 430 2.0 Array) hybridization was performed in the Regine-von-Ramin Laboratory for Molecular Rheumatology at the German Rheumatism Research Center. Complementary DNA (cDNA) was synthesized according to the technical manual *GeneChip Expression Analysis* from Affymetrix. Hybridization was performed using the GeneChip™ Hybridization, Wash, and Stain Kit in a Hybridization Oven 640. Subsequently chips washed and stained in the Fluidics Station FS450 and scanned with the Scanner 3000 7G. The data was analyzed with the Affymetrix GCOS/MAS5 software and transferred to the BioRetis Database (www.bioretis-analysis.de; Thomas Häupl, Charité). The further data processing was performed by Vikram Sunkara, PhD (FU-Berlin) using Python. In a first step, the Affymetrix detection call algorithms was applied while probes with $p > 0.065$ were declared as absent and excluded. For each treatment group two samples were examined via microarray (replicates). All probes which had a signal to noise ratio > 2.0 within the replicates were included. The further analysis was performed using the mean expression of the replicates. Expression data was normalized to the ACS control and probes with an average Log_2 fold change > 1.5 in one of the treatment groups were included.

➤ **qRT-PCR**

To verify the microarray data qRT-PCR was performed for chosen genes. Primers were designed in accordance with the gene sequences used for the probes on the Affymetrix chip and purchased from TIB Molbiol (Berlin, Germany; gene symbol) (Table 4).

cDNA was synthesized with the TaqMan Reverse Transcription Reagents Kit according to the manufacturer's protocol using the Stratagene Mx3000P with the following profile 10 min at 25°C (annealing), 30 min at 37°C (elongation) and 5 min at 95°C (denaturation). For primers and cDNA were diluted to concentration of 250 nM and 4 ng, respectively. RNA-expression analysis was performed using the DyNAmo Flash SYBR Green qPCR Kit and the Stratagene Mx3000P with the following temperature: 7 min at 95°C (initial denaturation); 45 cycles of 5 s at 95°C (denaturation), 7 s at 60°C (primer annealing), 9 s at 72°C (elongation); stepwise increase of the temperature from 50 to 98°C every 30 s (melting curve). For IL-6 and Col9a3 primer annealing was performed at 62°C . Data were normalized to the house keeper gene expression *ACTB* and the ACS only group, using the $\Delta\Delta\text{Ct}$ -method.

Table 4: Primer sequences

Gene	Forward	Reverse	Affymetrix index
<i>Ms4a1</i>	TGGAGTCCCTTTTGCATGAT	GAAACTGGAGATGGGCAAAG	1423226_at
<i>Cfd</i>	CGTACCATGACGGGGTAGTC	ATCCGGTAGGATGACACTCG	1417867_at
<i>HMOX1</i>	GTCCAATGTGGCCTTCTCTC	TTGGTGAGGGAAGTGTGTCA	1448239_at
<i>Hapln1</i>	CAAAGGGAATCAGTTGTCAGG	ACACTGTGCTGGCAGTCTTG	1438020_at
<i>MMP3</i>	AAGATCGATGCTGCCATTTTC	CCACCCTTGAGTCAACACCT	1418945_at
<i>Col10a1</i>	GCAGCATTACGACCCAAGAT	TCTGTGAGCTCCATGATTGC	1422253_at
<i>Cxcl9</i>	AAAATTTTCATCAGCCCTTG	TCTCCAGCTTGGTGAGGTCT	1418652_at
<i>IL-6</i>	GCTGGAGTCACAGAAGGAGTG	ACCACAGTGAGGAATGTCCA	1450297_at
<i>Col9a3</i>	AGGGATCTGCGACACTTCAG	GTAGCCAGCCACTGTCCATT	1460734_at
<i>Cxcl3</i>	CAACGGTGTCTGGATGTGTC	AGCCAAGGAATACTGCCTCA	1438148_at
<i>PECAM-1</i>	TGCAGGAGTCCTTCTCCACT	ACGGTTTGATTCCACTTTGC	-
<i>Emcn</i>	CAGTGAAGCCACTGAGACCA	ACGTCACCTTTTGGTCGTTCC	-
<i>ACTB</i>	AGCCATGTACGTAGCCATCC	CTCTCAGCTGTGGTGGTGAA	-

➤ Comparing microarray data to qRT-PCR results

For validation of microarray data with the qRT-PCR results, microarray data had to be normalized to *ACTB*. Therefore, a commonly used probe set was taken (1419734_at) and normalization was performed. Afterwards, corresponding data pairs were plotted against each other using reciprocal values and examine the correlation.

2.2.14 Statistical analysis

Statistical analysis was carried out with GraphPad Prism V.5 software. All values from *in vitro* assays were expressed as the mean \pm SD or SEM when measured in > duplicates and all values from animal experiments are depicted as median \pm ranges (box and whiskers plot). One and two-way ANOVA were performed where appropriate including Bonferroni's multiple comparison test to distinguish between groups and time points. Mann-Whitney U-test and Wilcoxon-signed rank test were used in case of lack of Gaussian distribution that was tested before via Kolmogorov-Smirnov test. A *p-value* <0.05 was considered as statistically significant. In some cases, statistical trends are indicated with a hashtag (#) when biological relevant. Power analysis was performed prior to animal tests by a statistician to determine the animal number with the results to use a minimum of 6 animals to attain worthwhile results and was provided in detail with the animal experiment application. Image analysis was blinded for treatment groups.

CHAPTER 3: Results

3.1 Characterization of bone marrow derived hMSCs

Since the *in vitro* studies were conducted with bone marrow derived hMSCs, it was essential to apply a standardized protocol to clearly characterize the isolated cells for their mesenchymal origin and stem cell character before use. Characterization was performed during passage 3, failure caused exclusion of these cells. The isolated hMSCs were tested for plastic adherence, several surface markers and the differentiation potential in at least two directions (here adipogenic and osteogenic) following the international recommendations [179]. All used hMSCs exhibited the positive surface markers CD13, CD44, CD90 and CD105 and were negative for CD45, CD14 and CD19 (Fig. 13A, B). Additionally, they showed the ability to differentiate into different mesenchymal lineages such as adipogenic and osteogenic (Fig. 13C, D).

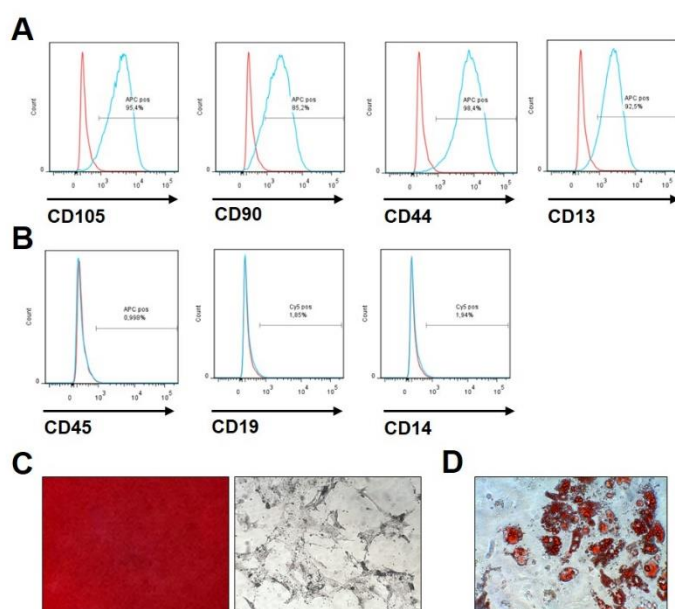


Figure 13: Characterization of hMSCs.

(A) Bone marrow derived hMSCs exhibit CD105, CD90, CD44, and CD13 expression (B) but do not express CD45, CD19, and CD14. (C) They are able to differentiate into the osteogenic lineage as shown by Alizarin red and ALP staining and (D) the adipogenic lineage as shown by Red oil staining.

As the donor's age, comorbidities and medications can impact the hMSC behavior *in vitro*, donor-related information was collected carefully and are summarized in Materials part (Chapter 2.1.1). Primary hMSCs were isolated from bone marrow that was obtained during total hip endoprosthesis. During the timespan of the work, the expansion protocol of hMSCs was changed in order to further optimize the proliferation capacity (not part of this study). Therefore, the used hMSCs in this work can be divided into two groups depending on the expansion medium (normal medium 1 – NM 1 vs. normal medium 2 – NM 2) (Chapter 2.1.3). The first experiments on the effect of glucocorticoids (GCs) on the osteogenic differentiation and the DFO/MIF titration were performed using group NM 1 while the *in vitro* experiments on the different scaffolds ACS-L and ACS-H were performed with hMSCs expanded in NM 2 while the osteogenic medium composition (OM 1 vs. OM 2) was adapted accordingly. In

the NM 1 group 11 donors were included, 7 females and 4 males with an age range of 48 – 82 and a mean age of 67.6 ± 11 years. The second NM 2 group consisted of 10 females and 6 males with an age range of 46 – 86 and a mean age of 71.3 ± 12 years. The exclusive reason for the TEP was hip osteoarthritis (OA) and all donors were treated with non-steroidal anti-inflammatory drugs (NSAIDs), age-appropriate further medications (e.g. blood thinner, antihypertensive) and only suffered from comorbidities that did not alter the quality of the bone marrow.

3.2 The effect of hypoxia or HIF-stabilizers on the inhibition of hMSC calcification by GCs in an *in vitro* setting

3.2.1 hMSC calcification was inhibited dose-dependent by GCs *in vitro*

To test and verify the effect of GCs on *in vitro* calcification of hMSCs as important part of osteogenesis, different concentrations of Dex (10^{-3} - 10^{-8} M) were applied to OM 1. In addition, cells were incubated under either normoxic (app. 18% O_2) or hypoxic (1% O_2) conditions. The calcification process was analyzed using a quantifiable Alizarin red staining method after 14, 21 and 28 days (Fig. 14).

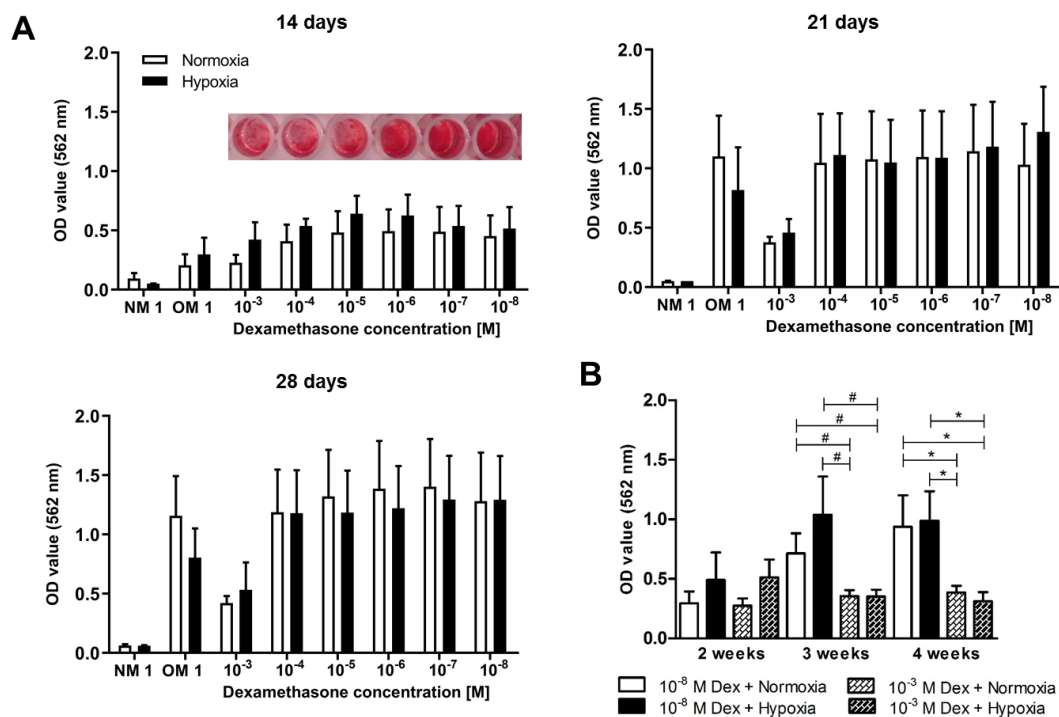


Figure 14: *In vitro* hMSC calcification - Titration of Dex concentrations revealed significant reduction for 10^{-3} M Dex which was further used for the titration studies with MIF and/or DFO.

(A) Application of Dex in different concentrations dose-dependently inhibited calcification (quantified Alizarin red staining) after 14 days which was not significantly counteracted by cultivation under hypoxia. (B) Application of Dex in high concentrations (10^{-3} M) to the OM 1 significantly inhibited calcification after 21 and 28 days compared to 10^{-8} M Dex which was only slightly counteracted by cultivation under hypoxia ($n = 5-7$; > triplicates). Data are shown as mean \pm SEM; Mann-Whitney U-test was used to determine the statistical significance; p -values are indicated with # $p < 0.07$; * $p < 0.05$.

A concentration-dependent inhibitory effect of Dex on the calcification was detectable after 14 days (Fig. 14A). The effects could be slightly antagonized by cultivation under hypoxia at day 14, but not at day 21 and 28. The treatment with 10^{-3} M Dex caused a long-lasting decrease in the calcification after 21 and 28 days (Fig. 14A). Comparing the 10^{-3} M Dex treatment group with the 10^{-8} M Dex treatment group, a reduction could be found after 21 days ($p < 0.07$) which became significant after 28 days ($p < 0.05$) (Fig 14B).

3.1.2 HIF-stabilizers diminished the inhibiting effect of GCs on hMSC calcification

Since the aim of the study was to evaluate the potential of MIF and DFO as supporting factors for bone regeneration, *in vitro* studies were performed to determine useful concentrations. Therefore, the application of high concentrations of Dex (10^{-3} M) was used as technical *in vitro* model to strongly induce delayed calcification as described in the previous chapter. Several concentrations of MIF and DFO alone and in combination were applied onto the hMSCs that were incubated with OM 1 and Dex 10^{-3} M for 21 and 28 days while as positive control OM 1 with 10^{-8} M was carried along on every 96-well plate for every hMSC donor. The application of DFO alone revealed significant increases in calcification after 28 days for 62.5, 125, 250 and 500 μ M which was also observed for 250 and 500 ng/ml MIF (Fig. 15A). The combination of MIF and DFO led to a significant increase in calcium deposition at 28 days for 125 μ M DFO + 50 ng/ml MIF and 125 μ M DFO + 100 ng/ml MIF (Fig. 15B). A double normalization to both controls (Dex 10^{-3} M and 10^{-8} M) yielded a 52.2% to 86.7% increase of the MIF/DFO combination towards the Dex 10^{-3} M control compared to a 40.5% to 45.9% or -10% to 10.5% increase for DFO or MIF alone, respectively, being significantly lower than the Dex 10^{-8} M control ($0.05 > p > 0.001$) (Fig. 16).

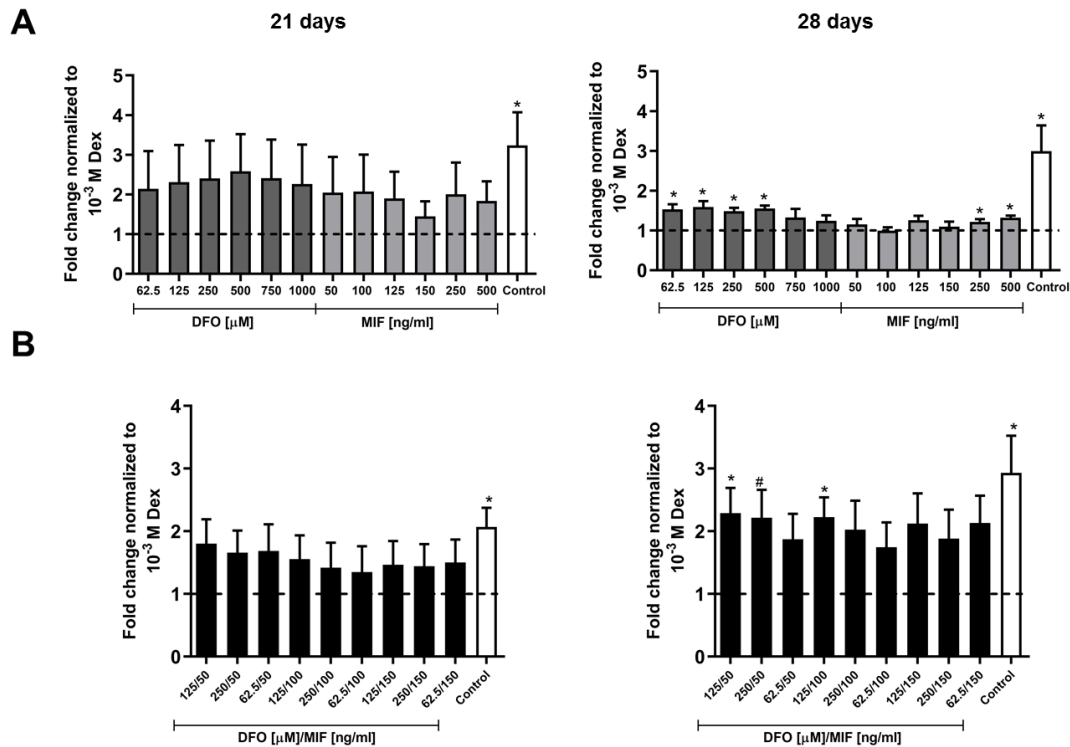


Figure 15: *In vitro* model simulating the inhibition of hMSC calcification via high concentration GC treatment showing the potential of HIF-stabilizers to counteract.

(A) The application of different concentrations of MIF and DFO alone to OM 1 + Dex 10^{-3} M showed a potential counteraction which was partly significant after 28 days of cultivation especially under DFO treatment. (B) The application of different concentrations combinations of MIF or DFO to OM 1 + Dex 10^{-3} M yielded a significant counteraction for two concentrations after 28 days. Data are normalized to Dex 10^{-3} M, compared to the control (OM 1 + Dex 10^{-8} M; white bar) ($n = 5-6$; > triplicates) and shown as mean \pm SEM; One sample t-test was used to determine statistical significance towards the hypothetical value of 1 (OM 1 + Dex 10^{-3} M). p -values are indicated with $0.07 > \#p > 0.05$; $*p < 0.05$.

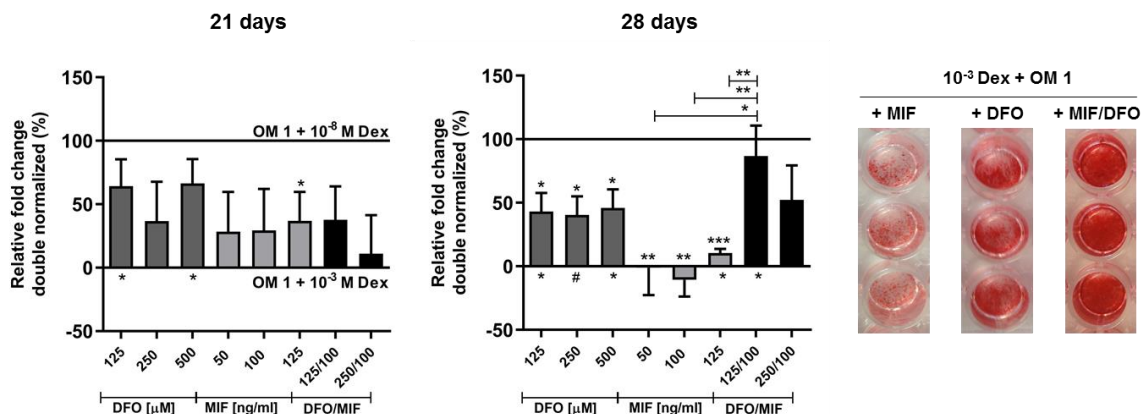


Figure 16: Double normalization to display the changes as percentage towards the Dex 10^{-3} M and 10^{-8} M demonstrate the superiority to combine MIF and DFO.

Comparing the potential of MIF and DFO alone and in two promising combinations to enhance calcification, data were double normalized to both controls (OM 1 + Dex 10^{-3} M = 0%; OM 1 + Dex 10^{-8} M = 100%) ($n = 5-6$). Data are shown as mean \pm SEM. Asterisks above and below the bars indicate significant difference towards the respective control as determined by one sample t-test. Mann-Whitney U-test was used to determine significant differences between treatment groups. p -values are indicated with $0.07 > \#p > 0.05$; $*p < 0.05$; $**p < 0.01$; $***p < 0.001$. Exemplary images of Alizarin red staining before quantification showing the counteraction via DFO and MIF alone and in combination.

In order to examine the cell cytotoxicity, the LDH-release was determined 24 h and 72 h after applying the OM 1. Therefore, a significant increase of LDH in the supernatant was measured after 72 h in the groups treated with Dex 10^{-3} M ($p < 0.001$) while the longer application of MIF and/or DFO seems to not further impact the cellular LDH-release (Fig. 17).

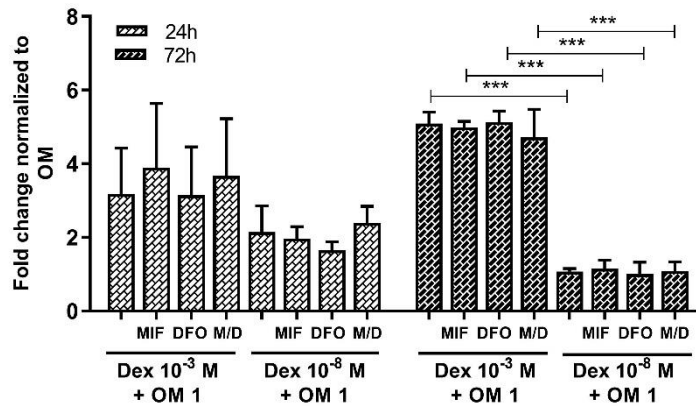


Figure 17: LDH-release indicated impact of Dex 10^{-3} M on cell survival.

LDH-release was measured at 24 h and 72 h for different concentrations of Dex and supplementation of MIF and/or DFO ($n = 3$). The application of Dex 10^{-3} M to the OM 1 showed a significant higher LDH-release after 72 h compared to the controls which was not further altered by application of MIF and/or DFO. Data are shown as mean \pm SEM; One-way ANOVA was used to determine statistical significance; p -values are indicated with *** $p < 0.001$.

3.3 Identification of a suitable scaffold for local delivery of MIF and DFO into the fracture gap

3.3.1 ACS-L and ACS-H contained high contents of collagens and further potential bone regeneration-linked proteins

Two clinically approved and commercially available bovine absorbable collagen (Col) I scaffolds known under the trademark Helistat[®] (ACS-H) – used to apply recombinant human bone morphogenetic protein-2 (rhBMP-2) in the clinics – and Lyostypt[®] (B. Braun Melsungen AG; ACS-L) – commonly used in research and oral surgery, were tested for their suitability as delivery system within this study. As there is nothing known on the production and composition of those two ACSs due to the companies' secrets, the first step was to clarify the protein composition of ACS-L and ACS-H. Therefore, scaffold protein extracts were analyzed by high-resolution liquid chromatography mass spectrometry (LC-MS/MS) in cooperation with Dr. Marieluise Kirchner (BIH Proteomics Core Facility). The intensity-based absolute quantification (iBAQ) algorithm was used to determine the protein abundance which is represented as the percentage of the sum of all protein iBAQ intensities. Since the preparation can strongly influence the outcomes, two different preparation protocols – without (Method 1) or with (Method 2) cryo-pulverizing before guanidine hydrochloride treatment were compared. Only robust protein identifications (minimum of 3 peptides identified; detection in all 3 replicates) were used for further analyses. Table 5 and 6 list all identified proteins grouped by biological function and properties. Collagen type I, alpha 1 (COL1A1) and Collagen type I, alpha 2 (COL1A2) chains were identified as the two most abundant proteins in ACS-L and ACS-H. In greater detail, in ACS-L, COL1A1 covers 49.7% and COL1A2 covers 33.2% of total protein content using Method 1 (Method 2: 44.8% COL1A1 and 20.8% COL1A2), whereas in ACS-H COL1A1 covers 23.5% and COL1A2 covers 31.7% of total protein content using Method 1 (Method 2: 42.0% COL1A1 and 47.4% COL1A2). Collagen 6 alpha-1-3 chains as other collagen species were present in both scaffolds (0.2 - 3.6%). Membrane and cytoskeleton proteins, enzymes and histones are only identified in ACS-L with different abundance levels ranging from 0.003% to 11.6% depending on the extraction methods. Several small leucine-rich proteoglycans (SLRP) were detected in both scaffolds. Decorin (DCN) revealed high abundances levels in ACS-L (0.5% - 8.7%) which was also the case for annexins (ANXA 1, 2, 5) (0.008 - 0.31%). Fibromodulin (FMOD) was most prominent in ACS-H (29% - 2.9%) while osteoglycin (OGN) was found only in low percentages in both scaffolds (0.1 - 0.48%).

Table 5: List of identified proteins from mass spectrometric measurements – Part 1 [174].

Protein Abbreviation and Name	ACS-L		ACS-H		
	Protein Abundance in % (Mean \pm SD)		Protein Abundance in % (Mean \pm SD)		
	Method 1	Method 2	Method 1	Method 2	
<u>Collagens</u>					
COL1A1	Collagen 1A1	49.72 \pm 7.24	44.84 \pm 3.75	23.49 \pm 2.70	41.94 \pm 3.99
COL1A2	Collagen 1A2	33.15 \pm 8.03	20.76 \pm 5.01	31.66 \pm 12.82	47.43 \pm 5.46
COL2A1	Collagen 2A1	-	-	0.04 \pm 0.03	-
COL3A1	Collagen 3A1	6.13 \pm 1.52	0.46 \pm 0.009	0.05 \pm 0.02	-
COL5A1	Collagen 5A1	0.04 \pm 0.02	-	-	-
COL6A1	Collagen 6A1	0.47 \pm 0.06	1.35 \pm 0.35	1.61 \pm 0.12	0.82 \pm 0.33
COL6A2	Collagen 6A2	0.28 \pm 0.05	0.82 \pm 0.05	3.27 \pm 0.67	0.71 \pm 0.29
COL6A3	Collagen 6A3	0.22 \pm 0.07	1.14 \pm 0.17	3.58 \pm 1.46	0.28 \pm 0.07
COL12A1	Collagen 12A1	-	0.15 \pm 0.004	0.07 \pm 0.02	-
COL14A1	Collagen 14A1	0.002 \pm 0.001	-	-	-
<u>Membrane & Cytoskeleton proteins</u>					
ANXA1	Annexin 1	0.07 \pm 0.06	-	-	-
ANXA2	Annexin 2	0.31 \pm 0.14	-	-	-
ANXA5	Annexin 5	0.008 \pm 0.004	-	-	-
TUBA1D	Tubulin alpha-1D chain	0.19 \pm 0.01	0.20 \pm 0.08	-	-
TUBB5	Tubulin beta-5 chain	0.05 \pm 0.02	0.28 \pm 0.16	-	-
MSN	Moesin	0.005 \pm 0.007	-	-	-
ACTB	Actin beta	0.48 \pm 0.33	1.09 \pm 0.42	-	-
<u>Small leucine-rich proteoglycans</u>					
VIM	Vimentin	0.05 \pm 0.02	0.21 \pm 0.13	0.19 \pm 0.13	-
DCN	Decorin	0.52 \pm 0.79	8.69 \pm 2.11	1.31 \pm 0.6	-
FMOD	Fibromodulin	0.02 \pm 0.02	0.14 \pm 0.10	29.00 \pm 8.98	2.86 \pm 0.49
OGN	Osteoglycin	0.10 \pm 0.04	0.48 \pm 0.31	0.14 \pm 0.06	-
ASPN	Asporin	0.05 \pm 0.02	-	-	-
ACTN1	Actinin alpha 1	0.04 \pm 0.03	0.02 \pm 0.02	-	-
DSTN	Destrin	0.05 \pm 0.04	-	-	-
PRELP	Prolargin	0.12 \pm 0.02	0.10 \pm 0.08	0.82 \pm 0.14	0.22 \pm 0.07

For each protein the mean protein abundance and standard deviation (n=3) is shown. Bold numbers underline obvious differences. Method 1 = direct extraction in guanidine hydrochloride; Method 2: Cryo-pulverization before guanidine hydrochloride treatment.

Table 6: List of identified proteins from mass spectrometric measurements – Part 2 [174].

Protein Abbreviation and Name	ACS-L		ACS-H		
	Protein Abundance in % (Mean ± SD)		Protein Abundance in % (Mean ± SD)		
	Method 1	Method 2	Method 1	Method 2	
Enzymes					
ATP5B	ATP synthase subunit beta	0.004 ± 0.00	-	-	-
PKM2	Pyruvate kinase isozymes M2	0.03 ± 0.03	-	-	-
PNP	Purine nucleoside phosphorylase	-	0.14 ± 0.08	-	-
Others					
TGFBI	Transforming growth factor beta induced	0.003 ± 0.002	-	-	-
CLTC	Clathrin heavy chain	0.009 ± 0.002	0.02 ± 0.01	-	-
HNRNPK	Heterogeneous nuclear ribonucleoprotein K	0.006 ± 0.003	-	-	-
EHD2	EH domain-containing protein 2	0.03 ± 0.005	-	-	-
MYH11	Myosin heavy chain 11	0.08 ± 0.07	-	0.008 ± 0.003	-
SRPX	Sushi repeat-containing protein	0.08 ± 0.02	0.11 ± 0.08	-	-
RPS16	Ribosomal protein S16	-	0.12 ± 0.05	-	-
Histones					
HIST2H2BE	Histone Cluster 1 H2 Family Member BE	-	0.063 ± 0.03	0.22 ± 0.17	-
HIST1H4J	Histone Cluster 1 H4 Family Member J	2.67 ± 0.53	11.59 ± 7.04	-	-
HIST2H3D	Histone Cluster 2 H3 Family Member D	0.58 ± 0.25	2.51 ± 0.53	0.60 ± 0.25	-

For each protein the mean protein abundance and standard deviation (n=3) is shown. Bold numbers underline obvious differences. Method 1 = direct extraction in guanidine hydrochloride; Method 2: Cryo-pulverization before guanidine hydrochloride treatment.

In summary, proteomics analysis revealed several proteins beside collagens especially in the ACS-L, but also in the ACS-H which can influence the bone healing process.

Based on literature search, potential bone-regeneration linked proteins were selected from the identified proteins:

- DCN, FMOD and OGN that play an important role in e.g. extracellular matrix (ECM) fibrillation, formation and degradation [180];
- ANXA 1, 2 and 5 are components of cell membranes [181, 182];
- Sushi repeat-containing protein (SRPX), a chondroitin sulfate proteoglycan, is not well known but involved in angiogenesis [183];
- Heterogeneous nuclear ribonucleoprotein K (HNRNPK) as repressor of osteocalcin expression is of great interest for callus mineralization [184].

Since the ACSs are bovine origin, the clarification of species differences was of great interest with regard to animal experimental and translational outcomes. Therefore, the selected proteins were examined for sequence homology (BLAST alignment for *Bos taurus* vs. *Mus musculus* and *Bos taurus* vs. *Homo sapiens*; Table 7). Alignment analysis showed 100% query cover for DCN, FMOD, ANXA1, 2, 5 and SRPX. OGN and HNRNPK showed a query cover $\geq 98\%$. These results indicate a possible functional impact on murine as well as human cells.

Table 7: List of query cover of potential bone regeneration-linked proteins [174].

Selected Proteins	Alignment <i>Bos taurus</i> against <i>Mus musculus</i>	Alignment <i>Bos taurus</i> against <i>Homo sapiens</i>
	Query cover	Query cover
Decorin	100%	100%
Fibromodulin	100%	100%
Osteoglycin	99%	99%
Annexin 1	100%	100%
Annexin 2	100%	100%
Annexin 5	100%	100%
Sushi repeat-containing protein	100%	100%
Heterogeneous nuclear ribonucleoprotein K	98%	98%

3.3.2 ACS-H and ACS-L showed structural differences

An additional observation was the form-stability of ACS-H. In contrast, the ACS-L was constricted and rounded with a reduction in the diameter of $48\% \pm 10\%$ compared to the ACS-H ($n = 4$) (Fig. 18).

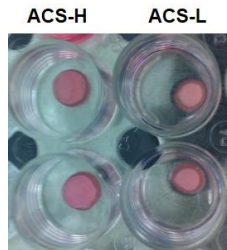


Figure 18: Macroscopic images of the ACS-H and ACS-L after applying medium revealing a form-instability of the ACS-L.

The initial size of the scaffolds was standardized by using a 8 mm diameter punching tool. Reproduced and modified from [174].

In order to analyze differences in the structure and accessibilities for cells to invade into the scaffold, electron microscopic images were examined. Dry ACS-L exhibit the common collagen fiber structure omitting porous-like structures allowing cell invasion (Fig. 19). The same was observed for ACS-H showing more layer-like than fibrillary structures (Fig. 20). Cellular colonization on the surface and matrix production was vaguely perceptible when applying hMSCs onto the scaffolds for 3 days and comparing to medium control (Fig. 19, 20).

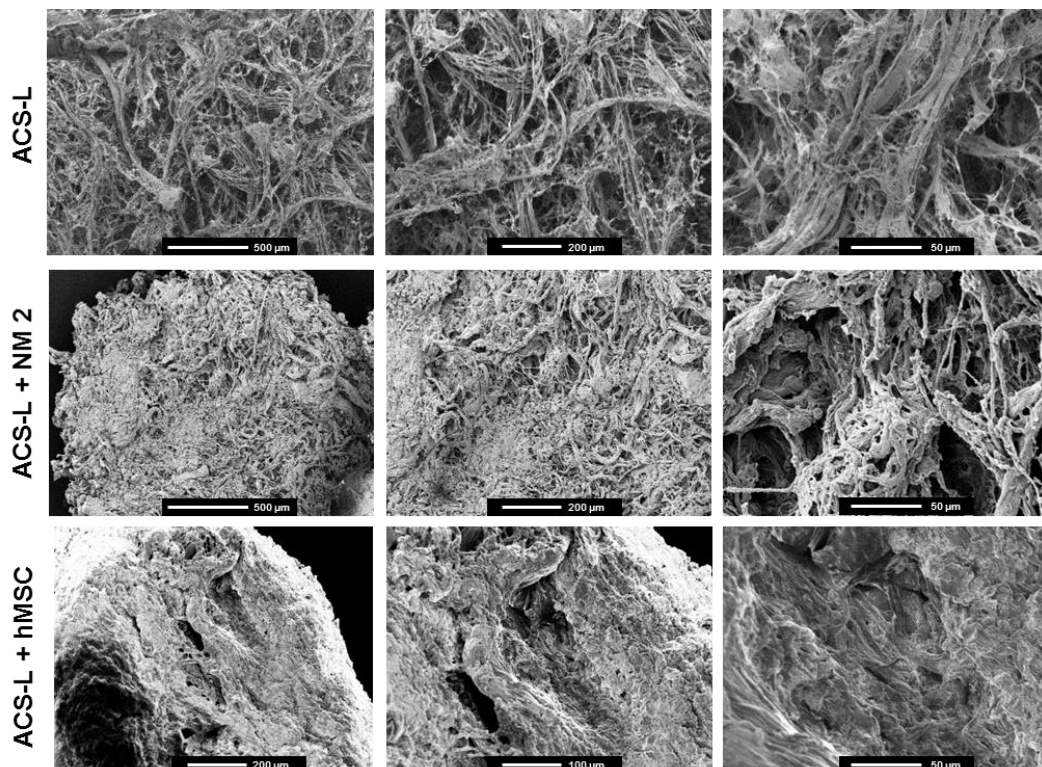


Figure 19: Structural evaluation of ACS-L using electron microscopy showing collagen fiber structures and cell matrix production.

Dry and untreated as well as medium-treated and hMSC-treated ACS-L (3 days) were analyzed via electron microscopy using a Jeoul JCM-6000 Plus Neo Scope™. The collagen fiber structure can be clearly seen in the untreated ACS-L revealing also porous-like structures which decreases after medium-treatment and are nearly missing when additionally applying cells indicating invasion. Exemplary images of $n = 3$. Scale bars show 500, 200, 100 or 50 μm as indicated in the images. Reproduced and modified from [174].

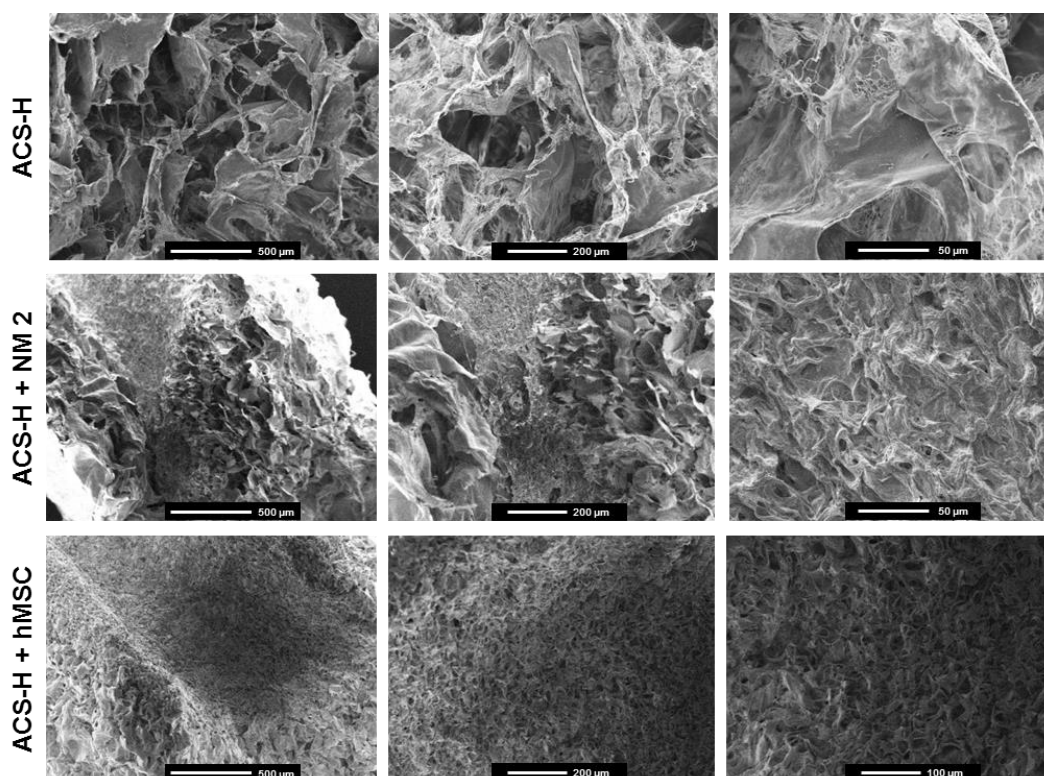


Figure 20: Structural evaluation of ACS-H using electron microscopy revealing a layer-like structures and little differences by cell application.

Dry and untreated as well as medium-treated and hMSC-treated ACS-H (3 days) were analyzed via electron microscopy using a Jeoul JCM-6000 Plus Neo Scope™. The strong layer-like structure is barely changed by medium- and or cell-treatment. Exemplary images of $n = 3$. Scale bars show 500, 200, 100 or 50 μm as indicated in the images. Reproduced and modified from [174].

3.3.3 ACS-H inhibited *in vitro* calcification of hMSCs while osteogenic gene expression was not affected

In a next step, an *in vitro* co-culture assay was performed to evaluate the functional effect of ACS-H or ACS-L on osteogenic differentiation in hMSCs. Therefore, osteogenic medium (OM 2) was applied for 21 days measuring the calcium deposition by quantification of Alizarin red staining. A significant decrease in calcium deposition was observed by co-cultivating hMSCs with ACS-H compared to co-cultivation with ACS-L ($p < 0.001$) and medium control (OM 2) ($p < 0.001$) (Fig. 21).

To evaluate the potential effect on the osteogenesis itself, osteopontin (OPN) was stained in the differentiated hMSCs after 14 days of co-cultivation with ACS-L or ACS-H as described above. In addition, RNA expression of two osteogenic markers – Runt-related transcription factor 2 (*RUNX2*) and Alkaline phosphatase (*ALP*) were analyzed after 7 days of co-cultivation. Control cells treated with OM 2 and hMSCs co-cultivated with ACS-L or ACS-H showed a higher amount of OPN per cell ($p = 0.03-0.06$) compared to the NM control indicating an osteogenic induction under all conditions (Fig. 10A). This was also supported by the significant upregulation of *RUNX2* and *ALP* expression for the OM 2 control ($p =$

0.02; $p = 0.002$) (Fig. 7B). In the ACS groups *ALP* was significantly increased towards the NM control (ACS-L: $p = 0.008$; ACS-H: $p = 0.02$) while *RUNX2* was not significantly induced. No differences between groups were found (Fig. 22).

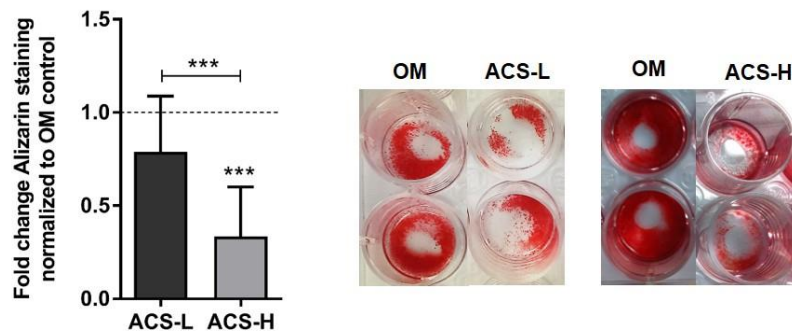


Figure 21: *In vitro* studies on hMSC calcification indicating a strong inhibiting effect of ACS-H. hMSCs were co-cultivated for 14 to 21 days with either ACS-H or ACS-L and osteogenic medium (OM 2). The Alizarin red staining was quantified and measured (wavelength = 562 nm). Co-cultivation with ACS-H significantly reduced calcification of hMSCs compared to the ACS-L co-cultivation and osteogenic control. Data are shown as mean \pm SEM (> 2 duplicates per experiment and hMSC donor) for $n = 9$ in three independent experiments. Mann-Whitney U-test and Wilcoxon signed ranked test were used to determine the statistical significance between groups and to the control, respectively; p -values are indicated with *** $p < 0.001$. Exemplary images show Alizarin red staining of different co-culture assays supporting the quantitative data. The light area in the middle of the well indicates the placement of the scaffold which was kept cell-free to exclude shear stress induced reactions by the hMSCs. Reproduced and modified from [174].

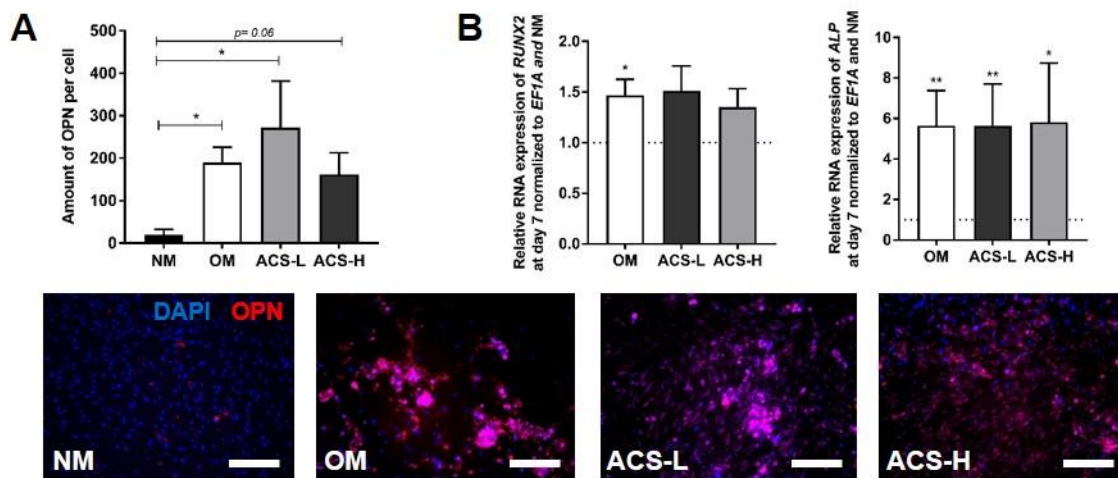


Figure 22: *In vitro* studies on hMSC osteogenesis revealed no effects of ACS-L or ACS-H. hMSCs were co-cultivated for 14 (OPN) or 7 (RNA) days with either normal medium (NM), ACS-H or ACS-L and/or osteogenic medium (OM 2). (A) Osteopontin (OPN) was stained via immunofluorescence and quantified via ImageJ as amount per cell. Cell number was determined via DAPI. Significant higher amounts of OPN in cultures treated with OM 2 indicate osteogenic induction. Data are shown as mean \pm SEM (> 4 images were evaluated per hMSC donor and condition) for $n = 4$. Mann-Whitney U-test were used to determine the statistical significance between groups; p -values are indicated with *** $p < 0.001$. Exemplary images show DAPI (blue) and OPN (red) staining in the different groups. Scale bars indicated 200 μ m. (B) RNA expression of *RUNX2* and *ALP* was normalized to the housekeeper (*EF1A*) and the NM control revealing an upregulation of both markers in OM 2 treated hMSCs. Co-cultivation with ACS-L and -H seemed to influence *RUNX2* expression rather than *ALP* expression. Mean \pm SEM (duplicates) for $n = 8$ in two independent experiments. Wilcoxon signed ranked test was used to determine the statistical significance towards the NM control (hypothetical value = 1); p -values are indicated with * $p < 0.05$ and ** $p < 0.01$. Reproduced and modified from [174].

3.3.4 ACS-H increased cell cytotoxicity and induced TNF α release from whole blood assay

In order to evaluate the suitability of the scaffolds to be colonized by cells, hMSCs were resuspended in NM 2, applied on to the scaffold and cultivated for 7 days. The subsequent LIVE/DEAD staining was quantified via ImageJ and revealed significant lower amounts of Calcein-AM⁺ cells (LIVE; $p < 0.001$) compared to the monolayer control (Fig. 23A). An increased number of dead (EthD1⁺) cells for the ACS-H was shown when compared to the control ($p = 0.02$). There was no significant difference between ACS-L and ACS-H ($p = 0.21$) (Fig. 23A). To further investigate the cell cytotoxicity, a LDH assay was conducted at day 3, 7, and 14 resulting in significant lower levels of LDH release in the presence of ACS-L compared to the control at day 3 ($p < 0.05$) while ACS-H caused a significant higher release of LDH at day 3 and day 7 compared to ACS-L ($p < 0.001$; $p < 0.05$) and the OM 2 control on day 7 ($p < 0.05$), respectively (Fig. 23B). The immunogenicity of the scaffolds was tested by a whole blood co-cultivation assay. TNF α release in the supernatant was measured via ELISA after 20 h. As a result, a significant higher TNF α release was observed in the ACS-H and ACS-L group compared to the control group (both $p < 0.001$) (Fig. 23C). Moreover, the ACS-H group revealed a significant higher TNF α release compared to the ACS-L group ($p < 0.001$). In addition, the ACS-L group showed a significantly lower TNF α release when compared with the positive control (LPS treatment) ($p < 0.001$) which was also the case for the negative control ($p < 0.001$) (Fig. 23C). In contrast, the results from the whole mouse blood assay revealed a significant lower TNF α release induce by ACS-L and ACS-H compared to the positive control ($p < 0.05$; $p = 0.06$) (Fig. 23D).

As the *in vitro* results revealed a negative effect of the ACS-H with regard to calcification, cell cytotoxicity and immunogenicity, which surpassed the ACS-L results, the latter was chosen for the *in vivo* study.

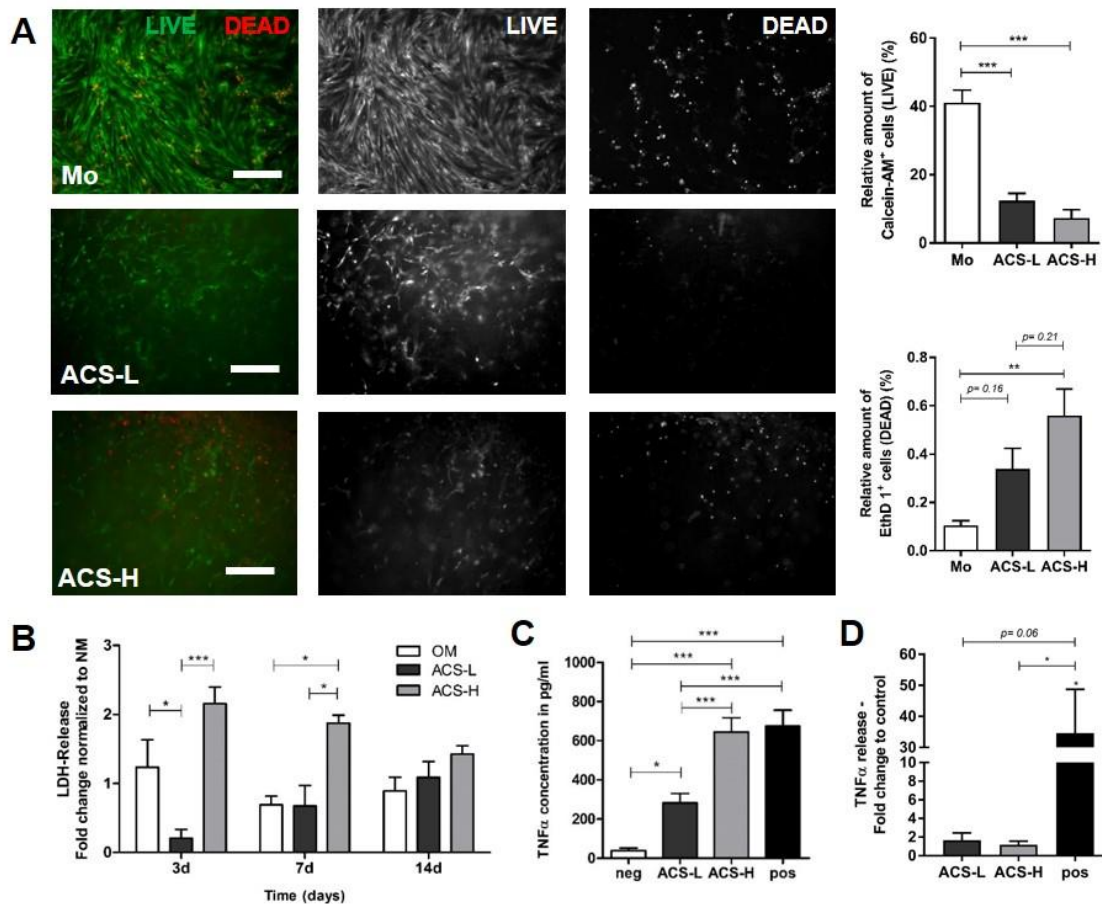


Figure 23: Cell cytotoxicity and immunogenicity showed negative effects of ACS-H on cell survival and TNF α release – cell vitality was also affected.

(A) hMSCs and medium were applied on to the scaffolds and cultivated for 7 days before performing LIVE/DEAD staining. As control hMSCs in monolayer were stained. Green and red colors discriminated between living and dead cells, respectively, showing more red stained cells in the ACS-H group than in the ACS-L group. This was also supported by quantification of Calcein-AM⁺ and EthD1⁺ cells via ImageJ. Representative images are shown. Scale bars representative for each row show 200 μ m. (B) LDH-assay was conducted to cover cell cytotoxicity over 14 days using supernatant from the osteogenic co-cultivation assays indicating a strong cell toxic effect of ACS-H compared to ACS-L at day 3 and 7. Data are shown as mean \pm SEM (triplicates) for $n = 3-6$. Two-way ANOVA was used to determine statistical significances between groups; p -values are indicated with $*p < 0.05$ and $***p < 0.001$. (C) A whole human blood co-cultivation assay was conducted for 20 h. Supernatants were used for TNF α ELISA. Both scaffolds induced TNF α release while the effect of ACS-H was significant stronger. Low control = blood + RPMI medium and the high control = LPS. Data are shown as mean \pm SEM (duplicates) for $n = 6$ in two independent experiments. One-way ANOVA was used to determine statistical significance between groups; p -values are indicated in the graphs with $*p < 0.05$ and $***p < 0.001$. (D) A whole mouse blood co-cultivation assay was performed for 20 h. Supernatants were used to measure TNF α release. In contrast to the results from the human whole blood assay, TNF α was significantly lower released compared to the positive control. Data are shown as mean \pm SEM (duplicates) for $n = 3$. One-way ANOVA was used to determine statistical significance between groups; p -values are indicated in the graphs with $*p < 0.05$. Reproduced and modified from [174].

3.3.5 ACS-L delayed mineralized callus formation *in vivo*

Based on the previous *in vitro* results, ACS-L was chosen to be tested *in vivo* as a potential delivery system to examine later the effect of MIF and DFO on the fracture healing. Thus, ACS-L was applied in a mouse-osteotomy-model with an osteotomy gap of 0.7 mm and a stable fixation via external fixator in 12 weeks old female C57BL/6N mice. As control, the gap was left empty. To measure the new formed mineralized bone in the gap, *ex vivo* quantitative μ CT analysis was performed 14 and 21 days after osteotomy. The total volume (TV) remained comparable between the two groups and over time indicating no differences in the callus size itself (Fig. 24A). In contrast, the bone volume (BV) and the bone volume fraction (BV/TV) were significantly decreased in the ACS-L group after 14 days in comparison to the empty control group ($p = 0.026$ and $p = 0.001$, respectively) (Fig. 24B, D). The BV and BV/TV were significantly increased within the ACS-L groups over time ($p = 0.015$ and $p = 0.021$, respectively) underlining the delayed mineralization process. Both groups showed comparable mineralization quality as verified by the significant increase of the bone mineral density (BMD) ($p = 0.008$; $p = 0.006$) (Fig. 24E).

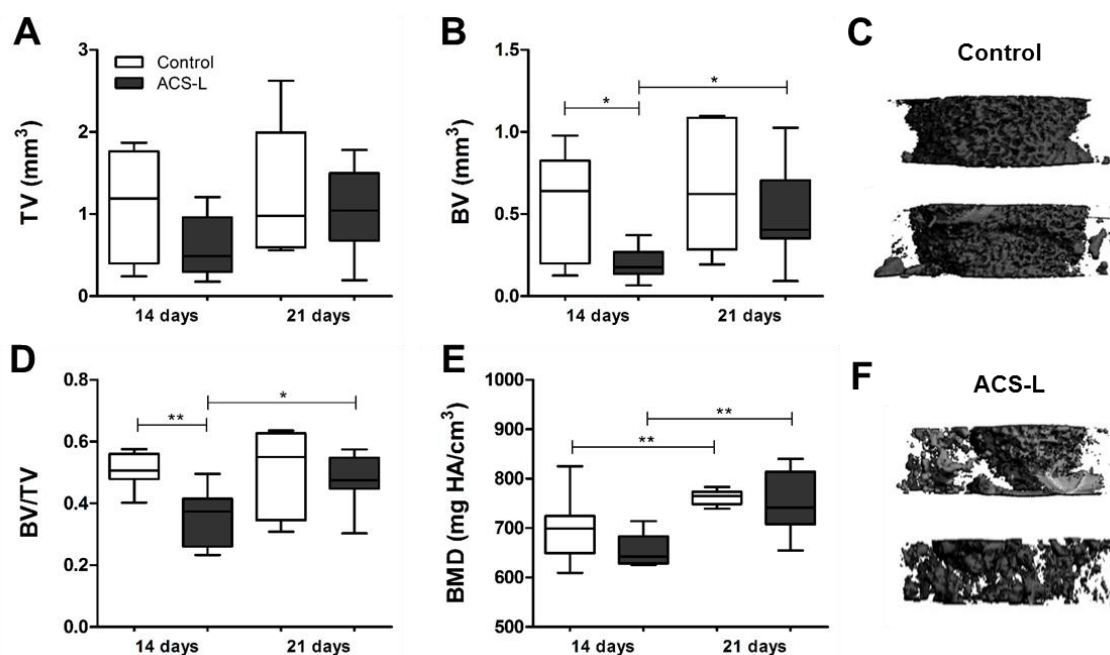


Figure 24: Ex vivo μ CT analysis 14 and 21 days after osteotomy revealed effect of ACS-L on callus mineralization.

Female C57BL/6N mice underwent osteotomy of the femur applying either NaCl (=control) or PBS-soaked ACS-L within the gap (0.7 mm). 14 and 21 days after osteotomy quantitative *ex vivo* μ CT analysis was performed using a Viva40 micro-CT scanning 191 slices. Post-processing included manually adjustment of the VOI (excluding the cortices) and automatic 3D callus tissue analysis (fixed 240 mg HA/cm³). Analyzed parameters were the total volume (TV) (A), the bone volume (BV) (B), the bone volume fraction (BV/TV) (D) and the bone mineral density (BMD) (E) in mg HA/cm³. ACS-L showed a negative effect on the bone volume and relative bone volume indicating a delayed mineralization process while the bone density (BMD) was comparable between the groups. Data are shown as box and whiskers plot with median \pm min/max for $n = 7-10$. Mann-Whitney U-test was used to determine statistical significance; p -values are indicated in the graphs with $*p < 0.05$, $**p < 0.01$ and $***p < 0.001$. (C, F) 3D reconstruction is exemplary depicted ($n=2$) for control and ACS-L group at 14 days supporting the quantified data. Reproduced and modified from [174].

Taken together, the results show a significant inhibitory effect of the mineralization at 14 days by the ACS-L resulting in delayed bone healing which was almost but not completely recovered after 21 days. To get a more precise view on the healing process, histological stainings were investigated in the subsequent step.

3.3.6 ACS-L remained partially in the osteotomy gap during the observation period

Histology was used to examine the regeneration processes on a tissue and cell level. Therefore, Movat's Pentachrome staining provides excellent features to assess different tissues formations at once. The combination with Von Kossa staining additionally provides the opportunity to clearly determine mineralized areas. The ACS-L was stained pale yellow which could be distinguished from the yellow-orange staining of the mineralized bone and therefore allowed for quantitative analysis in the next steps. As the images in Figure 25A clearly display, the ACS-L remains in the osteotomy gap over time undergoing slight changes and degradation. Additionally, several spots of ectopic bone formation were observed which were also revealed in the 3D reconstruction of μ CT analysis indicating an osteogenic potential (Fig. 25B, C).

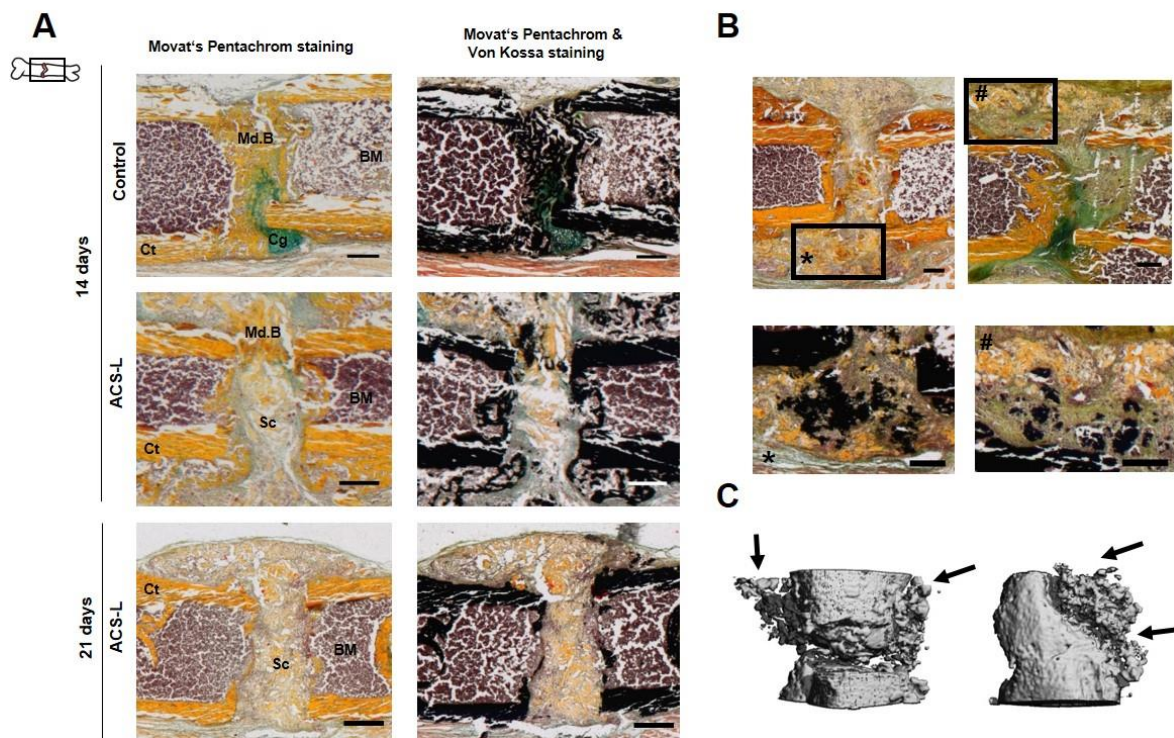


Figure 25: ACS-L was partially degraded in the osteotomy gap within 21 days.

(A) Images show Movat's Pentachrome staining alone and in combination with Von Kossa staining. Von Kossa staining supports the discrimination between mineralized bone and ACS-L. The presence of the ACS-L was observed over time. Images are exemplary for $n = 6-8$. Scale bars show $500 \mu\text{m}$. (B) Ectopic bone formation was found in the surrounding tissue as indicated by Van Kossa staining and (C) 3D μ CT reconstruction. Related sections are marked with * or #. Scale bars show $500 \mu\text{m}$ (B) Ct = corticalis; Md.B = mineralized bone; Cg = cartilage; BM = Bone marrow; Sc = scaffold. Reproduced and modified from [174].

3.3.7 Reduced cartilage formation and mineralization indicate inhibitory effect of ACS-L on transition from the soft to the hard callus phase

To quantitatively determine the influence of the ACS-L on the bone regeneration process histomorphometry analysis was applied for the Movat's Pentachrome staining. Therefore, the total callus area (Tt.Ar) was examined and subsequently divided in an endocortical (Ec; inside of the cortices) and an intracortical (Ic; between the cortical ends) area (Fig. 26). The analysis comprised cartilaginous (Cg) and mineralized tissue (Md.B) areas (Ar) as well as connective tissue (CoT) and scaffold (Sc) areas which were normalized to the corresponding Tt.Ar. Within the Tt.Ar, the ACS-L group showed a significantly reduced amount of Tt.Cg 14 days after osteotomy ($p < 0.001$) which was in accordance with the Tt.Md.B ($p < 0.001$) that was also reduced after 21 days as compared to the control group ($p = 0.051$) (Fig. 26A). As previously observed during *ex vivo* μ CT analysis, there was a significant increase in the Tt.Md.B.Ar within the ACS-L group over time ($p = 0.014$). In addition, the relative total connective tissue area (CoT.Ar) was significantly higher at 14 and 21 days in the ACS-L group compared to the control group ($p = 0.013$; $p = 0.022$) (Fig. 26A). The Ec.Cg.Ar and Ec.Md.B.Ar were significantly reduced at 14 days in the ACS-L group in comparison to the control group ($p = 0.001$; $p = 0.008$) and increased over time in the ACS-L group ($p = 0.054$; $p = 0.004$) (Fig. 26B). Mineralized tissue formation in the intracortical area (Ic.Md.B.Ar) would indicate a sufficient bridging between the cortical ends and revealed a significant reduction at 21 days in the ACS-L group as compared to the respective control groups ($p = 0.013$) (Fig. 26C). The ACS-L group showed at both time points significantly broader callus width (Cal.Wi) (both $p < 0.001$) and the Sc.Ar was not reduced over time (Fig. 26D, E).

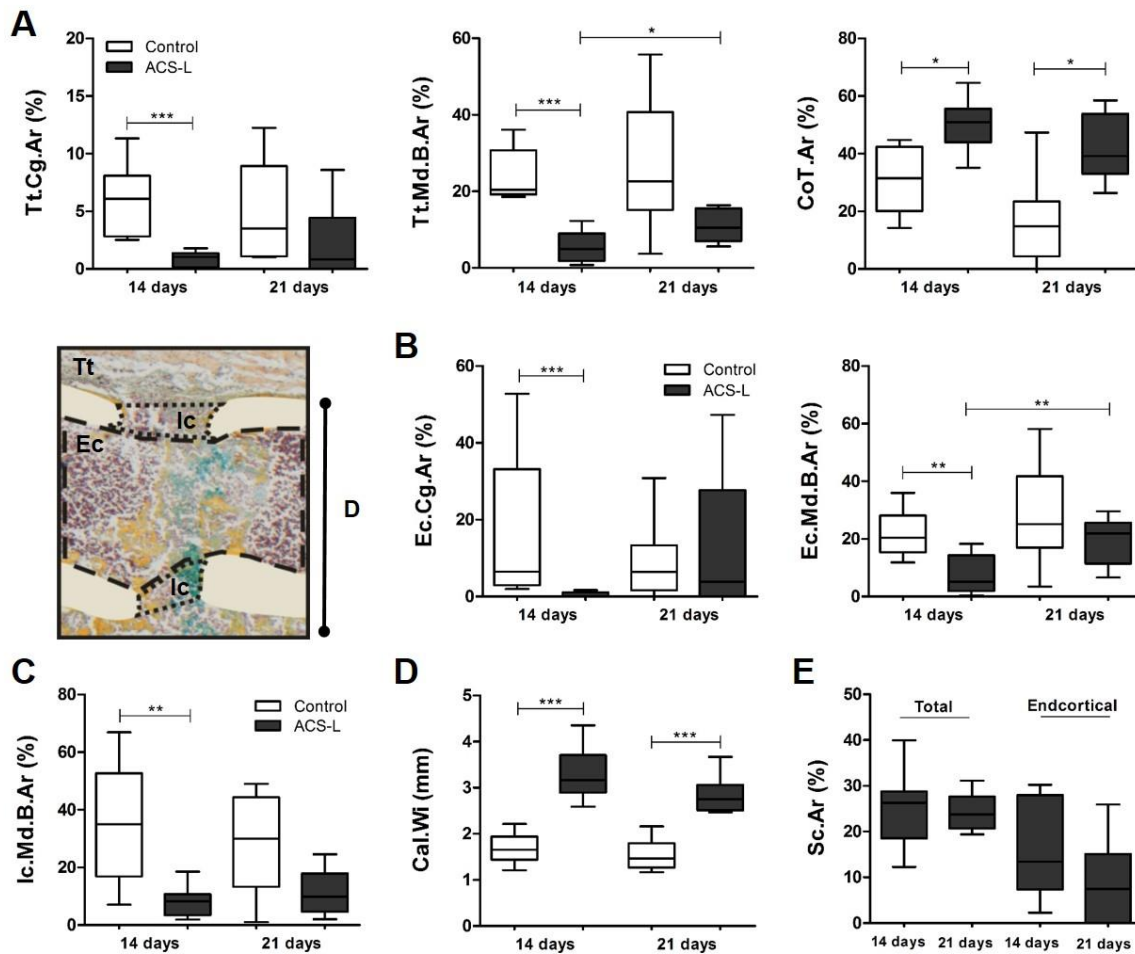


Figure 26: Inhibited transition from soft to hard callus phase by decreasing cartilage formation and mineralization.

Histomorphometry of the callus formation was conducted at 14 and 21 days after osteotomy. An ImageJ macro was used to determine the tissue areas. The manually selected callus area was subdivided into total (Tt), endocortical (Ec) and intracortical (Ic) area. Callus width was adjusted manually. Threshold adjustment was used to selected different tissue areas. Results are shown in relative numbers referring to either the total cartilage area (Tt.Cg.Ar.), the total mineralized bone area (Tt.Md.B.Ar), the total connective tissue area (CoT.Ar) (A), the endocortical cartilage (Ec.Cg.Ar) or mineralized bone (Ec.Md.B.Ar) area (B), intracortical mineralized bone area (Ic.Md.B.Ar) (C) or scaffold area (Sc.Ar) while void area was excluded. ACS-L groups had reduced cartilaginous and mineralized tissue areas and more connective tissue and showed larger callus width (Cal.Wi). Data are shown as box and whiskers plot with median \pm min/max for $n = 6-8$. Mann-Whitney U-test was used to determine statistical significance; p -values are indicated with $*p < 0.05$, $**p < 0.01$ and $***p < 0.001$. Reproduced and modified from [174].

These findings illustrate the negative influence of the ACS-L in the soft to hard callus transition which could be a result of reduced absorbance, cell invasion or vessel formation.

3.3.8 ACS-L diminished cell invasion and reduced CD31^{hi} Emcn^{hi} vessel formation

The cell invasion and vessel formation were examined in the next step. Immunofluorescence staining was performed focusing on DAPI, CD31 and endomucin (Emcn) (Fig. 27A, B). Staining positive areas were quantified and normalized to the total gap area. Representative DAPI stains and quantification of the relative cell number revealed reduced cell

numbers within the fracture gap in the ACS-L group after 14 days ($p = 0.059$), but not after 21 days (Fig. 27C). To confirm the previous data, brightfield images were used to identify the gap area and to quantify the relative mineralized callus area showing a significantly reduced area in the ACS-L groups 14 and 21 days after osteotomy compared to the controls ($p < 0.001$; $p = 0.03$) (Fig. 27C). Vessel formation is extremely important during bone regeneration allowing the removal of degraded material and the supply of nutrients, oxygen and cells. The analysis of vessel formation can serve as e.g. an indicator of invasion of cells into the scaffold and the status of regeneration. In 2014, the Adam's group published several studies on the presence of type-H vessels exhibiting the high expression of CD31^{hi} and Emcn^{hi}. Type-H vessels are described for the growth plate and were observed in drill hole setups [54, 138]. Nevertheless, to the date, they have not been described for fracture healing in an osteotomy setting. First, the amount of CD31^{hi} as well as Emcn^{hi} positive cells was determined yielding a decrease in the ACS-L group for CD31^{hi} 21 days after osteotomy ($p = 0.008$) and Emcn at 14 and 21 days ($p = 0.043$; $p = 0.035$) (Fig. 28A, B). Double positive cells (CD31^{hi} Emcn^{hi}) were significantly reduced after 21 days in the ACS-L group compared to the controls ($p = 0.035$) (Fig. 28B). In order to distinguish between type-H (CD31^{hi} Emcn^{hi}) and type-L (CD31^{low} Emcn^{low}) vessels, the mean intensity was determined in the fracture gap, around the fracture gap and in the bone marrow (Fig. 28C). The results show a clear significant higher expression of CD31 in the fracture gap at 14 and 21 days ($p = 0.004$; $p = 0.002$) compared to the bone marrow control which was also observed around the fracture gap ($p = 0.04$; $p = 0.004$) (Fig. 28D). Emcn was also higher expressed at 14 and 21 days in the fracture gap ($p = 0.009$; $p = 0.004$) and around the fracture gap (both time points $p = 0.009$) when compared to the bone marrow. In contrast, there was no significant difference in the ACS-L group indicating a reduced expression. Only the comparison of the CD31 expression around the fracture gap at 21 days revealed a significant difference towards the bone marrow ($p = 0.018$) (Fig. 28D).

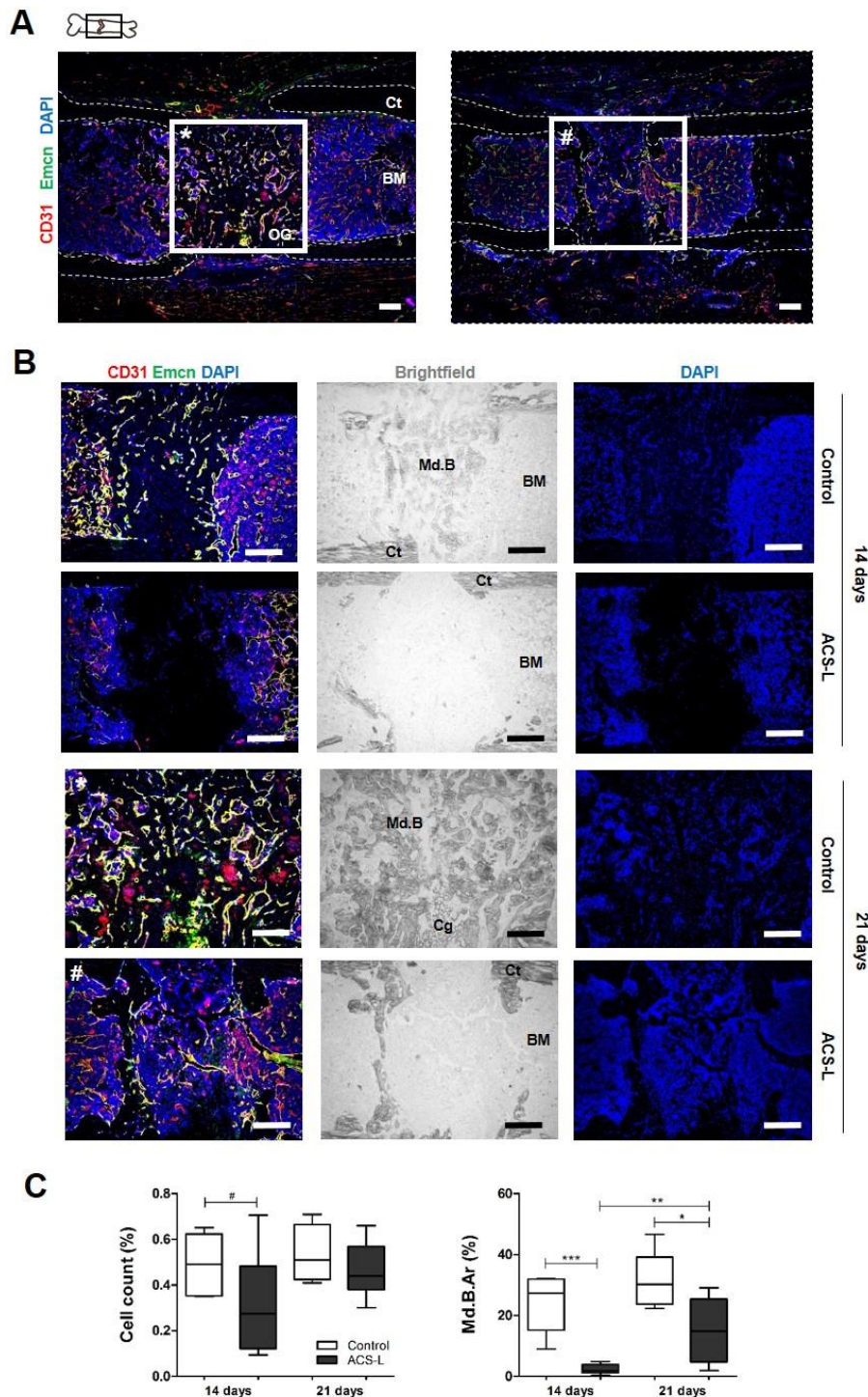


Figure 27: Diminished cell invasion and mineralization in ACS-L groups.

Immunofluorescence staining was performed to examine the cell number and the vessel formation within the osteotomy gap. (A) For standardization and comparable analysis similar sections were chosen between the cortical ends as indicated with white rectangles and * or # exemplary for 21 days. Ct = corticalis; BM = Bone marrow; OG = osteotomy gap. (B) Overview on CD31, Emcn and DAPI staining. Brightfield images were used to determine gap area and to quantify mineralized areas. Exemplary images for $n = 6-8$. Scale bars show $200 \mu\text{m}$. Md.B = mineralized bone; Sc = scaffold. (C) Cell numbers normalized to the gap area were determined by DAPI staining and ImageJ revealing lower cell numbers in the ACS-L group. Brightfield images were analyzed for mineralized callus tissue via grey threshold adjustment and calculated relative to the total gap area and confirmed previous data. Data are shown as box and whiskers plot with median \pm min/max for $n = 6-8$. Mann-Whitney U-test was used to determine statistical significance; p -values are indicated with $0.05 < \#p < 0.07$, $*p < 0.05$, $**p < 0.01$ and $***p < 0.001$. Reproduced and modified from [174].

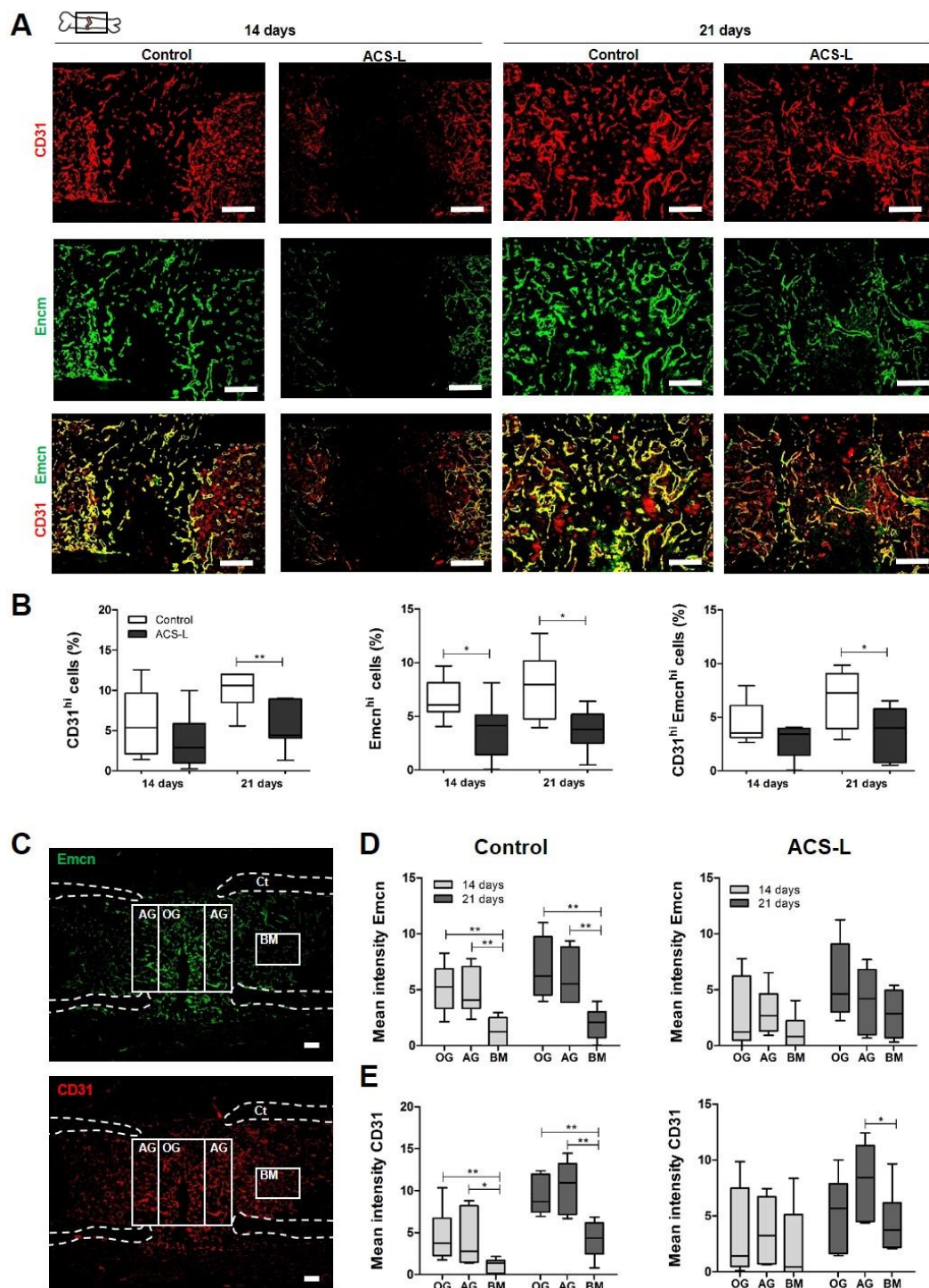


Figure 28: Reduced amount and expression of CD31^{hi} and Emcn^{hi} cells indicating disturbed vessel formation in the ACS-L groups.

Immunofluorescence staining was performed for quantitative analysis of type-H-like vessel formation. (A) Exemplary images for $n = 6-8$. Scale bar show 200 μm . (B) Positive stained cell areas were normalized to the gap area and are depicted as relative numbers showing a significant effect of ACS-L on the number of vessel-specific cells. (C) Mean intensity was determined via ImageJ for different areas – osteotomy gap (OG), around the gap (AG) and in the bone marrow (BM). Scale bar show 200 μm . Ct = corticalis. (D) Mean intensity of Emcn and (E) CD31 for the control and ACS-L groups. High expression of CD31 and Emcn demonstrated presence of type-H vessel in osteotomy gap in controls while ACS-L diminished the expression. Data are shown as box and whiskers plot with median \pm min/max for $n = 6-8$. Mann-Whitney U-test was used to determine statistical significance; p -values are indicated with $*p < 0.05$ and $**p < 0.01$. Reproduced and modified from [174].

3.3.9 ACS-L reduced TRAP⁺ cells while the number of macrophages and osteoblasts were comparable between groups

To investigate the effect of ACS-L on macrophages, osteoblasts and TRAP-positive cells (mainly osteoclasts), further stainings were applied using antibodies for F4/80 (macrophages) and Osterix (Osx; osteoblasts) and a TRAP staining kit afterwards. Staining positive areas were quantified and normalized to the total gap area. There were no group differences for F4/80⁺ and Osx⁺ areas (Fig. 29A, B) while more TRAP⁺ cells were found at 14 days in the control group compared to the ACS-L group ($p = 0.048$; Fig. 29C). These differences were not significant at 21 days ($p = 0.07$) although TRAP⁺ cells were scarcely detected in the collagen scaffold while in the control group TRAP⁺ cells were highly present throughout the mineralized callus (Fig. 30).

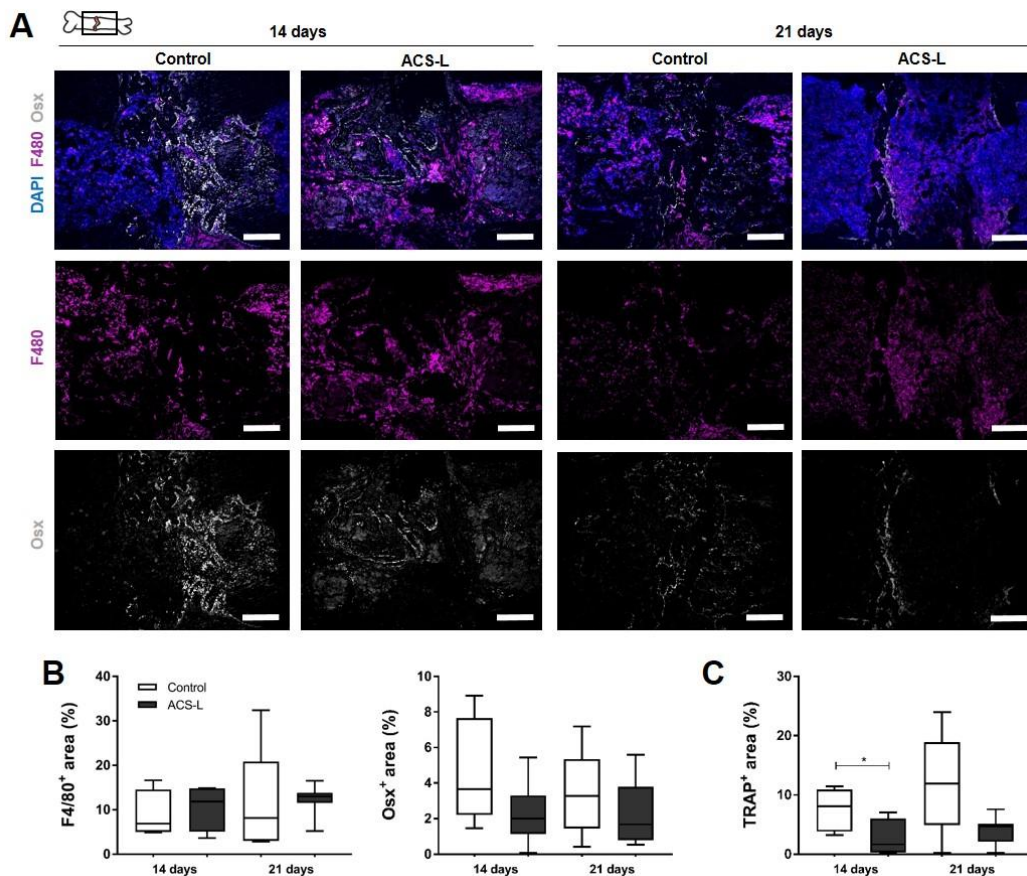


Figure 29: Comparable amount of F4/80⁺ and Osx⁺ cells between groups while TRAP⁺ cells were reduced.

Immunofluorescence staining was performed for quantitative analysis of macrophages (F4/80), osteoblasts (Osx) and activated macrophages/osteoclasts (TRAP). (A) Exemplary images for $n = 6-8$. Scale bar show 200 μm . (B) Positive stained cell areas were normalized to the gap area and are depicted as relative numbers showing no effect of ACS-L on the number of macrophages and osteoblasts. (C) TRAP staining revealed a lower amount of TRAP⁺ cells in the ACS-L groups. Data are shown as box and whiskers plot with median \pm min/max for $n = 6-8$. Mann-Whitney U-test was used to determine statistical significance; p -values are indicated with * $p < 0.05$.

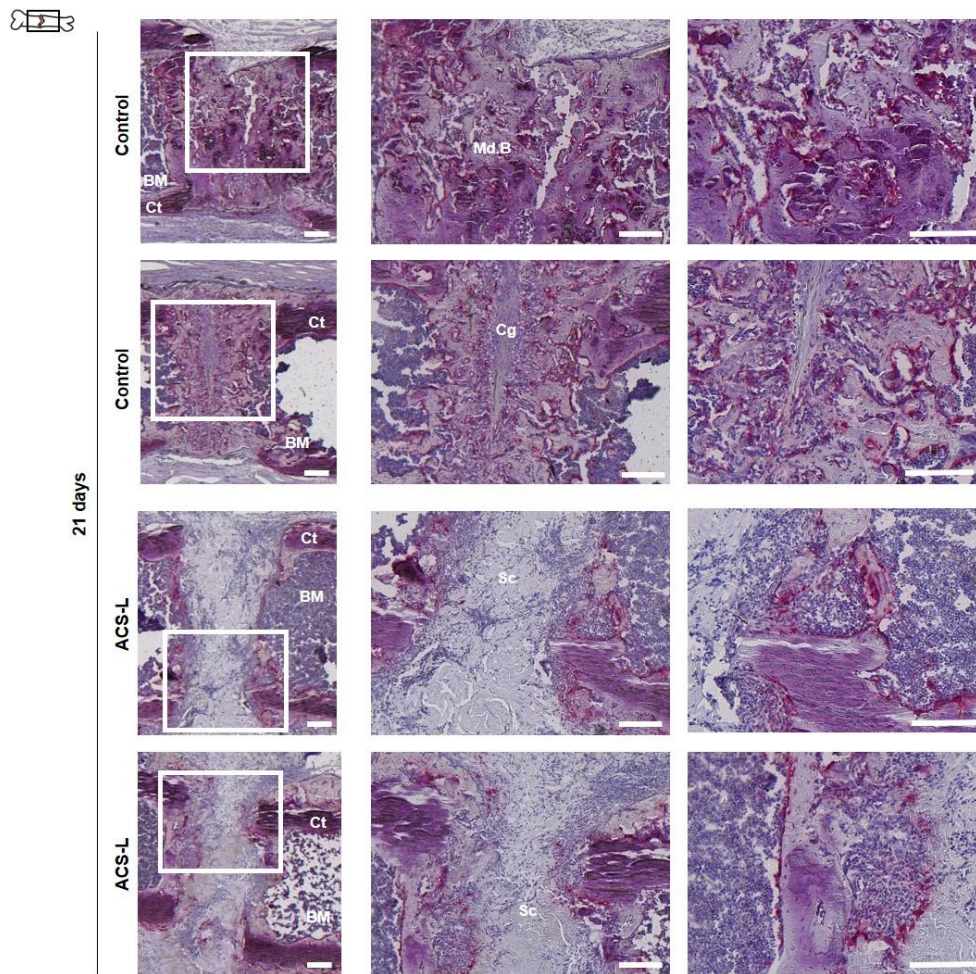


Figure 30: Marginal presence of TRAP⁺ cells in the ACS-L group 21 days after osteotomy.

Activated macrophages and osteoclasts were stained via TRAP staining (violet staining) and counter stained with HE. Different magnifications are presented in order to precisely determine the position of TRAP positive cells within the osteotomy gap. Within the ACS-L group TRAP⁺ cells are only found at the margin of the gap while controls indicate dissemination of those cells of the callus area. Related sections are marked with either * or #. Exemplary images for n = 4. Scale bars show 200 μ m. Ct = corticalis; BM = Bone marrow; Md.B = mineralized bone; Cg = cartilage; Sc = scaffold. Reproduced and modified from [174].

Although, there was no effect of ACS-L on the number of macrophages and osteoclasts detected, a reduction of activated macrophages and osteoclasts (TRAP⁺ cells) could be found. In summary, the results show an inhibitory effect of the ACS-L on cell invasion, vessel formation, CD31 and Emcn expression leading to the conclusion that the application of ACS-L leads to a delayed healing by inhibiting vascularization.

Taken together, the results of Chapter 3.3 clearly indicate that using ACS-L represents a rather delayed bone healing process than a normal healing process. Within this work, the effect of either MIF or DFO and their combination on the compromised conditions within this osteotomy model was subsequently examined.

3.4 Investigation on the influence of MIF and/or DFO on the regeneration process in a delayed healing model

3.4.1 Combined application of DFO and MIF and single application of DFO furthered the callus mineralization

After determining a beneficial concentration of MIF and DFO in combination in an *in vitro* setting (Chapter 3.2) and the evaluation and characterization of the fracture healing when applying ACS (Chapter 3.3), MIF and DFO were tested *in vivo* towards their potential to counteract a compromised bone regeneration process (induced by the application of the ACS-L). Therefore, MIF and DFO in concentrations of 100 ng/ml and 250 μ M, respectively, were applied on an ACS-L (further on termed ACS; ACS + MIF + DFO) for delivery in an osteotomy gap of 0.7 mm and a stable fixation via external fixator in 12 weeks old female C57BL/6N mice. In addition, MIF or DFO were applied alone (ACS + MIF; ACS + DFO). To measure the newly formed mineralized bone within the gap, *ex vivo* quantitative μ CT analysis was performed 7, 14 and 21 days after osteotomy. The TV was enhanced between 7 - 21 days in the groups treated either with ACS + DFO ($p < 0.01$) or ACS + MIF + DFO ($p < 0.05$) while no difference was observed between groups indicating a comparable callus size itself (Fig. 31A). The BV was increased over time in the ACS + DFO ($p < 0.001$) or ACS + MIF + DFO ($p < 0.05$) groups and was significantly higher in the ACS + DFO groups at 14 days compared to the ACS control ($p = 0.02$). This was also displayed in the BV/TV showing an increase between 7 and 21 days for the ACS + DFO ($p < 0.01$) or ACS + MIF + DFO ($p < 0.05$) groups and additionally in ACS and ACS + MIF + DFO group between 14 and 21 days (both $p < 0.05$). 14 days after osteotomy, the BV/TV was enhanced in the ACS + DFO ($p = 0.008$) or ACS + MIF + DFO ($p = 0.029$) group compared to the ACS control which was also seen at 21 days but was only statistically significant for the combination group ($p = 0.0499$). Moreover, there was a significant difference between the ACS + DFO ($p = 0.021$) or ACS + MIF + DFO ($p = 0.015$) groups in comparison to ACS + MIF group. All groups showed comparable bone density as displayed by the significant increase of the BMD ($p < 0.05$) (Fig. 31A). 3D reconstruction supported the quantitative data by demonstrating a clear gap in the ACS alone and ACS + MIF group and a pronounced mineralized callus in the ACS + DFO and ACS + MIF + DFO group (Fig. 31B).

Taken together, the combined application of DFO and MIF significantly enhanced the mineralization 14 and 21 days after osteotomy compared to the ACS control and the MIF only group at 21 days.

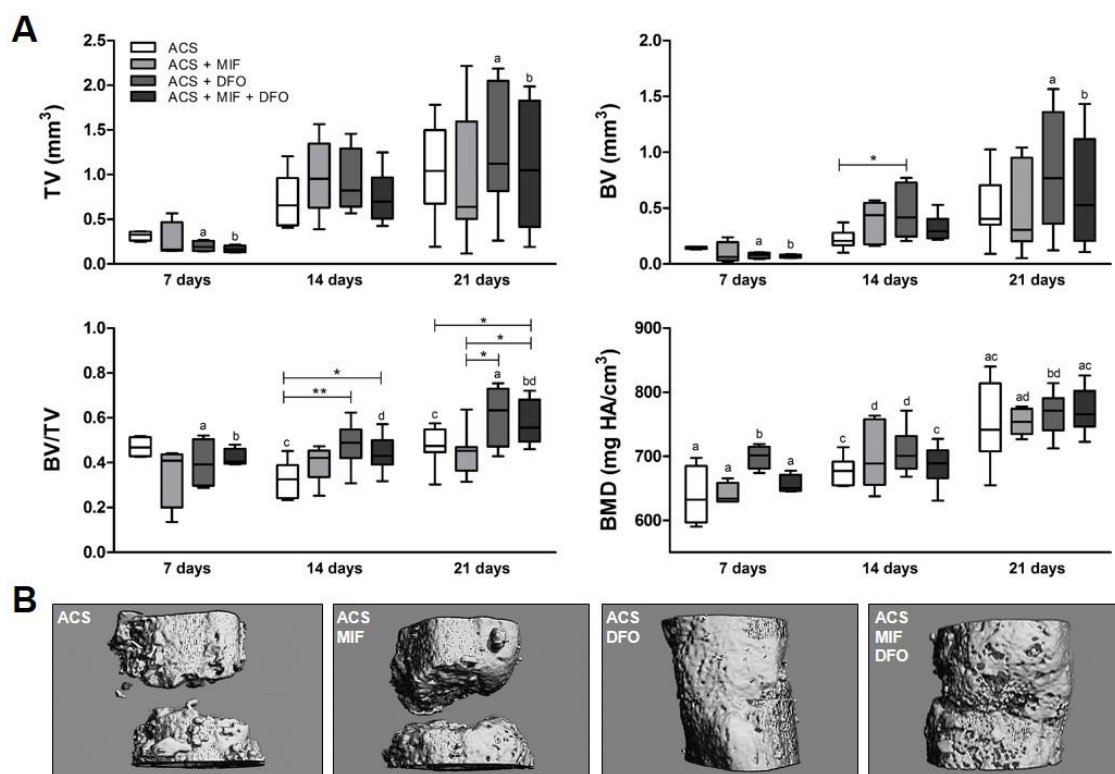


Figure 31: Increased bone volume fraction (BV/TV) after MIF/DFO or DFO treatment.

7, 14 and 21 days after osteotomy quantitative *ex vivo* μ CT analysis was performed using a Viva40 micro-CT scanning 191 slices. Post-processing included manually adjustment of the VOI (excluding the cortices) and automatic 3D callus tissue analysis. (A) Analyzed parameters were the total volume (TV), the bone volume (BV), the relative bone volume fraction (BV/TV) and the bone mineral density (BMD) in mg HA/cm³. The application of MIF and DFO on the ACS into the fracture gap at the time of the osteotomy showed a significant positive effect on healing processes as evidenced after 14 and 21 days by means of increased BV/TV compared to the respective ACS controls. Within the groups there was a significant increase of the BV, TV and BV/TV between 7 and 21 days. Data are shown as box and whiskers plot with median \pm min/max for $n = 4-8$. Mann-Whitney test was used to determine statistical significance between groups; p -values are indicated in the graphs with $*p < 0.05$ and $**p < 0.01$. Two-way ANOVA was used to determine significance for time differences within groups; small letters indicate correspondence. (B) 3D reconstruction is exemplary depicted for time point 21 days.

3.4.2 MIF and/or DFO enhanced mineralized tissue formation and ACS degradation

To verify the *ex vivo* μ CT data, Movat's pentachrome staining was applied on histological sections to analyze the processes on the tissue level while the combination with Von Kossa staining allowed to exactly identify mineralized tissue. Qualitative inspection of the stained sections revealed a strong presence of the ACS at day 14 and 21 for the ACS alone and ACS + MIF treated group, while treatment with ACS + DFO or ACS + MIF + DFO exhibited mainly mineralized tissue within the osteotomy gap which was also supported by Von Kossa staining (Fig. 32).

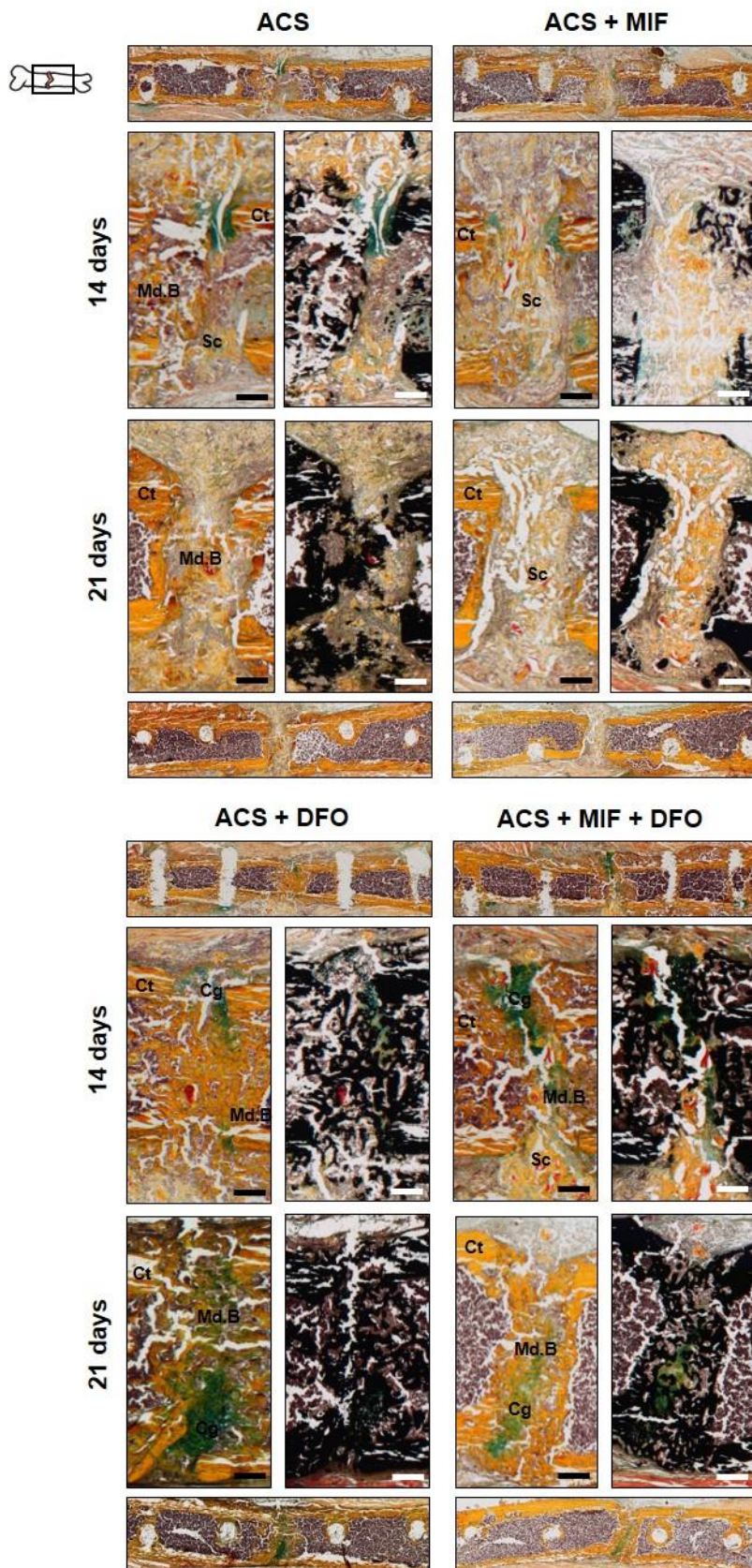


Figure 32: MIF/DFO and DFO further mineralized tissue formation and ACS degradation.

Images show Movat's Pentachrome staining alone and in combination with Von Kossa staining. Overview images are provided together with higher magnifications of gap area. The presence of the ACS-L was observed over time in the ACS only and ACS + MIF group. Mineralized callus tissue was dominant in ACS + DFO and ACS + MIF + DFO treated groups. Images are exemplary for n= 4-8. Scale bars show 200 μ m. Ct = corticalis; BM = Bone marrow; Md.B = mineralized bone; Cg = cartilage; Sc = scaffold.

Histomorphometry was done with ImageJ and used to quantify the observations and tissue appearances. Beside the total callus area (Tt.Ar), the endocortical (Ec.Ar.), the intracortical (Ic.Ar) area and the pericortical area (Pc.Ar; outside the cortices) were examined (see also Chapter 3.3.7; Fig. 26). The analysis comprised mineralized (Md.B.Ar) and cartilaginous tissue (Cg.Ar) areas which were normalized to the corresponding total Tt.Ar. The void area was subtracted to exclude technical errors. At 14 days after osteotomy, more Tt.Md.B could be found in the ACS + DFO treated group compared to the ACS control ($p = 0.02$) which partly reproduced the *ex vivo* μ CT (Fig. 33A compared to Fig. 31A). Nevertheless, there was no differences for the combination group at 14 days and between all groups at 21 days. Tt.Cg was more prominent in the ACS + DFO group compared to the ACS control ($p = 0.013$) and the ACS + MIF + DFO group ($p = 0.02$) (Fig. 33A). Contrarily, the Ec.Md.B was more enhanced in the ACS + MIF ($p = 0.013$), ACS + MIF + DFO group ($p = 0.02$) and to a certain amount in the ACS + DFO group ($p = 0.059$). The ACS + DFO additionally showed higher values for the Ic.Md.B at 14 days indicating a bridging of the gap ($p = 0.029$) (Fig. 33B, C).

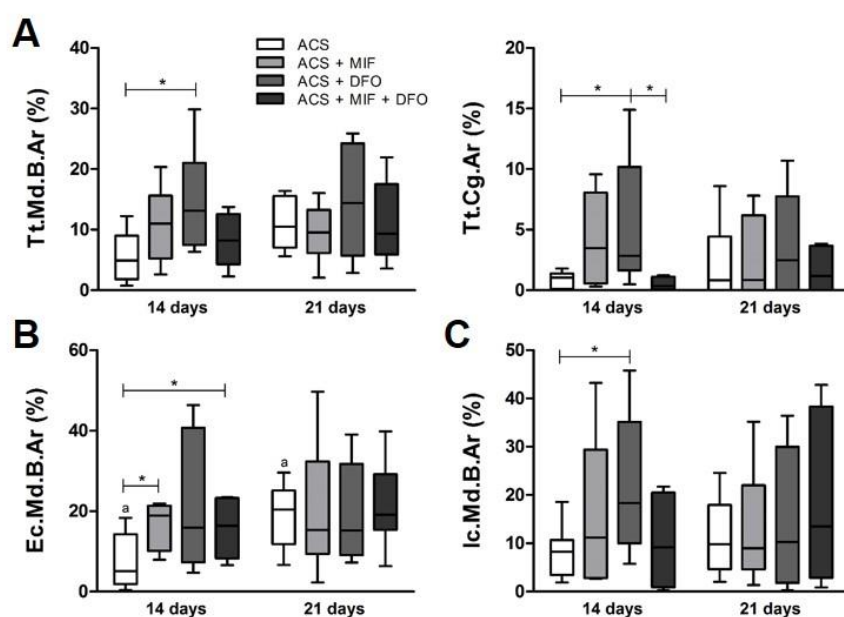


Figure 33: Treatment with MIF and/or DFO influenced mineralization.

To evaluate the influence on the tissue level, Movat's Pentachrom staining was quantified using an ImageJ macro. Different areas were distinguished: **(A)** total area (Tt.Ar; complete gap and callus area), **(B)** the endocortical (Ec.Ar; inside of the cortices) and **(C)** intracortical (Ic.Ar; between the cortical ends/bridging) area for mineralized bone (Md.B) and cartilage (Cg). Effects were observed 14 days post-osteotomy mainly for the ACS + DFO group (A, C) while the ACS + MIF + DFO group showed a significant higher amount of Ec.Md.B compared to the ACS control (B). Data are shown as box and whiskers plot with median \pm min/max for $n = 4-8$. Mann-Whitney U-test was used to determine statistical significance between groups; p -values are indicated in the graphs with $*p < 0.05$ and $**p < 0.01$. Two-way ANOVA was used to determine significance for time differences within groups; small letters indicate correspondence.

As shown previously the ACS was only partially removed from the osteotomy gap. Thus, the effect of the different treatments on the degradation of ACS was evaluated in detail. Therefore, the previously introduced divisions of the Tt.Ar was maintained. Over time the amount of remaining scaffold (Sc) in the Tt.Ar and Ec.Ar was significantly reduced in the ACS + MIF + DFO group ($p < 0.05$) (Fig. 34A). In addition, the Tt.Sc.Ar was less prominent in all treatment groups and significant for the ACS + MIF ($p = 0.014$) and ACS + MIF + DFO ($p = 0.04$) group at 21 days. This was also observed for the Ec.Sc.Ar for the MIF + DFO group compared to ACS control ($p = 0.044$) and ACS + MIF group ($p = 0.015$). Interestingly, there were also differences between the treatment groups depending on the time point. Treatment with DFO led to a significantly decreased Ec.Sc.Ar 14 days after osteotomy when compared to the ACS + MIF ($p = 0.042$), ACS + MIF + DFO ($p = 0.028$) and ACS group ($p = 0.016$) and remained low over time. In contrast, the Ec.Sc.Ar in the ACS + MIF + DFO treated group became significant lower at 21 days in comparison to the ACS control (Fig. 22A). The Pc.Sc.Ar was less prominent in the treatment groups 21 days after osteotomy and significant lower for the ACS + MIF treated group ($p = 0.021$) (Fig. 34A). The callus width (Cal.Wi) showed a negative trend without any significant difference (Fig. 34B).

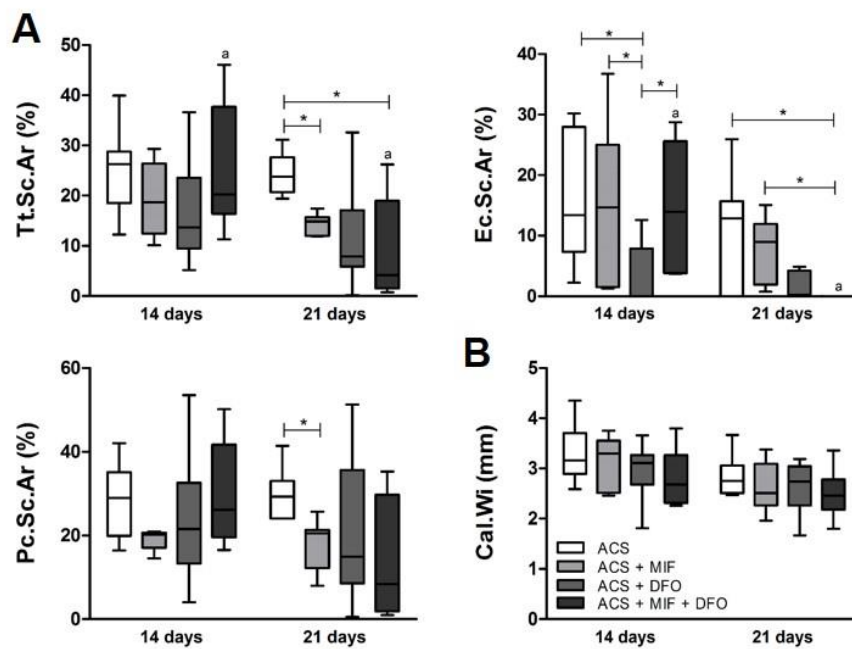


Figure 34: Treatment with MIF and DFO or DFO alone furthered degradation of ACS.

To evaluate the influence on the tissue level, Movat's Pentachrom staining was quantified using an ImageJ macro. (A) Different areas were distinguished: relative total area (complete gap and callus area), the endosteal (inside of the cortices) and periosteal (outside of the cortices) area for the ACS scaffold. The ACS + MIF + DFO group exhibited a significant reduction of the ACS scaffold at 21 days after osteotomy while (B) the callus widths showed no differences. Data are shown as box and whiskers plot with median \pm min/max for $n = 4-8$. Mann-Whitney U-test was used to determine statistical significance between groups; p -values are indicated in the graphs with $*p < 0.05$. Two-way ANOVA was used to determine significance for time differences within groups; small letters indicate correspondence.

In conclusion, the *ex vivo* μ CT could partly be reflected by the histomorphometric data regarding the mineralized bone formation, especially for the ACS + DFO treated group. A closer look towards the ACS presence in the Ec.Ar revealed a distinct effect for the ACS + DFO and ACS + MIF + DFO groups at different time points indicating a faster and more efficient degradation of the ACS as well as induction of an almost normal soft and hard callus formation.

3.4.3 Comparable amounts of macrophages and osteoblasts while TRAP⁺ cells were more prominent in treatment groups

As the presence of macrophages, osteoblasts and TRAP⁺ cells (activated macrophages and osteoclasts) are of great interest, a combination of immunofluorescence for F4/80 (macrophages), Osx (osteoblasts) and TRAP staining was performed. Staining positive areas were quantified and normalized to the total gap area. There were no group differences for F4/80⁺ and Osx⁺ areas (Fig. 35A, B). Comparing immunofluorescence with brightfield images revealed a potential negative correlation between the amount of F4/80⁺ areas and the Md.B.Ar which was also visible when plotting the corresponding data points together (Fig. 23C; linear fit $r = 0.38$; non-linear fit/one phase exponential decay $r = 0.39$) without considering group dependency. Quantification of TRAP showed no significant differences between groups (Fig. 36A). Nevertheless, from the images, treatment groups show a higher amount of TRAP positive cells around the gap area at 14 days compared to the ACS group (Fig. 36B) which is also displayed in the median differences (Fig. 36A). These observations justify the previous observation on the fast and efficient degradation of the ACS after 21 days which can be related to the higher number of TRAP⁺ cells at 14 days, but not to differences in amounts of macrophages.

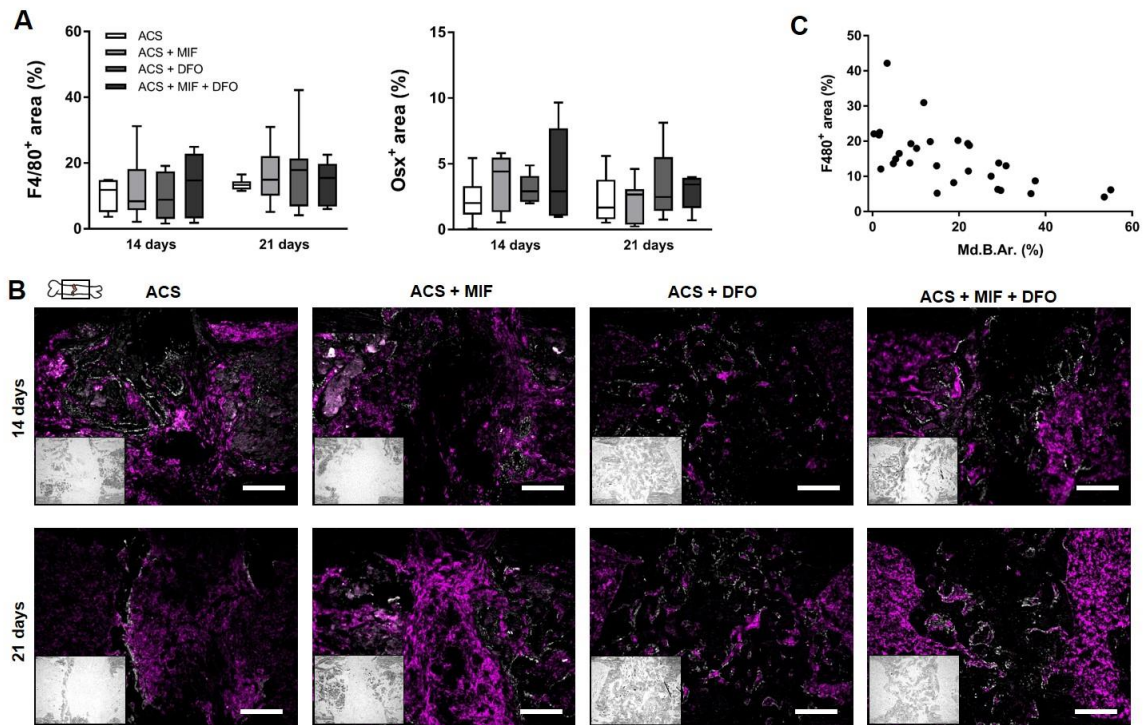


Figure 35: Comparable amounts of macrophages (F4/80) and osteoblasts (Osx) between groups.

Immunofluorescence staining was performed for quantitative analysis of macrophages (F4/80) and osteoblasts (Osx). **(A)** Positive stained cell areas were normalized to the gap area and are depicted as relative numbers showing no effect of ACS-L on the number of macrophages and osteoblasts. Data are shown as box and whiskers plot with median \pm min/max for $n = 6-8$. **(B)** Exemplary images for $n = 6-8$ including corresponding Brightfield images. Scale bar show 200 μm .

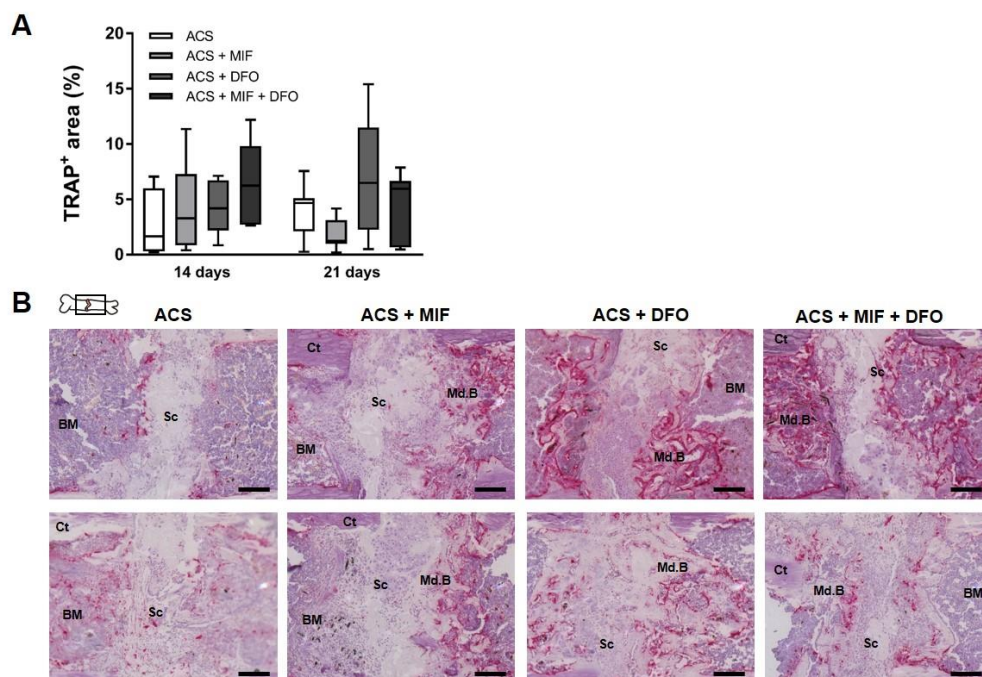


Figure 36: Higher amounts of TRAP⁺ cells were found in the treatment groups at 14 days.

TRAP staining was performed to quantify activated macrophages and osteoclasts. **(A)** Quantification showed lower amounts of TRAP⁺ cells in the ACS group at 14 days which is supported by the **(B)** exemplary images for $n = 4$. Scale bars show 200 μm . Ct = corticalis; BM = Bone marrow; Md.B = mineralized bone; Cg = cartilage; Sc = scaffold.

3.4.4 Amount of CD31^{hi} Emcn^{hi} vessels obviously did not depend on treatment but on mineralization status

The vessel formation is i) a crucial step within the bone regeneration process, ii) closely regulated and iii) accompanied by the microenvironment (e.g. hypoxia) and transitional tissue formations. Thus, within the next step, the effect of the different treatments on the vessel formation was investigated in detail. As markers CD31 and Emcn were used in order to describe the presence of H-type vessel (CD31^{hi} Emcn^{hi}) which was strongly diminished by the ACS alone as shown before. Quantification was performed using the thresholding tool in ImageJ after determining the osteotomy gap area (endocortical). Therefore, brightfield images were used which also served to measure the mineralization status (Md.B.Ar) in the chosen area while DAPI allowed for cell counting. When analyzing the images, it became obvious that the appearance of the vessels strongly depends on the mineralization status (Fig. 37A, B). In detail, if there is less tissue in the gap, there are only a few vessels visible showing isolated cell clusters or first vessels with a more elongated shape. In mineralized areas the vessel shape is adapting to the structure with a more network-like and directed shape. Additionally, the high presence of CD31 positive cells in the bone marrow was obvious at the margins of the selected gap area staining megakaryocytes or endothelial precursor cells and stem cells. Overall, treatment groups showed a more pronounced mineralization and therefore coordinated vessel formation while vessel shape was less developed in the ACS group (Fig. 37A, B). Analysis of the brightfield images confirmed the previously gained data evincing a significant higher amount of Md.B in the ACS + DFO ($p = 0.002$) and ACS + MIF + DFO ($p = 0.012$) treated group (Fig. 38A). Interestingly, the cell count showed no statistical differences, only a slight shift in the combination group at 21 days. Moreover, the amount of CD31^{hi} Emcn^{hi} cells was not different between the groups although the first qualitative inspection gave the impression towards a higher amount in the treatment groups including ACS + DFO (Fig. 38B). Considering the dependence of the vessel formation on the mineralization status, it becomes obvious that the amount itself must not lead to tangible conclusions as the amount is limited. Therefore, the amount of CD31^{hi} Emcn^{hi} cells relative to the Md.B.Ar was calculated at 14 days showing a significant difference between the treatment groups and the ACS control ($p = 0.015 - 0.038$) (Fig. 38C). It means in effect that the amount of mineralized tissue was higher than the amount of CD31^{hi} Emcn^{hi} cells indicating the indirect dependency of those measurements.

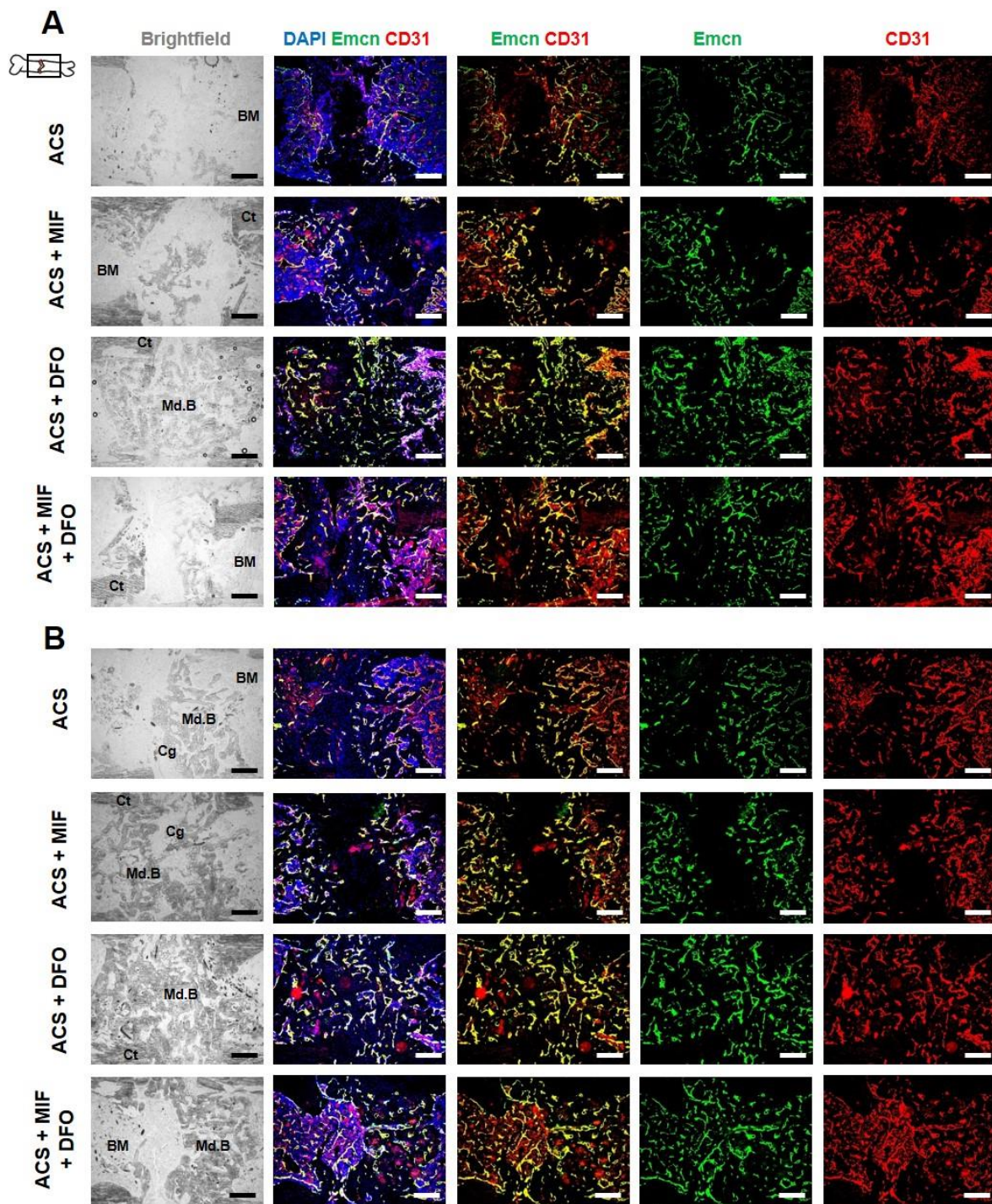


Figure 37: Different appearance of vessel formation can be observed depending on mineralization status.

Immunofluorescence staining was performed to examine the cell number (DAPI) and the vessel formation (CD31, Emcn) within the osteotomy gap (**A**) 14 days and (**B**) 21 days after osteotomy. Brightfield images were used to determine gap area and to quantify mineralized areas (Md.B.Ar). Md.B.Ar show stronger appearance of vessels than empty areas which can be either filled with scaffold or connective tissue (ACS + MIF) or cartilage (ACS + DFO). Most Md.B was observed in the ACS + DFO and ACS + MIF + DFO group. Exemplary images for $n = 4-8$. Scale bars show 200 μm . Ct = corticalis; BM = Bone marrow; Md.B = mineralized bone; Cg = cartilage.

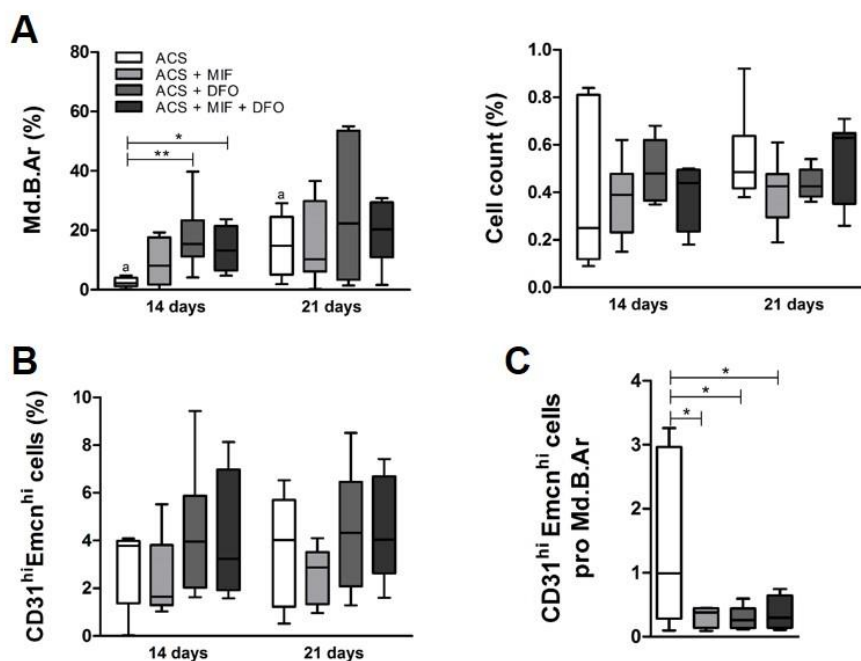


Figure 38: MIF and/or DFO treatment did not markedly influence cell invasion and amount of CD31^{hi} Emcn^{hi} cells, but high mineralized areas show lower amount of vessels.

Immunofluorescence staining was performed for quantitative analysis of type-H-like vessel formation. (A) Cell numbers normalized to the gap area were determined by DAPI staining and ImageJ showing no significant difference between the groups. Brightfield images were analyzed for mineralized tissue (Md.B.Ar) via grey threshold adjustment and calculated relative to the total gap area and confirmed previous data. (B) CD31 and Emcn double positive stained cell areas were normalized to the gap area and are depicted as relative numbers showing no significant effect of treatment. (C) The amount of CD31^{hi} Emcn^{hi} double positive cells was calculated relative to the Md.B.Ar showing a significant differences between the treatment and the ACS only group at 14 days. Data are shown as box and whiskers plot with median \pm min/max for $n = 4-8$. Mann-Whitney U-test was used to determine statistical significance; p -values are indicated with * $p < 0.05$ and ** $p < 0.01$.

Another assumption was that the amount of CD31^{hi} Emcn^{hi} cells is also influenced by the remaining scaffold. Hence, the amount of CD31^{hi} Emcn^{hi} cells at 21 days was charted against the corresponding Ec.Sc.Ar without including any group membership evincing a negative correlation (Fig. 39A). In detail, high amounts of CD31^{hi} Emcn^{hi} cells are found in samples with low amount of scaffold. In a next step, the Ec.Sc.Ar was divided into 4 groups (0-1%, 1-10%, 10-20% and 20-30%) allowing a better graphical and group-specific presentation. Consideration of the groups exhibits the more dominant presence of ACS + DFO and ACS + MIF + DFO group members in the 0-1% and 1-10% group while ACS and ACS + MIF group members were prominent in the higher Ec.Sc.Ar groups (Fig. 39A). Interestingly, there were two populations emerging separated by an imaginary line at 5% CD31^{hi} Emcn^{hi} cells. In order to evaluate the differences between those two populations (> 5% vs < 5%) the amount of Emcn^{hi} cells and CD31^{hi} cells was examined showing a significant difference between the populations ($p < 0.001$; $p = 0.0012$) (Fig. 39B). This was also the case for the Ec.Cg.Ar which was more present in the > 5% group ($p = 0.011$). This supports the data published by Ramasamy *et al.* 2014 describing the close regulation of vessel formation by VEGF released by chondrocytes in the growth plate [185]. Here, this relationship is shown

for the first time in a fracture healing setting. A clear treatment group specific difference could not be found.

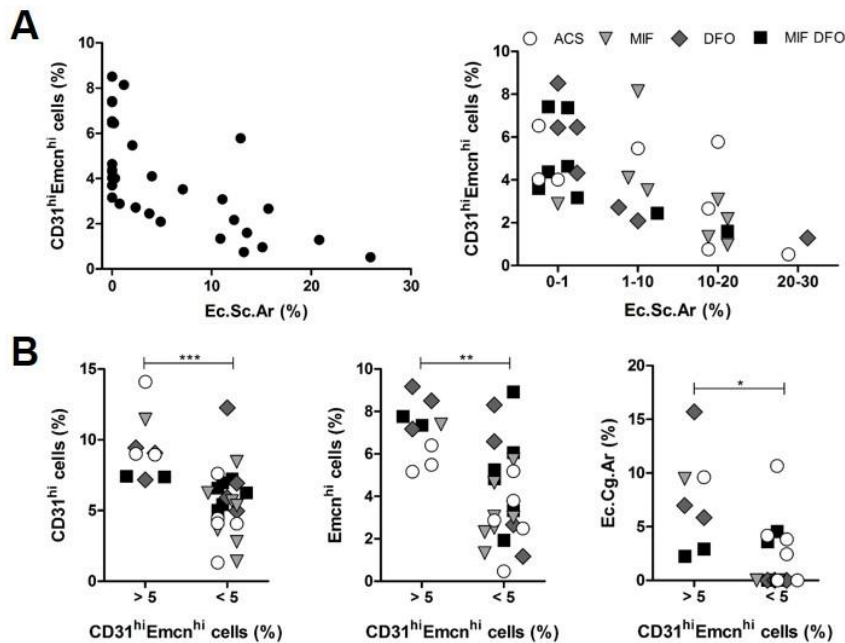


Figure 39: The amount of CD31^{hi} Emcn^{hi} cells negatively correlates with relative endosteal scaffold area (day 21).

(A) Osteotomy gaps with a high amount of relative scaffold in the endosteal area show small amounts of CD31^{hi} Emcn^{hi} cells as displayed in the xy-graph. Group membership was included in the next graph where the relative scaffold area was divided in 4 categories (0-1%, 1-10%, 10-20%, 20-30%). Interestingly, a distinct population (> 5% CD31^{hi} Emcn^{hi} cells) was identified. (B) The distinct population was drafted against the other population (< 5% CD31^{hi} Emcn^{hi} cells) and showed significant higher amounts of CD31, Emcn and cartilaginous tissue. Data are shown as scatter dot plot for $n = 4-8$. Mann-Whitney U-test was used to determine statistical significance; p -values are indicated with * $p < 0.05$, ** $p < 0.01$ and *** $p < 0.001$.

In order to assess the presence of H-type vessels (CD31^{hi} Emcn^{hi}) the mean intensity was measured in different areas – the gap area (OG), around the gap (AG) and in the bone marrow (BM) (Fig. 40). Differences were examined towards the BM as L-type vessels (CD31^{low} Emcn^{low}) are described to appear in the bone marrow. Since the ACS was shown to inhibit the expression intensity of CD31 and Emcn, it was of great importance to evaluate the effect of the different treatments. MIF treatment led to the significant difference between Emcn intensity in AG and BM at two and 21 days ($p = 0.009$; $p = 0.028$) and to an almost significant difference for CD31 (both $p = 0.065$) (Fig. 40). In contrast, DFO enhanced the activity at 14 days for Emcn ($p = 0.026$) and CD31 ($p = 0.002$) while at 21 days no significant differences were found. The combination of MIF and DFO influenced the Emcn activity at 14 and 21 days in the AG and partly the OG ($p = 0.057$; $p = 0.015$; $p = 0.028$). CD31 was more pronounced at 21 days in the AG ($p = 0.003$) (Fig. 40). The higher intensities of Emcn and CD31 predominantly at the margins of the osteotomy gap (=AG) supported qualitative observations and has not been described or investigated before.

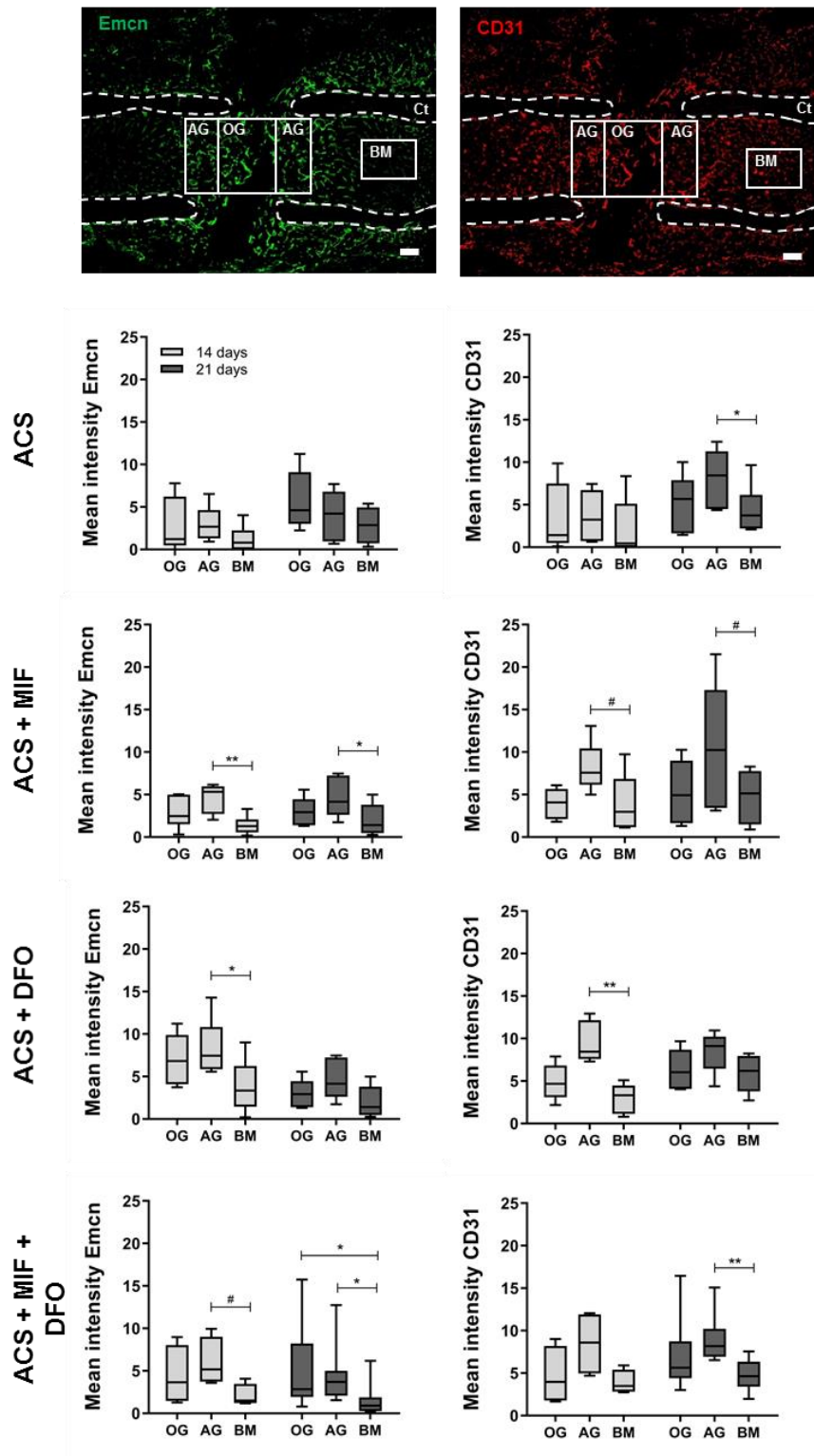


Figure 40: Mean intensity of Emcn and CD31 was enhanced by treatments.

Mean intensity was determined via ImageJ for different areas – osteotomy gap (OG), around the gap (AG) and in the bone marrow (BM) displayed in the exemplary images with a scale bar of 200 μ m. As shown previously the Mean intensity of Emcn and CD31 in the ACS group was only significant higher in AG compared to BM at 21 days. Significant higher intensity of CD31 and Emcn was shown for the treatment groups and demonstrated presence of type-H vessel in osteotomy gap. Data are shown as box and whiskers plot with median \pm min/max for n = 6-8. Mann-Whitney U-test was used to determine statistical significance; p-values are indicated with #*p* < 0.07, **p* < 0.05 and ***p* < 0.01. Ct = corticalis.

Taken together, the vessel appearance and formation were dependent on the mineralization status within the fracture gap and more pronounced in the treatment groups indicating a more physiological bone regeneration process. In addition, ACS + DFO and ACS + MIF + DFO groups exhibited lower relative areas of remaining scaffold and therefore, higher amounts of CD31^{hi} Emcn^{hi} cells. Moreover, the relation between the amount of cartilaginous tissue and CD31^{hi} Emcn^{hi} cells could be impressively shown and confirmed recently published studies [138, 185]. The mean intensity of Emcn or CD31 close to the osteotomy gap was positively influenced by the treatments especially by MIF + DFO (also in the OG) indicating the facilitation of H-type vessel formation.

3.4.5 Vessel formation was guided by tissue formation

Since less is known on the appearance and shape of type-H vessels during the different steps of fracture healing, different states and observations will be shortly described in the following and are displayed in Figure 41 and 42. At the beginning when tissue formation is starting isolated cell clusters can be found within the gap requiring the possibility to invade the area (Fig. 41A). In a next step, first vessel-like structures with a more elongated shape can be observed trying to bridge the gap and being surrounded by additional CD31 positive cells (Fig. 41B). When mineralization is starting from the margin, vessel shape shifts towards a more network-like shape being directed by the mineralization front missing the CD31 positive cells around (Fig. 41C). When cartilage is forming two different steps can be distinguished. In the first step there are no vessel directed towards the cartilage which is avascular (Fig. 41D). In a second step, vessel starts to penetrate the cartilage area with a more pronounced Emcn expression close to the cartilage (Fig. 42A, B). Total mineralization of the gap area led to adapted vessel shape and strong expression of Emcn and CD31 (Fig. 42C) The final step includes the remodeling leading to a channeling of the fracture gap and filling with bone marrow while vessel rebuilt towards physiological vessel network that can be found in the bone marrow (Fig. 42D).

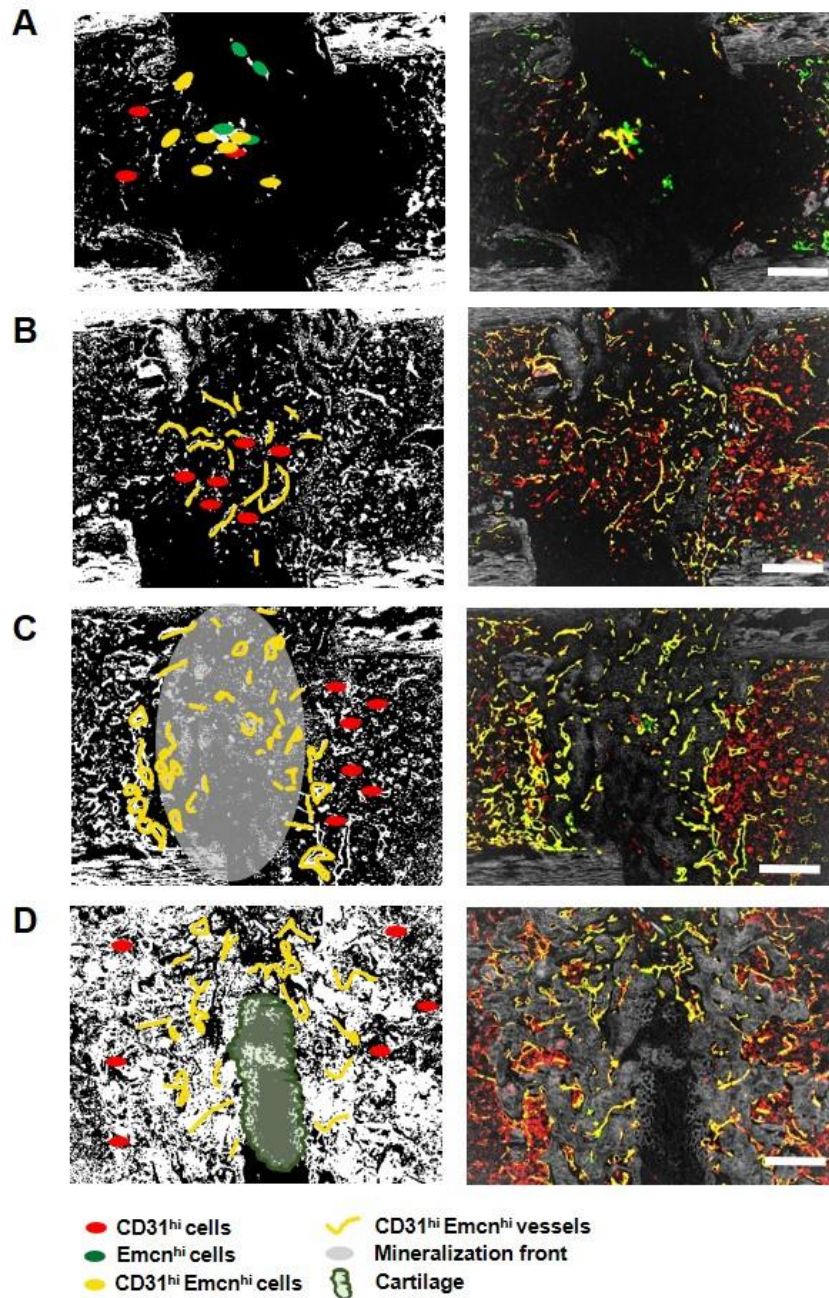


Figure 41: Different states of regeneration were accompanied by tissue dependent vessel formation – Part I.

In order to match images, brightfield images were inverted and composites were produced using ImageJ. On the left, important structures within the images are highlighted sketchily. (A) Isolated cell clusters within the gap are characteristic shortly after fracture, (B) before first vessel-like structures bridge the gap. (C) A more network-like vessel shape can be observed when mineralization starts while (D) cartilage is not vascularized. Scale bars show 200 μ m. Emcn = green; CD31 = red; inverted brightfield images = grey

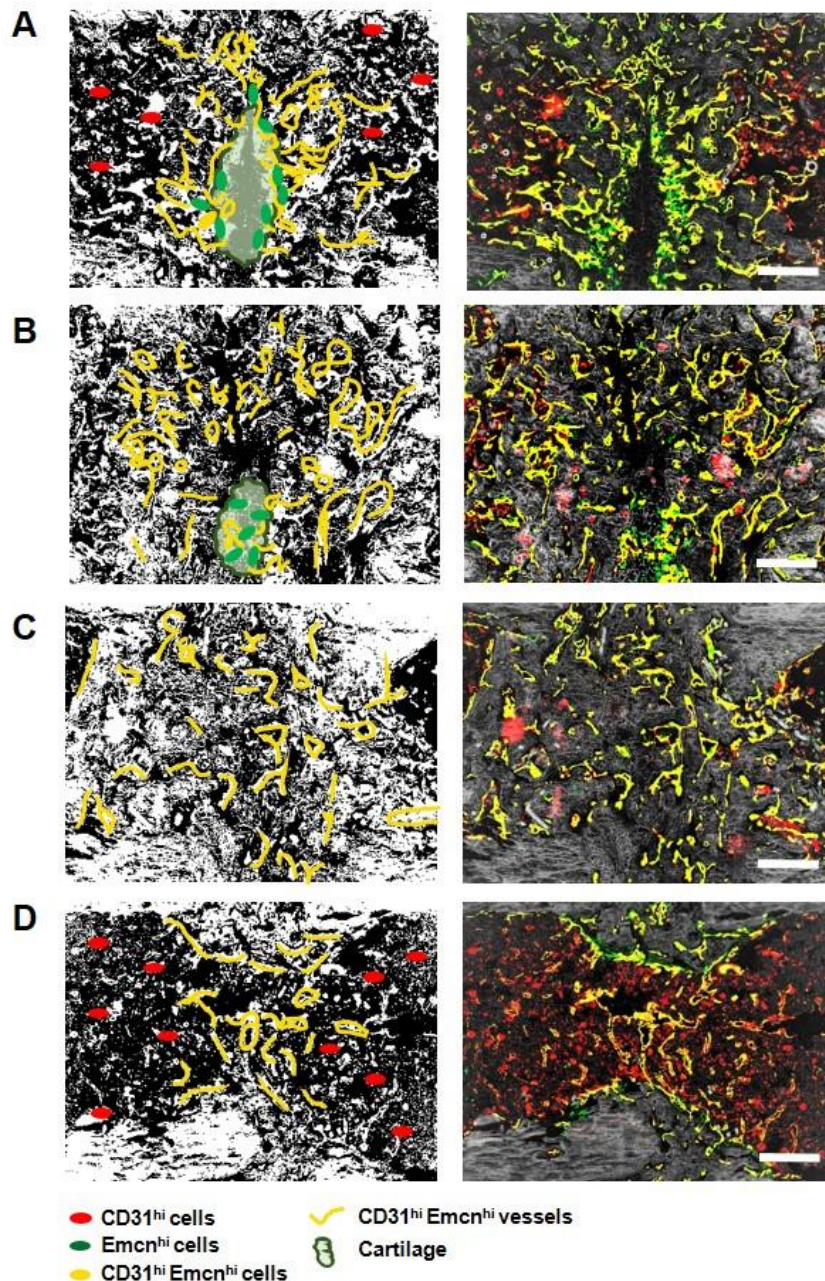


Figure 42: Different states of regeneration were accompanied by tissue dependent vessel formation – Part II.

In order to match images, brightfield images were inverted and composites were produced using ImageJ. On the left, important structures within the images are highlighted sketchily. (A, B) Vessels start to penetrate the cartilage showing a more pronounced Emcn expression. (C) Mineralization of the gap area results in adapted vessel shapes and strong expressions of Emcn and CD31. (D) During the final step the fracture gap is channeled and filled with bone marrow. Scale bars show 200 μm . Emcn = green; CD31 = red; inverted brightfield images = grey

In addition, higher resolutions revealed interesting findings as summarized in Figure 43. The vascularization of cartilaginous tissue seems to be driven by Emcn expressing ECs and invading vessel buds and arches-like structures could be identified. Furthermore, only CD31 positive vessel – arterioles were found within the fracture gap indicating the maintenance of the blood flow throughout the whole bone marrow.

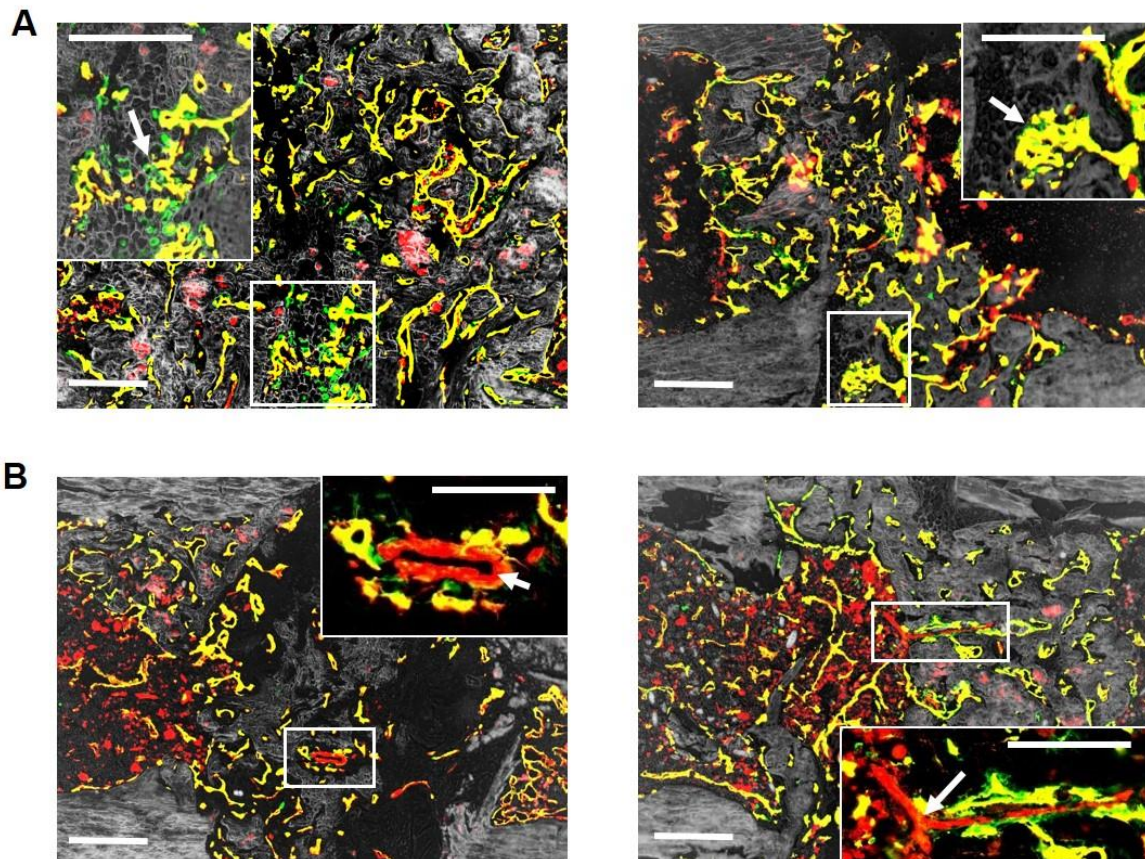


Figure 43: Vessel formation in cartilaginous areas seemed to be driven by $Emcn^{hi}$ cells and arterioles could be found in the gap area.

(A) Interesting observations supporting recently published findings indicating the facilitation of type H vessel formation by hypertrophic cartilage. $Emcn$ seems to be at first line during cartilage penetration. (B) Arterioles are only CD31 positive and responsible for the main blood supply. Their role and rebuilding during fracture healing are not well known. Scale bars show 200 μm . $Emcn$ = green; CD31 = red; inverted brightfield images = grey. [186].

3.4.6 Upregulation of immune response-related genes and downregulation of matrix-associated genes characterized gene profile at day 3 and 7

To identify potential differences between the treatment groups compared to the ACS group and to verify the supportive effect of DFO and MIF on RNA expression level, microarray analyses were conducted during the initial phase of fracture healing on day 3 and 7. RNA integrity, quality and amount were determined prior to the chip hybridization and scanning. Table 8 lists the results of the samples that were later used for the measurement. The mean RNA concentration on day 3 was $800.5 \text{ ng}/\mu\text{l} \pm 394.4 \text{ ng}/\mu\text{l}$ and $965.0 \pm 249.6 \text{ ng}/\mu\text{l}$ on day 7 while the mean RIN value was 9.3 ± 0.4 and 9.2 ± 0.2 on day 3 and 7, respectively. Therefore, samples were determined as suitable for further analyses.

Table 8: RNA concentration and RIN values of the samples used for microarray analyses.

Groups	3 days		7 days	
	Concentration (ng/μl)	RIN	Concentration (ng/μl)	RIN
ACS	955	9.6	772	9.4
	1,060	8.7	1,019	9.2
ACS + MIF	1,064	9.2	1,004	9.0
	705	9.1	1,283	8.9
ACS + DFO	693	9.5	868	9.2
	1,366	9.6	1,294	9.1
ACS + MIF + DFO	718	9.0	547	9.2
	906	9.7	933	9.2

For data analysis all treatment groups were normalized to the ACS group and clustered for genes with an expression Log_2 expression fold change > 1.5 in one of the treatment groups. An extensive literature search was performed in order to classify the identified genes for the potential function of the related protein or tissue (within the fracture healing process). Commonly used databases were not suitable as they normally focus on more general aspect for classification and pathway analysis. Seven different classes were identified including immune response and inflammation, cell metabolism and cell cycle, matrix formation, muscle function and metabolism, nervous system and myelination, fat metabolism and not classified genes. Related differentially expressed genes are listed in Tables 9 - 11. Clustering showed comparable expression fold changes at day 3 between the ACS + MIF and ACS + DFO group while at day 7 ACS + DFO closer clustered with the ACS + MIF + DFO group. 13 genes were found to be differentially expressed especially in the combination group (ACS + MIF + DFO) at day 3 (Table 9). At day 7, a total of 42 genes were differentially expressed mainly in the ACS + MIF group (Table 10, 11).

Table 9: Gene expression profiles discriminating the different treatment groups normalized to the ACS group at day 3.

Differentially expressed genes and names classified for function	Log ₂ expression fold change of treatment groups Mean of two individual samples		
	ACS + MIF + DFO	ACS + DFO	ACS + MIF
Clustering			
<u>Immune response, inflammation</u>			
<i>Igh6</i> <i>Immunoglobulin heavy chain 6</i>	3	0.27	-0.3
<i>Ms4a1</i> <i>Membrane spanning 4-domains A1</i>	1.6	0.089	0.093
<i>Cxcl3</i> <i>C-X-C motif chemokine ligand 3</i>	1.8	0.8	0.0046
<i>C1qtnf3</i> <i>Complement C1q tumor necrosis factor-related</i>	-1.6	-0.65	0.41
<u>Cell metabolism, cell cycle</u>			
<i>Aldh2</i> <i>Aldehyde dehydrogenase 2</i>	-1.4 / -1.6	-1.7 / -1.4	-1.8 / -1.3
<u>Matrix formation</u>			
<i>Fmod</i> <i>Fibromodulin</i>	-1.6	-0.22	-1
<u>Muscle function, metabolism</u>			
<i>Myh1</i> <i>Myosin heavy chain 1</i>	-2.3	-1.7	-1.5
<i>Asb15</i> <i>Ankyrin repeat and SOCS box-containing 15</i>	-1.5	-0.79	-0.31
<i>Phkg1</i> <i>Phosphorylase kinase catalytic subunit gamma 1</i>	-1.6	-0.59	-0.43
<u>Nervous system, myelination</u>			
<i>Stfa3</i> <i>Stefin A3</i>	1.6	0.95	1.2
<u>Not classified</u>			
<i>Scn4b</i> <i>Sodium voltage-gated channel beta subunit</i>	-2.1	-1.1	-0.88
<i>Ces5a</i> <i>Carboxylesterase 5A</i>	-1.3	-1.6	0.39
<i>Chac 1</i> <i>ChaC glutathione specific gamma-glutamylcyclotransferase 1</i>	-1.8	-0.92	-0.55

Expression fold changes of different probe sets are divided by a slash (/). Bold numbers indicate markedly different expression levels compared to ACS control.

Table 10: Gene expression profiles discriminating the different treatment groups normalized to the ACS group at day 7.

Differentially expressed genes and names classified for function	Log ₂ expression fold change of treatment groups Mean of two individual samples		
	ACS + MIF + DFO	ACS + DFO	ACS + MIF
Clustering			
<u>Immune response, inflammation</u>			
<i>Il1b</i> <i>Interleukin 1 beta</i>	0.4	0.1	1.5
<i>Il6</i> <i>Interleukin 6</i>	0.8	0.67	2.5
<i>Gbp2</i> <i>Guanylate-binding protein 2</i>	0.18/0.01	0.78/0.55	2.2/1.7
<i>Gbp10</i> <i>Guanylate-binding protein 10</i>	0.67	1.1	2.6
<i>Slamf8</i> <i>SLAM Family Member 8</i>	0.56	0.83	1.9
<i>Ear1</i> <i>Eosinophil cationic protein 1</i>	-0.75	-1.7	-1.5
<i>Socs3</i> <i>Suppressor of cytokine signaling 3</i>	0.72	0.13	1.6
<i>Cxcl1</i> <i>C-X-C motif chemokine ligand 1</i>	0.72/0.62	0.56/0.62	1.8/1.9
<i>Cxcl3</i> <i>C-X-C motif chemokine ligand 3</i>	0.88	-0.12	1.8
<i>Cxcl9</i> <i>C-X-C motif chemokine ligand 9</i>	0.67/0.073	1.6/0.95	3.6/3.1
<i>Cxcl10</i> <i>C-X-C motif chemokine ligand 10</i>	0.11	0.001	2.3
<i>Cxcl14</i> <i>C-X-C motif chemokine ligand 14</i>	0.56/0.74	0.52/0.23	1.7/1.7
<i>Ccl5</i> <i>C-C motif chemokine ligand 5</i>	0.15	0.12	1.7
<i>Ccl21</i> <i>C-C motif chemokine ligand 21</i>	1.2	1.3	2.1
<i>Capg</i> <i>Macrophage-capping protein</i>	1.9	1.6	2.6
<i>Saa3</i> <i>Serum amyloid A</i>	0.31	0.3	1.9
<i>Cd274</i> <i>Programmed cell death 1 ligand 1</i>	0.33	0.38	1.8
<i>Lyve</i> <i>Lymphatic Vessel Endothelial Hyaluronan Receptor 1</i>	1.6	1.6	1.6
<u>Cell metabolism, cell cycle</u>			
<i>Pdk4</i> <i>Pyruvate dehydrogenase lipoamide kinase isozyme 4</i>	1.7	1.3	1.1
<i>Hmox1</i> <i>Heme Oxygenase 1</i>	-0.1	-1.7	-0.39
<i>Crabp1</i> <i>Cellular retinoic acid-binding protein 1</i>	-1.2	-2.1	-1.8
<i>Niacr1</i> <i>Niacin receptor 1</i>	0.62	0.23	2.3
<i>Scd1</i> <i>Stearoyl-CoA desaturase-1</i>	2	1.3	1.7

Expression fold changes of different probe sets are divided by a slash (/). Bold numbers indicate markedly different expression levels compared to ACS control.

Table 11: Gene expression profiles discriminating the different treatment groups normalized to the ACS group at day 7 continued from Table 10.

Differentially expressed genes and names classified for function	Log ₂ expression fold change of treatment groups Mean of two individual samples		
	ACS + MIF + DFO	ACS + DFO	ACS + MIF
<u>Matrix formation</u>			
<i>Epyc</i> <i>Epiphycan</i>	2.1	-0.048	0.62
<i>Mmp3</i> <i>Matrix metalloproteinase 3</i>	1.3	1.2	2.3
<i>Col2a1</i> <i>Collagen 2A1</i>	0.43	-1.7	0.72
<i>Col9a3</i> <i>Collagen 9A3</i>	1.2	-1.7	1.1
<i>Col10a1</i> <i>Collagen 10A1</i>	-0.49	-2.5	0.36
<i>Lect1</i> <i>Chondromodulin-1</i>	1.6	-1.4	1.5
<i>Hapln1</i> <i>Hyaluronan and proteoglycan link protein 1</i>	1.2/1.2/0.93	-1.5/-1.5/-1.7	0.55/0.9/1
<u>Muscle function, metabolism</u>			
<i>Myl3</i> <i>Myosin light chain</i>	1.5/1.4	1.6/1.6	1.3/1.3
<i>Abra</i> <i>Actin-binding Rho-activating protein</i>	2.1	0.78	0.82
<i>Xirp</i> <i>Xin actin-binding repeat-containing protein</i>	1.6	0.35	0.46
<i>Ankrd2</i> <i>Ankyrin Repeat Domain 2</i>	1.6	0.86	0.65
<i>Myoc</i> <i>Myocilin</i>	1.3	1.2	1.5
<u>Nervous system, myelination</u>			
<i>Plp1</i> <i>Proteolipid Protein 1</i>	2.3	0.63	-0.04
<i>Mbp</i> <i>Myelin basic protein</i>	3	1.7	0.84
<u>Fat metabolism</u>			
<i>Apod</i> <i>Apolipoprotein D</i>	1.7/1.5	0.91/0.69	0.33/0.24
<u>Not classified</u>			
<i>Plekhb1</i> <i>Pleckstrin Homology Domain Containing B1</i>	1.5	0.52	0.41
<i>Bc023105</i> -	0.28	1.6	2.5
<i>Chl1</i> <i>Cell Adhesion Molecule L1 Like</i>	0.95	0.91	1.9
<i>Ubd</i> <i>Ubiquitin D</i>	0.4	0.3	2.3

Expression fold changes of different probe sets are divided by a slash (/). Bold numbers indicate markedly different expression levels compared to ACS control.

The highest number of differentially expressed genes were related to immune response or inflammation on day 3 and 7 (4 and 18 number of genes, respectively) followed by the genes related to matrix formation (1 and 5 number of genes, respectively) and cell metabolism or cell cycle (1 and 5 number of genes, respectively). Several genes could be sorted for their relation to muscle function or metabolism, nervous system or myelination, fat metabolism or could not be classified. Since the initial phase is characterized by inflammatory processes, it is interesting that in the ACS + MIF + DFO group related genes such as C-X-C motif chemokine ligand 3 (*Cxcl3*), immunoglobulin heavy chain 6 (*Ihg6*) and membrane spanning 4-domains A1 (*Ms4a*) are highly upregulated at day 3 encoding for proteins that are involved in B-cell maturation and neutrophil attraction. In contrast, aldehyde dehydrogenase 2 (*Aldh2*) and *Fmod* were downregulated in all groups. While *Aldh2* leads to detoxification and interferes with the reactive oxygen species (ROS) pathway, *Fmod* is a modulator of the extracellular matrix. Muscle-related genes were mainly downregulated in all treatment groups compared to the ACS control. At day 7, genes related to the immune response were mainly upregulated in the ACS + MIF group including classical inflammatory cytokines such as interleukin 1 β (*Il1b*) and -6 (*Il6*), but also chemokines and attractants (*Cxcl1*, 3, 9, 14). Macrophage-capping protein (*Capg*), which is important for macrophage activity and the lymphatic vessel endothelial hyaluronan receptor 1 (*Lyve*), important for the immune cell migration, were upregulated in all treatment groups. Heme Oxygenase 1 (*Hmox1*), which is known to be highly expressed in periosteum during the initial fracture healing phase, was reduced expressed while the pyruvate dehydrogenase lipoamide kinase isozyme 4 (*Pdk4*) and Stearoyl-CoA desaturase-1 (*Scd1*) were upregulated especially in the ACS + DFO group at day 7. Cellular retinoic acid-binding protein 1 (*Crap1*) was downregulated in all groups - retinoic acid is essential for osteoblastogenesis. Matrix-related genes that are needed for endochondral ossification such as *Col2a1*, *Col9a3* and *Col10a1* were prominently downregulated in the ACS + DFO group at day 7. Interestingly, two gene related to cartilage formation (hypertrophy of chondrocytes) - chondromodulin-1 (*Lect1*) and hyaluronan and proteoglycan link protein 1 (*Hapln1*) are regulated comparably at 7 days. Both genes are upregulated in the ACS + MIF + DFO and the ACS + MIF group and downregulated in the ACS + DFO group. Genes related to muscle and the nervous system were mainly upregulated in the combination group at day 7.

In order to verify the microarray data ($n=2$), qRT-PCR was performed for selected highly regulated genes ($n=4$) such as *Cxcl3*, *Hmox1*, *Hapln1*, *MMP3*, *Col10a1*, *Cxcl9*, *IL-6*, *Col9a3* and *Ms4a1*. Primers were designed according to the sequences from corresponding probe sets on the Affymetrix chip. For correlation, microarray and qRT-PCR data were normalized to a commonly used housekeeper actin β (*Actb*). Only corresponding data pairs were plotted ($n=2$) (Fig. 44). Correlation revealed a Spearman's Rho (r_s) of 0.84 and the direction of

change in expression in agreement (up-/downregulation) of all datasets was 80.77 % indicating a sufficient correlation and the verification of the microarray data.

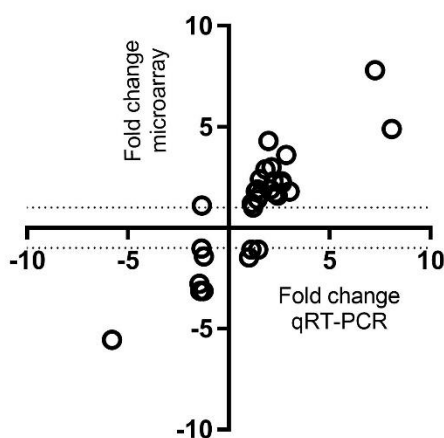


Figure 44: Correlation of fold change data from microarray and qRT-PCR.

The mean (n=2) of fold change expression is displayed for 9 genes + *Cxcl3* at day 3 and 7 = 30 data points. Correlation indicated verification of microarray data.

In a next step, the qRT-PCR results for n > 2 per treatment group including those not corresponding to microarray samples were examined for day 3 and 7 more in detail and compared to the normalized and raw microarray data if applicable (not all genes were regulated and displayed at day 3 in the microarrays). Statistical analysis was not applied as n-numbers strongly varied due to quality restriction of the qRT-PCR (dissociation curve) and were overall too small for statistical analysis. Nevertheless, qRT-PCR results revealed interesting trends which were partly supported by microarray data.

Table 12: qRT-PCR results of selected inflammation-related genes compared to the corresponding microarray results.

Both datasets were normalized to *Actb* and ACS control. Data in bold indicated correlation towards qRT-PCR data. Data are shown as mean for n = 2-4.

Microarray	<i>Il6</i>						<i>Cxcl3</i>						<i>Cxcl9</i>					
	3 days			7 days			3 days			7 days			3 days			7 days		
	MIF	DFO	MIF + DFO	MIF	DFO	MIF + DFO	MIF	DFO	MIF + DFO	MIF	DFO	MIF + DFO	MIF	DFO	MIF + DFO	MIF	DFO	MIF + DFO
Microarray	-	-	-	4.9	1.6	1.7	-1.0	1.9	3.6	3	-1.1	1.8	-	-	-	10	3	1.6
qRT-PCR	2.6	-1.9	-1.8	-3.1	-1.7	-4.7	1.6	2.2	3	0.4	-1.1	-0.2	-2.8	-4	-0.8	5.7	0.1	-0.4

qRT-PCR data revealed an upregulation of *Il6* at day 3 and *Cxcl9* at day 7 in the ACS + MIF group and *Cxcl3* in all groups at day 3 (Table 12). *Il6* was downregulated at day 7 which was the opposite result observed in the microarray data. The slight downregulation or upregulation of *Cxcl3* and *Cxcl9* at day 7 was mainly displayed by the microarray data. Fold change expression of *Ms4a1* and *Hmox1* were mainly positive at day 3 and negative at day 7 supported by the microarray data (Table 13). In contrast, *Hapln1* was downregulated during early phase and upregulated in the ACS + MIF and ACS + MIF+ DFO group a week after osteotomy.

Table 13: qRT-PCR results of selected metabolism-related genes compared to the corresponding microarray results.

Both datasets were normalized to *Actb* and ACS control. Data in bold indicated correlation towards qRT-PCR data. Data are shown as mean for n = 2-4.

	<i>Ms4a1</i>						<i>Hmox1</i>						<i>Hapln1</i>					
	3 days			7 days			3 days			7 days			3 days			7 days		
	MIF	DFO	MIF + DFO	MIF	DFO	MIF + DFO	MIF	DFO	MIF + DFO	MIF	DFO	MIF + DFO	MIF	DFO	MIF + DFO	MIF	DFO	MIF + DFO
Microarray	1	1.2	3.2	-	-	-	-	-	-	-1.4	-3.3	-1.1	-	-	-	1.3	-2.9	2.4
qRT-PCR	-0.2	0.5	1.3	-1.4	-1.9	-2.6	1.2	1.3	1.4	-1.5	-2	-0.3	-1.1	-2.5	-3.9	4.1	-1.4	6.5

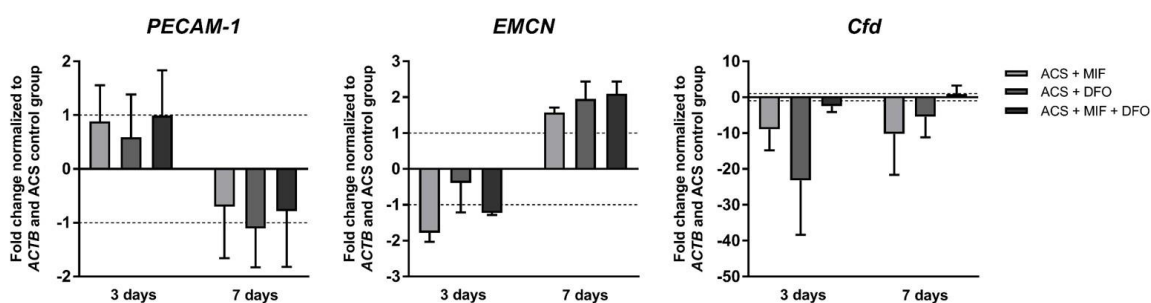
Mmp3 was strongly downregulated in the qRT-PCR data for all groups and time points which was contrarily to the microarray data indicating an upregulation (Table 14). Fold change expression of *Col9a3* and *Col10a1* were positive in the ACS + MIF group at both time points and the other groups at day 7, but more negative at day 3.

In addition, to the genes that were examined to verify microarray data, three other genes of interest were analyzed via qRT-PCR (Fig. 45). Platelet endothelial cell adhesion molecule (*Pecam-1*; CD31) and endomucin (*Emcn*) are endothelial markers indicating vessel formation as described in Chapter 3.3.8 and 3.4.4. Complement Factor D (*Cfd*) is part of the alternative complement pathway. Interestingly, *Pecam-1* and *Emcn* are oppositely regulated in the qRT-PCR data. While *Pecam-1* is more positively and *Emcn* is negatively regulated at day 3, it is the other way around at day 7. *Cfd* is mainly downregulated in all groups at both time points

Table 14: qRT-PCR results of selected matrix-related genes compared to the corresponding microarray results.

Both datasets were normalized to *Actb* and ACS control. Data in bold indicated correlation towards qRT-PCR data. Data are shown as mean for n = 2-4.

	<i>Mmp3</i>						<i>Col9a3</i>						<i>Col10a1</i>					
	3 days			7 days			3 days			7 days			3 days			7 days		
	MIF	DFO	MIF + DFO	MIF	DFO	MIF + DFO	MIF	DFO	MIF + DFO	MIF	DFO	MIF + DFO	MIF	DFO	MIF + DFO	MIF	DFO	MIF + DFO
Microarray	-	-	-	4.3	2.3	2.4	-	-	-	1.8	-3.3	2.2	-	-	-	1.1	-5	-1.4
qRT-PCR	-1.4	-1.7	-3	-1.8	-0.9	-2.5	6.2	-0.8	-1.2	5.5	1.2	1.7	-1.5	-0.3	-0.2	3.4	-0.05	0.3

**Figure 45: qRT-PCR results of further interesting genes.**

Pecam-1 and *Emcn* were oppositely regulated while *Cfd* was mainly downregulated. Data are shown as mean \pm SEM for n = 4.

Analysis of qRT-PCR data indicated an upregulation and downregulation of immune response- and matrix- and metabolism-related genes in the early phase at day 3 and 7 depending on the genes and time points which was more differentiated in the qPCR than in the microarray. In summary, ACS + MIF differently regulated inflammation- and matrix-related genes compared to the other two groups. All treatments groups showed downregulation of *Col9a3*, *Col10a1* and *Cfd* and influences on the expression of *Il6*, *Cxcl3* and *Cxcl9*.

In summary, the results provide clear evidence that the application of HIF-stabilizers especially DFO can effectively counteract inhibitory influences as induced by the ACS-L which significantly inhibit the bone healing process at various steps. Although a clear beneficial effect of applying additionally MIF to the DFO could not be shown, the results of this thesis further support the high potential of HIF-stabilizers especially DFO to be used as new therapeutic and regenerative strategy towards fracture healing disorders.

CHAPTER 4: Discussion

The present work covers three main parts on the potential effects of HIF-stabilizers on fracture healing outcomes and aims at providing evidence towards a new therapeutic approach for fracture healing under compromised conditions.

- 1) The first part mainly focused on the *in vitro* testing of hypoxia and HIF-stabilizers to counteract a delayed calcification approach in bone marrow derived mesenchymal stromal cells (hMSCs) induced by high concentrations of the glucocorticoid (GC) Dexamethasone (Dex). Different concentrations of the HIF-stabilizers deferoxamine (DFO) and macrophage migration inhibitory factor (MIF) were tested alone and in combination to define an effective concentration also for further *in vivo* testing.
- 2) Within the second part, the potential delivery systems, in this work, two absorbable bovine Col I scaffolds (ACSs; Lyostypt[®], ACS-L; Helistat[®], ACS-H) were examined for their suitability while one was chosen for further *in vivo* testing. Unexpectedly, it was shown for the first time that this scaffold (ACS-L) negatively influenced the bone healing process although it is routinely applied in research and clinic. The results clearly indicated a delayed fracture healing which parallel observations from fracture healing disorders due to compromised conditions known from RA patients or smokers.
- 3) Subsequently, the combination of MIF and DFO was examined in this mouse model of compromised conditions to verify the counteracting ability in a setting of compromised conditions. In addition, within this work the presence of H-type vessel that have been described in other models before, was proven for the first time in a fracture healing approach – a mouse-osteotomy-model.

The results of the work are intensively discussed below and are currently included in three publications, which have been published or are in preparation.

Lang, A., Kirchner, M., Stefanowski, J., Durst, M., Weber, M.-C., Pfeiffenberger, M., Damerau, A., Hauser, A.E., Hoff, P., Duda, G.N., Buttgereit, F., Schmidt-Bleek, K. & T. Gaber (2019) Collagen I-based scaffolds negatively impact fracture healing in a mouse-osteotomy-model although used routinely in research and clinical application. *Acta Biomaterialia*. 86:171-184. doi: 10.1016/j.actbio.2018.12.043.

Stefanowski, J.*, Lang, A.*, Rauch, A., Aulich, L., Köhler, M., Fiedler, A.F., Buttgereit, F., Schmidt-Bleek, K., Duda, G., Gaber, T., Niesner, R. & A. Hauser (2019) Spatial Distribution of Macrophages during Callus Formation and Maturation Reveals Close Crosstalk between Macrophages and Newly Forming Vessels. *Frontiers Immunology*. 10 (2588). doi: 10.3389/fimmu.2019.02588

Lang et al. (2019) Immunological dysregulation and inadequate hypoxia adaptation - HIF-stabilization as possible prevention of fracture healing disorders in RA or immune-suppressed patients. *In preparation*.

4.1 Characterization of bone marrow derived hMSCs

Since bone marrow derived hMSCs were used for the *in vitro* studies during the first part of the present study, the precise characterization via surface markers and appropriate differentiation assays were essential. According to the guidelines published by the *The International Society for Cellular Therapy* in 2006, the minimal criteria for the characterization include i) plastic adherence, ii) presence of positive surface markers (e.g. CD13, CD44, CD90, CD105) and absence of negative surface markers (e.g. CD45, CD14, CD19) and iii) the potential to differentiate in at least two different lineages [179]. All these criteria were considered in the present study and only cells that have been positively characterized were enrolled in the studies (Fig. 13). Nevertheless, there are ongoing discussions in the scientific community on the appropriate and specific characterization of hMSCs due to their high heterogeneity – the presence of several subpopulations which are not addressed by the current criteria. First, in former days hMSCs were named as “stem” cells which was changed during the last years towards “stromal” cells in order to consider the heterogenic mixture of distinct stem cells and other cells. Additionally, several further positive markers have been proposed such as stromal cell surface marker (STRO)-1, CD271, CD146, CD73 or sushi domain-containing protein 2 (SUSD2) [187]. Unfortunately, none of those markers is exclusive for hMSCs being one of the major challenges today in order to e.g. track those cells *in vivo*. Chan *et al.* recently described the identification of a specific human skeletal stem cell population defined by the following markers: PDPN⁺ CD146⁻ CD73⁺ CD164⁺ [188] (PDPN - podoplanin). This study could have great impact on hMSC therapy towards fracture healing disorders and *in vitro* differentiation protocols [189], but was however too late to influence the here presented data.

4.2 The effect of hypoxia or HIF-stabilizers on the inhibition of osteogenic hMSC differentiation by GCs in an *in vitro* setting

Glucocorticoids (GCs) are produced by the adrenal cortex as class of corticosteroids and control the immune system e.g. during inflammation. Two different GC-mediated modes of action can be distinguished: genomic and non-genomic effects. GC can easily pass through the plasma membrane due to their lipophilic structure and binds to the cytosolic GC receptor (GCR). The following genomic effects are mediated by promoting the expression of anti-inflammatory genes in the nucleus (transactivation) or inhibiting the translocation of transcription factors for pro-inflammatory cytokines from the cytosol to the nucleus (transrepression). Non-genomic effects have been recently classified in three categories: nonspecific interactions of glucocorticoids with cellular membranes; non-genomic effects mediated by the GCR; and specific interactions with membrane-bound GCR (mGCR) [190]. Beside their interaction with the immune system, GCs are responsible for the synthesis and

secretion of sex hormones, the regulation of calcium reabsorption in the kidney and absorption in the intestine influencing the levels of parathyroid hormone (PTH) and PTH sensitivity [191]. In addition, GCs are known to increase apoptosis and decrease proliferation and metabolism of osteoblasts accompanied by an increased proliferation and activity of osteoclast leading to disorders such as osteoporosis [191].

Several studies describe the controversial effects of GCs on hMSC proliferation and osteogenic differentiation. In greater detail, GCs have been shown to be essential for osteogenic differentiation in low concentrations while high concentrations inhibit osteogenic differentiation and proliferation favoring adipogenesis [192-197]. Therefore, Dex was chosen to effectively inhibit *in vitro* calcification of hMSCs and to test the potential counteracting role of HIF-stabilizers within the present study. As a result, a concentration-dependent inhibitory effect of Dex on the calcification of hMSCs was obvious after 14 days while the treatment with 10^{-3} M Dex caused a long-lasting significant decrease in the calcification after 21 and 28 days (Fig. 14). Moreover, supplementation with 10^{-3} M Dex also strongly increased LDH activity after 24 and 72h, indicating a negative impact on cell survival (Fig. 17). Comparing those results with the literature, 10^{-3} M Dex is an extraordinary high concentration compared to the normally described strongly varying supraphysiological concentrations of 10^{-5} M [198], 10^{-6} M [192] or 10^{-7} M [197]. In contrast, as physiological or supporting concentrations 10^{-7} M or 10^{-8} M Dex are defined and recommended to be added for osteogenic differentiation [199].

One possible reason why the strong inhibitory effect was only seen with a concentration of 10^{-3} M Dex could be differences in the composition of the osteogenic medium. It has been previously discussed that ascorbic acid is able to diminish the effect of high GC concentrations which could explain differences between studies due to varying concentrations of ascorbic acid in the differentiation medium [197]. Cárcamo Orive *et al.* reported inhibitory effects on hMSCs after treatment with 10^{-6} M Dex using 0.05 mM ascorbic acid-2-phosphate, while in the present study 0.1 mM ascorbic acid-2-phosphate was applied into the osteogenic medium (OM) [192]. Similar observations were described by Walsh and colleagues [197]. They described the inhibitory effect of high GC concentration on the proliferation of human osteoblast precursors indicated by lower cell numbers while recruitment and maturation were unaffected [197]. An additional aspect of interest was that they used bone marrow suspension which they treated with different concentrations of Dex over 28 days. Their results indicate that the crosstalk between different cells in the bone marrow could additionally mask the effect of high GC concentrations which is further supported by the recently published study from Kohno *et al.* [200]. They compared the effect of high Dex concentrations on isolated rat MSCs and bone marrow suspension reporting only strong

inhibitory effects of osteogenesis in the isolated MSCs. Since the hMSCs for the present study were isolated from bone marrow via migration rather than density gradient centrifugation, the heterogeneity of cells could be higher compared to other studies despite the positive characterization. This could additionally explain the requirement to apply those high concentrations of Dex.

Nevertheless, the aim of the study was to examine the potential counteracting ability of HIF-stabilizers towards inhibition of osteogenesis/calcification and therefore, a primary significant inhibitory effect was chosen in order to heighten any positive influences. Clear conclusions for the clinical translation cannot be made from this *in vitro* study as clinical applied dosages achieve far lower concentrations in the tissue [190]. However, as underlying mechanism for the inhibitory effect of high GC concentrations on osteogenesis or calcification, different pathways have been described involving i) the GCR [201], ii) the crosstalk between GCR and AP-1 [192] or the Histone deacetylase 6 [198], iii) the activation of the CCAAT/enhancer-binding protein alpha (C/EBP α), an enhancer of adipogenesis [202, 203] or the inhibition of osteoactivin downstream genes [204]. In addition, several mechanism have been proposed explaining the supporting effect of low GC concentrations on osteogenesis [205-210]. Based on these results, new therapeutic approaches have been developed applying low concentrations of Dex on scaffolds to enhance bone formation *in vivo* [211-216].

Besides the different Dex concentrations and the different time points, calcification in the hMSCs was compared between cultivation under normoxic (app. 18% O₂) or hypoxic (1% O₂) conditions. There were slight differences visible after 14 days showing higher calcification under hypoxia independent of the Dex concentration applied (Fig. 14). After 21 and 28 days, no differences were found. Interestingly for the OM only control group it seemed as if hypoxia would rather inhibit calcification at 21 and 28 days. In a previous study, our group showed that hypoxia promotes osteogenesis while diminishing adipogenesis in hMSC after 2 weeks using Alizarin red and Von Kossa staining without quantification [47]. These findings are somehow reproduced in a quantitative manner by the present data at 14 days - treatment group with 10⁻⁸ M Dex which is in our hands defined as physiological concentration (Fig. 14). Although the effect was not significant, Wagegg *et al.* additionally reported the upregulation of *HIF1A* on RNA level and the HIF-1-dependence of this effect by knock-down experiments [47]. A comparable effect was observed by Zou *et al.* describing higher expression levels of angiogenic, cartilaginous and osteogenic genes after HIF-1 α transduction [64]. The positive influence of hypoxia on osteogenic differentiation was further shown in other studies including also hMSCs from different sources e.g. placenta or fat [217-219]. However, many studies have been published during the last decade reporting an inhibitory effect of hypoxia on osteogenesis while the positive influence on chondrogenesis has been

widely scientifically accepted [220-224]. As underlying mechanism for the inhibition, Yang *et al.* described the direct regulation of *RUNX2* by *TWIST* a downstream gene of HIF-1 α while Zhang *et al.* proposed a prominent role of the p38-RUNX2 signaling pathway [225, 226]. In addition, Xu *et al.* showed an association between the inhibition of osteogenesis via hypoxia and increased levels and activity of Notch1 which can bind *RUNX2* and inhibit its transcriptional activity [227]. In the present study, no significance was found when comparing cultivation under normoxia and hypoxia which somehow resembles the controversy situation in the literature (Fig. 14). Nevertheless, the cultivation under hypoxic conditions was interrupted weekly by medium change which had to be performed under normoxic conditions.

Interestingly, from a bioenergetic point of view, it has been shown that undifferentiated hMSCs have increased glycolysis and high expression levels of glycolytic HIF target genes. In contrast during osteogenic differentiation, *HIF1A* mRNA and protein expression has been described to be reduced leading to diminished glycolysis and induction of oxidative metabolism [228]. Shum *et al.* performed bioenergetic profiling combined with transcriptomics and described the activation of the mitochondrial process of oxidative phosphorylation during osteogenesis which requires downregulation of HIF-1 α expression [229]. Unfortunately, they proved their hypotheses only by examining the *ALP*-expression and not functional parameters such as calcification. ALP activity has been described to be independent of subsequent calcification and therefore not a suitable parameter to be used alone for determine osteogenic differentiation success [194]. The described findings can be explained by the assumption that hypoxia regulates osteogenesis in a time-dependent manner which was shown by e.g. Ding *et al.* [230]. In detail, in early stages of osteogenesis HIF-1 α may be required to enhance proliferation and prepare differentiation while at later stages mitochondrial activation is more prominent and decreases the need for HIF-1 α [229, 230]. This goes hand in hand with studies showing a positive effect on bone formation after pretreatment of hMSCs with hypoxia [231-233]. For the *in vivo* situation it can be proposed that hMSCs are recruited to the fracture site due to the hypoxic environment which would require the cells to migrate and proliferate while during endochondral ossification first chondrogenic differentiation is activated under hypoxia while mineralization and osteogenic differentiation is initiated when new vessels penetrates the soft callus [104]. Due to the natural bone marrow niche and its low oxygen tensions, hMSC proliferation and stemness can be improved *in vitro* by cultivation under hypoxia (5 % O₂) [234-236].

Despite those findings, in the present study, cells were treated continuously via hypoxia or HIF-stabilizers – despite a weekly change of medium under normoxic conditions. But for the subsequent *in vivo* test, DFO and MIF were only applied during fracture initiation.

The application of DFO alone *in vitro* on hMSCs revealed significant increases in calcification despite the treatment with 10^{-3} M Dex, while MIF alone showed no counteracting potential (Fig. 15). The combination of DFO and MIF was significantly favorable for the calcification at 28 days especially for concentrations of 125 μ M DFO + 50 ng/ml MIF and 125 μ M DFO + 100 ng/ml MIF (Fig. 15, 16). Beside the stabilization of HIF-1 α , DFO has been described to directly influence hMSC differentiation via beta-catenin signaling cascades [237]. In addition, Yu and colleagues reported the STAT3-dependent increase of osteogenic differentiation initiated by Cobalt(II) chloride, another HIF-stabilizer [238]. Nevertheless, there is no study found in the literature addressing the counteracting potential of DFO for GC-induced inhibition of differentiation as shown in the present study. Interestingly, investigating the pathogenesis of GC-induced osteonecrosis of the femoral head the combination of hypoxia and GC seems to be disturbing rather than supporting [239]. In contrast, hypoxia has been shown to upregulate GCR activity while GCs have been shown to inhibit HIF in CD4⁺ T-cells or to be able to stabilize HIF in the liver of zebrafish [166, 240, 241]. Those data must be proven and reproduced during the next years and further studies are needed to clarify the potential crosstalk between GC and HIF in hMSCs and bone regeneration.

The ability of MIF to stabilize HIF-1 α was independently shown by two groups [166, 242]. In context of the results from the present study, the influence of MIF alone via stabilization of HIF and the properties as natural antagonist of GCs do not seem to be beneficial to overcome the strong inhibitory effect. Yet, it seems to have a supporting effect when combined with DFO. One reason for the disability to counteract alone could be the missing HIF-unrelated mechanism to influence osteogenesis as it has been described for DFO or the timing as discussed before. Taken together, the *in vitro* studies revealed a concentration-dependent inhibitory effect of Dex on hMSC calcification which could not be counteracted by hypoxia or application of MIF alone while the application of DFO and the DFO + MIF yielded beneficial effects towards significant upregulation of calcification despite the strong inhibitory effect of high Dex concentrations under normoxic conditions. Important conclusions could be drawn towards the dose finding for the *in vivo* proof of concept study.

4.3 Identification of a suitable scaffold for local delivery of MIF and DFO into the fracture gap

Biomaterials are of crucial importance for orthopedic medicine and research in order to fill large bone defects (osteoconduction) or to serve as a carrier for progenitor cells or osteoinductive factors in order to facilitate osteogenesis. Since absorbable bovine Col I scaffolds (ACS) are approved and routinely used in the clinics and research, two different ACS were tested in the second part of the present work for their suitability to be used in the proof of

concept study on DFO and MIF in fracture healing. The extracellular matrix (ECM) of bone consists of inorganic and organic components while 85-90% of bone protein are Col I [243]. Col I is a highly conserved protein with no potential interspecies differences.

Therefore, two ACS (Helistat®, H vs. Lyostypt®, L) were firstly examined via proteomics analysis followed by several *in vitro* experiments. Due to company secrets it was not possible to clarify the production strategies for ACS-L and ACS-H to get insights into the composition and structure. However, during proteomics analysis, several interesting proteins were identified beside Col I. Indeed, most abundant were the two alpha chains of Col I (COL1A1, COL1A2) followed by other collagens such as COL6A1-3 (Table 5 and 6). Membrane and cytoskeleton proteins such as Annexin (ANXA) 1, 2, 5, Actin beta or Tubulin were only found in ACS-L, while small leucine-rich proteoglycans (SLRP) such as vimetin, decorin (DCN), fibromodulin (FMOD) or osteoglycin (OGN) were found in both scaffolds. Comparing this proteomics analysis to a published study by Li *et al.* on rat-tail Col I, overlaps in the following identified proteins: Col1A2, Col1A1, DCN, vimentin, ANXA1 and 2 and Col5A1 and Col11A1 [244]. SLRP have small protein cores (36-42 kDa) and are integral components of the ECM in e.g. the skeleton. In bone, SLRP are involved in the bone formation process including the deposition of organic and inorganic matrix and can therefore interfere with the bone regeneration. Due to their structural specification, they can be divided into 5 classes. Examples for class I SLRP are DCN and asporin while FMOD is class II and OGN class III [245, 246]. DCN and FMOD besides biglycan and asporin bind TGFβ [247]. The formed complexes are eliminated via the circulation or urinary excretion or can be included in the ECM inactivating TGFβ functions [248, 249]. DCN knock-out mice exhibit irregular collagen fibrils which is more evident with biglycan depletion in parallel [250-252]. However, DCN can also enhance the bioactivity of TGFβ influence in the fate of MSCs [253, 254]. TGFβ plays a crucial role during fracture healing being strongly enhanced during callus formation, but also interfering with immune cells during the hematoma phase [255]. Thus, class I SLRP are strongly involved in cartilaginous callus formation and mineralization. OGN was firstly described to inhibit PTH-stimulated multinucleated cells formation *in vitro* [256]. Bentz *et al.* showed the osteoinductive ability of OGN *in vivo* [257]. ANXA2 and 5 are Ca²⁺-binding proteins, essential for osteoblast differentiation and mechanoreceptors regulating Ca²⁺ ion channels [258]. ANXA1 is involved in the regulation of endothelial activation, leukocyte infiltration and neutrophil apoptosis [259, 260]. Further roles and functions of identified proteins are summarized in Table 15.

Table 15: Results of the literature search on biological functions of selected proteins potentially being involved in bone-regeneration. Reproduced from [174].

Selected Proteins	Protein Group/ Family	Described Function and Relation to Bone Biology or Bone Healing	Affected Cells	Ref.
Decorin (DCN)	Small leucine-rich proteoglycan	<ul style="list-style-type: none"> modulates collagen fibril formation downregulates bioactivity of TGFβ inhibits fibrous encapsulation by inducing fibroblast apoptosis improves osteoblast calcification <i>in vitro</i> important regulatory role in bone mineralization 	ECM-producing cells Osteoblasts	[250] [251] [261] [180]
Osteoglycin (OGN)	Small leucine-rich proteoglycan	<ul style="list-style-type: none"> osteoinductive factor osteoblast differentiation, bone development inhibits multiple nucleated cells <i>in vitro</i> 	osteoblasts (osteoclasts)	[256, 262]
Fibromodulin (FMOD)	Small leucine-rich proteoglycan	<ul style="list-style-type: none"> binding with collagens - modulation of ECM important in wound healing pro-angiogenic effects <i>in vitro</i> maintenance of stem cell niches and modulating bioactivity of growth factors 	ECM-producing cells	[263- 265]
Sushi repeat-containing protein (SRPX)	Chondroitin sulfate proteoglycan	<ul style="list-style-type: none"> enhances angiogenesis down regulated by BMP-2 	endothelial pro- genitors	[183, 266]
Annexin 1 (ANXA 1)	Membrane protein	<ul style="list-style-type: none"> regulated by glucocorticoids – inhibits phospholipase A2 regulates innate immune cells clearance of inflammation, wound repair and restoration of mucosal homeostasis 	immune cells	[267, 268] [181, 259, 260]
Annexin 2 and 5 (ANXA 2, 5)	Membrane protein	<ul style="list-style-type: none"> identified in matrix vesicles of osteoblasts and hypertrophic chondrocytes during calcification process – membrane stability; formation of ion channels ANXA5 is central to osteoblast mechanotransduction ANXA2 expressed in osteoblasts and MSCs with osteogenic potential 	osteoblasts and hypertrophic chondrocytes	[182, 269] [270]
Heterogeneous nuclear ribonucleoprotein K (HNRNPK)	Transcription factor	<ul style="list-style-type: none"> major pre-mRNA-binding protein repressor of osteocalcin gene transcription 	(osteoblasts)	[184]

Since the ACSs are bovine origin, the clarification of species differences was of great interest with regard to the performed animal experiments in mice and therefore, sequence homology was analyzed for selected proteins revealing almost 100 % query cover (Table 7). Thus, specific proteins that were identified in the scaffold might have an effect in a murine or even human system. Taken together, there are several proteins in both of the two scaffolds which can be either advantageous or disadvantageous according to the literature. The manufacturing process of those scaffold often fail to remove all contamination or unwanted proteins leading to additional peptides after degradation which might have negative effects.

The ideal scaffold should fulfill different requirements such as i) providing a 3D porous network allowing cells to invade, ii) being biocompatible and bioresorbable with controlled degradation and resorption rates, iii) providing an optimal surface chemistry allowing cells to attach and iv) being able to adapt to mechanical properties at the implantation site [271].

Therefore, ACS-L and ACS-H were analyzed for structure, biocompatibility and cell invasion. In general, both scaffolds exhibited clear structural differences (Fig. 18). While ACS-L showed a fibrillar-network and was less form-stable during wetting, ACS-H consisted of tissue-layer – a wall-like structure and is strongly form-stable (Fig. 19 and 20). Col I based scaffolds can be produced from different resources such as skin, pericard, intestine or tendons. ACS-L is often described as fleece which is reflected by the fibrillar structure and softness while the wall-like structure of ACS-H is typical of porous sponges. It is known that ACS-H is manufactured from bovine deep flexor tendon. The common way of scaffold manufacturing starts with the production of a collagen solution. In a next step the collagen molecules are enforced to self-assemble by pH neutralization and incubation below denaturation temperature followed by freeze-drying [272]. In order to enhance the stability and mechanical properties different cross-linking techniques can be applied e.g. formaldehyde, dehydrothermal (DHT), glutaraldehyde (GTA), and carbodiimide (EDC). The composition of the scaffold as well as the cross-linking might influence the cellular response and biocompatibility [273-275]. Although natural cross-linking of collagens is essential for e.g. fracture healing [276]. Haugh *et al.* described the effect of GTA and EDC on stiffness which additionally favored the differentiation of osteoblasts [277]. Moreover, DHT cross-linking was shown to have a positive effect on *OPN* and *OC* expression of MC3T3 cells [278]. In contrast, Lee *et al.* reported a negative effect of cross-linking on osteogenic hMSC differentiation [279]. It is quite well known that cells react to the biomechanical properties of the surrounding environment and sense the stiffness of different tissue which influence the differentiation and maturation [280]. For example, stiffer scaffolds enhance osteogenic differentiation of hMSCs [281, 282]. Interestingly, in the current study the ACS-H, which exhibited stiffer properties than the ACS-L diminished hMSC calcification, although osteogenesis was not strongly affected, and cells were seeded around and not on the scaffold (Fig. 21-23).

The co-cultivation assay from this study is more comparable with a degradation assay focusing on the bioactivity of released peptides. Nevertheless, the inhibitory effect of ACS-H on hMSC calcification has not been described before (Fig. 21). It can be speculated that the loading of the scaffold led to the binding of e.g. glycerophosphate which is applied within the osteogenic medium and essential for calcification. The ACS-H as well as the ACS-L have been developed for hemostatic platelet activation and adsorption of blood where the loading and surface tension is essential for fast activation of the complement system and absorption [283]. Pure Col I is supposed to be favorable for hMSC adhesion, survival and proliferation as shown by Somaiah *et al.* when coating cell culture flasks with Col I [284]. The proteomics data revealed a higher abundance of FMOD in the ACS-H which perhaps could be released during the 3 weeks of cultivation. Interestingly, Li *et al.* used FMOD to reprogram fibroblasts which showed enhanced osteogenic properties *in vitro* [285]. FMOD

is highly expressed in chondrocytes and osteoblasts during fetal bone development and is essential for ECM maturation [264, 286]. Goldberg *et al.* described a dual function of FMOD during alveolar bone formation with an inhibitory function during the bone accumulation and developing step [287]. Additionally, another reason for the diminished calcification induced by ACS-H can be the reduced cell survival indicated by a higher LDH release, although collected RNA concentrations were comparable between treatment groups (Fig. 23). LIVE/DEAD staining revealed higher percentage of dead cells on ACS-H compared to the control which can be caused by the scaffold stiffness, surface tension/loading or cross-linking [288]. Nevertheless, most publications indicate the facilitation of cell attachment and differentiation as well as the recruitment of e.g. hMSCs to the implantation site when using ECM scaffolds [289-292].

Whole blood assays using human and murine blood showed a high TNF α release in the human system and no release in the murine system. Low doses of TNF α were recently described as promotional for bone regeneration when applied within 24 h after injury to recruit neutrophil granulocytes and monocytes [54]. Thus, the high TNF α release, induced by ACS-H, but also ACS-L, must not necessarily be disturbing in the human system (Fig. 23). It is not clear while there is a difference between the human and murine system in this approach, although several differences with regard to the immune system and response are widely discussed [293, 294]. Some mechanisms have been described how the immune system responds to biomaterials especially in terms of xenogeneic approaches. During the processing of the ECM and cross-linking most of cells, DNA, antigenic epitopes or damage associated molecular patterns (DAMP) are removed, although residual contaminants can activate an immune response. In a xenogeneic context, the Gal epitope (Gal α 1,3-Gal β 1-4GlcNAc-R) plays an important role and is most often found in animal-based scaffolds [295]. In order to examine the interaction of the immune system with the biomaterial dendritic cells (DCs) or macrophages are often used *in vitro* [296]. Therefore, Poudel *et al.* reported the enhanced maturation and function of DCs by Col I and that the Col I induced TNF α is crucial for activated and functionalized DCs [297]. In addition, Bayrak *et al.* intensively studied the properties of porcine and bovine Col I from the heart valve with the results that neither DCs nor T- or B-cells were triggered by the Col I [298]. But the co-cultivation with human immune cells revealed strong immune response (including TNF α) for the naïve and decellularized scaffolds while GTA cross-linking diminished these effects [299]. Nevertheless, without the concrete information on the manufacturing process of the two scaffolds underlying mechanism to our conclusions are only speculative.

Based on the *in vitro* data ACS-L was chosen to be tested *in vivo* and used as delivery system for DFO and MIF. Unexpectedly, there was an inhibition of bone healing observed

after two and three weeks (Fig. 24 and 26). Beside a significant inhibition of bone mineralization, cell invasion and vessel formation were reduced compared to the empty control. To exclude limitations such as the size or filling techniques, the used protocol was standardized and only two experienced surgeons performed the animal trials with no differences in their outcomes.

ACS-L and ACS-H are marked as hemostatic agents which promote platelet aggregation and physically block injured vessels due to strong adherence [300-303]. In 1978, Harris *et al.* reported no interfering effects with bone healing in total hip replacement when applying this scaffold as hemostatic agent [304]. Controversially, Schonhauer *et al.* listed animal studies with no impeding effect of Col I in their review but stated that Col I scaffold may interfere with bone healing [303]. The ACS-L was used by Fügl *et al.* for alveolar bone regeneration with the result of an inhibition at day 7 and 21 hypothesizing that increased resorptive activity alters regeneration which has been also described by Lindhe *et al.* using BioOss® [112, 305]. In addition, the soft mechanical properties may reduce MSC recruitment and differentiation capacity which is supported by lower cell numbers in the fracture gap at 2 weeks. Moreover, degradation might release bioactive peptides inhibiting the fracture healing process. For example, DCN was shown to regulate mineralization during development and regeneration while high expression have been shown at the bony ends of non-unions [261]. Furthermore, the presence of these ANXA might be beneficial for osteoblast differentiation, whereas ANXA1 is supposed to interfere with the initial phase of bone healing and might deactivate cells that are important for hematoma resorption [181]. HNRNPK is a transcription factor and described as a repressor of *OCN* gene transcription and therefore may negatively affect osteoblast differentiation [184]. Further studies are needed to examine the role of potential interfering and bioactive peptides released from Col I scaffolds during degradation within fracture healing more in detail.

However, the degradation and constructive remodeling of natural biomaterials mainly depend on the ability to modulate the host response. Anderson *et al.* divides the foreign body reaction in 7 steps - injury, blood-material interactions, provisional matrix formation, acute and chronic inflammation, granulation tissue development [306]. These steps can either lead to remodeling and degradation of the biomaterial or a fibrosis/fibrous capsule development. During the first hours post-implantation neutrophils are followed by macrophages at around 72 h [307]. The presence of macrophages is associated with chronic inflammation but is essential for constructive remodeling and may depend on the M1 or M2 phenotype [308-310]. Scaffolds with high concentrations of cellular residuals promote rather a M1 than

M2 response which delays the healing process [311]. Furthermore, cross-linking can influence the host response and prevent degradation [312, 313]. Since the ACS-L was not degraded over 3 weeks and cell invasion was low at 2 weeks it can be speculated that perhaps the cross-linking inhibits the immune response, or the scaffold is unreactive and does not sufficiently induce an inflammatory reaction (Fig. 25). This is also supported by the comparable numbers of macrophages between the control and ACS-L group at 2 and 3 weeks, although the differential staining for M1 and M2 macrophages would have been beneficial as well as the examination of earlier time points via histology (Fig. 29).

Furthermore, the presence and invasion of foreign body giant cells (FBGCs) are well known especially in a chronic process [306]. The main difference towards osteoclast is the not necessarily mineralized surrounding, since FBGCs also express TRAP [314]. Therefore, the distribution of TRAP⁺ cells within this study might indicate the presence of FBGCs at the interface between scaffold and bone-marrow, while osteoclasts can be found in the mineralized callus areas of the controls (Fig. 30). Interestingly, adherent macrophages and FBGCs close to the biomaterial produce a privileged environment which is characterized by e.g. reactive oxygen intermediates or high acidity (pH < 4) [315]. Nevertheless, it can be assumed that the slow degradation of the ACS-L caused the delayed healing process; therefore, these parameters should be considered more carefully before using those scaffolds in research or clinical application. Unfortunately, most of those important parameters are not available and the corresponding experiments are time-consuming and expensive. I assume that especially those circumstances are the main reasons for missing clinical translation and the gap between academia and pharmaceutical industry.

However, DeLustro and colleagues stated 1990 that the presence of immunity against collagenous and non-collagenous components does not necessarily predict adverse clinical outcomes. Immunity can exist as an epiphenomenon with no effect on e.g. osteogenesis [316]. This might be true with regard to clinical application, but in research those observations and considerations are of utmost importance in order to provide precise and reproducible data as well as valuable conclusions.

Nevertheless, Col I scaffolds in fracture healing are mainly used together with rhBMP-2. There are many controversially observations described in the literature on the effectiveness of this combination including potential adverse effects such as hematoma formation, higher incidence of infection and heterotopic bone formation [107]. However, adverse effects were never attributed to the carrier e.g. we observed ectopic/heterotopic bone formation that might be supported by rhBMP-2 in the clinic. In addition, inhibiting effects of the ACS-H scaffold in clinical application might be masked by the low pH solvent (pH: 4.5; hydrochloric

acid - HCl solution) for rhBMP-2 [317-319]. HCl enhances degradation by acting as an enzymatic pre-treatment although the effect of HCl on the initial phase of bone healing are unclear. Clinical studies using rhBMP-2 lack controls of only ACS which is reasonable due to ethical issues. In those studies controls are combinations of ACS and allograft [320].

Vessel formation is an important step during fracture healing as impaired angiogenesis can lead to delayed and non-unions. Some years ago, the group of Ralf Adams described the presence of a distinct vessel type in the growth plate of mice - type H vessels – consisting of endothelial cells (ECs) highly expressing CD31 and Emcn [52, 138, 185]. Here, we were able to show for the first time the presence of CD31^{hi}Emcn^{hi} ECs in the fracture gap and in the close area around the gap (Fig. 27 and 28). In addition, ACS-L treated mice showed abundant vessel formation as well as the loss of CD31^{hi}Emcn^{hi} ECs in the fracture gap and in the close area around the gap (Fig. 28). The underlying mechanisms are unclear, although several studies described that Col I scaffolds can be used to induce vessel formation *in vitro* including the development of capillary structures [117]. It can be speculated that the diminished cell invasion impacts the vessel formation and the low amount of cartilage which normally promote vessel formation by VEGF release [15].

These data show for the first time a negative influence of clinically routinely applied absorbable Col I scaffolds. For basic research, it is strongly recommended, when using those scaffolds as a delivery system for new substances, to consider the impaired healing character of the model. In terms of clinical applications, conclusions should be drawn carefully since the study was performed in a mouse model. However, these results greatly support the need for more sophisticated delivery systems and might help to convince the authorities to approve new innovative scaffolds with less potential adverse effects.

4.4 Investigation on the influence of MIF and/or DFO on the regeneration process in a delayed healing model

During the initial fracture healing phase, the hypoxic microenvironment is essential for activating the subsequent immune cell-driven healing cascade finally leading to regeneration [10]. Fracture hematomas collected from immunologically restricted patients showed an up-regulated *HIF1A* mRNA expression, but a decreased expression of *LDHA* and *PGK1* – two HIF target genes [102]. The missing adaptation to hypoxia may result in impaired fracture healing. HIF is the key regulator of cellular adaption under hypoxic conditions regulated by the activity of O₂ sensitive prolyl hydroxyls (PHDs). Stabilization of HIF leads to activation of angiogenic, proliferative or osteogenic target genes which can also be achieved by factors such as DFO and/or MIF. Therefore, the combination of MIF and DFO was examined in the previously described mouse-osteotomy-model of compromised conditions (inhibition

of mineralization and vascularization by ACS-L application) to verify the counteracting ability in a setting being much closer to clinical observations [174].

Quantitative *ex vivo* μ CT analysis and histomorphometry revealed enhanced mineralized callus formation after 14 and 21 days when applying DFO alone or in combination with MIF (Fig. 31). This is in accordance with several studies on DFO administered in rat- or mouse-osteotomy-models of *Ossa irregularia* (mandibula or zygomatic arch) and long bones (femur or tibia) [123-132, 134, 136, 143-147, 149, 174, 321]. All studies showed a strong positive effect of DFO on bone and vessel formation although the application routes and concentrations differed. The group of Prof. Buchman published several studies using mandibular osteotomy or distraction combined with or without radiation in rats applying DFO in a concentration of 200 μ M every other day with a total of 5 doses [99, 124-127, 130, 143-146]. Matsumoto *et al.* induced a cortical drilling hole in the tibia of rats and combined it with hindlimb unloading showing a positive effect on bone formation after 2 - 5 doses of 200 μ mol/l DFO every other day [132]. Much more comparable to the present work are the studies of Wan *et al.* and Yao *et al.* using the mouse-osteotomy-model with medullary pin fixation, but with a repeated local injection of 200 μ M DFO every other day [123, 135]. The hypothesis of the present study was that a single-dose of DFO in combination with MIF is sufficient to accelerate bone formation which was shown by the enhanced mineralized bone formation at later time points (14 and 21 days). The efficiency of a single-dose of DFO has been also shown before in osteotomy studies of long bones and the application of DFO on different scaffolds. Therefore, it could be speculated that a single-dose would be enough to enhance bone healing and avoid the application of several doses which could be difficult in a clinical setting. Nevertheless, all these studies focus on the application of DFO alone. In the present study, the combination with MIF was supposed to further enhance the DFO effect which could not be clearly shown in the data on callus mineralization and bone formation. It can be speculated that the DFO effect alone is strong enough and therefore masks the potential additional effect of MIF. However, comparing the histomorphometric results on mineralized bone formation endosteal or intracortical, MIF alone and in combination with DFO showed significantly more mineralized bone in the endosteal compartment after 14 days (Fig. 32-34). In contrast, DFO alone enhanced the bone formation intracortical compared to the ACS control. Willie *et al.* stated in their according study from 2011 that bony bridging in the intracortical or periosteal area indicates bone remodeling and healing while endosteal bridging does not [322]. Therefore, MIF could be assumed to delay fracture healing to a certain amount while underlying pathways have not been described in detail. Due to the prominent involvement of MIF in inflammatory processes, it can be hypothesized that the administration of MIF during the initial phase prolongs the pro-inflammatory phase and delays the anti-inflammatory phase which can negatively influence the following healing

cascade. This is in accordance with the gene expression data from day 7 and will be discussed below. In addition, in a previous study by Hoff *et al.* high levels of MIF were measured in fracture hematomas from immunologically restricted patients which are more predisposed to suffer from delayed bone healing or non-unions [39]. Nevertheless, MIF is a target gene of HIF-1 α , but also regulates and enhances the HIF stabilization itself as it has been described in CD4⁺ T-cells [157]. Within the present study, the additional stabilization of HIF-1 α was assumed to further accelerate bone healing. It can be not excluded that MIF acts concentration-dependent, since the concentration for the *in vivo* study has been extrapolated from *in vitro* calcification assays that additionally included GC treatment.

However, the effect of hypoxia on bone formation and underlying mechanism have been previously investigated over the last decades. Beside the upregulation of *VEGF* – a HIF target gene and key driver of vessel formation – the HIF-1 α induced upregulation of the Wnt/ β -catenin signaling pathway via downregulation of sclerostin (*Sost*) is of main interest. Genetos *et al.* showed the enhanced β -catenin reporter activity in osteoblasts and osteocytes under hypoxic conditions which was further accompanied by the increase of gremlin and noggin and a decrease of Smad-1/5/8 phosphorylation [66]. Moreover, Chen *et al.* described an upregulation of *Sost* in osteoblasts under hypoxia which led to an inhibition of Wnt signaling, but enhanced osteoblast proliferation [323]. In contrast, most recently, Stegen *et al.* reported that enhanced HIF-1 α signaling decreased *Sost* expression in osteocytes via Sirtuin 1-dependent deacetylation of the *Sost* promoter [324]. Therefore, the expression of *Sost* seems to have cell-specific effects. Since Wnt/ β -catenin signaling is especially important during the soft to hard callus formation influencing the osteo-chondro-progenitor differentiation, the potential inhibition of *Sost* has been studied by Kruck *et al.* [325]. Interestingly, they found that the application of a sclerostin antibody negatively influence the later stages of fracture healing such as a delayed callus mineralization and bone marrow reconstitution. In addition, HIF-stabilization can also activate BMP-2 signaling – a key driver during bone formation [104]. Since I observed more mineralized bone formation in the MIF + DFO and DFO alone group at day 14, it can be hypothesized that the stabilization of HIF-1 α might have upregulated *Sost* as well as induced BMP-2 signaling leading to enhanced osteoblast proliferation and to accelerated transformation from soft to hard callus. However, there was no upregulation seen at day 3 and 7 in the microarrays which suggest a potential earlier or later impact.

On a cellular level, the conditions of the initial phase are also prone to attract cells to the injury site especially macrophages, leukocytes and MSCs. Wu *et al.* demonstrated that DFO and DMOG are able to upregulate the expression of CXCR4 on MSCs [326]. In addition,

MIF has been shown to support homing of CXCR4⁺ osteoclast precursors as well as agonistically mimicking CXCL12 to interact with CXCR4 for leukocyte recruitment [327, 328]. Interestingly, CXCL12 has a hypoxia-response element on the promoter and is therefore mainly responsible for the cell recruitment to the fracture site [329]. In summary, the combination of MIF + DFO but also DFO alone are beneficial for cell recruitment which might explain the more pronounced mineralization being only possible when progenitor cells are at the fracture's site. This is further supported by Yao *et al.* who reported that MIF is essential during HIF-1 α regulated chondro-osteogenic differentiation by interacting with the SOX9 and *RUNX2* promoter – in human cartilage endplate stem cells [330].

In addition to the enhanced mineralization, a faster degradation of the ACS was observed especially in the MIF + DFO group (Fig. 34). The macrophage (F4/80⁺) staining did not show any significant effects although TRAP⁺ cells were slightly more pronounced in the combination group (Fig. 35 and 36). Drager *et al.* showed that DFO strongly supported resorption of biomaterial by enhancing osteoclast activity [129]. Interestingly, several studies describe the inhibition of osteoclasts induced by DFO or comparable substances [137, 331, 332]. In the present study TRAP staining does not reflect these observations, although TRAP staining is not osteoclast specific and also present in activated macrophages. However, MIF has been known to support osteoclastogenesis by interacting with the RANKL pathway [171, 172, 333, 334]. This might explain the high presence of TRAP positive cells in the combination group (Fig. 36). Macrophages are essential for fracture healing in general, but especially for vascularization and angiogenesis by degrading ECM, and releasing angiogenic factors [335, 336]. The degradation of the ECM enables the migration of endothelial progenitors and activate the angiogenic potential of some ECM molecules which has been shown e.g. for fragments of hyaluronic acid [337]. In addition, macrophages also release factors that attract, activate or even inhibit angiogenic cells depending on the phase of vascularization. Studies from mouse development revealed the tight association of macrophages with capillaries and the subsequent enhancement of angiogenesis [338, 339]. Interestingly, macrophages have been shown to regulate vessel permeability comparable to pericytes [340]. *Vice versa*, ECs also promote the selective growth and differentiation of macrophages, especially the switch towards the M2 phenotype which requires the direct contact with the endothelium and the regulation via M-CSF signaling [341]. In the present study, I did not perform specific stainings for M1 and M2 macrophage, but stainings of macrophages together with vessels indicate a close crosstalk especially under disturbed conditions (data not shown). This will be more closely investigated in a follow-up study.

However, beside macrophages, the HIF-1 α induced *VEGF* expression in different cell types is the major driver of vascularization during fracture healing. Wang *et al.* reported the up-regulation of VEGF by HIF-1 α stabilization in osteoblast which enhanced osteogenesis and angiogenesis [342]. This was also confirmed in several studies applying DFO to accelerate bone formation [133, 143, 321]. In 2014, Kusumbe *et al.* described CD31^{hi}Emcn^{hi} ECs to be part of a bone tissue specific vessel subtype linking angiogenesis and bone formation via Notch and HIF-1 α signaling. CD31^{hi}Emcn^{hi} ECs are situated at the bone surfaces and in the growth plate [138, 185]. Most recently, the presence of these ECs was observed in response to bone tissue injury – irradiation [138], after implantation of a microendoscope [54], adjacent to subchondral bone of aged and osteoarthritic joints [343], and after tibia drill hole injury [344] [174]. In the present study, the presence of CD31^{hi}Emcn^{hi} ECs in a complete fracture healing has been demonstrated for the first time. However, it is not clear why CD31^{hi}Emcn^{hi} ECs were inhibited by ACS, since bovine Col I scaffolds have been reported to induce vessel formation *in vitro* especially in CD31⁺ capillary structures [117]. However, the appearance CD31^{hi}Emcn^{hi} ECs was restored by application of DFO or MIF + DFO which is in accordance with a study indicating the restoration of H-type vessels in aged mice after DFO treatment (Fig. 38-40) [138, 174]. It can be proposed that the assessment of vessel formation and the presence of CD31^{hi}Emcn^{hi} ECs is essential to evaluate fracture healing outcomes although the underlying mechanism and functions of type-H vessels have not yet been fully characterized.

In order to get more insights into the early phase of fracture healing microarray analysis were performed from callus tissue collected at day 3 and 7 (Table 9-11). Note, the initial phase of fracture healing including pro-inflammatory processes are supposed to take place within the first 72 h after injury and are replaced by anti-inflammatory, regenerative processes. Therefore, it can be speculated that the pro-inflammatory phase should be diminished at day 3. The MIF + DFO group had higher expressions of *Igh6* and *Ms4a1* (CD20) which are related to B-cell development, maturation and immune response that is essential during fracture healing to suppress pro-inflammatory signals [32, 37, 345-347]. Normally, B-cells have been described to be present at later stages during fracture healing. In addition, *Cxcl3* – a neutrophil attractant which has been described to be upregulated during fracture healing – was more pronounced expressed in the combination group while *C1qtnf3*, which is connected to the innate immune system and bioenergetically protection, was down-regulated [22, 24, 348-350]. These results may indicate a more pronounced switch from pro- to anti-inflammatory signaling in the MIF + DFO group that later resulted in a faster mineralization. *Aldh2* is essential for detoxification of endogenous and exogenous aldehydes and counteracts ROS production at early stages of oxidative stress injuries [351, 352]. The downregulation in all treatment groups compared to ACS might be a sign of more

adequate and fast cellular adaptation to the microenvironment. At day 7, the MIF alone group showed upregulated expression of inflammation-related genes such as *IL1b*, *IL6*, *Gbp2*, *10* or several chemokines [21, 353-355]. *Capg* was upregulated in all treatment groups indicating enhanced macrophage motility, phagocytosis, and membrane ruffling further facilitating the cell invasion into collagen [356, 357]. Additionally, *Ear1* was downregulated in all groups – a cellular marker of eosinophils that is in accordance with the literature describing the presence of eosinophils at later stages during fracture healing [358, 359]. Moreover, *Lyve* was also upregulated in all treatment groups supporting immune cell migration during inflammation [360]. Taken together, these data indicate a more pronounced activation of macrophages and other useful inflammatory cells at day 7 in the treatment groups in order to degrade the ACS resulting in a better healing outcome at day 21 compared to the ACS. In addition, MIF seems to prolong the pro-inflammatory phase until day 7 explaining the delayed fracture healing.

Regarding the cell metabolism at day 7, *Pdk4* – a hypoxia-induce regulator of the glycolysis was induced in all groups, but mainly in the MIF + DFO group [361, 362]. Interestingly, *Hmox-1* was downregulated which has been described to be upregulated during the initial phase of fracture healing within the periosteum [13, 107, 363]. Retinoic acid is essential during bone healing and needs to be transported into the cells via *Crabp1* that was downregulated at day 7 in the treatment groups which might indicate counter-regulative mechanism in the ACS group to support regeneration. It additionally regulates BMP-2 expression and osteoblastogenesis [364]. Note, matrix-related genes were mainly upregulated in the MIF + DFO and MIF group indicating a beneficial effect of MIF, since matrix formation is strongly required at day 7 to support the soft callus formation which is represented by *Col2a1*, *Col10a1*, *Lect1* and *Hapln1* expression. All these genes are associated with cartilage formation, an essential step during endochondral ossification [365-369].

Several additional genes with regard to the muscle or fat metabolism or nervous system have been found, although their roles in the process of fracture healing have not been clarified, it is important to rather analyze and list than classifying them as contaminants. Fracture healing is a complex process involving several tissues surrounding the injury and we are only at the beginning of understanding all the cellular and molecular mechanism.

The last step was to compare the microarray data to the qRT-PCR for selected genes that were mostly comparable (Fig. 44). Nevertheless, there were also differences such as for *Mmp3* or *Il6* which may be based on the low n-numbers tested in the microarrays (n= 2) which was increased in the qRT-PCR (n= 2-4) (Table 12-14). Therefore, further detailed studies are needed, although the presented results in this study give interesting insights and provide evidence for further mechanistical hypotheses.

In summary, our data support the previously published studies on the potential of DFO to accelerate bone healing by enhancing mineralization and vessel formation. In addition, MIF alone used in a concentration of 100 ng/ml rather showed inhibitory properties in the regeneration process by potentially prolonging the pro-inflammatory phase. The additional effect of MIF on top of the DFO effect was only slightly seen at some points – e.g. faster ACS degradation or enhanced matrix formation at day 7. Therefore, it can be supposed that MIF acts concentration-dependent and further studies on the dosage finding are needed. However, to this end, it was clearly shown that the combination of HIF-stabilizers can counteract delayed fracture healing.

4.5 Limitations

➤ *In vitro* studies on hMSCs

In the present study, hMSCs were isolated via migration from the bone marrow although normal protocols recommend density gradient centrifugation. The protocol in our lab was established as the cell number was markedly higher after migration compared to the density gradient centrifugation. Nevertheless, the increased cell number can be an indication for higher heterogeneity in the following cell culture which can influence the experimental outcomes. Density gradient centrifugation also has disadvantages e.g. losing smaller cell populations such as high proliferative hMSCs or the varying protocols that can be found in the literature which does also not ensure reproducibility [370]. Furthermore, there is strong evidence in the literature that freshly isolated hMSCs differ in their transcriptome and secretome from isolated and cultivated hMSCs indicating that conclusion from *in vitro* studies should be translated carefully towards *in vivo* assumptions [187]. In the present study, the *in vitro* studies were rather used as a tool to get insights for further *in vivo* studies than investigating specific pathways.

Moreover, it has been known for many years that hMSCs are affected by ageing, therefore the donor age as well as the ageing *in vitro* can influence experimental outcomes. In the present study the mean age for the NM 1 group was 67.6 ± 11 years, while the mean age of the NM 2 group was 71.3 ± 12 years. Beside the lower number of hMSCs that can be obtained from bone marrow aspirates in elderly patients, the proliferation capacity and the differentiation potential can be strongly affected [371, 372]. That is why, in our lab the expansion medium (NM 1 vs. NM 2) was changed during the time of this study. By supplementing the expansion medium with 20 % of the StemMACS™ MSC Expansion Media, the proliferation capacity and velocity was significantly enhanced while donor-differences and variations were strongly diminished. The change of the medium did not disturb the first part of this study. Cells expanded with the new medium were firstly used in the second part of this study. Nevertheless, Fickert *et al.* showed that the osteogenic capacity (ALP activity)

was the highest in hMSCs from donors aged > 65 years [353]. With regard to *in vitro* ageing, the current applied protocols do only include hMSCs between passage 4 - 7, a state that is considered to be not strongly influenced by passaging [373].

For the *in vitro* studies on GC and DFO/MIF, all hMSCs were expanded and cultivated in monolayer under normoxic condition which does not parallel the normal bone marrow niche – 3D and hypoxia [374, 375]. Moreover, a heterogenic population of hMSCs was used for the assays while distinct subpopulations can be influenced differently by the treatments [376]. In addition, high Dex concentrations were required to mimic significant inhibitory effects of GCs *in vitro*. Those concentrations do not resemble clinically used dosages. For cell survival, a LDH assay was performed and showed higher LDH releases under DFO and DFO + GC treatment which can be an effect of HIF-upregulated LDH expression (HIF target gene). Therefore, the LDH release is much higher from one apoptotic cell compared to a control. For further studies the determination of the cell number could be much more reliable in order to evaluate influences on apoptosis and proliferation. Therefore, different approaches must be evaluated which can be combined with the Alizarin red staining and quantification. Interestingly, MTT assay has been shown to be influenced by DFO which should be taken into account when choosing appropriate assays [377]. Finally, it is important to mention that steroid effects and regulation can be affected by gender differences [206]. In the present study the results of male and female hMSCs were pooled and no detailed evaluation of gender differences were applied. In context of the ongoing debates on gender differences, it should be self-evident that in following studies the potential gender difference is considered more in detail.

➤ **Animal models**

Nevertheless, it should be taken into account that the present study was conducted in mice and the interpolation to the human can be limited. In general, in orthopedic research rodents as well as large animal models are most commonly used. Mice are favored for basic research questions due to the possibility of genetical modifications. In contrast, sheep or pigs are preferred for translational approaches and rats are more often used for pharmacological interventions and toxicological studies. Most animal species show slight analogies to the human bone macro- and microstructure. Main differences in mice are based on permanent opening of the growth plate in the epiphyses of long bones leading to a lifelong skeletal modeling, the lack of a Haversian system and low cancellous bone content at the epiphyses of long bones [378, 379]. Here, a mouse-osteotomy-model was used which does not completely heal within a time period of 21 days (osteotomy gap 0.7 mm) in the control group. Thus, an improvement in the healing process can be seen in treated groups. This model only works in female mice since the bone healing process is slower in females than in males

[380]. In addition, the BL6 strain is known for good bone healing qualities – bone growth is “adult” at around 12 weeks and bone reaches its peak bone mass at around 16 weeks [174]. However, it is not always possible to determine the exact time frames for every phase during the fracture healing process which makes the interpretation much more complex and might impact especially small differences. This might be a reason while the beneficial effect of MIF is not clearly visible indicating a more technical and methodical challenge rather than a biological non-function.

CHAPTER 5: Conclusion and Future Perspectives

This study shows that a single-dose application of DFO alone and in combination with MIF can counteract e.g. a GC induced inhibition of calcification *in vitro* or a bovine Col I scaffold-based delay of fracture healing *in vivo* in a mouse-osteotomy-model. Therefore, additional evidence is provided for the beneficial effect of HIF-1 α stabilization during fracture healing which is definitively a promising therapeutic approach for further regenerative strategies. Furthermore, the results report for the first time inhibitory effects of clinically applied scaffolds. Therefore, more sophisticated and appropriate transfer/delivery systems with more promising characteristics are urgently required. Biological activity of those delivery systems should be carefully examined early in the development and reconsidered also during clinical use enforcing a paradigm shift within biomaterial research to fasten up the translational process.

Fracture healing combines spatiotemporal fine-tuned and tightly regulated regenerative processes which lead to a complete restoration of the broken bone without formation of a fibrous scar. However, 10 % of patients with fractures suffer from fracture healing disorders such as delayed healing or non-unions leading to immobility, pain and a loss in quality of life and to an economic burden for the society [2, 3]. Patients with fracture healing disorders often require several further revision surgeries. Usually, regeneration processes during fracture healing are completed within 4 months. If healing takes longer, it is termed 'delayed'. If bridging of the fracture gap does not take place after 9 months, it is termed 'non-union' [72]. Although there are treatment strategies available including rh BMP-2 for local delivery into the fracture gap [381], low effectiveness and observations of several adverse effects strongly restrict the clinical use of this approach. Therefore, new delivery strategies and further therapeutic alternatives are needed.

The HIF-stabilizer DFO has been proven to be effective in preventing fracture healing disorders and is a cost-effective and low-risk alternative to recombinant human growth factors such as BMP-2. Based on previous results, the FDA approved DFO, which is commercially available as Desferal[®] (Novartis) and listed on *World Health Organization's List of Essential Medicines*, can be considered as suitable for rapid clinical translation to improve fracture healing and the treatment of bone healing disorders. Therefore, we are currently striving to start a multi-centric confirmatory study with the long-term goal of clinical translation. In addition, further studies on MIF are under way using our own developed *in vitro* models to simulate the initial phase of fracture healing in order to actively implement the 3R-principle in our laboratory routine.

Summary

HIF-stabilization to accelerate fracture healing – Evaluation of a new therapeutic strategy to treat delayed bone regeneration

The hypoxic microenvironment during the initial phase of fracture healing is essential for initiating immunological process that further the regeneration and restoration of the bone. The hypoxia-inducible factor (HIF)-1 α closely regulates the cellular adaption under hypoxic conditions. HIF-1 α can be chemically stabilized by different factors which either inhibit the O₂-sensing prolyl hydroxylase e.g. deferoxamine (DFO) or directly interfere with the downstream effects after nuclear translocation e.g. the macrophage-migration inhibitory factor (MIF). As a transcription factor, HIF-1 α initiates the consecutive processes of bone regeneration and human mesenchymal stromal cell (hMSC) differentiation. Hence, the aim was to promote the cellular adaptation towards hypoxia in order to specifically accelerate fracture healing under compromised conditions (inhibited mineralization and vascularization). First, *in vitro* studies were performed to i) evaluate the potential of DFO and MIF in combination to counteract a glucocorticoid-induced inhibition of hMSC calcification and ii) determine an effective concentration of both substances for further testing in a mouse-osteotomy-model. Concurrently, two absorbable bovine Col I scaffolds (ACSs) were tested for their suitability to be used as a delivery system of these substances into the osteotomy gap. Finally, both HIF-stabilizers were evaluated for their potential to accelerate fracture healing in a mouse-osteotomy-model.

In vitro, a concentration-dependent inhibitory effect of the glucocorticoid dexamethasone was observed on osteogenic differentiation and calcification of hMSCs via a quantitative Alizarin red assay. This inhibition was counteracted by applying different concentrations DFO and MIF in combination. As suitable scaffolds for the *in vivo* application Lyostypt® (ACS-L) and Helistat® (ACS-H) were investigated *in vitro* for their structural components and impact on hMSC osteogenesis, cytotoxicity and immunogenicity. Proteomics analysis of both scaffolds yielded several proteins beside collagens that might be advantageous or disadvantageous regarding the fracture healing outcomes. Moreover, ACS-H induced a strong tumor necrosis factor (TNF α) release when applied to whole human blood and inhibited the calcification during the osteogenic differentiation of hMSCs. Consequently, ACS-L was examined in more detail in a mouse-osteotomy-model and revealed an inhibitory effect on mineralized callus formation, cellular recruitment to the osteotomy gap and vessel formation. The application of DFO and MIF in combination and DFO alone during the initial healing phase accelerated the vessel formation, the ACS degradation and the callus mineralization.

The results support the fact that stabilization of HIF-1 α enhances osteogenic differentiation *in vitro* and is capable to counteract e.g. glucocorticoid-induced inhibition. Both ACSs negatively influenced either the hMSC differentiation *in vitro* or the bone healing process *in vivo*, although being routinely used in research and clinic routine. These results display a delayed healing process that parallels observed compromised conditions in Rheumatoid arthritis patients or smokers – reduced vessel and bone formation. The combination of MIF and DFO was evaluated in this model of compromised condition to test their counteracting ability in this clinically relevant model. This study provides evidence for a promising therapeutic strategy to accelerate fracture healing capacities and to prevent disorders by applying potent HIF-stabilizers in a specific patient cohort with a higher risk of a bone healing delay.

Zusammenfassung

HIF-Stabilisierung zur Verbesserung der Frakturheilung – Evaluation eines neuen therapeutischen Ansatzes zur Behandlung von Frakturheilungsstörungen

Das hypoxische Mikromilieu während der initialen Phase der Frakturheilung ist essenziell für die Knochenregeneration und -wiederherstellung. Dadurch werden wichtige immunologische Prozesse für den weiteren Verlauf der Heilung angeschoben. Der Hypoxie-induzierte Faktor (HIF)-1 α reguliert maßgeblich die zelluläre Adaptation unter hypoxischen Bedingungen. HIF-1 α kann durch verschiedene Faktoren chemisch stabilisiert werden, wobei diese entweder die O₂-sensitive Prolyl-Hydroxylase hemmen, wie z.B. Deferoxamin (DFO) oder direkt mit dem Signalweg nach HIF-Translokation in den Nukleus interagieren, wie z.B. der Macrophage-migration Inhibitory Factor (MIF). Als Transkriptionsfaktor aktiviert HIF-1 α wichtige Schritte der Knochenregeneration, wie z.B. die Differenzierung von humanen Mesenchymalen Stromazellen (hMSC) oder die Gefäßbildung. Dementsprechend ist die Förderung der zellulären Adaptation gegenüber Hypoxie ein vielversprechender Ansatz und Inhalt dieser Arbeit, um die Frakturheilung vor allem unter kompromittierten Bedingungen (Hemmung der Mineralisierung und Vaskularisierung) zu verbessern. In einem ersten Schritt wurden *In-vitro*-Studien durchgeführt um (i) das Potential von MIF und DFO in Kombination zu testen, einer Glukokortikoid-induzierten Hemmung der Kalzifizierung von hMSCs entgegenzuwirken und (ii) die optimale Dosierung beider Substanzen für weitere Studien *in vivo* zu bestimmen. Parallel dazu wurden zwei absorbierbare bovine Kollagen-I Scaffolds (ACS) auf ihre Eignung, als Trägermaterialien für die Substanzkombination für die weiteren *In-vivo*-Testung zu dienen, evaluiert. Im letzten Schritt wurde der Effekt von MIF und DFO nach lokaler Applikation in einem Maus-Osteotomie-Modell untersucht.

In vitro wurde ein konzentrationsabhängiger hemmender Effekt des Glukokortikoids Dexamethason auf die osteogene Differenzierung und Kalzifizierung von hMSC mittels quantitativem Alizarin-Rot-Assay beobachtet. Diese Hemmung konnte durch Applikation von verschiedenen Konzentrationen von MIF und DFO in Kombination aufgehoben werden. Die ausgewählten Scaffolds für die *In-vivo*-Studien, Lyostypt® (ACS-L) und Helistat® (ACS-H), wurden einer genaueren Analyse ihrer strukturelle Beschaffenheit und ihres potentiellen Einfluss auf die osteogene Differenzierung von hMSC, Zytotoxizität und Immunogenität unterzogen. Mittels Proteomics-Analysen konnten neben den zu erwartenden Kollagenen weitere Proteine, die potenziell die Knochenregeneration beeinflussen können, nachgewiesen werden. Weiterhin induzierte ACS-H eine signifikante Freisetzung des Tumor-Nekrosefaktors (TNF)- α in humanem Vollblut und hemmte die Kalzifizierung von hMSC während der Osteogenese. Folglich wurde nur ACS-L für weitere *In-vivo*-Studien eingesetzt. Dieser zeigte nach Applikation in einem Maus-Osteotomie-Modell eine hemmende Wirkung auf die

mineralisierte Kallusformation, die Zellmigration in den Osteotomiespalt und die Gefäßbildung. Die Applikation von DFO und MIF oder nur DFO allein konnte diesem hemmenden Effekt entgegenwirken.

Die Ergebnisse der Studie unterstützen den Fakt, dass die Stabilisierung von HIF-1 α , die osteogene Differenzierung *in vitro* fördert und z.B. Glukokortikoid-induzierten negativen Effekten entgegenwirken kann. Interessanterweise zeigten beide Scaffolds eine hemmende Wirkung auf hMSC *in vitro* oder den Knochenregenerationsprozess *in vivo*, obwohl sie beide routinemäßig in der Klinik oder Forschung zur Behandlung von Knochenbrüchen eingesetzt werden. Die Nutzung des ACS-L, als Trägermaterial, für die *In-vivo*-Studien ist entsprechend den hier gewonnen Daten eher vergleichbar mit kompromittierenden Bedingungen, wie sie z.B. während der Knochenheilung in Rheuma-Patienten oder Rauchern beobachtet werden (reduzierte Knochen- und Gefäßbildung). Die Kombination von MIF und DFO wurde in diesem Modell untersucht und konnte in einem klinisch-relevanten Modell ihr Potential zur Verbesserung der Knochenregeneration zeigen. Die Ergebnisse dieser Arbeit sind äußerst vielversprechend im Hinblick auf die mögliche Therapie von spezifischen Patientenkohorten, die zu Frakturheilungsstörungen neigen, mit HIF-Stabilisatoren, um die Knochenregeneration nebenwirkungsarm zu fördern.

References

- [1] B. McKibbin, "The biology of fracture healing in long bones," (in eng), *The Journal of bone and joint surgery. British volume*, vol. 60-b, no. 2, pp. 150-62, May 1978.
- [2] D. J. Hak *et al.*, "Delayed union and nonunions: epidemiology, clinical issues, and financial aspects," (in eng), *Injury*, vol. 45 Suppl 2, pp. S3-7, Jun 2014.
- [3] K. D. Hankenson, G. Zmmerman, and R. Marcucio, "Biological Perspectives of Delayed Fracture Healing," *Injury*, vol. 45, no. 0 2, pp. S8-S15, 2014.
- [4] N. K. Kanakaris and P. V. Giannoudis, "The health economics of the treatment of long-bone non-unions," (in eng), *Injury*, vol. 38 Suppl 2, pp. S77-84, May 2007.
- [5] P. Baldwin, D. J. Li, D. A. Auston, H. S. Mir, R. S. Yoon, and K. J. Koval, "Autograft, allograft, and bone graft substitutes: clinical evidence and indications for use in the setting of orthopaedic trauma surgery," (in eng), *Journal of orthopaedic trauma*, Jan 8 2019.
- [6] T. Winkler, F. A. Sass, G. N. Duda, and K. Schmidt-Bleek, "A review of biomaterials in bone defect healing, remaining shortcomings and future opportunities for bone tissue engineering: The unsolved challenge," *Bone & Joint Research*, vol. 7, no. 3, pp. 232-243, 05/05 2018.
- [7] T. A. Einhorn and L. C. Gerstenfeld, "Fracture healing: mechanisms and interventions," (in eng), *Nature reviews. Rheumatology*, vol. 11, no. 1, pp. 45-54, Jan 2015.
- [8] R. Marsell and T. A. Einhorn, "The biology of fracture healing," (in eng), *Injury*, vol. 42, no. 6, pp. 551-5, Jun 2011.
- [9] K. Schmidt-Bleek, A. Petersen, A. Dienelt, C. Schwarz, and G. N. Duda, "Initiation and early control of tissue regeneration - bone healing as a model system for tissue regeneration," (in eng), *Expert opinion on biological therapy*, vol. 14, no. 2, pp. 247-59, Feb 2014.
- [10] P. Kolar *et al.*, "The early fracture hematoma and its potential role in fracture healing," (in eng), *Tissue engineering. Part B, Reviews*, vol. 16, no. 4, pp. 427-34, Aug 2010.
- [11] L. Claes, S. Recknagel, and A. Ignatius, "Fracture healing under healthy and inflammatory conditions," (in eng), *Nature reviews. Rheumatology*, vol. 8, no. 3, pp. 133-43, Jan 31 2012.
- [12] P. Kolar, T. Gaber, C. Perka, G. N. Duda, and F. Buttgerit, "Human early fracture hematoma is characterized by inflammation and hypoxia," (in eng), *Clinical orthopaedics and related research*, vol. 469, no. 11, pp. 3118-26, Nov 2011.
- [13] H. Schell, G. N. Duda, A. Peters, S. Tsitsilonis, K. A. Johnson, and K. Schmidt-Bleek, "The haematoma and its role in bone healing," (in eng), *Journal of experimental orthopaedics*, vol. 4, no. 1, p. 5, Dec 2017.
- [14] X. Wang, T. Friis, V. Glatt, R. Crawford, and Y. Xiao, "Structural properties of fracture haematoma: current status and future clinical implications," *Journal of tissue engineering and regenerative medicine*, vol. 11, no. 10, pp. 2864-2875, 2017.

- [15] K. Schmidt-Bleek, B. J. Kwee, D. J. Mooney, and G. N. Duda, "Boon and Bane of Inflammation in Bone Tissue Regeneration and Its Link with Angiogenesis," *Tissue Engineering. Part B, Reviews*, vol. 21, no. 4, pp. 354-364, 2015 2015.
- [16] R. J. O'Keefe, "Fibrinolysis as a Target to Enhance Fracture Healing," (in eng), *The New England journal of medicine*, vol. 373, no. 18, pp. 1776-8, Oct 29 2015.
- [17] M. Yuasa *et al.*, "Fibrinolysis is essential for fracture repair and prevention of heterotopic ossification," (in eng), *The Journal of clinical investigation*, vol. 125, no. 8, pp. 3117-31, Aug 3 2015.
- [18] C. H. Rundle, X. Wang, J. E. Wergedal, S. Mohan, and K. H. Lau, "Fracture healing in mice deficient in plasminogen activator inhibitor-1," (in eng), *Calcified tissue international*, vol. 83, no. 4, pp. 276-84, Oct 2008.
- [19] O. Grundnes and O. Reikeras, "The importance of the hematoma for fracture healing in rats," (in eng), *Acta orthopaedica Scandinavica*, vol. 64, no. 3, pp. 340-2, Jun 1993.
- [20] S. H. Park, M. Silva, W. J. Bahk, H. McKellop, and J. R. Lieberman, "Effect of repeated irrigation and debridement on fracture healing in an animal model," (in eng), *Journal of orthopaedic research : official publication of the Orthopaedic Research Society*, vol. 20, no. 6, pp. 1197-204, Nov 2002.
- [21] P. Hoff *et al.*, "Immunological characterization of the early human fracture hematoma," (in eng), *Immunologic research*, vol. 64, no. 5-6, pp. 1195-1206, Dec 2016.
- [22] O. W. Bastian, L. Koenderman, J. Alblas, L. P. Leenen, and T. J. Blokhuis, "Neutrophils contribute to fracture healing by synthesizing fibronectin+ extracellular matrix rapidly after injury," (in eng), *Clinical immunology (Orlando, Fla.)*, vol. 164, pp. 78-84, Mar 2016.
- [23] R. Chung, J. C. Cool, M. A. Scherer, B. K. Foster, and C. J. Xian, "Roles of neutrophil-mediated inflammatory response in the bony repair of injured growth plate cartilage in young rats," (in eng), *Journal of leukocyte biology*, vol. 80, no. 6, pp. 1272-80, Dec 2006.
- [24] A. Kovtun, S. Bergdolt, R. Wiegner, P. Radermacher, M. Huber-Lang, and A. Ignatius, "The crucial role of neutrophil granulocytes in bone fracture healing," (in eng), *European cells & materials*, vol. 32, pp. 152-62, Jul 25 2016.
- [25] M. Bozlar, B. Aslan, A. Kalaci, L. Baktiroglu, A. N. Yanat, and A. Tasci, "Effects of human granulocyte-colony stimulating factor on fracture healing in rats," (in eng), *Saudi medical journal*, vol. 26, no. 8, pp. 1250-4, Aug 2005.
- [26] D. Moukoko *et al.*, "Granulocyte-colony stimulating factor enhances bone fracture healing," (in eng), *Clinical biomechanics (Bristol, Avon)*, vol. 58, pp. 62-68, Oct 2018.
- [27] K. A. Alexander *et al.*, "Osteal macrophages promote in vivo intramembranous bone healing in a mouse tibial injury model," (in eng), *Journal of bone and mineral research : the official journal of the American Society for Bone and Mineral Research*, vol. 26, no. 7, pp. 1517-32, Jul 2011.
- [28] K. A. Alexander *et al.*, "Resting and injury-induced inflamed periosteum contain multiple macrophage subsets that are located at sites of bone growth and regeneration," *Immunology & Cell Biology*, vol. 95, no. 1, pp. 7-16, 2017.

- [29] L. Batoon, S. M. Millard, L. J. Raggatt, and A. R. Pettit, "Osteomacs and Bone Regeneration," (in eng), *Curr Osteoporos Rep*, vol. 15, no. 4, pp. 385-395, Aug 2017.
- [30] C. Schlundt *et al.*, "Macrophages in bone fracture healing: Their essential role in endochondral ossification," (in eng), *Bone*, vol. 106, pp. 78-89, Jan 1 2015.
- [31] L. Vi *et al.*, "Macrophage cells secrete factors including LRP1 that orchestrate the rejuvenation of bone repair in mice," *Nature communications*, vol. 9, no. 1, pp. DOI: 10.1038/s41467-018-07666-0, 2018/12/05 2018.
- [32] D. Toben *et al.*, "Fracture healing is accelerated in the absence of the adaptive immune system," *Journal of Bone and Mineral Research*, vol. 26, no. 1, pp. 113-124, 2011.
- [33] N. T. Colburn, K. J. Zaal, F. Wang, and R. S. Tuan, "A role for gamma/delta T cells in a mouse model of fracture healing," (in eng), *Arthritis and rheumatism*, vol. 60, no. 6, pp. 1694-703, Jun 2009.
- [34] S. Reinke *et al.*, "Terminally differentiated CD8(+) T cells negatively affect bone regeneration in humans," (in eng), *Science translational medicine*, vol. 5, no. 177, p. 177ra36, Mar 20 2013.
- [35] F. Grassi *et al.*, "T cell subsets differently regulate osteogenic differentiation of human mesenchymal stromal cells in vitro," (in eng), *Journal of tissue engineering and regenerative medicine*, vol. 10, no. 4, pp. 305-14, Apr 2016.
- [36] M. O. Al-Sebaei *et al.*, "Role of Fas and Treg cells in fracture healing as characterized in the fas-deficient (*lpr*) mouse model of lupus," (in eng), *Journal of bone and mineral research : the official journal of the American Society for Bone and Mineral Research*, vol. 29, no. 6, pp. 1478-91, Jun 2014.
- [37] I. Konnecke *et al.*, "T and B cells participate in bone repair by infiltrating the fracture callus in a two-wave fashion," (in eng), *Bone*, vol. 64, pp. 155-65, Jul 2014.
- [38] G. Sun *et al.*, "STAT3 promotes bone fracture healing by enhancing the FOXP3 expression and the suppressive function of regulatory T cells," (in eng), *APMIS : acta pathologica, microbiologica, et immunologica Scandinavica*, vol. 125, no. 8, pp. 752-760, Aug 2017.
- [39] P. Hoff *et al.*, "A Pronounced Inflammatory Activity Characterizes the Early Fracture Healing Phase in Immunologically Restricted Patients," (in eng), *International journal of molecular sciences*, vol. 18, no. 3, p. DOI: 10.3390/ijms18030583, Mar 08 2017.
- [40] F. Gao *et al.*, "Mesenchymal stem cells and immunomodulation: current status and future prospects," (in eng), *Cell Death Dis*, vol. 7, p. e2062, Jan 21 2016.
- [41] T. Gaber *et al.*, "CTLA-4 Mediates Inhibitory Function of Mesenchymal Stem/Stromal Cells," *International journal of molecular sciences*, vol. 19, no. 8, p. 2312, 2018.
- [42] T. Furuta *et al.*, "Mesenchymal Stem Cell-Derived Exosomes Promote Fracture Healing in a Mouse Model," (in eng), *Stem cells translational medicine*, vol. 5, no. 12, pp. 1620-1630, Dec 2016.
- [43] F. Granero-Molto *et al.*, "Regenerative effects of transplanted mesenchymal stem cells in fracture healing," (in eng), *Stem cells (Dayton, Ohio)*, vol. 27, no. 8, pp. 1887-98, Aug 2009.

- [44] S. Herberg *et al.*, "Mesenchymal stem cell expression of stromal cell-derived factor-1beta augments bone formation in a model of local regenerative therapy," (in eng), *Journal of orthopaedic research : official publication of the Orthopaedic Research Society*, vol. 33, no. 2, pp. 174-84, Feb 2015.
- [45] Z. Lu, Y. Chen, C. Dunstan, S. Roohani-Esfahani, and H. Zreiqat, "Priming Adipose Stem Cells with Tumor Necrosis Factor-Alpha Preconditioning Potentiates Their Exosome Efficacy for Bone Regeneration," (in eng), *Tissue engineering. Part A*, vol. 23, no. 21-22, pp. 1212-1220, Nov 2017.
- [46] P. M. Mountziaris, S. N. Tzouanas, and A. G. Mikos, "Dose effect of tumor necrosis factor-alpha on in vitro osteogenic differentiation of mesenchymal stem cells on biodegradable polymeric microfiber scaffolds," (in eng), *Biomaterials*, vol. 31, no. 7, pp. 1666-75, Mar 2010.
- [47] M. Wagegg *et al.*, "Hypoxia promotes osteogenesis but suppresses adipogenesis of human mesenchymal stromal cells in a hypoxia-inducible factor-1 dependent manner," (in eng), *PLoS One*, vol. 7, no. 9, p. e46483, 2012.
- [48] Z. S. Ai-Aql, A. S. Alagl, D. T. Graves, L. C. Gerstenfeld, and T. A. Einhorn, "Molecular mechanisms controlling bone formation during fracture healing and distraction osteogenesis," (in eng), *J Dent Res*, vol. 87, no. 2, pp. 107-18, Feb 2008.
- [49] P. J. Bouletreau *et al.*, "Hypoxia and VEGF up-regulate BMP-2 mRNA and protein expression in microvascular endothelial cells: implications for fracture healing," (in eng), *Plastic and reconstructive surgery*, vol. 109, no. 7, pp. 2384-97, Jun 2002.
- [50] K. Hu and B. R. Olsen, "The roles of vascular endothelial growth factor in bone repair and regeneration," (in eng), *Bone*, vol. 91, pp. 30-8, Oct 2016.
- [51] J. Filipowska, K. A. Tomaszewski, L. Niedzwiedzki, J. A. Walocha, and T. Niedzwiedzki, "The role of vasculature in bone development, regeneration and proper systemic functioning," (in eng), *Angiogenesis*, vol. 20, no. 3, pp. 291-302, Aug 2017.
- [52] S. K. Ramasamy, "Structure and Functions of Blood Vessels and Vascular Niches in Bone," (in eng), *Stem cells international*, vol. 2017, p. 5046953, 2017.
- [53] J. Lienau *et al.*, "Differential regulation of blood vessel formation between standard and delayed bone healing," (in eng), *Journal of orthopaedic research : official publication of the Orthopaedic Research Society*, vol. 27, no. 9, pp. 1133-40, Sep 2009.
- [54] D. Reismann *et al.*, "Longitudinal intravital imaging of the femoral bone marrow reveals plasticity within marrow vasculature," (in eng), *Nature communications*, vol. 8, no. 1, pp. DOI: 10.1038/s41467-017-01538-9, Dec 18 2017.
- [55] H. Aro, E. Eerola, A. J. Aho, and J. Niinikoski, "Tissue oxygen tension in externally stabilized tibial fractures in rabbits during normal healing and infection," (in eng), *The Journal of surgical research*, vol. 37, no. 3, pp. 202-7, Sep 1984.
- [56] D. R. Epari, J. Lienau, H. Schell, F. Witt, and G. N. Duda, "Pressure, oxygen tension and temperature in the periosteal callus during bone healing--an in vivo study in sheep," (in eng), *Bone*, vol. 43, no. 4, pp. 734-9, Oct 2008.

- [57] O. Grundnes and O. Reikeras, "Blood flow and mechanical properties of healing bone. Femoral osteotomies studied in rats," (in eng), *Acta orthopaedica Scandinavica*, vol. 63, no. 5, pp. 487-91, Oct 1992.
- [58] T. Gaber, R. Dziurla, R. Tripmacher, G. R. Burmester, and F. Buttgereit, "Hypoxia inducible factor (HIF) in rheumatology: low O₂! See what HIF can do!," *Annals of the rheumatic diseases*, vol. 64, no. 7, pp. 971-980, 2005.
- [59] C. Maes, G. Carmeliet, and E. Schipani, "Hypoxia-driven pathways in bone development, regeneration and disease," *Nature Reviews Rheumatology*, Review Article vol. 8, p. 358, 03/27/online 2012.
- [60] D. E. Komatsu and M. Hadjiargyrou, "Activation of the transcription factor HIF-1 and its target genes, VEGF, HO-1, iNOS, during fracture repair," (in eng), *Bone*, vol. 34, no. 4, pp. 680-8, Apr 2004.
- [61] T. Cramer *et al.*, "HIF-1alpha is essential for myeloid cell-mediated inflammation," (in eng), *Cell*, vol. 112, no. 5, pp. 645-57, Mar 7 2003.
- [62] D. Burke, M. Dishowitz, M. Sweetwyne, E. Miedel, K. D. Hankenson, and D. J. Kelly, "The role of oxygen as a regulator of stem cell fate during fracture repair in TSP2-null mice," (in eng), *Journal of orthopaedic research : official publication of the Orthopaedic Research Society*, vol. 31, no. 10, pp. 1585-96, Oct 2013.
- [63] X. Sun and Y. Wei, "The role of hypoxia-inducible factor in osteogenesis and chondrogenesis," (in eng), *Cytotherapy*, vol. 11, no. 3, pp. 261-7, 2009.
- [64] N. Zhou *et al.*, "HIF-1alpha as a Regulator of BMP2-Induced Chondrogenic Differentiation, Osteogenic Differentiation, and Endochondral Ossification in Stem Cells," (in eng), *Cellular physiology and biochemistry : international journal of experimental cellular physiology, biochemistry, and pharmacology*, vol. 36, no. 1, pp. 44-60, 2015.
- [65] L. F. Raheja, D. C. Genetos, and C. E. Yellowley, "The effect of oxygen tension on the long-term osteogenic differentiation and MMP/TIMP expression of human mesenchymal stem cells," (in eng), *Cells, tissues, organs*, vol. 191, no. 3, pp. 175-84, 2010.
- [66] D. C. Genetos *et al.*, "Hypoxia decreases sclerostin expression and increases Wnt signaling in osteoblasts," (in eng), *Journal of cellular biochemistry*, vol. 110, no. 2, pp. 457-67, May 15 2010.
- [67] D. S. Steinbrech *et al.*, "Hypoxia increases insulinlike growth factor gene expression in rat osteoblasts," (in eng), *Annals of plastic surgery*, vol. 44, no. 5, pp. 529-34; discussion 534-5, May 2000.
- [68] R. I. Stirling, "The Report of an Investigation into the Process of the Healing of Fractured Bones, with Some Clinical Applications," (in eng), *Edinburgh medical journal*, vol. 39, no. 12, pp. T203-t228, Dec 1932.
- [69] Z. Zhang *et al.*, "Acidic pH environment induces autophagy in osteoblasts," *Scientific Reports*, Article vol. 7, p. 46161, 04/06/online 2017.
- [70] R. J. Newman, R. B. Duthie, and M. J. Francis, "Nuclear magnetic resonance studies of fracture repair," (in eng), *Clinical orthopaedics and related research*, no. 198, pp. 297-303, Sep 1985.

- [71] J. P. Frolke and P. Patka, "Definition and classification of fracture non-unions," (in eng), *Injury*, vol. 38 Suppl 2, pp. S19-22, May 2007.
- [72] E. Gomez-Barrena, P. Rosset, D. Lozano, J. Stanovici, C. Ermthaller, and F. Gerbhard, "Bone fracture healing: cell therapy in delayed unions and nonunions," (in eng), *Bone*, vol. 70, pp. 93-101, Jan 2015.
- [73] S. Olson and D. Hahn, "Surgical treatment of non-unions: A case for internal fixation," (in eng), *Injury*, vol. 37, no. 8, pp. 681-90, Aug 2006.
- [74] A. H. Karladani, H. Granhed, J. Karrholm, and J. Styf, "The influence of fracture etiology and type on fracture healing: a review of 104 consecutive tibial shaft fractures," (in eng), *Archives of orthopaedic and trauma surgery*, vol. 121, no. 6, pp. 325-8, Jun 2001.
- [75] R. Zura *et al.*, "Epidemiology of Fracture Nonunion in 18 Human Bones," (in eng), *JAMA surgery*, vol. 151, no. 11, p. e162775, Nov 16 2016.
- [76] M. Bhandari *et al.*, "Predictors of reoperation following operative management of fractures of the tibial shaft," (in eng), *Journal of orthopaedic trauma*, vol. 17, no. 5, pp. 353-61, May 2003.
- [77] S. Tsitsilonis *et al.*, "The effect of traumatic brain injury on bone healing: an experimental study in a novel in vivo animal model," (in eng), *Injury*, vol. 46, no. 4, pp. 661-5, Apr 2015.
- [78] R. Gruber, H. Koch, B. A. Doll, F. Tegtmeier, T. A. Einhorn, and J. O. Hollinger, "Fracture healing in the elderly patient," (in eng), *Experimental gerontology*, vol. 41, no. 11, pp. 1080-93, Nov 2006.
- [79] R. Zura *et al.*, "Bone fracture nonunion rate decreases with increasing age: A prospective inception cohort study," (in eng), *Bone*, vol. 95, pp. 26-32, Feb 2017.
- [80] J. A. Donigan, D. C. Fredericks, J. V. Nepola, and J. D. Smucker, "The effect of transdermal nicotine on fracture healing in a rabbit model," (in eng), *Journal of orthopaedic trauma*, vol. 26, no. 12, pp. 724-7, Dec 2012.
- [81] S. E. Porter and E. N. Hanley, Jr., "The musculoskeletal effects of smoking," (in eng), *The Journal of the American Academy of Orthopaedic Surgeons*, vol. 9, no. 1, pp. 9-17, Jan-Feb 2001.
- [82] J. A. Scolaro, M. L. Schenker, S. Yannascoli, K. Baldwin, S. Mehta, and J. Ahn, "Cigarette smoking increases complications following fracture: a systematic review," (in eng), *The Journal of bone and joint surgery. American volume*, vol. 96, no. 8, pp. 674-81, Apr 16 2014.
- [83] D. A. Chakkalakal *et al.*, "Inhibition of bone repair in a rat model for chronic and excessive alcohol consumption," (in eng), *Alcohol (Fayetteville, N.Y.)*, vol. 36, no. 3, pp. 201-14, Jul 2005.
- [84] P. Giannoudis, C. Tzioupis, T. Almalki, and R. Buckley, "Fracture healing in osteoporotic fractures: is it really different? A basic science perspective," (in eng), *Injury*, vol. 38 Suppl 1, pp. S90-9, Mar 2007.
- [85] P. Hadji *et al.*, "The epidemiology of osteoporosis--Bone Evaluation Study (BEST): an analysis of routine health insurance data," (in eng), *Deutsches Arzteblatt international*, vol. 110, no. 4, pp. 52-7, Jan 2013.

- [86] M. Kampschulte *et al.*, "Neovascularization of osteoporotic metaphyseal bone defects: A morphometric micro-CT study," (in eng), *Microvascular research*, vol. 105, pp. 7-14, May 2016.
- [87] N. Mathavan, M. Tagil, and H. Isaksson, "Do osteoporotic fractures constitute a greater recalcitrant challenge for skeletal regeneration? Investigating the efficacy of BMP-7 and zoledronate treatment of diaphyseal fractures in an open fracture osteoporotic rat model," (in eng), *Osteoporosis international : a journal established as result of cooperation between the European Foundation for Osteoporosis and the National Osteoporosis Foundation of the USA*, vol. 28, no. 2, pp. 697-707, Feb 2017.
- [88] R. M. McCann *et al.*, "Effect of osteoporosis on bone mineral density and fracture repair in a rat femoral fracture model," (in eng), *Journal of orthopaedic research : official publication of the Orthopaedic Research Society*, vol. 26, no. 3, pp. 384-93, Mar 2008.
- [89] W. Liu *et al.*, "Alkaline biodegradable implants for osteoporotic bone defects--importance of microenvironment pH," (in eng), *Osteoporosis international : a journal established as result of cooperation between the European Foundation for Osteoporosis and the National Osteoporosis Foundation of the USA*, vol. 27, no. 1, pp. 93-104, Jan 2016.
- [90] J. Alblowi *et al.*, "High levels of tumor necrosis factor-alpha contribute to accelerated loss of cartilage in diabetic fracture healing," (in eng), *Am J Pathol*, vol. 175, no. 4, pp. 1574-85, Oct 2009.
- [91] A. Gandhi, H. A. Beam, J. P. O'Connor, J. R. Parsons, and S. S. Lin, "The effects of local insulin delivery on diabetic fracture healing," (in eng), *Bone*, vol. 37, no. 4, pp. 482-90, Oct 2005.
- [92] B. Dominiak, W. Oxberry, and P. Chen, "Study on a nonhealing fracture from a patient with systemic lupus erythematosus and its pathogenetic mechanisms," (in eng), *Ultrastructural pathology*, vol. 29, no. 2, pp. 107-20, Mar-Apr 2005.
- [93] B. Stromqvist, "Hip fracture in rheumatoid arthritis," (in eng), *Acta orthopaedica Scandinavica*, vol. 55, no. 6, pp. 624-8, Dec 1984.
- [94] O. Bissinger *et al.*, "A biomechanical, micro-computertomographic and histological analysis of the influence of diclofenac and prednisolone on fracture healing in vivo," (in eng), *BMC musculoskeletal disorders*, vol. 17, no. 1, p. 383, Sep 5 2016.
- [95] A. Marquez-Lara, I. D. Hutchinson, F. Nunez, Jr., T. L. Smith, and A. N. Miller, "Nonsteroidal Anti-Inflammatory Drugs and Bone-Healing: A Systematic Review of Research Quality," (in eng), *JBJS reviews*, vol. 4, no. 3, Mar 15 2016.
- [96] I. Pountos, T. Georgouli, G. M. Calori, and P. V. Giannoudis, "Do nonsteroidal anti-inflammatory drugs affect bone healing? A critical analysis," (in eng), *TheScientificWorldJournal*, vol. 2012, p. 606404, 2012.
- [97] R. K. Hernandez, T. P. Do, C. W. Critchlow, R. E. Dent, and S. S. Jick, "Patient-related risk factors for fracture-healing complications in the United Kingdom General Practice Research Database," (in eng), *Acta orthopaedica*, vol. 83, no. 6, pp. 653-60, Dec 2012.
- [98] J. Li *et al.*, "Perioperative glucocorticosteroid treatment delays early healing of a mandible wound by inhibiting osteogenic differentiation," (in eng), *Injury*, vol. 43, no. 8, pp. 1284-9, Aug 2012.

- [99] C. A. Luppen *et al.*, "Recombinant human bone morphogenetic protein-2 enhances osteotomy healing in glucocorticoid-treated rabbits," (in eng), *Journal of bone and mineral research : the official journal of the American Society for Bone and Mineral Research*, vol. 17, no. 2, pp. 301-10, Feb 2002.
- [100] K. Schmidt-Bleek *et al.*, "Inflammatory phase of bone healing initiates the regenerative healing cascade," (in eng), *Cell and tissue research*, vol. 347, no. 3, pp. 567-73, Mar 2012.
- [101] O. Grundnes and O. Reikeraas, "Effects of macrophage activation on bone healing," (in eng), *Journal of orthopaedic science : official journal of the Japanese Orthopaedic Association*, vol. 5, no. 3, pp. 243-7, 2000.
- [102] P. Hoff *et al.*, "Immunologically restricted patients exhibit a pronounced inflammation and inadequate response to hypoxia in fracture hematomas," (in eng), *Immunologic research*, vol. 51, no. 1, pp. 116-22, Oct 2011.
- [103] E. Bogoch, N. Gschwend, B. Rahn, E. Moran, and S. Perren, "Healing of cancellous bone osteotomy in rabbits--Part II: Local reversal of arthritis-induced osteopenia after osteotomy," (in eng), *Journal of orthopaedic research : official publication of the Orthopaedic Research Society*, vol. 11, no. 2, pp. 292-8, Mar 1993.
- [104] E. Muinos-Lopez *et al.*, "Hypoxia and Reactive Oxygen Species Homeostasis in Mesenchymal Progenitor Cells Define a Molecular Mechanism for Fracture Nonunion," (in eng), *Stem cells (Dayton, Ohio)*, vol. 34, no. 9, pp. 2342-53, Sep 2016.
- [105] S. Govender *et al.*, "Recombinant human bone morphogenetic protein-2 for treatment of open tibial fractures: a prospective, controlled, randomized study of four hundred and fifty patients," (in eng), *The Journal of bone and joint surgery. American volume*, vol. 84-a, no. 12, pp. 2123-34, Dec 2002.
- [106] M. R. Urist and B. S. Strates, "Bone Morphogenetic Protein," *Journal of Dental Research*, vol. 50, no. 6, pp. 1392-1406, 1971/11/01 1971.
- [107] S. P. Lad *et al.*, "Cancer After Spinal FusionThe Role of Bone Morphogenetic Protein," *Neurosurgery*, vol. 73, no. 3, pp. 440-449, 2013.
- [108] V. Alt, S. T. Donell, A. Chhabra, A. Bentley, A. Eicher, and R. Schnettler, "A health economic analysis of the use of rhBMP-2 in Gustilo-Anderson grade III open tibial fractures for the UK, Germany, and France," (in eng), *Injury*, vol. 40, no. 12, pp. 1269-75, Dec 2009.
- [109] C. W. DiGiovanni *et al.*, "Recombinant human platelet-derived growth factor-BB and beta-tricalcium phosphate (rhPDGF-BB/beta-TCP): an alternative to autogenous bone graft," (in eng), *The Journal of bone and joint surgery. American volume*, vol. 95, no. 13, pp. 1184-92, Jul 3 2013.
- [110] H. Kawaguchi *et al.*, "A local application of recombinant human fibroblast growth factor 2 for tibial shaft fractures: A randomized, placebo-controlled trial," (in eng), *Journal of bone and mineral research : the official journal of the American Society for Bone and Mineral Research*, vol. 25, no. 12, pp. 2735-43, Dec 2010.
- [111] Z. Sheikh, S. Najeeb, Z. Khurshid, V. Verma, H. Rashid, and M. Glogauer, "Biodegradable Materials for Bone Repair and Tissue Engineering Applications," *Materials*, vol. 8, no. 9, p. 5273, 2015.

- [112] A. Fugl *et al.*, "Alveolar bone regeneration in response to local application of calcitriol in vitamin D deficient rats," (in eng), *Journal of clinical periodontology*, vol. 42, no. 1, pp. 96-103, Jan 2015.
- [113] T. Pekkarinen, T. Jamsa, M. Maatta, O. Hietala, and P. Jalovaara, "Reindeer BMP extract in the healing of critical-size bone defects in the radius of the rabbit," (in eng), *Acta orthopaedica*, vol. 77, no. 6, pp. 952-9, Dec 2006.
- [114] C. Schwarz, D. Wulsten, A. Ellinghaus, J. Lienau, B. M. Willie, and G. N. Duda, "Mechanical load modulates the stimulatory effect of BMP2 in a rat nonunion model," (in eng), *Tissue engineering. Part A*, vol. 19, no. 1-2, pp. 247-54, Jan 2013.
- [115] A. S. Spiro *et al.*, "BMP-7-induced ectopic bone formation and fracture healing is impaired by systemic NSAID application in C57BL/6-mice," (in eng), *Journal of orthopaedic research : official publication of the Orthopaedic Research Society*, vol. 28, no. 6, pp. 785-91, Jun 2010.
- [116] D. Wulsten *et al.*, "Time kinetics of bone defect healing in response to BMP-2 and GDF-5 characterised by in vivo biomechanics," (in eng), *European cells & materials*, vol. 21, pp. 177-92, Feb 11 2011.
- [117] E. C. Chan *et al.*, "Three Dimensional Collagen Scaffold Promotes Intrinsic Vascularisation for Tissue Engineering Applications," *PLoS ONE*, vol. 11, no. 2, p. e0149799, 2016.
- [118] E. Garcia-Gareta, M. J. Coathup, and G. W. Blunn, "Osteoinduction of bone grafting materials for bone repair and regeneration," (in eng), *Bone*, vol. 81, pp. 112-21, Dec 2015.
- [119] A. M. Ferreira, P. Gentile, V. Chiono, and G. Ciardelli, "Collagen for bone tissue regeneration," (in eng), *Acta biomaterialia*, vol. 8, no. 9, pp. 3191-200, Sep 2012.
- [120] C. K. Davis, S. A. Jain, O. N. Bae, A. Majid, and G. K. Rajanikant, "Hypoxia Mimetic Agents for Ischemic Stroke," (in eng), *Frontiers in cell and developmental biology*, vol. 6, p. 175, 2018.
- [121] G. L. Semenza, "Pharmacologic Targeting of Hypoxia-Inducible Factors," (in eng), *Annual review of pharmacology and toxicology*, vol. 59, pp. 379-403, Jan 6 2019.
- [122] L. Fan, J. Li, Z. Yu, X. Dang, and K. Wang, "The hypoxia-inducible factor pathway, prolyl hydroxylase domain protein inhibitors, and their roles in bone repair and regeneration," (in eng), *Biomed Res Int*, vol. 2014, p. 239356, 2014.
- [123] C. Wan *et al.*, "Activation of the hypoxia-inducible factor-1alpha pathway accelerates bone regeneration," (in eng), *Proceedings of the National Academy of Sciences of the United States of America*, vol. 105, no. 2, pp. 686-91, Jan 15 2008.
- [124] A. Donneys *et al.*, "Deferoxamine restores callus size, mineralization, and mechanical strength in fracture healing after radiotherapy," (in eng), *Plastic and reconstructive surgery*, vol. 131, no. 5, pp. 711e-9e, May 2013.
- [125] A. Donneys *et al.*, "Targeting angiogenesis as a therapeutic means to reinforce osteocyte survival and prevent nonunions in the aftermath of radiotherapy," (in eng), *Head & neck*, vol. 37, no. 9, pp. 1261-7, Sep 2015.

- [126] A. Donneys *et al.*, "Prevention of radiation-induced bone pathology through combined pharmacologic cytoprotection and angiogenic stimulation," (in eng), *Bone*, vol. 84, pp. 245-252, Mar 2016.
- [127] A. Donneys *et al.*, "Localized deferoxamine injection augments vascularity and improves bony union in pathologic fracture healing after radiotherapy," (in eng), *Bone*, vol. 52, no. 1, pp. 318-25, Jan 2013.
- [128] J. Drager, J. L. Ramirez-GarciaLuna, A. Kumar, U. Gbureck, E. J. Harvey, and J. E. Barralet, "(*) Hypoxia Biomimicry to Enhance Monetite Bone Defect Repair," (in eng), *Tissue engineering. Part A*, vol. 23, no. 23-24, pp. 1372-1381, Dec 2017.
- [129] J. Drager, Z. Sheikh, Y. L. Zhang, E. J. Harvey, and J. E. Barralet, "Local delivery of iron chelators reduces in vivo remodeling of a calcium phosphate bone graft substitute," (in eng), *Acta biomaterialia*, vol. 42, pp. 411-419, Sep 15 2016.
- [130] A. S. Farberg *et al.*, "Deferoxamine reverses radiation induced hypovascularity during bone regeneration and repair in the murine mandible," (in eng), *Bone*, vol. 50, no. 5, pp. 1184-7, May 2012.
- [131] S. Guzey, A. Aykan, S. Ozturk, H. Avsever, Y. Karslioglu, and A. Ertan, "The Effects of Desferroxamine on Bone and Bone Graft Healing in Critical-Size Bone Defects," (in eng), *Annals of plastic surgery*, vol. 77, no. 5, pp. 560-568, Nov 2016.
- [132] T. Matsumoto and S. Sato, "Stimulating angiogenesis mitigates the unloading-induced reduction in osteogenesis in early-stage bone repair in rats," (in eng), *Physiological reports*, vol. 3, no. 3, Mar 2015.
- [133] X. Shen *et al.*, "Prolyl hydroxylase inhibitors increase neoangiogenesis and callus formation following femur fracture in mice," (in eng), *Journal of orthopaedic research : official publication of the Orthopaedic Research Society*, vol. 27, no. 10, pp. 1298-305, Oct 2009.
- [134] R. Stewart, J. Goldstein, A. Eberhardt, G. T. Chu, and S. Gilbert, "Increasing vascularity to improve healing of a segmental defect of the rat femur," (in eng), *Journal of orthopaedic trauma*, vol. 25, no. 8, pp. 472-6, Aug 2011.
- [135] Q. Yao, Y. Liu, J. Tao, K. M. Baumgarten, and H. Sun, "Hypoxia-Mimicking Nanofibrous Scaffolds Promote Endogenous Bone Regeneration," (in eng), *ACS applied materials & interfaces*, vol. 8, no. 47, pp. 32450-32459, Nov 30 2016.
- [136] W. Zhang, G. Li, R. Deng, L. Deng, and S. Qiu, "New bone formation in a true bone ceramic scaffold loaded with desferrioxamine in the treatment of segmental bone defect: a preliminary study," (in eng), *Journal of orthopaedic science : official journal of the Japanese Orthopaedic Association*, vol. 17, no. 3, pp. 289-98, May 2012.
- [137] H. Kang *et al.*, "Desferrioxamine reduces ultrahigh-molecular-weight polyethylene-induced osteolysis by restraining inflammatory osteoclastogenesis via heme oxygenase-1," *Cell death & disease*, vol. 7, no. 10, pp. e2435-e2435, 2016.
- [138] A. P. Kusumbe, S. K. Ramasamy, and R. H. Adams, "Coupling of angiogenesis and osteogenesis by a specific vessel subtype in bone," (in eng), *Nature*, vol. 507, no. 7492, pp. 323-8, Mar 20 2014.

- [139] J. Li, L. Fan, Z. Yu, X. Dang, and K. Wang, "The effect of deferoxamine on angiogenesis and bone repair in steroid-induced osteonecrosis of rabbit femoral heads," (in eng), *Experimental biology and medicine (Maywood, N.J.)*, vol. 240, no. 2, pp. 273-80, Feb 2015.
- [140] X. Liu, Y. Tu, L. Zhang, J. Qi, T. Ma, and L. Deng, "Prolyl hydroxylase inhibitors protect from the bone loss in ovariectomy rats by increasing bone vascularity," (in eng), *Cell biochemistry and biophysics*, vol. 69, no. 1, pp. 141-9, May 2014.
- [141] L. Wang *et al.*, "Synergistic protection of bone vasculature and bone mass by desferrioxamine in osteoporotic mice," (in eng), *Molecular medicine reports*, vol. 16, no. 5, pp. 6642-6649, Nov 2017.
- [142] U. Kuchler *et al.*, "Dimethyloxalyglycine lyophilized onto bone substitutes increase vessel area in rat calvarial defects," (in eng), *Clinical oral implants research*, vol. 26, no. 5, pp. 485-91, May 2015.
- [143] A. Donneys, A. S. Farberg, C. N. Tchanque-Fossuo, S. S. Deshpande, and S. R. Buchman, "Deferoxamine enhances the vascular response of bone regeneration in mandibular distraction osteogenesis," (in eng), *Plastic and reconstructive surgery*, vol. 129, no. 4, pp. 850-6, Apr 2012.
- [144] A. S. Farberg, D. Sarhaddi, A. Donneys, S. S. Deshpande, and S. R. Buchman, "Deferoxamine enhances bone regeneration in mandibular distraction osteogenesis," (in eng), *Plastic and reconstructive surgery*, vol. 133, no. 3, pp. 666-71, Mar 2014.
- [145] A. Donneys *et al.*, "Deferoxamine expedites consolidation during mandibular distraction osteogenesis," (in eng), *Bone*, vol. 55, no. 2, pp. 384-90, Aug 2013.
- [146] P. A. Felice, S. Ahsan, A. Donneys, S. S. Deshpande, N. S. Nelson, and S. R. Buchman, "Deferoxamine administration delivers translational optimization of distraction osteogenesis in the irradiated mandible," (in eng), *Plastic and reconstructive surgery*, vol. 132, no. 4, pp. 542e-548e, Oct 2013.
- [147] K. M. Urlaub *et al.*, "Histologic Improvements in Irradiated Bone Through Pharmaceutical Intervention in Mandibular Distraction Osteogenesis," (in eng), *Journal of oral and maxillofacial surgery : official journal of the American Association of Oral and Maxillofacial Surgeons*, vol. 76, no. 12, pp. 2660-2668, Dec 2018.
- [148] B. S. Grewal, B. Keller, P. Weinhold, and L. E. Dahners, "Evaluating effects of deferoxamine in a rat tibia critical bone defect model," (in eng), *Journal of orthopaedics*, vol. 11, no. 1, pp. 5-9, Mar 2014.
- [149] Y. Yan *et al.*, "Vascularized 3D printed scaffolds for promoting bone regeneration," *Biomaterials*, vol. 190-191, pp. 97-110, 2019/01/01/ 2019.
- [150] P. Jia *et al.*, "Deferoxamine released from poly(lactic-co-glycolic acid) promotes healing of osteoporotic bone defect via enhanced angiogenesis and osteogenesis," vol. 104, no. 10, pp. 2515-2527, 2016.
- [151] C. Guo *et al.*, "SF-deferoxamine, a bone-seeking angiogenic drug, prevents bone loss in estrogen-deficient mice," (in eng), *Bone*, vol. 120, pp. 156-165, Oct 30 2018.
- [152] B. R. Bloom and B. Bennett, "Mechanism of a reaction in vitro associated with delayed-type hypersensitivity," *Science*, vol. 153, no. 3731, pp. 80-2, Jul 1 1966.

- [153] J. R. David, "Delayed hypersensitivity in vitro: its mediation by cell-free substances formed by lymphoid cell-antigen interaction," *Proceedings of the National Academy of Sciences of the United States of America*, vol. 56, no. 1, pp. 72-7, Jul 1966.
- [154] J. P. Bach, B. Rinn, B. Meyer, R. Dodel, and M. Bacher, "Role of MIF in inflammation and tumorigenesis," *Oncology*, vol. 75, no. 3-4, pp. 127-33, 2008.
- [155] L. Leng *et al.*, "MIF signal transduction initiated by binding to CD74," (in eng), *J Exp Med*, vol. 197, no. 11, pp. 1467-76, Jun 2 2003.
- [156] L. L. Santos and E. F. Morand, "Macrophage migration inhibitory factor: a key cytokine in RA, SLE and atherosclerosis," (in eng), *Clinica chimica acta; international journal of clinical chemistry*, vol. 399, no. 1-2, pp. 1-7, Jan 2009.
- [157] M. Bacher *et al.*, "MIF expression in the rat brain: implications for neuronal function," *Mol Med*, vol. 4, no. 4, pp. 217-30, Apr 1998.
- [158] M. Bacher *et al.*, "Migration inhibitory factor expression in experimentally induced endotoxemia," *Am J Pathol*, vol. 150, no. 1, pp. 235-46, Jan 1997.
- [159] T. Calandra and T. Roger, "Macrophage migration inhibitory factor: a regulator of innate immunity," (in eng), *Nature reviews. Immunology*, vol. 3, no. 10, pp. 791-800, Oct 2003.
- [160] T. Nishino, J. Bernhagen, H. Shiiki, T. Calandra, K. Dohi, and R. Bucala, "Localization of macrophage migration inhibitory factor (MIF) to secretory granules within the corticotrophic and thyrotrophic cells of the pituitary gland," (in eng), *Mol Med*, vol. 1, no. 7, pp. 781-8, Nov 1995.
- [161] X. Shi *et al.*, "CD44 is the signaling component of the macrophage migration inhibitory factor-CD74 receptor complex," (in eng), *Immunity*, vol. 25, no. 4, pp. 595-606, Oct 2006.
- [162] R. Kleemann *et al.*, "Intracellular action of the cytokine MIF to modulate AP-1 activity and the cell cycle through Jab1," (in eng), *Nature*, vol. 408, no. 6809, pp. 211-6, Nov 9 2000.
- [163] H. Lue *et al.*, "Rapid and transient activation of the ERK MAPK signalling pathway by macrophage migration inhibitory factor (MIF) and dependence on JAB1/CSN5 and Src kinase activity," (in eng), *Cellular signalling*, vol. 18, no. 5, pp. 688-703, May 2006.
- [164] H. Flaster, J. Bernhagen, T. Calandra, and R. Bucala, "The macrophage migration inhibitory factor-glucocorticoid dyad: regulation of inflammation and immunity," (in eng), *Molecular endocrinology (Baltimore, Md.)*, vol. 21, no. 6, pp. 1267-80, Jun 2007.
- [165] S. Oda *et al.*, "Macrophage migration inhibitory factor activates hypoxia-inducible factor in a p53-dependent manner," (in eng), *PLoS One*, vol. 3, no. 5, p. e2215, May 21 2008.
- [166] T. Gaber *et al.*, "Macrophage migration inhibitory factor counterregulates dexamethasone-mediated suppression of hypoxia-inducible factor-1 alpha function and differentially influences human CD4+ T cell proliferation under hypoxia," (in eng), *Journal of immunology (Baltimore, Md. : 1950)*, vol. 186, no. 2, pp. 764-74, Jan 15 2011.
- [167] S. Onodera, J. Nishihira, M. Yamazaki, T. Ishibashi, and A. Minami, "Increased expression of macrophage migration inhibitory factor during fracture healing in rats," *Histochem Cell Biol*, vol. 121, no. 3, pp. 209-17, Mar 2004.

- [168] S. C. Gilliver, E. Emmerson, J. Bernhagen, and M. J. Hardman, "MIF: a key player in cutaneous biology and wound healing," *Exp Dermatol*, vol. 20, no. 1, pp. 1-6, Jan 2011.
- [169] S. Onodera *et al.*, "Macrophage migration inhibitory factor up-regulates matrix metalloproteinase-9 and -13 in rat osteoblasts. Relevance to intracellular signaling pathways," *The Journal of biological chemistry*, vol. 277, no. 10, pp. 7865-74, Mar 8 2002.
- [170] D. J. Behonick *et al.*, "Role of matrix metalloproteinase 13 in both endochondral and intramembranous ossification during skeletal regeneration," *PLoS One*, vol. 2, no. 11, p. e1150, 2007.
- [171] T. Kobayashi *et al.*, "Impaired fracture healing in macrophage migration inhibitory factor-deficient mice," *Osteoporosis international : a journal established as result of cooperation between the European Foundation for Osteoporosis and the National Osteoporosis Foundation of the USA*, vol. 22, no. 6, pp. 1955-65, Jun 2011.
- [172] R. Gu *et al.*, "Macrophage migration inhibitory factor is essential for osteoclastogenic mechanisms in vitro and in vivo mouse model of arthritis," (in eng), *Cytokine*, vol. 72, no. 2, pp. 135-45, Apr 2015.
- [173] C. Jacquin *et al.*, "Macrophage migration inhibitory factor inhibits osteoclastogenesis," (in eng), *Bone*, vol. 45, no. 4, pp. 640-9, Oct 2009.
- [174] A. Lang *et al.*, "Collagen I-based scaffolds negatively impact fracture healing in a mouse-osteotomy-model although used routinely in research and clinical application," (in eng), *Acta biomaterialia*, vol. 86, pp. 171-184, Mar 1 2019.
- [175] J. Rappsilber, Y. Ishihama, and M. Mann, "Stop and go extraction tips for matrix-assisted laser desorption/ionization, nanoelectrospray, and LC/MS sample pretreatment in proteomics," (in eng), *Analytical chemistry*, vol. 75, no. 3, pp. 663-70, Feb 01 2003.
- [176] M. L. Boussein, S. K. Boyd, B. A. Christiansen, R. E. Guldberg, K. J. Jepsen, and R. Muller, "Guidelines for assessment of bone microstructure in rodents using micro-computed tomography," (in eng), *Journal of bone and mineral research : the official journal of the American Society for Bone and Mineral Research*, vol. 25, no. 7, pp. 1468-86, Jul 2010.
- [177] T. Kawamoto and K. Kawamoto, "Preparation of thin frozen sections from nonfixed and undecalcified hard tissues using Kawamoto's film method (2012)," (in eng), *Methods in molecular biology (Clifton, N.J.)*, vol. 1130, pp. 149-64, 2014.
- [178] D. D. W *et al.*, "Standardized nomenclature, symbols, and units for bone histomorphometry: A 2012 update of the report of the ASBMR Histomorphometry Nomenclature Committee," *Journal of Bone and Mineral Research*, vol. 28, no. 1, pp. 2-17, 2013.
- [179] M. Dominici *et al.*, "Minimal criteria for defining multipotent mesenchymal stromal cells. The International Society for Cellular Therapy position statement," (in eng), *Cytotherapy*, vol. 8, no. 4, pp. 315-7, 2006.
- [180] R. J. Waddington, H. C. Roberts, R. V. Sugars, and E. Schonherr, "Differential roles for small leucine-rich proteoglycans in bone formation," (in eng), *European cells & materials*, vol. 6, pp. 12-21, Oct 06 2003.
- [181] S. E. Headland and L. V. Norling, "The resolution of inflammation: Principles and challenges," (in eng), *Seminars in immunology*, vol. 27, no. 3, pp. 149-60, May 2015.

- [182] T. Kirsch, H. D. Nah, I. M. Shapiro, and M. Pacifici, "Regulated production of mineralization-competent matrix vesicles in hypertrophic chondrocytes," (in eng), *The Journal of cell biology*, vol. 137, no. 5, pp. 1149-60, Jun 02 1997.
- [183] K. Liu, J. Fan, and J. Wu, "Sushi repeat-containing protein X-linked 2 promotes angiogenesis through the urokinase-type plasminogen activator receptor dependent integrin alphavbeta3/focal adhesion kinase pathways," (in eng), *Drug discoveries & therapeutics*, vol. 11, no. 4, pp. 212-217, 2017.
- [184] J. P. Stains, F. Lecanda, D. A. Towler, and R. Civitelli, "Heterogeneous nuclear ribonucleoprotein K represses transcription from a cytosine/thymidine-rich element in the osteocalcin promoter," (in eng), *The Biochemical journal*, vol. 385, no. Pt 2, pp. 613-23, Jan 15 2005.
- [185] S. K. Ramasamy, A. P. Kusumbe, L. Wang, and R. H. Adams, "Endothelial Notch activity promotes angiogenesis and osteogenesis in bone," (in eng), *Nature*, vol. 507, no. 7492, pp. 376-80, Mar 20 2014.
- [186] J. Stefanowski *et al.*, "Spatial Distribution of Macrophages During Callus Formation and Maturation Reveals Close Crosstalk Between Macrophages and Newly Forming Vessels," (in English), *Frontiers in Immunology*, Original Research vol. 10, no. 2588, 2019-November-26 2019.
- [187] H. Li, R. Ghazanfari, D. Zacharaki, H. C. Lim, and S. Scheduling, "Isolation and characterization of primary bone marrow mesenchymal stromal cells," (in eng), *Annals of the New York Academy of Sciences*, vol. 1370, no. 1, pp. 109-18, Apr 2016.
- [188] C. K. F. Chan *et al.*, "Identification of the Human Skeletal Stem Cell," (in eng), *Cell*, vol. 175, no. 1, pp. 43-56.e21, Sep 20 2018.
- [189] F. P. Luyten and S. J. Roberts, "Close to the bone — in search of the skeletal stem cell," *Nature Reviews Rheumatology*, vol. 14, no. 12, pp. 687-688, 2018/12/01 2018.
- [190] C. Stahn and F. Buttgerit, "Genomic and nongenomic effects of glucocorticoids," *Nature Clinical Practice Rheumatology*, Review Article vol. 4, p. 525, 09/02/online 2008.
- [191] D. Patschan, K. Loddenkemper, and F. Buttgerit, "Molecular mechanisms of glucocorticoid-induced osteoporosis," (in eng), *Bone*, vol. 29, no. 6, pp. 498-505, Dec 2001.
- [192] I. Carcamo-Orive *et al.*, "Regulation of human bone marrow stromal cell proliferation and differentiation capacity by glucocorticoid receptor and AP-1 crosstalk," (in eng), *Journal of bone and mineral research : the official journal of the American Society for Bone and Mineral Research*, vol. 25, no. 10, pp. 2115-25, Oct 2010.
- [193] P. L. Chang *et al.*, "Comparison of fetal and adult marrow stromal cells in osteogenesis with and without glucocorticoids," (in eng), *Connective tissue research*, vol. 47, no. 2, pp. 67-76, 2006.
- [194] C. D. Hoemann, H. El-Gabalawy, and M. D. McKee, "In vitro osteogenesis assays: influence of the primary cell source on alkaline phosphatase activity and mineralization," (in eng), *Pathologie-biologie*, vol. 57, no. 4, pp. 318-23, Jun 2009.
- [195] I. H. Song, A. I. Caplan, and J. E. Dennis, "In vitro dexamethasone pretreatment enhances bone formation of human mesenchymal stem cells in vivo," (in eng), *Journal of orthopaedic*

- research : official publication of the Orthopaedic Research Society*, vol. 27, no. 7, pp. 916-21, Jul 2009.
- [196] G. Tan, P. D. Kang, and F. X. Pei, "Glucocorticoids affect the metabolism of bone marrow stromal cells and lead to osteonecrosis of the femoral head: a review," (in eng), *Chinese medical journal*, vol. 125, no. 1, pp. 134-9, Jan 2012.
- [197] S. Walsh, G. R. Jordan, C. Jefferiss, K. Stewart, and J. N. Beresford, "High concentrations of dexamethasone suppress the proliferation but not the differentiation or further maturation of human osteoblast precursors in vitro: relevance to glucocorticoid-induced osteoporosis," (in eng), *Rheumatology (Oxford, England)*, vol. 40, no. 1, pp. 74-83, Jan 2001.
- [198] M. G. Rimando *et al.*, "Glucocorticoid receptor and Histone deacetylase 6 mediate the differential effect of dexamethasone during osteogenesis of mesenchymal stromal cells (MSCs)," *Scientific reports*, vol. 6, pp. 37371-37371, 2016.
- [199] F. Langenbach and J. Handschel, "Effects of dexamethasone, ascorbic acid and β -glycerophosphate on the osteogenic differentiation of stem cells in vitro," *Stem cell research & therapy*, vol. 4, no. 5, pp. 117-117, 2013.
- [200] Y. Kohno *et al.*, "Osteogenic ability of rat bone marrow concentrate is at least as efficacious as mesenchymal stem cells in vitro," *Journal of Biomedical Materials Research Part B: Applied Biomaterials*, vol. 0, no. 0, 2019/02/19 2019.
- [201] L. Hong *et al.*, "Effects of glucocorticoid receptor small interfering RNA delivered using poly lactic-co-glycolic acid microparticles on proliferation and differentiation capabilities of human mesenchymal stromal cells," (in eng), *Tissue engineering. Part A*, vol. 18, no. 7-8, pp. 775-84, Apr 2012.
- [202] Q. Chen *et al.*, "Fate decision of mesenchymal stem cells: adipocytes or osteoblasts?," *Cell death and differentiation*, vol. 23, no. 7, pp. 1128-1139, 2016.
- [203] J. Li *et al.*, "Dexamethasone shifts bone marrow stromal cells from osteoblasts to adipocytes by C/EBPalpha promoter methylation," (in eng), *Cell Death Dis*, vol. 4, p. e832, Oct 3 2013.
- [204] H. Hu *et al.*, "Osteoactivin inhibits dexamethasone-induced osteoporosis through up-regulating integrin β 1 and activate ERK pathway," *Biomedicine & Pharmacotherapy*, vol. 105, pp. 66-72, 2018/09/01/ 2018.
- [205] M. Ahlstrom, M. Pekkinen, and C. Lamberg-Allardt, "Dexamethasone downregulates the expression of parathyroid hormone-related protein (PTHrP) in mesenchymal stem cells," (in eng), *Steroids*, vol. 74, no. 2, pp. 277-82, Feb 2009.
- [206] L. Hong, H. Sultana, K. Paulius, and G. Zhang, "Steroid regulation of proliferation and osteogenic differentiation of bone marrow stromal cells: a gender difference," (in eng), *The Journal of steroid biochemistry and molecular biology*, vol. 114, no. 3-5, pp. 180-5, Apr 2009.
- [207] Y. C. Liu *et al.*, "CCL5/RANTES is important for inducing osteogenesis of human mesenchymal stem cells and is regulated by dexamethasone," (in eng), *Bioscience trends*, vol. 8, no. 3, pp. 138-43, Jun 2014.
- [208] Y. Mikami, M. Lee, S. Irie, and M. J. Honda, "Dexamethasone modulates osteogenesis and adipogenesis with regulation of osterix expression in rat calvaria-derived cells," (in eng), *Journal of cellular physiology*, vol. 226, no. 3, pp. 739-48, Mar 2011.

- [209] S. Oshima *et al.*, "Macrophage migration inhibitory factor-deficient mice are resistant to ovariectomy-induced bone loss," *FEBS Lett*, vol. 580, no. 5, pp. 1251-6, Feb 20 2006.
- [210] H.-L. Wang *et al.*, "Dexamethasone-induced cellular tension requires a SGK1-stimulated Sec5-GEF-H1 interaction," *Journal of cell science*, vol. 128, no. 20, pp. 3757-3768, 2015.
- [211] P. G. Alexander, R. Gottardi, H. Lin, T. P. Lozito, and R. S. Tuan, "Three-dimensional osteogenic and chondrogenic systems to model osteochondral physiology and degenerative joint diseases," *Experimental biology and medicine (Maywood, N.J.)*, vol. 239, no. 9, pp. 1080-1095, 2014.
- [212] Y. Chen, S. Chen, N. Kawazoe, and G. Chen, "Promoted Angiogenesis and Osteogenesis by Dexamethasone-loaded Calcium Phosphate Nanoparticles/Collagen Composite Scaffolds with Microgroove Networks," *Scientific reports*, vol. 8, no. 1, pp. 14143-14143, 2018.
- [213] Y. Chen, N. Kawazoe, and G. Chen, "Preparation of dexamethasone-loaded biphasic calcium phosphate nanoparticles/collagen porous composite scaffolds for bone tissue engineering," (in eng), *Acta biomaterialia*, vol. 67, pp. 341-353, Feb 2018.
- [214] C. R. Nuttelman, M. C. Tripodi, and K. S. Anseth, "Dexamethasone-functionalized gels induce osteogenic differentiation of encapsulated hMSCs," (in eng), *Journal of biomedical materials research. Part A*, vol. 76, no. 1, pp. 183-95, Jan 2006.
- [215] C. Wang, X. Cao, and Y. Zhang, "A novel bioactive osteogenesis scaffold delivers ascorbic acid, beta-glycerophosphate, and dexamethasone in vivo to promote bone regeneration," (in eng), *Oncotarget*, vol. 8, no. 19, pp. 31612-31625, May 9 2017.
- [216] B. Zhang *et al.*, "Surface-decorated hydroxyapatite scaffold with on-demand delivery of dexamethasone and stromal cell derived factor-1 for enhanced osteogenesis," *Materials Science and Engineering: C*, vol. 89, pp. 355-370, 2018/08/01/ 2018.
- [217] B. Y. Binder, J. E. Sagun, and J. K. Leach, "Reduced serum and hypoxic culture conditions enhance the osteogenic potential of human mesenchymal stem cells," (in eng), *Stem cell reviews*, vol. 11, no. 3, pp. 387-93, Jun 2015.
- [218] Q. Gu, Y. Gu, Q. Shi, and H. Yang, "Hypoxia Promotes Osteogenesis of Human Placental-Derived Mesenchymal Stem Cells," (in eng), *The Tohoku journal of experimental medicine*, vol. 239, no. 4, pp. 287-96, Aug 2016.
- [219] S. P. Hung, J. H. Ho, Y. R. Shih, T. Lo, and O. K. Lee, "Hypoxia promotes proliferation and osteogenic differentiation potentials of human mesenchymal stem cells," (in eng), *Journal of orthopaedic research : official publication of the Orthopaedic Research Society*, vol. 30, no. 2, pp. 260-6, Feb 2012.
- [220] S. H. Hsu, C. T. Chen, and Y. H. Wei, "Inhibitory effects of hypoxia on metabolic switch and osteogenic differentiation of human mesenchymal stem cells," (in eng), *Stem cells (Dayton, Ohio)*, vol. 31, no. 12, pp. 2779-88, Dec 2013.
- [221] J. Leijten, N. Georgi, L. Moreira Teixeira, C. A. van Blitterswijk, J. N. Post, and M. Karperien, "Metabolic programming of mesenchymal stromal cells by oxygen tension directs chondrogenic cell fate," (in eng), *Proceedings of the National Academy of Sciences of the United States of America*, vol. 111, no. 38, pp. 13954-9, Sep 23 2014.

- [222] G. Pattappa, S. D. Thorpe, N. C. Jegard, H. K. Heywood, J. D. de Bruijn, and D. A. Lee, "Continuous and uninterrupted oxygen tension influences the colony formation and oxidative metabolism of human mesenchymal stem cells," (in eng), *Tissue engineering. Part C, Methods*, vol. 19, no. 1, pp. 68-79, Jan 2013.
- [223] E. Potier *et al.*, "Hypoxia affects mesenchymal stromal cell osteogenic differentiation and angiogenic factor expression," (in eng), *Bone*, vol. 40, no. 4, pp. 1078-87, Apr 2007.
- [224] J. H. Kim *et al.*, "Hypoxia Suppresses Spontaneous Mineralization and Osteogenic Differentiation of Mesenchymal Stem Cells via IGFBP3 Up-Regulation," (in eng), *International journal of molecular sciences*, vol. 17, no. 9, Aug 24 2016.
- [225] D. C. Yang, M. H. Yang, C. C. Tsai, T. F. Huang, Y. H. Chen, and S. C. Hung, "Hypoxia inhibits osteogenesis in human mesenchymal stem cells through direct regulation of RUNX2 by TWIST," (in eng), *PLoS One*, vol. 6, no. 9, p. e23965, 2011.
- [226] P. Zhang, N. Ha, Q. Dai, S. Zhou, C. Yu, and L. Jiang, "Hypoxia suppresses osteogenesis of bone mesenchymal stem cells via the extracellular signalregulated 1/2 and p38mitogen activated protein kinase signaling pathways," (in eng), *Molecular medicine reports*, vol. 16, no. 4, pp. 5515-5522, Oct 2017.
- [227] N. Xu *et al.*, "Hypoxia inhibits the differentiation of mesenchymal stem cells into osteoblasts by activation of Notch signaling," (in eng), *Experimental and molecular pathology*, vol. 94, no. 1, pp. 33-9, Feb 2013.
- [228] S. Palomaki *et al.*, "HIF-1alpha is upregulated in human mesenchymal stem cells," (in eng), *Stem cells (Dayton, Ohio)*, vol. 31, no. 9, pp. 1902-9, Sep 2013.
- [229] L. C. Shum, N. S. White, B. N. Mills, K. L. d. M. Bentley, and R. A. Eliseev, "Energy Metabolism in Mesenchymal Stem Cells During Osteogenic Differentiation," *Stem cells and development*, vol. 25, no. 2, pp. 114-122, 2016.
- [230] H. Ding *et al.*, "Continuous hypoxia regulates the osteogenic potential of mesenchymal stem cells in a time-dependent manner," (in eng), *Molecular medicine reports*, vol. 10, no. 4, pp. 2184-90, Oct 2014.
- [231] G. Ciapetti *et al.*, "Effects of hypoxia on osteogenic differentiation of mesenchymal stromal cells used as a cell therapy for avascular necrosis of the femoral head," (in eng), *Cytotherapy*, vol. 18, no. 9, pp. 1087-99, Sep 2016.
- [232] M. G. Valorani *et al.*, "Pre-culturing human adipose tissue mesenchymal stem cells under hypoxia increases their adipogenic and osteogenic differentiation potentials," (in eng), *Cell proliferation*, vol. 45, no. 3, pp. 225-38, Jun 2012.
- [233] E. Volkmer *et al.*, "Hypoxic preconditioning of human mesenchymal stem cells overcomes hypoxia-induced inhibition of osteogenic differentiation," (in eng), *Tissue engineering. Part A*, vol. 16, no. 1, pp. 153-64, Jan 2010.
- [234] C. Fehrer *et al.*, "Reduced oxygen tension attenuates differentiation capacity of human mesenchymal stem cells and prolongs their lifespan," (in eng), *Aging cell*, vol. 6, no. 6, pp. 745-57, Dec 2007.

- [235] D. S. Kim *et al.*, "Effect of low oxygen tension on the biological characteristics of human bone marrow mesenchymal stem cells," (in eng), *Cell stress & chaperones*, vol. 21, no. 6, pp. 1089-1099, Nov 2016.
- [236] J. S. Lee, S. K. Kim, B. J. Jung, S. B. Choi, E. Y. Choi, and C. S. Kim, "Enhancing proliferation and optimizing the culture condition for human bone marrow stromal cells using hypoxia and fibroblast growth factor-2," (in eng), *Stem cell research*, vol. 28, pp. 87-95, Apr 2018.
- [237] Z. H. Qu, X. L. Zhang, T. T. Tang, and K. R. Dai, "Promotion of osteogenesis through beta-catenin signaling by desferrioxamine," (in eng), *Biochem Biophys Res Commun*, vol. 370, no. 2, pp. 332-7, May 30 2008.
- [238] X. Yu *et al.*, "CoCl₂, a mimic of hypoxia, enhances bone marrow mesenchymal stem cells migration and osteogenic differentiation via STAT3 signaling pathway," (in eng), *Cell biology international*, vol. 42, no. 10, pp. 1321-1329, Sep 2018.
- [239] H. Yamamoto *et al.*, "Heme oxygenase-1 prevents glucocorticoid and hypoxia-induced apoptosis and necrosis of osteocyte-like cells," (in eng), *Medical molecular morphology*, Jan 31 2019.
- [240] A. Vettori *et al.*, "Glucocorticoids promote Von Hippel Lindau degradation and Hif-1 α stabilization," *Proceedings of the National Academy of Sciences of the United States of America*, vol. 114, no. 37, pp. 9948-9953, 2017.
- [241] W. Zou *et al.*, "Hypoxia enhances glucocorticoid-induced apoptosis and cell cycle arrest via the PI3K/Akt signaling pathway in osteoblastic cells," (in eng), *Journal of bone and mineral metabolism*, vol. 33, no. 6, pp. 615-24, Nov 2015.
- [242] M. Winner, A. C. Koong, B. E. Rendon, W. Zundel, and R. A. Mitchell, "Amplification of tumor hypoxic responses by macrophage migration inhibitory factor-dependent hypoxia-inducible factor stabilization," (in eng), *Cancer research*, vol. 67, no. 1, pp. 186-93, Jan 1 2007.
- [243] J. Scheinpflug *et al.*, "Journey into Bone Models: A Review," (in eng), *Genes*, vol. 9, no. 5, May 10 2018.
- [244] Q. Li *et al.*, "Proteomic analysis of naturally-sourced biological scaffolds," (in eng), *Biomaterials*, vol. 75, pp. 37-46, Jan 2016.
- [245] L. Schaefer and R. V. Iozzo, "Biological Functions of the Small Leucine-rich Proteoglycans: From Genetics to Signal Transduction," *The Journal of Biological Chemistry*, vol. 283, no. 31, pp. 21305-21309, 2008.
- [246] D. Nikitovic, J. Aggelidakis, M. F. Young, R. V. Iozzo, N. K. Karamanos, and G. N. Tzanakakis, "The biology of small leucine-rich proteoglycans in bone pathophysiology," *The Journal of biological chemistry*, vol. 287, no. 41, pp. 33926-33933, 2012.
- [247] A. Hildebrand *et al.*, "Interaction of the small interstitial proteoglycans biglycan, decorin and fibromodulin with transforming growth factor beta," (in eng), *The Biochemical journal*, vol. 302 (Pt 2), pp. 527-34, Sep 1 1994.
- [248] N. Abdel-Wahab, S. J. Wicks, R. M. Mason, and A. Chantry, "Decorin suppresses transforming growth factor-beta-induced expression of plasminogen activator inhibitor-1 in human mesangial cells through a mechanism that involves Ca²⁺-dependent

- phosphorylation of Smad2 at serine-240," (in eng), *The Biochemical journal*, vol. 362, no. Pt 3, pp. 643-9, Mar 15 2002.
- [249] E. Schonherr, M. Broszat, E. Brandan, P. Bruckner, and H. Kresse, "Decorin core protein fragment Leu155-Val260 interacts with TGF-beta but does not compete for decorin binding to type I collagen," (in eng), *Archives of biochemistry and biophysics*, vol. 355, no. 2, pp. 241-8, Jul 15 1998.
- [250] K. G. Danielson, H. Baribault, D. F. Holmes, H. Graham, K. E. Kadler, and R. V. Iozzo, "Targeted disruption of decorin leads to abnormal collagen fibril morphology and skin fragility," (in eng), *The Journal of cell biology*, vol. 136, no. 3, pp. 729-43, Feb 10 1997.
- [251] Y. Yamaguchi, D. M. Mann, and E. Ruoslahti, "Negative regulation of transforming growth factor-beta by the proteoglycan decorin," (in eng), *Nature*, vol. 346, no. 6281, pp. 281-4, Jul 19 1990.
- [252] A. Corsi *et al.*, "Phenotypic effects of biglycan deficiency are linked to collagen fibril abnormalities, are synergized by decorin deficiency, and mimic Ehlers-Danlos-like changes in bone and other connective tissues," (in eng), *Journal of bone and mineral research : the official journal of the American Society for Bone and Mineral Research*, vol. 17, no. 7, pp. 1180-9, Jul 2002.
- [253] Y. Bi *et al.*, "Extracellular matrix proteoglycans control the fate of bone marrow stromal cells," (in eng), *The Journal of biological chemistry*, vol. 280, no. 34, pp. 30481-9, Aug 26 2005.
- [254] Y. Takeuchi, Y. Kodama, and T. Matsumoto, "Bone matrix decorin binds transforming growth factor-beta and enhances its bioactivity," (in eng), *The Journal of biological chemistry*, vol. 269, no. 51, pp. 32634-8, Dec 23 1994.
- [255] L. A. Poniatowski, P. Wojdasiewicz, R. Gasik, and D. Szukiewicz, "Transforming growth factor Beta family: insight into the role of growth factors in regulation of fracture healing biology and potential clinical applications," (in eng), *Mediators of inflammation*, vol. 2015, p. 137823, 2015.
- [256] A. Kukita, L. Bonewald, D. Rosen, S. Seyedin, G. R. Mundy, and G. D. Roodman, "Osteoinductive factor inhibits formation of human osteoclast-like cells," (in eng), *Proceedings of the National Academy of Sciences of the United States of America*, vol. 87, no. 8, pp. 3023-6, Apr 1990.
- [257] H. Bentz *et al.*, "Purification and characterization of a unique osteoinductive factor from bovine bone," (in eng), *The Journal of biological chemistry*, vol. 264, no. 34, pp. 20805-10, Dec 05 1989.
- [258] D. C. Genetos, A. Wong, T. J. Weber, N. J. Karin, and C. E. Yellowley, "Impaired osteoblast differentiation in annexin A2- and -A5-deficient cells," (in eng), *PLoS One*, vol. 9, no. 9, p. e107482, 2014.
- [259] M. C. Basil and B. D. Levy, "Specialized pro-resolving mediators: endogenous regulators of infection and inflammation," (in eng), *Nature reviews. Immunology*, vol. 16, no. 1, pp. 51-67, Jan 2016.
- [260] C. N. Serhan, "Pro-resolving lipid mediators are leads for resolution physiology," (in eng), *Nature*, vol. 510, no. 7503, pp. 92-101, Jun 05 2014.

- [261] X. G. Han, D. K. Wang, F. Gao, R. H. Liu, and Z. G. Bi, "Bone morphogenetic protein 2 and decorin expression in old fracture fragments and surrounding tissues," (in eng), *Genetics and molecular research : GMR*, vol. 14, no. 3, pp. 11063-72, Sep 21 2015.
- [262] S. Deckx, S. Heymans, and A. P. Papageorgiou, "The diverse functions of osteoglycin: a deceitful dwarf, or a master regulator of disease?," (in eng), *FASEB journal : official publication of the Federation of American Societies for Experimental Biology*, vol. 30, no. 8, pp. 2651-61, Aug 2016.
- [263] Y. Bi *et al.*, "Identification of tendon stem/progenitor cells and the role of the extracellular matrix in their niche," *Nat Med*, 10.1038/nm1630 vol. 13, no. 10, pp. 1219-1227, 10//print 2007.
- [264] M. Goldberg, D. Septier, Å. Oldberg, M. F. Young, and L. G. Ameye, "Fibromodulin-deficient Mice Display Impaired Collagen Fibrillogenesis in Predentin as Well as Altered Dentin Mineralization and Enamel Formation," *Journal of Histochemistry & Cytochemistry*, vol. 54, no. 5, pp. 525-537, 2006/05/01 2006.
- [265] Z. Zheng *et al.*, "Fibromodulin Enhances Angiogenesis during Cutaneous Wound Healing," *Plastic and Reconstructive Surgery Global Open*, vol. 2, no. 12, p. e275.
- [266] M. W. Izzo, B. Pucci, R. S. Tuan, and D. J. Hall, "Gene expression profiling following BMP-2 induction of mesenchymal chondrogenesis in vitro," (in eng), *Osteoarthritis and cartilage*, vol. 10, no. 1, pp. 23-33, Jan 2002.
- [267] J. D. Croxtall and R. J. Flower, "Antisense oligonucleotides to human lipocortin-1 inhibit glucocorticoid-induced inhibition of A549 cell growth and eicosanoid release," (in eng), *Biochemical pharmacology*, vol. 48, no. 9, pp. 1729-34, Nov 01 1994.
- [268] M. Perretti and F. D'Acquisto, "Annexin A1 and glucocorticoids as effectors of the resolution of inflammation," (in eng), *Nature reviews. Immunology*, vol. 9, no. 1, pp. 62-70, Jan 2009.
- [269] T. Kirsch and H. Claassen, "Matrix vesicles mediate mineralization of human thyroid cartilage," (in eng), *Calcified tissue international*, vol. 66, no. 4, pp. 292-7, Apr 2000.
- [270] T. L. Haut Donahue, D. C. Genetos, C. R. Jacobs, H. J. Donahue, and C. E. Yellowley, "Annexin V disruption impairs mechanically induced calcium signaling in osteoblastic cells," (in eng), *Bone*, vol. 35, no. 3, pp. 656-63, Sep 2004.
- [271] D. W. Hutmacher, "Scaffolds in tissue engineering bone and cartilage," (in eng), *Biomaterials*, vol. 21, no. 24, pp. 2529-43, Dec 2000.
- [272] V. Irawan, T.-C. Sung, A. Higuchi, and T. Ikoma, "Collagen Scaffolds in Cartilage Tissue Engineering and Relevant Approaches for Future Development," *Tissue Engineering and Regenerative Medicine*, vol. 15, no. 6, pp. 673-697, 2018/12/01 2018.
- [273] T. Bou-Akl, R. Banglmaier, R. Miller, and P. VandeVord, "Effect of crosslinking on the mechanical properties of mineralized and non-mineralized collagen fibers," (in eng), *Journal of biomedical materials research. Part A*, vol. 101, no. 9, pp. 2507-14, Sep 2013.
- [274] E. Jorge-Herrero *et al.*, "Influence of different chemical cross-linking treatments on the properties of bovine pericardium and collagen," (in eng), *Biomaterials*, vol. 20, no. 6, pp. 539-45, Mar 1999.

- [275] A. Rahmanian-Schwarz *et al.*, "In vivo biocompatibility and biodegradation of a novel thin and mechanically stable collagen scaffold," (in eng), *Journal of biomedical materials research. Part A*, vol. 102, no. 4, pp. 1173-9, Apr 2014.
- [276] H. Fernandes *et al.*, "The role of collagen crosslinking in differentiation of human mesenchymal stem cells and MC3T3-E1 cells," (in eng), *Tissue engineering. Part A*, vol. 15, no. 12, pp. 3857-67, Dec 2009.
- [277] M. G. Haugh, C. M. Murphy, R. C. McKiernan, C. Altenbuchner, and F. J. O'Brien, "Crosslinking and mechanical properties significantly influence cell attachment, proliferation, and migration within collagen glycosaminoglycan scaffolds," (in eng), *Tissue engineering. Part A*, vol. 17, no. 9-10, pp. 1201-8, May 2011.
- [278] M. B. Keogh, F. J. O'Brien, and J. S. Daly, "Substrate stiffness and contractile behaviour modulate the functional maturation of osteoblasts on a collagen-GAG scaffold," *Acta biomaterialia*, vol. 6, no. 11, pp. 4305-4313, 2010/11/01/ 2010.
- [279] J. C. Lee *et al.*, "Optimizing Collagen Scaffolds for Bone Engineering: Effects of Cross-linking and Mineral Content on Structural Contraction and Osteogenesis," (in eng), *The Journal of craniofacial surgery*, vol. 26, no. 6, pp. 1992-1996, 2015.
- [280] D. E. Discher, P. Janmey, and Y. L. Wang, "Tissue cells feel and respond to the stiffness of their substrate," (in eng), *Science*, vol. 310, no. 5751, pp. 1139-43, Nov 18 2005.
- [281] R. Olivares-Navarrete *et al.*, "Substrate Stiffness Controls Osteoblastic and Chondrocytic Differentiation of Mesenchymal Stem Cells without Exogenous Stimuli," (in eng), *PloS one*, vol. 12, no. 1, pp. e0170312-e0170312, 2017.
- [282] M. Sun *et al.*, "Extracellular matrix stiffness controls osteogenic differentiation of mesenchymal stem cells mediated by integrin $\alpha 5$," (in eng), *Stem cell research & therapy*, vol. 9, no. 1, pp. 52-52, 2018.
- [283] A. Y. Wang, J. Rafalko, M. MacDonald, X. Ming, and R. Kocharian, "Absorbable Hemostatic Aggregates," *ACS Biomaterials Science & Engineering*, vol. 3, no. 12, pp. 3675-3686, 2017/12/11 2017.
- [284] C. Somaiah *et al.*, "Collagen Promotes Higher Adhesion, Survival and Proliferation of Mesenchymal Stem Cells," *PloS one*, vol. 10, no. 12, pp. e0145068-e0145068, 2015.
- [285] C.-S. Li *et al.*, "Fibromodulin reprogrammed cells: A novel cell source for bone regeneration," *Biomaterials*, vol. 83, pp. 194-206, 2016.
- [286] F. Gori, E. Schipani, and M. B. Demay, "Fibromodulin is expressed by both chondrocytes and osteoblasts during fetal bone development," (in eng), *Journal of cellular biochemistry*, vol. 82, no. 1, pp. 46-57, Apr 2-27 2001.
- [287] M. Goldberg *et al.*, "Fibromodulin-deficient mice reveal dual functions for fibromodulin in regulating dental tissue and alveolar bone formation," (in eng), *Cells, tissues, organs*, vol. 189, no. 1-4, pp. 198-202, 2009.
- [288] M. Meyer, "Processing of collagen based biomaterials and the resulting materials properties," *BioMedical Engineering OnLine*, vol. 18, no. 1, p. 24, 2019/03/18 2019.

- [289] S. F. Badylak, K. Park, N. Peppas, G. McCabe, and M. Yoder, "Marrow-derived cells populate scaffolds composed of xenogeneic extracellular matrix," (in eng), *Experimental hematology*, vol. 29, no. 11, pp. 1310-8, Nov 2001.
- [290] X. Liu *et al.*, "Repairing goat tibia segmental bone defect using scaffold cultured with mesenchymal stem cells," (in eng), *Journal of biomedical materials research. Part B, Applied biomaterials*, vol. 94, no. 1, pp. 44-52, Jul 2010.
- [291] T. Zantop, T. W. Gilbert, M. C. Yoder, and S. F. Badylak, "Extracellular matrix scaffolds are repopulated by bone marrow-derived cells in a mouse model of achilles tendon reconstruction," (in eng), *Journal of orthopaedic research : official publication of the Orthopaedic Research Society*, vol. 24, no. 6, pp. 1299-309, Jun 2006.
- [292] T. Schmidt, S. Stachon, A. Mack, M. Rohde, and L. Just, "Evaluation of a thin and mechanically stable collagen cell carrier," (in eng), *Tissue engineering. Part C, Methods*, vol. 17, no. 12, pp. 1161-1170, 2011.
- [293] M. A. Ingersoll *et al.*, "Comparison of gene expression profiles between human and mouse monocyte subsets," (in eng), *Blood*, vol. 115, no. 3, pp. e10-e19, 2010.
- [294] J. Mestas and C. C. W. Hughes, "Of Mice and Not Men: Differences between Mouse and Human Immunology," vol. 172, no. 5, pp. 2731-2738, 2004.
- [295] S. F. Badylak and T. W. Gilbert, "Immune response to biologic scaffold materials," (in eng), *Seminars in immunology*, vol. 20, no. 2, pp. 109-116, 2008.
- [296] L. M. Delgado, Y. Bayon, A. Pandit, and D. I. Zeugolis, "To cross-link or not to cross-link? Cross-linking associated foreign body response of collagen-based devices," (in eng), *Tissue engineering. Part B, Reviews*, vol. 21, no. 3, pp. 298-313, 2015.
- [297] B. Poudel, H. H. Ki, Y. M. Lee, and D. K. Kim, "Collagen I-induced dendritic cells activation is regulated by TNF-alpha production through down-regulation of IRF4," (in eng), *Journal of biosciences*, vol. 40, no. 1, pp. 71-8, Mar 2015.
- [298] A. Bayrak, P. Pruger, U. A. Stock, and M. Seifert, "Absence of immune responses with xenogeneic collagen and elastin," (in eng), *Tissue engineering. Part A*, vol. 19, no. 13-14, pp. 1592-600, Jul 2013.
- [299] A. Bayrak *et al.*, "Human immune responses to porcine xenogeneic matrices and their extracellular matrix constituents in vitro," (in eng), *Biomaterials*, vol. 31, no. 14, pp. 3793-803, May 2010.
- [300] B. M. Achauer, K. S. Black, D. M. Grosmark, and T. F. Hayamizu, "A comparison of hemostatic agents in microvascular surgery," (in eng), *Journal of microsurgery*, vol. 3, no. 4, pp. 242-7, Summer 1982.
- [301] M. R. Hait, "Microcrystalline collagen. A new hemostatic agent," (in eng), *American journal of surgery*, vol. 120, no. 3, p. 330, Sep 1970.
- [302] L. Morgenstern, "Microcrystalline collagen used in experimental splenic injury. A new surface hemostatic agent," (in eng), *Archives of surgery (Chicago, Ill. : 1960)*, vol. 109, no. 1, pp. 44-7, Jul 1974.

- [303] C. Schonauer, E. Tessitore, G. Barbagallo, V. Albanese, and A. Moraci, "The use of local agents: bone wax, gelatin, collagen, oxidized cellulose," (in eng), *European spine journal : official publication of the European Spine Society, the European Spinal Deformity Society, and the European Section of the Cervical Spine Research Society*, vol. 13 Suppl 1, pp. S89-96, Oct 2004.
- [304] W. H. Harris, O. D. Crothers, B. J. Moyen, and R. B. Bourne, "Topical hemostatic agents for bone bleeding in humans. A quantitative comparison of gelatin paste, gelatin sponge plus bovine thrombin, and microfibrillar collagen," (in eng), *The Journal of bone and joint surgery. American volume*, vol. 60, no. 4, pp. 454-6, Jun 1978.
- [305] J. Lindhe, D. Cecchinato, M. Donati, C. Tomasi, and B. Liljenberg, "Ridge preservation with the use of deproteinized bovine bone mineral," (in eng), *Clinical oral implants research*, vol. 25, no. 7, pp. 786-90, Jul 2014.
- [306] J. M. Anderson, A. Rodriguez, and D. T. Chang, "Foreign body reaction to biomaterials," (in eng), *Seminars in immunology*, vol. 20, no. 2, pp. 86-100, 2008.
- [307] J. E. Valentin, J. S. Badylak, G. P. McCabe, and S. F. Badylak, "Extracellular matrix bioscaffolds for orthopaedic applications. A comparative histologic study," (in eng), *The Journal of bone and joint surgery. American volume*, vol. 88, no. 12, pp. 2673-86, Dec 2006.
- [308] K. A. Alberti and Q. Xu, "Biocompatibility and degradation of tendon-derived scaffolds," (in eng), *Regenerative biomaterials*, vol. 3, no. 1, pp. 1-11, 2016.
- [309] S. F. Badylak, J. E. Valentin, A. K. Ravindra, G. P. McCabe, and A. M. Stewart-Akers, "Macrophage phenotype as a determinant of biologic scaffold remodeling," (in eng), *Tissue engineering. Part A*, vol. 14, no. 11, pp. 1835-42, Nov 2008.
- [310] B. N. Brown *et al.*, "Macrophage phenotype as a predictor of constructive remodeling following the implantation of biologically derived surgical mesh materials," (in eng), *Acta biomaterialia*, vol. 8, no. 3, pp. 978-87, Mar 2012.
- [311] B. N. Brown, J. E. Valentin, A. M. Stewart-Akers, G. P. McCabe, and S. F. Badylak, "Macrophage phenotype and remodeling outcomes in response to biologic scaffolds with and without a cellular component," (in eng), *Biomaterials*, vol. 30, no. 8, pp. 1482-91, Mar 2009.
- [312] B. N. Brown and S. F. Badylak, "Extracellular matrix as an inductive scaffold for functional tissue reconstruction," (in eng), *Translational research : the journal of laboratory and clinical medicine*, vol. 163, no. 4, pp. 268-285, 2014.
- [313] J. E. Valentin, A. M. Stewart-Akers, T. W. Gilbert, and S. F. Badylak, "Macrophage participation in the degradation and remodeling of extracellular matrix scaffolds," (in eng), *Tissue engineering. Part A*, vol. 15, no. 7, pp. 1687-1694, 2009.
- [314] Y. Kadoya, N. al-Saffar, A. Kobayashi, and P. A. Revell, "The expression of osteoclast markers on foreign body giant cells," (in eng), *Bone and mineral*, vol. 27, no. 2, pp. 85-96, Nov 1994.
- [315] A. Haas, "The phagosome: compartment with a license to kill," (in eng), *Traffic (Copenhagen, Denmark)*, vol. 8, no. 4, pp. 311-30, Apr 2007.

- [316] F. DeLustro, J. Dasch, J. Keefe, and L. Ellingsworth, "Immune responses to allogeneic and xenogeneic implants of collagen and collagen derivatives," (in eng), *Clinical orthopaedics and related research*, no. 260, pp. 263-79, Nov 1990.
- [317] I. El Bialy, W. Jiskoot, and M. Reza Nejadnik, "Formulation, Delivery and Stability of Bone Morphogenetic Proteins for Effective Bone Regeneration," *Pharmaceutical Research*, vol. 34, no. 6, pp. 1152-1170.
- [318] W. Friess, H. Uludag, S. Foskett, and R. Biron, "Bone regeneration with recombinant human bone morphogenetic protein-2 (rhBMP-2) using absorbable collagen sponges (ACS): influence of processing on ACS characteristics and formulation," (in eng), *Pharmaceutical development and technology*, vol. 4, no. 3, pp. 387-96, Aug 1999.
- [319] L. F. Vallejo and U. Rinas, "Optimized procedure for renaturation of recombinant human bone morphogenetic protein-2 at high protein concentration," (in eng), *Biotechnology and bioengineering*, vol. 85, no. 6, pp. 601-9, Mar 20 2004.
- [320] G. S. Krishnakumar, A. Roffi, D. Reale, E. Kon, and G. Filardo, "Clinical application of bone morphogenetic proteins for bone healing: a systematic review," (in eng), *International orthopaedics*, Apr 19 2017.
- [321] B. P. Hertzberg, J. B. Holt, R. D. Graff, S. R. Gilbert, and L. E. Dahners, "An evaluation of carrier agents for desferoxamine, an up-regulator of vascular endothelial growth factor," (in eng), *Journal of biomaterials applications*, vol. 27, no. 8, pp. 1046-54, May 2013.
- [322] B. M. Willie, R. Blakytyn, M. Glockelmann, A. Ignatius, and L. Claes, "Temporal variation in fixation stiffness affects healing by differential cartilage formation in a rat osteotomy model," (in eng), *Clinical orthopaedics and related research*, vol. 469, no. 11, pp. 3094-101, Nov 2011.
- [323] D. Chen *et al.*, "HIF-1alpha inhibits Wnt signaling pathway by activating Sost expression in osteoblasts," (in eng), *PLoS One*, vol. 8, no. 6, p. e65940, 2013.
- [324] S. Stegen *et al.*, "Osteocytic oxygen sensing controls bone mass through epigenetic regulation of sclerostin," (in eng), *Nature communications*, vol. 9, no. 1, p. 2557, Jul 2 2018.
- [325] B. Kruck *et al.*, "Sclerostin Neutralizing Antibody Treatment Enhances Bone Formation but Does Not Rescue Mechanically Induced Delayed Healing," (in eng), *Journal of bone and mineral research : the official journal of the American Society for Bone and Mineral Research*, vol. 33, no. 9, pp. 1686-1697, Sep 2018.
- [326] Y. Wu, A. Jin, C. Feng, Y. Zhao, and X. Liu, "DFO and DMOG up-regulate the expression of CXCR4 in bone marrow mesenchymal stromal cells," (in eng), *Die Pharmazie*, vol. 68, no. 10, pp. 835-8, Oct 2013.
- [327] A. Movila *et al.*, "Macrophage Migration Inhibitory Factor (MIF) Supports Homing of Osteoclast Precursors to Peripheral Osteolytic Lesions," (in eng), *Journal of bone and mineral research : the official journal of the American Society for Bone and Mineral Research*, vol. 31, no. 9, pp. 1688-700, Sep 2016.
- [328] D. Rajasekaran *et al.*, "Macrophage Migration Inhibitory Factor-CXCR4 Receptor Interactions: EVIDENCE FOR PARTIAL ALLOSTERIC AGONISM IN COMPARISON WITH CXCL12 CHEMOKINE," (in eng), *The Journal of biological chemistry*, vol. 291, no. 30, pp. 15881-15895, 2016.

- [329] C. Yellowley, "CXCL12/CXCR4 signaling and other recruitment and homing pathways in fracture repair," (in eng), *BoneKEy reports*, vol. 2, pp. 300-300, 2013.
- [330] Y. Yao *et al.*, "MIF Plays a Key Role in Regulating Tissue-Specific Chondro-Osteogenic Differentiation Fate of Human Cartilage Endplate Stem Cells under Hypoxia," *Stem cell reports*, vol. 7, no. 2, pp. 249-262, 2016.
- [331] A. J. Leger *et al.*, "Inhibition of osteoclastogenesis by prolyl hydroxylase inhibitor dimethylxallyl glycine," (in eng), *Journal of bone and mineral metabolism*, vol. 28, no. 5, pp. 510-9, Sep 2010.
- [332] P. Vinzenz, S. Schrockmair, R. Gruber, and H. Agis, "Bone substitute materials supplemented with prolyl hydroxylase inhibitors decrease osteoclastogenesis in vitro," (in eng), *Journal of biomedical materials research. Part B, Applied biomaterials*, vol. 103, no. 6, pp. 1198-203, Aug 2015.
- [333] S. H. Mun, H. Y. Won, P. Hernandez, H. L. Aguila, and S. K. Lee, "Deletion of CD74, a putative MIF receptor, in mice enhances osteoclastogenesis and decreases bone mass," (in eng), *Journal of bone and mineral research : the official journal of the American Society for Bone and Mineral Research*, vol. 28, no. 4, pp. 948-59, Apr 2013.
- [334] L. Zheng *et al.*, "Macrophage migration inhibitory factor (MIF) inhibitor 4-IPP suppresses osteoclast formation and promotes osteoblast differentiation through the inhibition of the NF-kappaB signaling pathway," (in eng), *FASEB journal : official publication of the Federation of American Societies for Experimental Biology*, p. fj201802364RR, Mar 20 2019.
- [335] R. P. Pirraco, R. L. Reis, and A. P. Marques, "Effect of monocytes/macrophages on the early osteogenic differentiation of hBMSCs," (in eng), *Journal of tissue engineering and regenerative medicine*, vol. 7, no. 5, pp. 392-400, May 2013.
- [336] L. J. Raggatt *et al.*, "Fracture healing via periosteal callus formation requires macrophages for both initiation and progression of early endochondral ossification," (in eng), *Am J Pathol*, vol. 184, no. 12, pp. 3192-204, Dec 2014.
- [337] F. M. Spinelli, D. L. Vitale, G. Demarchi, C. Cristina, and L. Alaniz, "The immunological effect of hyaluronan in tumor angiogenesis," *Clinical & translational immunology*, vol. 4, no. 12, pp. e52-e52, 2015.
- [338] S. Al-Roubaie, J. H. Hughes, M. B. Filla, R. Lansford, S. Lehoux, and E. A. Jones, "Time-lapse microscopy of macrophages during embryonic vascular development," (in eng), *Developmental dynamics : an official publication of the American Association of Anatomists*, vol. 241, no. 9, pp. 1423-31, Sep 2012.
- [339] A. Fantin *et al.*, "Tissue macrophages act as cellular chaperones for vascular anastomosis downstream of VEGF-mediated endothelial tip cell induction," (in eng), *Blood*, vol. 116, no. 5, pp. 829-40, Aug 5 2010.
- [340] H. He *et al.*, "Perivascular Macrophages Limit Permeability," *Arteriosclerosis, thrombosis, and vascular biology*, vol. 36, no. 11, pp. 2203-2212, 2016.
- [341] H. He *et al.*, "Endothelial cells provide an instructive niche for the differentiation and functional polarization of M2-like macrophages," (in eng), *Blood*, vol. 120, no. 15, pp. 3152-62, Oct 11 2012.

- [342] Y. Wang *et al.*, "The hypoxia-inducible factor alpha pathway couples angiogenesis to osteogenesis during skeletal development," (in eng), *The Journal of clinical investigation*, vol. 117, no. 6, pp. 1616-26, Jun 2007.
- [343] J. Lu *et al.*, "Positive-Feedback Regulation of Subchondral H-Type Vessel Formation by Chondrocyte Promotes Osteoarthritis Development in Mice," (in eng), *Journal of bone and mineral research : the official journal of the American Society for Bone and Mineral Research*, vol. 33, no. 5, pp. 909-920, May 2018.
- [344] J. Wang *et al.*, "CD31hiEmcnhi Vessels Support New Trabecular Bone Formation at the Frontier Growth Area in the Bone Defect Repair Process," *Scientific Reports*, vol. 7, pp. DOI: 10.1038/s41598-017-04150-5, 2017.
- [345] N. Manabe *et al.*, "Connection between B lymphocyte and osteoclast differentiation pathways," (in eng), *Journal of immunology (Baltimore, Md. : 1950)*, vol. 167, no. 5, pp. 2625-31, Sep 1 2001.
- [346] P. Mastroeni, C. Simmons, R. Fowler, C. E. Hormaeche, and G. Dougan, "Igh-6(-/-) (B-Cell-Deficient) Mice Fail To Mount Solid Acquired Resistance to Oral Challenge with Virulent Salmonella enterica Serovar Typhimurium and Show Impaired Th1 T-Cell Responses to Salmonella Antigens," *Infection and Immunity*, vol. 68, no. 1, pp. 46-53.
- [347] G. Sun, Y. Wang, Y. Ti, J. Wang, J. Zhao, and H. Qian, "Regulatory B cell is critical in bone union process through suppressing proinflammatory cytokines and stimulating Foxp3 in Treg cells," (in eng), *Clinical and experimental pharmacology & physiology*, vol. 44, no. 4, pp. 455-462, Apr 2017.
- [348] B. Edderkaoui, "Potential Role of Chemokines in Fracture Repair," *Frontiers in Endocrinology*, vol. 8, p. 39.
- [349] M. Hou, J. Liu, F. Liu, K. Liu, and B. Yu, "C1q tumor necrosis factor-related protein-3 protects mesenchymal stem cells against hypoxia- and serum deprivation-induced apoptosis through the phosphoinositide 3-kinase/Akt pathway," (in eng), *International journal of molecular medicine*, vol. 33, no. 1, pp. 97-104, Jan 2014.
- [350] M. Timlin *et al.*, "Fracture hematoma is a potent proinflammatory mediator of neutrophil function," (in eng), *The Journal of trauma*, vol. 58, no. 6, pp. 1223-9, Jun 2005.
- [351] C.-H. Chen, J. C. B. Ferreira, E. R. Gross, and D. Mochly-Rosen, "Targeting Aldehyde Dehydrogenase 2: New Therapeutic Opportunities," *Physiological Reviews*, vol. 94, no. 1, pp. 1-34, 2014.
- [352] G. Prasad, M. S. Dhillon, M. Khullar, and O. N. Nagi, "Evaluation of oxidative stress after fractures. A preliminary study," (in eng), *Acta orthopaedica Belgica*, vol. 69, no. 6, pp. 546-51, Dec 2003.
- [353] S. Fickert *et al.*, "Human mesenchymal stem cell proliferation and osteogenic differentiation during long-term ex vivo cultivation is not age dependent," (in eng), *Journal of bone and mineral metabolism*, vol. 29, no. 2, pp. 224-35, Mar 2011.
- [354] J. Lange *et al.*, "Action of IL-1 β during fracture healing," *Journal of orthopaedic research : official publication of the Orthopaedic Research Society*, vol. 28, no. 6, pp. 778-784, 2010.
- [355] T. Tanaka, M. Narazaki, and T. Kishimoto, "IL-6 in Inflammation, Immunity, and Disease," *Cold Spring Harbor Perspectives in Biology*, vol. 6, no. 10, p. a016295, 2014.

- [356] V. De Corte *et al.*, "Increased importin-beta-dependent nuclear import of the actin modulating protein CapG promotes cell invasion," (in eng), *Journal of cell science*, vol. 117, no. Pt 22, pp. 5283-92, Oct 15 2004.
- [357] W. Witke, W. Li, D. J. Kwiatkowski, and F. S. Southwick, "Comparisons of CapG and gelsolin-null macrophages: demonstration of a unique role for CapG in receptor-mediated ruffling, phagocytosis, and vesicle rocketing," (in eng), *The Journal of cell biology*, vol. 154, no. 4, pp. 775-84, Aug 20 2001.
- [358] J. Bystrom, K. Amin, and D. Bishop-Bailey, "Analysing the eosinophil cationic protein - a clue to the function of the eosinophil granulocyte," *Respiratory Research*, vol. 12, no. 1, pp. 10-10.
- [359] A. Serra, I. Könnecke, K. Schmidt-Bleek, H. Schell, A. Radbruch, and G. Duda, "Lymphocytes control bone fracture healing by programming the mineralisation capacity of migratory osteogenic precursors," *Annals of the Rheumatic Diseases*, vol. 71, no. Suppl 1, pp. A63-A63, 2012.
- [360] N. W. Gale *et al.*, "Normal Lymphatic Development and Function in Mice Deficient for the Lymphatic Hyaluronan Receptor LYVE-1," *Molecular and Cellular Biology*, vol. 27, no. 2, pp. 595-604.
- [361] J. H. Lee *et al.*, "Hypoxia Induces PDK4 Gene Expression through Induction of the Orphan Nuclear Receptor ERR γ ," *PLoS ONE*, vol. 7, no. 9, p. e46324.
- [362] S. J. Lee *et al.*, "Pyruvate Dehydrogenase Kinase 4 Promotes Vascular Calcification via SMAD1/5/8 Phosphorylation," *Scientific Reports*, Article vol. 5, p. 16577, 11/12/online 2015.
- [363] C. A. Piantadosi *et al.*, "Heme Oxygenase-1 Couples Activation of Mitochondrial Biogenesis to Anti-inflammatory Cytokine Expression," *The Journal of Biological Chemistry*, vol. 286, no. 18, pp. 16374-16385.
- [364] K. Tanaka, S. Tanaka, A. Sakai, T. Ninomiya, Y. Arai, and T. Nakamura, "Deficiency of vitamin A delays bone healing process in association with reduced BMP2 expression after drill-hole injury in mice," (in eng), *Bone*, vol. 47, no. 6, pp. 1006-12, Dec 2010.
- [365] A. Aspberg, "The different roles of aggrecan interaction domains," (in eng), *The journal of histochemistry and cytochemistry : official journal of the Histochemistry Society*, vol. 60, no. 12, pp. 987-96, Dec 2012.
- [366] J. Gu *et al.*, "Identification and characterization of the novel Col10a1 regulatory mechanism during chondrocyte hypertrophic differentiation," *Cell Death & Disease*, vol. 5, no. 10, p. e1469.
- [367] S. Mebarki *et al.*, "De novo HAPLN1 expression hallmarks Wnt-induced stem cell and fibrogenic networks leading to aggressive human hepatocellular carcinomas," *Oncotarget*, vol. 7, no. 26, pp. 39026-39043.
- [368] F. Nakajima *et al.*, "Spatial and temporal gene expression in chondrogenesis during fracture healing and the effects of basic fibroblast growth factor," (in eng), *Journal of orthopaedic research : official publication of the Orthopaedic Research Society*, vol. 19, no. 5, pp. 935-44, Sep 2001.
- [369] X. Zhang, I. Prasad, W. Fang, R. Crawford, and Y. Xiao, "Chondromodulin-1 ameliorates osteoarthritis progression by inhibiting HIF-2 α activity," (in eng), *Osteoarthritis and cartilage*, vol. 24, no. 11, pp. 1970-1980, Nov 2016.

- [370] N. Y. Naung, S. Suttapreyasri, S. Kamolmatyakul, and T. Nuntanaranont, "Comparative study of different centrifugation protocols for a density gradient separation media in isolation of osteoprogenitors from bone marrow aspirate," *Journal of oral biology and craniofacial research*, vol. 4, no. 3, pp. 160-168, Sep-Dec 2014.
- [371] M. J. Peffers *et al.*, "Age-related changes in mesenchymal stem cells identified using a multi-omics approach," (in eng), *European cells & materials*, vol. 31, pp. 136-59, Feb 8 2016.
- [372] Y.-H. K. Yang, "Aging of mesenchymal stem cells: Implication in regenerative medicine," *Regenerative therapy*, vol. 9, pp. 120-122, 2018.
- [373] P. Ganguly, J. J. El-Jawhari, P. V. Giannoudis, A. N. Burska, F. Ponchel, and E. A. Jones, "Age-related Changes in Bone Marrow Mesenchymal Stromal Cells: A Potential Impact on Osteoporosis and Osteoarthritis Development," *Cell transplantation*, vol. 26, no. 9, pp. 1520-1529, 2017.
- [374] A. Papadimitropoulos *et al.*, "Expansion of human mesenchymal stromal cells from fresh bone marrow in a 3D scaffold-based system under direct perfusion," (in eng), *PLoS One*, vol. 9, no. 7, p. e102359, 2014.
- [375] Y. Zhou, H. Chen, H. Li, and Y. Wu, "3D culture increases pluripotent gene expression in mesenchymal stem cells through relaxation of cytoskeleton tension," *Journal of cellular and molecular medicine*, vol. 21, no. 6, pp. 1073-1084, 2017.
- [376] H. Oshina *et al.*, "Effects of continuous dexamethasone treatment on differentiation capabilities of bone marrow-derived mesenchymal cells," (in eng), *Bone*, vol. 41, no. 4, pp. 575-83, Oct 2007.
- [377] A. S. Muller *et al.*, "Deferoxamine but Not Dimethylxalylglycine, L-Mimosine, or Cobalt Dichloride Can Interfere with the MTT Assay," (in eng), *Biomed Res Int*, vol. 2018, p. 5872865, 2018.
- [378] P. S. Gomes and M. H. Fernandes, "Rodent models in bone-related research: the relevance of calvarial defects in the assessment of bone regeneration strategies," (in eng), *Laboratory animals*, vol. 45, no. 1, pp. 14-24, Jan 2011.
- [379] M. Peric *et al.*, "The rational use of animal models in the evaluation of novel bone regenerative therapies," (in eng), *Bone*, vol. 70, pp. 73-86, Jan 2015.
- [380] M. Mehta *et al.*, "A 5-mm femoral defect in female but not in male rats leads to a reproducible atrophic non-union," (in eng), *Archives of orthopaedic and trauma surgery*, vol. 131, no. 1, pp. 121-9, Jan 2011.
- [381] E. A. Barcak and M. J. Beebe, "Bone Morphogenetic Protein: Is There Still a Role in Orthopedic Trauma in 2017?," (in eng), *The Orthopedic clinics of North America*, vol. 48, no. 3, pp. 301-309, Jul 2017.

Publications

A. From the present work

Publications (Peer reviewed)

Lang, A., Kirchner, M., Stefanowski, J., Durst, M., Weber, M.-C., Pfeiffenberger, M., Damerau, A., Hauser, A.E., Hoff, P., Duda, G.N., Buttgereit, F., Schmidt-Bleek, K. & T. Gaber (2019) Collagen I-based scaffolds negatively impact fracture healing in a mouse-osteotomy-model although used routinely in research and clinical application. *Acta Biomaterialia*. 86:171-184. doi: 10.1016/j.actbio.2018.12.043.

Stefanowski, J.*, **Lang, A.***, Rauch, A., Aulich, L., Köhler, M., Fiedler, A.F., Buttgereit, F., Schmidt-Bleek, K., Duda, G., Gaber, T., Niesner, R. & A. Hauser (2019) Spatial Distribution of Macrophages during Callus Formation and Maturation Reveals Close Crosstalk between Macrophages and Newly Forming Vessels. *Frontiers Immunology*. 10 (2588). doi: 10.3389/fimmu.2019.02588

Lang, A. et al. (2019) Immunological dysregulation and inadequate hypoxia adaptation - HIF-stabilization as possible prevention of fracture healing disorders in RA or immune-suppressed patients. *In preparation*.

Abstracts & Participation in Conferences

Lang, A., Gaber, T., Hoff, P., Schmidt-Bleek, K., Buttgereit, F. (2019) Application of HIF-Stabilizers Enhances Bone Regeneration in a Mouse Model of Compromised Conditions. ORS Meeting, Austin, Texas – Poster Presentation

Lang, A., Gaber, T., Schmidt-Bleek, K., Buttgereit, F. (2017) Bovine Col I-based scaffold inhibits bone healing in a mouse-osteotomy-model – Time to rethink delivery systems Bone-tec Meeting, Munich – Oral Presentation

Lang, A., Fügner, S., Hoff, P., Schmidt-Bleek, K., Gaber, T., Buttgereit, F. (2016) Fracture healing disorders as adverse effect of anti-inflammatory medications - How can HIF-stabilization be used for prevention in OA or RA patients? OARSI Congress, Amsterdam – Oral Presentation

Lang, A., Fügner, S., Hoff, P., Schmidt-Bleek, K., Gaber, T. & F. Buttgereit (2015) Immunological Dysregulation and Inadequate Hypoxia Adaptation - HIF-Stabilization As Possible Prevention of Fracture Healing Disorders in RA or Immune-Suppressed Patients. ACR/ARHP Annual Meeting, San Francisco – Poster Presentation

Fügner, S., **Lang, A.**, Rakow, A., Gaber, T., Burmester, G.-R., Simon, P., Buttgereit, F. & P. Hoff, (2015) Logistic regression method identifies RA as risk factors for delayed fracture-healing – An update of a single-center retrospective study. Annual European Congress of Rheumatology EULAR, Rome – Poster Presentation

Lang, A., Schmidt-Bleek, K., Jakstadt, M., Hoff, P., Gaber, T., Duda, G. & F. Buttgerit (2015) Der Einfluss von Glukokortikoiden auf mesenchymale Stromazellen – hat Hypoxie entgegengesetzte Effekte? Osteologiekongress, Berlin – Oral Presentation

Lang, A., Fügenger, S., Hoff, P., Rakow, A., Jackstadt, M., Gaber, T., Burmester, G.-R., Perka, K. & F. Buttgerit (2014) Impaired Bone Healing in Patients Suffering from Rheumatoid Arthritis - Anti-inflammatory Therapy as Confounder. ACR/ARHP Annual Meeting, Boston - Poster Presentation

Lang, A., Schmidt-Bleek, K., Jackstadt, M., Hoff, P., Gaber, T., Duda, G. & F. Buttgerit (2014) Impact of Glucocorticoids on Mesenchymal Stromal Cell Differentiation - Can Hypoxia counteract? Annual European Congress of Rheumatology EULAR, Paris - Poster Presentation

Fügenger, S., Hoff, P., **Lang, A.**, Gaber, T., Perka, K. & F. Buttgerit (2014) Potential Risk Factors for Fracture Bone Healing Complications at the Charité Berlin. Annual European Congress of Rheumatology EULAR Congress, Paris - Poster Presentation

Lang A., Wagegg M., Lohanatha F.L., Jackstadt M., Gaber T., Duda G. & F. Buttgerit (2013) GC and NSAID induced Impact on MSC Differentiation - How can Hypoxia counteract? PhD Symposium, Berlin-Brandenburg School of Regenerative Therapies (BSRT), Berlin - Poster Presentation

B. From additional work

Publications (Peer reviewed)

Pfeiffenberger, M.* , Bartsch, J.* , Hoff, P., Ponomarev, I., Barnewitz, D., Thöne-Reineke, C., Buttgerit, F., Gaber, T.* & **A. Lang*** (2019) Hypoxia and mesenchymal stromal cells as key drivers of initial fracture healing in an equine *in vitro* fracture hematoma model. *PlosONE*. Apr 4;14(4).

Jirkof, P.* , Durst, M.* , Klopffleisch, R., Palme, R., Thöne-Reineke, C., Buttgerit, F., Schmidt-Bleek, K. & **A. Lang** (2019) Tramadol and Buprenorphine via the drinking water as analgesia in a mouse-osteotomy model – Why dosage matters! *In revision after review for Scientific Reports*.

Gaber, T., Schönbeck, K., Hoff, H., Tran, C.L., Strehl, C., **Lang, A.**, Ohrndorf, S., Pfeiffenberger, M., Röhner, E., Matziolis, G., Burmester, G.R., Buttgerit, F. & P. Hoff (2018) CTLA-4 Mediates Inhibitory Function of Mesenchymal Stem/Stromal Cells. *International Journal of Molecular Sciences*. Aug 7;19(8).

Hoff, P., Gaber, T., Strehl, C., Jakstadt, M., Hoff, H., Schmidt-Bleek, K., **Lang, A.**, Röhner, E., Huscher, D., Matziolis, G., Burmester, G.R., Schmidmaier, G., Perka, C., Duda, G.N. & F. Buttgerit (2017) A Pronounced Inflammatory Activity Characterizes the Early Fracture Healing Phase in Immunologically Restricted Patients. *International Journal of Molecular Sciences*. Mar 8;18(3).

Hoff, P., Gaber, T., Strehl, C., Schmidt-Bleek, K., **Lang, A.**, Huscher, D., Burmester, G.R., Schmidmaier, G., Perka, C., Duda, G.N. & F. Buttgerit (2016) Immunological characterization of the early human fracture hematoma. *Immunologic Research*. 64(5-6): 1195-1206.

Lang, A., Neuhaus, J., Pfeiffenberger, M., Schröder, E., Weber, Y., Ponomarev, I., Gaber, T. & M.F.G. Schmidt (2014) Optimization of a non-viral transfection system to evaluate Cox-2 controlled IL-4 expression for osteoarthritis gene therapy *in vitro*. *Journal of Gene Medicine*. Nov-Dec; 16(11-12): 352-63.

Hoff, P., Belavý, D.L., Huscher, D., **Lang, A.**, Hahne, M., Kuhlmeier, A., Maschmeyer, P., Armbrrecht, G., Fitzner, R., Perschel, F.H., Gaber, T., Burmester, G.R., Straub, R.H., Felsenberg, D. & F. Buttgerit (2014) Effects of 60-days bed rest with and without exercise on cellular and humoral immunological parameters. *Cellular & Molecular Immunology*. Nov 10.

Lang, A., De Vries, M., Feineis, S., Müller, E, Osterrieder, N. & A.M. Damiani (2013) Development of a peptide ELISA for discrimination between serological responses to equine herpesvirus type 1 and 4. *Journal of Virological Methods*. 193: 667– 673.

Reviews, Monograph and Book chapters

Scheinpflug, J.* , Pfeiffenberger, M.* , Damerau, A., Schwarz, F., Textor, M., **Lang, A.** & F. Schulze (2018) Journey into human bone models - A review. *Genes*. 9 (5).

Lang, A. et al. (2018) *In silico* methods - Computational alternatives to animal testing. Workshop report. *Altex* 35, 124-126.

Lang, A., Schulz, A., Ellinghaus, A. & K. Schmidt-Bleek (2016) Osteotomy models - the current status on pain scoring and management in small rodents. *Laboratory animals*, 50(6): 433-441.

A. Lang (2016) Reviewing Challenges in Osteoarthritis Gene Therapy and Introduction of a Molecular Therapeutic Approach in an Equine Model System. Inaugural-Dissertation Dr. med. vet. Freie Universität Berlin. In: Mensch und Buch Verlag. Berlin, Germany. ISBN 978-3-86387-707-1

Rai, M.F., **Lang, A.**, Sieber, M. & M.F.G. Schmidt (2011) Conditioning and Scaffolding of Chondrocytes: Smart Steps towards Osteoarthritis Gene Therapy. In: Chunsheng Kang (ed.), Gene Therapy Application. In: Tech Open Access Publisher. Rijeka, Croatia. ISBN 978-953-307-541-9

Danksagung

Mein erster Dank gilt **Prof. Frank Buttgerit**, der mir die Möglichkeit gab, Teil seiner Arbeitsgruppe zu werden und meine Expertisen auch im Bereich der Knochenbiologie auszubauen. Weiterhin bedanke ich mich herzlich für seine tolle und stetige Unterstützung im Aufbau und der Initiierung neuer Projekte z.B. im Bereich der 3R-Forschung, wodurch ich die Möglichkeit bekam, mich frei zu entfalten und unabhängig zu agieren.

Ganz herzlich möchte ich mich bei **Dr. Timo Gaber** bedanken, für seine Offenheit und Zuversicht mir eines seiner Projekte anzuvertrauen und seiner unermüdlichen fachlichen Unterstützung. Außerdem möchte ich mich bei der gesamten AG Buttgerit bedanken für die herzliche Aufnahme, die Unterstützung in experimentellen oder administrativen Belangen und die Bereicherung des Laboralltages durch z.B. Schokolade. Namentlich sind dabei besonders zu erwähnen: **Manuela Jakstadt**, **Gabriele May** und **Cindy Strehl**. Einen besonderen Dank gilt auch meinen direkten Laborkollegen, Studenten oder Praktikanten, die bei dem ein oder anderen Experiment helfend zur Seite standen – **Marie-Christin Weber**, **Mattea Durst**, **Kerstin Schönbeck**, **Moritz Pfeiffenberger** und **Alexandra Damerau**.

Weiterhin gilt mein tiefer Dank **Dr. Katharina Schmidt-Bleek**, die mich nicht nur in die Welt der Tierexperimente eingeführt hat, sondern auch eine großartige Mentorin und konstruktive Projektpartnerin ist und mich bei all meinen Ideen immer unterstützt. Danken möchte ich dabei auch ihrer Arbeitsgruppe – **Norma Schulze**, **Claudia Schlundt** und **Christian Bucher** - für die fachmännische Unterstützung, die Einführung in die Methoden und den fachlichen Austausch. **Prof. Georg Duda** möchte ich auf diesem Wege danken, für die Übernahmen meiner Zweitbetreuung im Rahmen der BSRT, die fachlichen Diskussionen, die offene Aufnahme in seinem Institut sowie die Erlaubnis die entsprechenden Einrichtungen und Geräte zu benutzen.

Der **BSRT** (Berlin-Brandenburg School for Regenerative Therapies) möchte ich danken für die Unterstützung im Rahmen eines Promotionsstipendiums, das mir die Anfertigung dieser Arbeit ermöglicht hat, ebenso wie das überaus großzügige und breite Angebot an Kursen und auch die Unterstützung von Konferenzreisen oder kleineren Projekten. Eine bessere Graduiertenschule hätte ich mir nicht wünschen können. Weiter so! Außerdem danke ich auch der DRS Biomedical Sciences für die Aufnahme und Unterstützung, um den PhD an der FU-Berlin zu erhalten.

Prof. Dr. Robert Klopffleisch danke ich für die Betreuung an der FU-Berlin und die ein oder anderen Kooperationen.

Ich danke meinen Kooperationspartnern – **Dr. Marieluise Kirchner, Vikram Sunkara, PhD** und **Jonathan Stefanowski** für die großartige Zusammenarbeit.

Zu guter Letzt danke ich meinen **Freunden** und **Mitbewohnern** für ihre Unterstützung, ebenso wie meinem Partner – **Andreas Benn** und meinem Hund **Mephisto**. Ein besonderer Dank gilt meiner **Familie**, die mich unermüdlich auch bei der zweiten Doktorarbeit unterstützt haben – Danke **Mama** und **Papa**, dass ihr mich weiterhin fliegen lasst!

Anteilsenkärung von Dr. med. vet. Annemarie Lang

Anteilsenkärung von Annemarie Lang an der vorliegenden Monografie gemäß § 8 Abschnitt 3 Promotionsordnung des Fachbereichs Veterinärmedizin der Freien Universität Berlin (Stand 14.09.2011)

Dr. med. vet. Annemarie Lang hat die Experimente, Ergebnisse und Abbildungen/Tabellen, die in dieser Monografie dargestellt sind, selbständig durchgeführt, analysiert und erstellt. Abbildungen/Tabellen und Ergebnisse, die in Zusammenarbeit mit anderen Wissenschaftlern entstanden und in anderen Arbeiten/Veröffentlichungen publiziert sind, werden im Folgenden detailliert aufgelistet:

Figure 1-6: Die Abbildungen wurden aus Publikationen entnommen, welche entsprechend in der Legende vermerkt sind. Die Genehmigungen zur Verwendung in dieser Monografie liegen Dr. med. vet. Annemarie Lang vor und können auf Rückfrage vorgewiesen werden.

Figure 9-13, 18-28, 30, 43 und Table 5-7, 15: Die Abbildungen und Tabellen wurden von Annemarie Lang eigenständig für die Veröffentlichung in den folgenden Publikationen erstellt und sind in dieser Arbeit z.T. modifiziert dargestellt. Die Genehmigung zur Verwendung in dieser Monografie liegen Dr. med. vet. Annemarie Lang vor und kann auf Rückfrage vorgewiesen werden.

Lang, A., Kirchner, M., Stefanowski, J., Durst, M., Weber, M.-C., Pfeiffenberger, M., Damerau, A., Hauser, A.E., Hoff, P., Duda, G.N., Buttgerit, F., Schmidt-Bleek, K. & T. Gaber (2019) *Acta Biomaterialia*. Jan 4. doi: 10.1016/j.actbio.2018.12.043.

Stefanowski, J.*, Lang, A.*, Rauch, A., Aulich, L., Köhler, M., Fiedler, A.F., Buttgerit, F., Schmidt-Bleek, K., Duda, G., Gaber, T., Niesner, R. & A. Hauser (2019). *Front Immunol.* 10 (2588). doi: 10.3389/fimmu.2019.02588

Proteomics-Analysen: Die Proteomics-Analysen wurden von Dr. Marieluise Kirchner von der BIH Core Facility für Proteomics durchgeführt. Die Aufarbeitung, Darstellung und Interpretation der Daten erfolgte selbständig von Dr. med. vet. Annemarie Lang.

Microarray-Analysen: Die Durchführung der Microarray-Analysen erfolgte im Regine-von-Raminlabor (DRFZ, Berlin). Die Daten wurden von Prof. Thomas Häupl aufgearbeitet und von Vikram Sunkara, PhD (FU-Berlin) analysiert. Die Darstellung und Interpretation der Daten erfolgte selbständig von Dr. med. vet. Annemarie Lang.

BioAnalyzer: Die Untersuchung der Integrität der RNA-Proben mittels BioAnalyzer erfolgte in der Service-Einrichtung des DRFZ, Berlin.

Finanzierungsquellen

Die Arbeiten wurden finanziell unterstützt durch das Berlin-Brandenburg Center for Regenerative Therapies (BCRT). Dr. med. vet. Annemarie Lang erhielt ein dreijähriges Stipendium der Berlin-Brandenburg School for Regenerative Therapies (BSRT). Einzelne Daten wurden im Rahmen einer BfR/Bf3R geförderten Studie (RefineMOMo; Projektnr.: 1328-542) erhoben.

Interessenskonflikte

Es bestehen keine Interessenskonflikte.

Selbstständigkeitserklärung

Hiermit bestätige ich, dass ich die hier vorliegende Arbeit selbstständig angefertigt habe. Ich versichere, dass ich ausschließlich die angegebenen Quellen und Hilfen in Anspruch genommen habe.

Berlin, den 28.11.2019

Dr. med. vet. Annemarie Lang



9 783967 290264
mbvberlin | mensch und buch verlag

49,90 Euro | ISBN: 978-3-96729-026-4